

**STUDIES OF GEL POLYMER ELECTROLYTES FOR
LITHIUM AND SODIUM BATTERIES**

KHAIRUL BAHYAH BINTI MD ISA

**DESSERTATION SUBMITTED IN FULFILMENT OF
THE REQUIREMENTS FOR THE DEGREE OF DOCTOR
OF PHILOSOPHY**

**FACULTY OF SCIENCE
UNIVERSITY OF MALAYA
KUALA LUMPUR**

2016

UNIVERSITY OF MALAYA
ORIGINAL LITERARY WORK DECLARATION

Name of Candidate: Khairul Bahiyah Md Isa (I.C/Passport No:

Registration/Matric No: SHC 100089

Name of Degree: Doctor of Philosophy

Title of Project Paper/Research Report/Dissertation/Thesis (“this Work”):

Studies of Gel Polymer Electrolytes for Lithium and Sodium Batteries

Field of Study: Advanced Materials

I do solemnly and sincerely declare that:

- (1) I am the sole author/writer of this Work;
- (2) This Work is original;
- (3) Any use of any work in which copyright exists was done by way of fair dealing and for permitted purposes and any excerpt or extract from, or reference to or reproduction of any copyright work has been disclosed expressly and sufficiently and the title of the Work and its authorship have been acknowledged in this Work;
- (4) I do not have any actual knowledge nor do I ought reasonably to know that the making of this work constitutes an infringement of any copyright work;
- (5) I hereby assign all and every rights in the copyright to this Work to the University of Malaya (“UM”), who henceforth shall be owner of the copyright in this Work and that any reproduction or use in any form or by any means whatsoever is prohibited without the written consent of UM having been first had and obtained;
- (6) I am fully aware that if in the course of making this Work I have infringed any copyright whether intentionally or otherwise, I may be subject to legal action or any other action as may be determined by UM.

Candidate’s Signature

Date:

Subscribed and solemnly declared before,

Witness’s Signature

Date:

Name:

Designation:

ABSTRACT

In the present work, gel polymer electrolytes (GPEs) comprising polyvinylidene-co-hexafluoropropylene (PVdF-HFP) as host polymer in a mixture of ethylene carbonate (EC) and propylene carbonate (PC) plasticizing solvent with various concentrations of lithium triflate and sodium triflate dopant salts have been prepared by the solution casting technique. Three systems of polymer electrolytes films have been prepared; these systems are the plasticized-PVdF-HFP system i.e. PVdF-HFP/EC/PC system and two plasticized-salted PVdF-HFP systems i.e. PVdF-HFP/EC/PC/LiCF₃SO₃ and PVdF-HFP/EC/PC/NaCF₃SO₃. The pure PVdF-HFP film serves as reference. Using results from impedance spectroscopy, ionic conductivity for each film in all systems has been calculated. The room temperature conductivity for pure PVdF-HFP film and plasticized-PVdF-HFP film is $1.86 \times 10^{-11} \text{ S cm}^{-1}$ and $3.31 \times 10^{-8} \text{ S cm}^{-1}$, respectively. The room temperature-conductivity for the highest conducting film in PVdF-HFP/EC/PC/LiCF₃SO₃ system and PVdF-HFP/EC/PC/NaCF₃SO₃ system are $1.40 \times 10^{-3} \text{ S cm}^{-1}$ and $2.50 \times 10^{-3} \text{ S cm}^{-1}$ respectively. The conductivity of the PVdF-HFP-based polymer electrolyte has been found to be salt concentration dependent which is attributed to the increase in the number of mobile ions within the polymer matrix. The binary plasticizing solvent helps to increase the amorphous content of the polymer matrix and tend to dissociate ion-pairs into free cations and anions thereby leading to an overall enhancement in conductivity. The conductivity-temperature studies are then performed on the highest conducting film from the in PVdF-HFP/EC/PC/LiCF₃SO₃ system and PVdF-HFP/EC/PC/NaCF₃SO₃ system. The plots of conductivity versus inverse temperature for both systems follow the VTF rule. The activation energy for all the GPE films are determined to be in the range of 0.08 - 0.102 eV. The transport number of lithium and sodium ions in the GPEs was evaluated using the combination of

AC impedance spectroscopy and DC polarization techniques. DSC studies show that the T_g of the GPE film decreases upon addition of the plasticizing solvents and the salts. This result is in good agreement with the conductivity behaviour. TGA analysis shows that the samples with higher salt concentrations have greater thermal stability. FTIR and Raman studies confirm that conductivity enhancement is due to increase in free ions and decrease in ion aggregates. XRD studies show the occurrence of complexation between the polymer, the plasticizing solvents and the salts. The FESEM micrographs show that the presence of the plasticizing solvents in PVdF-HFP/salt system helped to obtain regular pore structure, which can increase ion mobility and conductivity. The electrochemical stability of the GPE films has been tested using linear sweep voltammetry (LSV) and the value of working voltage range appears to be high enough to be used as an electrolyte in lithium and sodium cells. Studies based on AC impedance and cyclic voltammetry (CV) confirmed the lithium and sodium ion conduction in the GPE films from both systems. The LiNiCoO_2 | GPE | Li and MnO_2 | GPE | Na cells have been assembled and their performances have been evaluated. The cells that containing LiCF_3SO_3 and NaCF_3SO_3 salt exhibits the first capacity of 164 mAhg^{-1} and 168 mAhg^{-1} , respectively.

ABSTRAK

Dalam kajian ini, elektrolit gel polimer (GPE) yang mengandungi polivinilidinafluorid-hesafloropropilena (PVdF-HFP) sebagai polimer asas di dalam campuran larutan agen pemplastik, etilena karbonat (EC) dan propilena karbonat (PC) berserta lithium triflat dan natrium triflat sebagai garam pendopan dengan jumlah kandungan yang berbeza telah disediakan dengan menggunakan teknik tuangan larutan. Terdapat tiga sistem elektrolit gel polimer yang telah disediakan iaitu sistem PVdF-HFP/EC/PC, sistem PVdF-HFP/EC/PC/LiCF₃SO₃ dan sistem PVdF-HFP/EC/PC/NaCF₃SO₃. Filem PVdF-HFP tulen digunakan sebagai rujukan. Kekonduksian bagi setiap filem dalam semua sistem diukur dengan menggunakan spektroskopi impedans. Kekonduksian pada suhu bilik bagi filem PVdF-HFP tulen dan PVdF-HFP/ EC/ PC adalah masing-masing bernilai $1.86 \times 10^{-11} \text{ S cm}^{-1}$ dan $3.31 \times 10^{-8} \text{ S cm}^{-1}$. Kekonduksian tertinggi dalam sistem PVdF-HFP/EC/PC/LiCF₃SO₃ dan sistem PVdF-HFP/EC/PC/ NaCF₃SO₃ adalah masing-masing pada kepekatan garam 25 wt.% LiCF₃SO₃ dan 20 wt.% NaCF₃SO₃ dengan nilai kekondusian $1.40 \times 10^{-3} \text{ S cm}^{-1}$ and $2.50 \times 10^{-3} \text{ S cm}^{-1}$. Kekonduksian filem-filem ini menunjukkan kebergantungan kepada kandungan garam pendopan yang disebabkan peningkatan jumlah bilangan ion bergerak di dalam matrik polimer. Pelarut pemplastik juga membantu meningkatkan kandungan amorfus dalam matrik polimer dan dapat meleraikan pasangan ion kepada ion-ion bebas seterusnya meningkatkan kekonduksian filem. Kajian seterusnya dilakukan ke atas filem-filem pada kepekatan minimum, maksimum dan yang mempunyai kekonduksian tertinggi daripada setiap sistem untuk menyiasat kesan suhu ke atas nilai kekonduksian. Plot-plot kekonduksian melawan suhu songsangan menunjukkan filem-filem tersebut mematuhi hukum VTF dengan julat tenaga pengaktifan adalah antara 0.08 - 0.102 eV. Bilangan pengangkutan ion litium dan ion natrium dalam filem GPE telah diukur menggunakan gabungan spektroskopi

impedans AC dan polarisasi teknik DC dan kajian ini juga menentukan pembawa cas dalam filem elektrolit. Keputusan ujikaji DSC menunjukkan nilai T_g bagi setiap filem berkurangan dengan penambahan pelarut pemplastik dan kandungan garam. Keputusan ini adalah selari dengan nilai-nilai kekonduksian. Analisis TGA pula menunjukkan filem yang mengandungi kepekatan garam yang tinggi lebih stabil daripada segi terma. Kajian FTIR dan Raman ke atas filem-filem elektrolit membuktikan peningkatan nilai kekonduksian adalah disebabkan peningkatan bilangan ion-ion bebas dan pengurangan ion agregat. Keputusan XRD menunjukkan pengkompleksan berlaku di antara polimer, pelarut pemplastik dan garam pendopan. Mikrograf daripada ujikaji FESEM menunjukkan bahawa kehadiran agen pemplastik telah menghasilkan struktur berliang yang seragam di mana ianya memudahkan pergerakan ion-ion seterusnya meningkatkan kekonduksian. Kestabilan elektrokimia filem telah diukur dengan menggunakan kaedah voltammetri sapu linear (LSV) dan julat keupayaan kerja bagi filem yang diukur didapati mencukupi untuk digunakan sebagai elektrolit dalam sistem bateri. Ujikaji berdasarkan impedans AC dan voltammetri berkisar (CV) memastikan konduksi ion lithium dan ion natrium dalam filem. Sel – sel $\text{LiNiCoO}_2 | \text{GPE} | \text{Li}$ dan $\text{MnO}_2 | \text{GPE} | \text{Na}$ difabrikasikan dan diuji. Sel tersebut yang masing-masing mengandungi garam LiCF_3SO_3 dan NaCF_3SO_3 menunjukkan nilai kapasiti pertama sebanyak 164 mAhg^{-1} dan 168 mAhg^{-1} .

ACKNOWLEDGEMENTS

In the name of Allah, the Almighty Lord, the most Gracious and the most Merciful. Alhamdulillah, I thank to God for His Help and Bless, finally, I was able to finish my dissertation successfully. Peace be upon His messenger Muhammad and his honourable family.

I would like to express my deepest gratitude to my supervisors, Assoc. Prof. Dr. Zurina Osman and Prof. Dr. Abdul Kariem Arof for the encouragement, excellent guidance, caring, patience and support from the initial to the final level enabled me to develop an understanding of this project.

Special thanks to Lisani Othman, who as a good friend, was always willing to help and give her best suggestions. I am also grateful to my lab mates, Siti Mariam Samin, Nurul Husna Zainol, Diyana Hambali and Zaffan Zainuddin for their help and long term friendship. Thanks also due to Dzurainey Abu Bakar, the Materials Science Laboratory assistant at Physics Department for the technical support rendered.

I would also like to convey thanks to the Ministry of Higher Education and University of Malaya for providing the financial support and laboratory facilities.

I also wishes to express my love and gratitude to my beloved families and my husband, Mohd Amran Ahmad for their understanding and endless love, through the duration of my studies. They were always supporting and encouraging me with their best wishes. Last but certainly not least, appreciation is expressed to all the individuals who have directly or indirectly assisted me during the preparation of this thesis.

TABLE OF CONTENTS

Abstract	iii
Abstrak	v
Acknowledgements	vii
Table of Contents	viii
List of Figures	xii
List of Tables.....	xix
List of Symbols and Abbreviations.....	xxii
CHAPTER 1: INTRODUCTION.....	1
1.1 Background of the Present Work.....	1
1.2 Objectives of the Present Work	3
1.3 Organization of the Thesis.....	4
CHAPTER 2: LITERATURE REVIEW.....	6
2.1 Electrolytes and Batteries	6
2.1.1 Development of Lithium Ion Rechargeable Battery	11
2.1.2 Development of Sodium Ion Rechargeable Battery	14
2.2 Polymer Electrolytes in Lithium-Polymer Batteries.....	15
2.2.1 Development of Polymer Electrolytes.....	19
2.2.1.1 Polymer Matrix	20
2.2.1.2 Salts	24
2.2.1.3 Plasticizing Agent	25
2.3 Development of PVdF-HFP-based polymer electrolytes	29
2.4 Ionic Mechanism in Conducting Polymer Electrolytes	32

CHAPTER 3: EXPERIMENTAL TECHNIQUES	38
3.1 Sample Preparation	38
3.1.1 Materials	38
3.1.2 Preparation of Gel Polymer Electrolytes Systems	39
3.2 Characterizations of Gel Polymer Electrolytes Films	39
3.3 Experimental Techniques	42
3.3.1 Electrochemical Impedance Spectroscopy (EIS)	42
3.3.2 Transport number measurements	49
3.3.3 Differential Scanning Calorimetry (DSC).....	52
3.3.4 Thermogravimetry Analysis.....	54
3.3.5 Fourier Transfer Infrared Spectroscopy (FTIR).....	58
3.3.6 Raman Spectroscopy	62
3.3.7 X-Ray Diffraction.....	67
3.3.8 Field Emission Scanning Electron Microscopy (FESEM).....	70
3.3.9 Linear Sweep Voltammetry.....	73
3.3.10 Cyclic Voltammetry	75
3.3.11 Battery Fabrication	77
CHAPTER 4: ELECTRICAL STUDIES	80
4.1 Impedance Spectroscopy Analysis.....	80
4.1.1 Room Temperature Impedance Spectroscopy Studies	80
4.1.1.1 Pure PVdF-HFP film and PVdF-HFP/EC/PC film	80
4.1.1.2 GPE system with LiCF_3SO_3 salt and NaCF_3SO_3 salt.....	83
4.1.2 Conductivity-Temperature Dependence Studies	88
4.2 Transport Number Studies	93
4.1.2 Ionic Transport Measurement	93
4.1.3 Cationic Transport Number Measurement, t_{Li^+} and t_{Na^+}	96

CHAPTER 5: THERMAL ANALYSIS	99
5.1 Differential Scanning Calorimetry (DSC) Analysis	100
5.1.1 Pure PVdF-HFP	100
5.1.2 PVdF-HFP/EC/PC.....	101
5.1.3 PVdF-HFP/ EC/ PC/ LiCF ₃ SO ₃ and PVdF-HFP/ EC/ PC/ NaCF ₃ SO ₃ systems.	102
5.2 Thermogravimetric Analysis (TGA)	108
5.2.1 Pure PVdF-HFP	108
5.2.2 PVdF-HFP/EC/PC.....	109
5.2.3 PVdF-HFP/ EC/ PC/ LiCF ₃ SO ₃ and PVdF-HFP/ EC/ PC/ NaCF ₃ SO ₃ systems.	110
CHAPTER 6: STRUCTURAL AND MORPHOLOGICAL ANALYSIS	113
6.1 Fourier Transform Infrared Spectroscopy (FTIR) analysis	113
6.1.1 Pure PVdF-HFP	113
6.1.2 PVdF-HFP/EC/PC.....	115
6.1.3 PVdF-HFP/EC/PC/ LiCF ₃ SO ₃ and PVdF-HFP/EC/PC/ NaCF ₃ SO ₃ systems	118
6.2 Raman Spectroscopy Analysis	127
6.2.1 Pure PVdF-HFP and PVdF-HFP/EC/PC film.....	128
6.2.2 PVdF-HFP/EC/PC/ LiCF ₃ SO ₃ and PVdF-HFP/EC/PC/ NaCF ₃ SO ₃ systems	129
6.3 X-Ray Diffraction Analysis	135
6.3.1 Pure PVdF-HFP and PVdF-HFP/EC/PC.....	135
6.3.2 LiCF ₃ SO ₃ and NaCF ₃ SO ₃ Salts.....	137
6.3.3 PVdF-HFP/EC/PC/ LiCF ₃ SO ₃ and PVdF-HFP/EC/PC/ NaCF ₃ SO ₃ systems	

6.4	Field Emission Scanning Electron Microscope Analysis.....	142
6.4.1	Pure PVdF-HFP and PVdF-HFP/EC/PC.....	142
6.4.2	PVdF-HFP/EC/PC/LiCF ₃ SO ₃	144
6.4.3	PVdF-HFP/EC/PC/NaCF ₃ SO ₃ System.....	146

CHAPTER 7: ELECTROCHEMICAL STUDIES..... 149

7.1	Linear Sweep Voltammetry.....	149
7.2	Cyclic Voltammetry.....	151

CHAPTER 8: CELL PERFORMANCES 155

8.1	Performances of Lithium Cell	155
8.2	Performances of Sodium Cell.....	158

CHAPTER 9: DISCUSSION, CONCLUSION AND SUGGESTIONS FOR FURTHER WORK 161

References.....	168
List of Publications and Papers Presented	178
Appendix A.....	179
Appendix B.....	180
.....	180

LIST OF FIGURES

Figure 1.1: Molecular structure of PVdF-HFP	1
Figure 1.2: The chemical structure of (a) lithium triflate and (b) sodium triflate.....	3
Figure 2.1: Basic structure of primary battery	6
Figure 2.2: Schematic representation of the working mechanism of a zinc-copper battery	7
Figure 2.3: Schematic of charge and discharge process for secondary battery	8
Figure 2.4: Examples of commercial (a) primary lithium-battery and (b) lithium-ion rechargeable batteries.....	12
Figure 2.5: Structure of Li-ion battery	14
Figure 2.6: This Ragone plot for the new cathode material (red circles) and other cathode materials for Na-ion batteries show that the new cathode has the highest energy density for a wide range of charge and discharge rates	15
Figure 2.7: Ions move in polymer chain	19
Figure 2.8: Conceptual structure of lithium polymer battery.....	19
Figure 2.9: Chemical structure of (a) lithium triflate and (b) sodium triflate	25
Figure 2.10: Chemical structure of (a) ethylene carbonate (EC) and (b) propylene carbonate (PC).....	27
Figure 2.11: Chemical structures of PVdF-HFP copolymer and PVdF homopolymer ..	30
Figure 2.12: Representation of cation motion in polymer electrolyte (a) assisted by polymer chain motion only; (b) taking account of ionic cluster contributions.....	33
Figure 3.1: The experimental flow chart for the sample preparation method and characterization of the GPE films	41
Figure 3.2: A.C. waveform for an applied potential and a resulting current.	43
Figure 3.3: Vector in terms of Angle (θ) and Magnitude ($ Z $) Inset figure: Vector in terms of x and y coordinates	44
Figure 3.4: Vector in Terms of Real (I') and Imaginary (I'') coordinates	45

Figure 3.5: Experimental setup for conductivity measurement.	48
Figure 3.6: A typical current versus time plot for DC polarization measurement.....	50
Figure 3.7: Schematic diagrams Differential Scanning Calorimeter	52
Figure 3.8: Typical DSC thermogram.....	54
Figure 3.9: Schematic principle of TGA measurement	55
Figure 3.10: Typical TGA curve.....	57
Figure 3.11: TGA -DTA Curve. Note the plateau of constant weight (region A), the mass loss portion (region B), and another plateau of constant mass (region C).....	58
Figure 3.12: A Schematic of a generic Michelson interferometer.....	59
Figure 3.13: The sample analysis process.....	61
Figure 3.14: The IR spectrum of pure PVdF-HFP, plotted as transmission (left) and absorbance (right).....	62
Figure 3.15: Diagram for the most important processes involved in light scattering by molecules.....	65
Figure 3.16: Schematic of typical Raman system.....	66
Figure 3.17: A typical Raman spectra.....	66
Figure 3.18: A schematic of an x-ray diffractometer.....	67
Figure 3.19: Constructive and destructive interferences.....	68
Figure 3.20: A simple schematic of the Young's double split experiment.....	69
Figure 3.21: Bragg's Law reflection.....	70
Figure 3.22: The schematic diagram of FESEM microscope	72
Figure 3.23: Schematic representation of the voltammetry experimental setup.....	74
Figure 3.24: Current-Voltage profile of electrolytes cell under LSV	75
Figure 3.25: Current-voltage in cyclic voltammetry	76
Figure 4.1: Cole-Cole plot for pure PVdF-HFP film	81
Figure 4.2: Cole-Cole plot for PVdF-HFP/EC/PC gel polymer electrolytes film	82

Figure 4.3: Cole-Cole plots for PVdF-HFP/EC/PC/LiCF ₃ SO ₃ gel polymer electrolytes film containing (a) 5 wt.% (b) 10 wt.% (c) 15 wt.% (d) 20 wt.% (e) 25 wt.% and (f) 30wt.% of LiCF ₃ SO ₃ salt	83
Figure 4.4: Variation of ionic conductivity with LiCF ₃ SO ₃ salt in the GPE films	85
Figure 4.5: Cole-Cole plots for PVdF-HFP/EC/PC/NaCF ₃ SO ₃ gel polymer electrolytes film containing (a) 5 wt.% (b) 10 wt.% (c) 15 wt.% (d) 20 wt.% (e) 25 wt.% and (f) 30wt.% of NaCF ₃ SO ₃ salt.	87
Figure 4.6: Variation of ionic conductivity with NaCF ₃ SO ₃ salt in the GPE films	87
Figure 4.7: Log σ versus 1000/T plot for the GPE film containing (a) 5 wt.% (b) 25 wt.% and (c) 30wt.% of LiCF ₃ SO ₃ salt	90
Figure 4.8: Log σ versus 1000/T plot for the GPE film containing (a) 5 wt.% (b) 20 wt.% and (c) 30wt.% of NaCF ₃ SO ₃ salt.....	90
Figure 4.9: Log $\sigma T^{1/2}$ versus 1000/ (T-T ₀) plots for the GPE films containing (a) 5wt.% (b) 25 wt.% and (c) 30 wt.% of LiCF ₃ SO ₃ salt.....	92
Figure 4.10: Log $\sigma T^{1/2}$ versus 1000/ (T-T ₀) plots for the GPE films containing (a) 5wt.% (b) 20 wt.% and (c) 30 wt.% of NaCF ₃ SO ₃ salt.....	93
Figure 4.11: Normalized current versus time plots for films in PVdF-HFP/ EC/ PC/ LiCF ₃ SO ₃ system.....	95
Figure 4.12: Normalized current versus time plots for films in PVdF-HFP/ EC/ PC/ NaCF ₃ SO ₃ system.....	95
Figure 4.13: Normalized current versus time plot for PVdF-HFP/EC/PC + 25wt.% LiCF ₃ SO ₃ film. Inset figure: Impedance plots of the cell before and after polarization.	97
Figure 4.14: Normalized current versus time plot for PVdF-HFP/ EC/PC + 20 wt.% NaCF ₃ SO ₃ film. Inset figure: Impedance plots of the cell before and after polarization.	97
Figure 5.1: DSC thermogram of pure PVdF-HFP film.....	100
Figure 5.2: DSC thermogram of pure PVdF-HFP/EC/PC film.	101
Figure 5.3: DSC thermogram of PVdF-HFP/EC/ PC/ 5 wt.% LiCF ₃ SO ₃ film.....	104
Figure 5.4: DSC thermogram of PVdF-HFP/ EC/ PC/25 wt.% LiCF ₃ SO ₃	104
Figure 5.5: DSC thermogram of PVdF-HFP/EC/PC/ 30 wt.% LiCF ₃ SO ₃	105
Figure 5.6: DSC thermogram of PVdF-HFP/ EC/ PC/5 wt.% NaCF ₃ SO ₃	105

Figure 5.7: DSC thermogram of PVdF-HFP/EC/PC/20 wt.% NaCF ₃ SO ₃	106
Figure 5.8: DSC thermogram of PVdF-HFP/ EC/ PC/ 30 wt.% NaCF ₃ SO ₃	106
Figure 5.9: Melting temperature of (a) GPE + LiCF ₃ SO ₃ system and (b) GPE + NaCF ₃ SO ₃ system	107
Figure 5.10: TGA thermograms of pure PVdF-HFP film.....	108
Figure 5.11: TGA thermograms of PVdF-HFP/EC/PC film.....	109
Figure 5.12: TGA plot for the films containing 5 wt.%, 25 wt.% and 30 wt.% of LiCF ₃ SO ₃	110
Figure 5.13: TGA plot for the films containing 5 wt.%, 20 wt.% and 30 wt.% of NaCF ₃ SO ₃	111
Figure 6.1: FTIR spectra of pure PVdF-HFP film in the region 650 cm ⁻¹ and 3150 cm ⁻¹	113
Figure 6.2: FTIR spectra of (a) pure PC and (b) pure EC in the range of 650 cm ⁻¹ and 2250 cm ⁻¹	116
Figure 6.3: FTIR spectra of pure PVdF-HFP film and PVdF-HFP/EC/PC film.	116
Figure 6.4: FTIR spectrum of LiCF ₃ SO ₃ salt.....	118
Figure 6.5: FTIR spectrum of NaCF ₃ SO ₃ salt.....	119
Figure 6.6: FTIR spectra of pure PVdF-HFP, PVdF-HFP/EC/PC and GPE films with different amount of LiCF ₃ SO ₃ salt contents.	122
Figure 6.7: FTIR spectra of pure PVdF-HFP, PVdF-HFP/EC/PC and GPE films with different amount of NaCF ₃ SO ₃ salt contents.	122
Figure 6.8: Deconvolution of FTIR spectra between 1000-1100 cm ⁻¹ for GPE films containing (a) 5 wt.% (b) 10 wt.% (c) 15 wt.% (d) 20 wt.% (e) 25 wt.% and (f) 30wt.% of LiCF ₃ SO ₃ salt in the region (I) free triflate ions (II) ion pairs (III) ion aggregates (IV) ring breathing of the plasticizing solvent	124
Figure 6.9: Deconvolution of FTIR spectra between 1000-1100 cm ⁻¹ for GPE films containing (a) 5 wt.% (b) 10 wt.% (c) 15 wt.% (d) 20 wt.% (e) 25 wt.% and (f) 30wt.% of NaCF ₃ SO ₃ salt in the region (I) free triflate ions (II) ion pairs (III) ion aggregates (IV) ring breathing of the plasticizing solvent	125
Figure 6.10: The plots of area under assigned decomposed of free ions band with conductivity versus the concentration of (a) LiCF ₃ SO ₃ (b) NaCF ₃ SO ₃ salt.....	126

Figure 6.11: The plots of area under assigned decomposed of ion pair band with conductivity versus the concentration of (a) LiCF_3SO_3 (b) NaCF_3SO_3 salt.....	126
Figure 6.12: The plots of area under assigned decomposed of ion aggregate band with conductivity versus the concentration of (a) LiCF_3SO_3 (b) NaCF_3SO_3 salt.....	127
Figure 6.13: Raman Spectra of pure PVdF-HFP	128
Figure 6.14: Raman spectra of PVdF-HFP/EC/PC film	128
Figure 6.15: Raman spectrum of pure PVdF-HFP, PVdF-HFP/EC/PC and PVdF-HFP/EC/PC/ LiCF_3SO_3 GPE with different salt compositions in the range of 600-1000 cm^{-1}	131
Figure 6.16: Raman spectrum of pure PVdF-HFP, PVdF-HFP/EC/PC and PVdF-HFP/EC/PC/ NaCF_3SO_3 GPE with different salt compositions in the range of 600-1000 cm^{-1}	132
Figure 6.17: Raman spectrum of pure PVdF-HFP, PVdF-HFP/EC/PC and PVdF-HFP/EC/PC/ LiCF_3SO_3 GPE with different salt compositions in the range of 1000 - 1300 cm^{-1}	133
Figure 6.18: Raman spectrum of pure PVdF-HFP, PVDF-HFP/EC/PC and PVDFHFP/EC/PC/ NaCF_3SO_3 GPE with different salt compositions in the range of 1000-1300 cm^{-1}	134
Figure 6.19: X-ray diffractogram of pure PVdF-HFP film.....	136
Figure 6.20: X-ray diffractogram of PVdF-HFP/EC/PC film.....	136
Figure 6.21: X-ray diffractogram of LiCF_3SO_3 salt.	137
Figure 6.22: X-ray diffractogram of NaCF_3SO_3 salt.....	138
Figure 6.23: X-ray diffractogram of the GPE films in the PVdF-HFP/EC/PC/ LiCF_3SO_3 system.....	140
Figure 6.24: X-ray diffractogram of the GPE films in the PVdF-HFP/EC/PC/ NaCF_3SO_3 system.....	141
Figure 6.25: (a) Micrograph of pure PVdF-HFP film with the magnification factor of 3000X (b) Micrograph of pure PVdF-HFP film with the magnification factor of 12000X	143
Figure 6.26: (a) Micrograph of PVdF-HFP/EC/PC film with the magnification factor of 3000X. (b) Micrograph of PVdF-HFP/EC/PC film with the magnification factor of 12000X.....	143

Figure 6.27: (a) Micrograph of PVdF-HFP/EC/PC/5wt.% of LiCF_3SO_3 film with the magnification factor of 3000X. (b) Micrograph of the film with the magnification factor of 12000X	144
Figure 6.28: (a) Micrograph of PVdF-HFP/EC/PC/25wt.% of LiCF_3SO_3 film with the magnification factor of 3000X. (b) Micrograph of the film with the magnification factor of 12000X	145
Figure 6.29: (a) Micrograph of PVdF-HFP/EC/PC/30wt.% of LiCF_3SO_3 film with the magnification factor of 3000X. (b) Micrograph of the film with the magnification factor of 12000X	145
Figure 6.30: (a) Micrograph of PVdF-HFP/EC/PC/5 wt.% of NaCF_3SO_3 film with the magnification factor of 3000X. (b) Micrograph of the film with the magnification factor of 12000X	147
Figure 6.31: (a) Micrograph of PVdF-HFP/EC/PC/20 wt.% of NaCF_3SO_3 film with the magnification factor of 3000X. (b) Micrograph of the film with the magnification factor of 12000X	147
Figure 6.32: (a) Micrograph of PVdF-HFP/EC/PC/30 wt.% of NaCF_3SO_3 film with the magnification factor of 3000X. (b) Micrograph of the film with the magnification factor of 12000X	148
Figure 7.1: Linear sweep voltammogram of SS GPE Li cell for GPE containing 25 wt.% of LiCF_3SO_3 salt at scan rate of 5 mV s^{-1}	150
Figure 7.2: Linear sweep voltammogram of SS GPE Na cell for GPE containing 20 wt.% of NaCF_3SO_3 salt at scan rate of 5 mV s^{-1}	151
Figure 7.3: Cyclic voltammogram of cell-I: SS GPE-Li SS with 25 wt.% of LiCF_3SO_3 salt at scan rate of 5 mV s^{-1}	153
Figure 7.4: Cyclic voltammogram of cell-II: SS GPE-Na SS with 20 wt.% of NaCF_3SO_3 salt at scan rate of 5 mV s^{-1}	153
Figure 7.5: Cyclic voltammogram of cell-III: Li GPE Li with 25 wt.% of LiCF_3SO_3 salt at scan rate of 5 mVs^{-1}	154
Figure 7.6: Cyclic voltammogram of cell-IV: Na GPE Na with 20 wt.% of NaCF_3SO_3 salt at scan rate of 5 mVs^{-1}	154
Figure 8.1: Variation of voltage of LiNiCoO_2 GPE Li cell during discharge with a current of 0.05 mA.	157
Figure 8.2: Discharge capacities of LiNiCoO_2 GPE Li cell as a function of cycle number.....	157

Figure 8.3: Variation of voltage of MnO₂ | GPE | Na cell during discharge with a current of 0.5 mA. 159

Figure 8.4: Discharge capacities of MnO₂ | GPE | Na cell as a function of cycle number. 160

University of Malaya

LIST OF TABLES

Table 2.1: Commercial primary battery systems	10
Table 2.2: Commercial secondary battery systems	11
Table 2.3: Physical properties of some organic solvents	28
Table 3.1: Amounts of PVdF-HFP, plasticizers and salts in each group of gel.....	38
Table 3.2: Example of equivalent circuits and the impedance plots in A.C impedance measurements.....	47
Table 4.1: The compositions, the bulk resistance, R_b and the conductivity, σ of films in the PVdF-HFP/EC/PC/LiCF ₃ SO ₃ system	84
Table 4.2: The compositions, the bulk resistance, R_b and the conductivity, σ of films in the PVdF-HFP/ EC/PC/NaCF ₃ SO ₃ system	88
Table 4.3: VTF parameters for the GPE films from LiCF ₃ SO ₃ system and NaCF ₃ SO ₃ system.....	92
Table 4.4: Ionic transport number for the GPE film in PVdF-HFP/ EC/ PC/ LiCF ₃ SO ₃ and PVdF-HFP/ EC/PC/NaCF ₃ SO ₃ systems.....	94
Table 4.5: Transport number data and conductivity values for the GPE films in PVdF-HFP/ EC/PC/ LiCF ₃ SO ₃ and PVdF-HFP/EC/PC/NaCF ₃ SO ₃ systems.....	96
Table 5.1: Thermal and conductivity data for the GPE films.	103
Table 5.2: Decomposition temperatures and weight loss percentages of GPE films obtained from the TGA thermograms	112
Table 6.1: The vibrational modes and wavenumbers of pure PVdF-HFP	114
Table 6.2: The vibrational modes and wavenumbers of pure EC and pure PC.	117
Table 6.3: The vibrational modes and wavenumbers of LiCF ₃ SO ₃ salt.....	120
Table 6.4: The vibrational modes and wavenumbers of NaCF ₃ SO ₃ salt.....	120
Table 9.1: The compositions, and the conductivity, σ of films in the GPE films	161
Table 9.2: VTF parameters for the GPE films from LiCF ₃ SO ₃ system and NaCF ₃ SO ₃ system.....	164

Table 9.3: Ionic and cation transport number values for the GPE films in PVdF-HFP/
EC/PC/ LiCF₃SO₃ and PVdF-HFP/EC/PC/NaCF₃SO₃ systems 165

University of Malaya

LIST OF SYMBOLS AND ABBREVIATIONS

BTL	:	γ -Butyrolactone
E_a	:	Activation energy
AC	:	Alternating current
$\text{NH}_4\text{CF}_3\text{SO}_3$:	Ammonium triflate,
i_{pa}	:	Anodic peak current
E_{pa}	:	Anodic peak potential
AsF_6	:	Arsenic Fluoride
T_b	:	Boiling temperature
k	:	Boltzmann constant
R_b	:	Bulk resistance
Cd	:	Cadmium
C = O	:	Carbonyl
i_{pc}	:	Cathodic peak current
E_{pc}	:	Cathodic peak potential
t_+	:	Cationic transference number
σ	:	Conductivity
CuCNS	:	Copper (1) thiocyanate
CuCF_3SO_3	:	Copper triflate
T_c	:	Crystallization temperature
CV	:	Cyclic voltammetry
ϵ	:	Dielectric constant
DEC	:	Diethyl carbonate
DSC	:	Differential Scanning Calorimetry
DMC	:	Dimethyl carbonate

DMC	:	Dimethyl carbonate
DMSO	:	Dimethyl sulfoxide
DMF	:	Dimethylformamide
DC	:	Direct Current
DC	:	Direct Current
EIS	:	Electrochemical impedance spectroscopy
t_e	:	Electronic transference number
EMC	:	Ethyl methyl carbonate
EC	:	Ethylene carbonate
FESEM	:	Field Emission Scanning Electron Microscopy
FTIR	:	Fourier Transform Infrared Spectroscopy
ω	:	Frequency in radians per second
GPEs	:	Gel Polymer Electrolytes
T_g	:	Glass transitions temperature
t_i	:	Ionic transference number
LSV	:	Linear Sweep Voltammery
LiBr	:	Lithium Bromide
LiCl	:	Lithium Chloride
LiCoO ₂	:	Lithium cobalt oxides
LiPF ₆	:	Lithium hexafluorophosphate
LiI	:	Lithium Iodide
LiFePO ₄	:	Lithium iron phosphate
LiMn ₂ O ₄	:	Lithium manganese oxides
LiNiCoO ₂	:	Lithium Nickel Cobalt Oxide
LiClO ₄	:	Lithium perchlorate
Li ₂ SO ₄	:	Lithium sulfate

LiBF ₄	:	Lithium tetrafluoroborate
LiTPSB	:	Lithium tetrakis borate
LiCF ₃ SO ₃	:	Lithium trifluorosulfonate / triflate
MnO ₂	:	Manganese dioxides
T _m	:	Melting temperature
Hg	:	Mercury
μ	:	Mobility
OCV	:	Open circuit voltage
θ	:	Phase shift
Pb	:	Plumbum
PVdF	:	Poly (vynillidene flouride)
PAN	:	Poly(acrylonitrile)
PEMA	:	Poly(ethyl methacrylate)
PMMA	:	Poly(methyl methacrylate)
PPO	:	Poly(propylene oxide)
PVC	:	Poly(vinyl chloride)
PAN	:	Polyacrylonitrile
PEO	:	Polyethylene oxide
PMMA	:	Polymethyl methacrylate
PVdF	:	Polyvinylidene fluoride
PC	:	Propylene carbonate
R ²	:	Regression value
SiO ₂	:	Silicon dioxide / silica
NaPF ₆	:	Sodium hexafluorophosphate
NaClO ₄	:	Sodium perchlorate
NaCF ₃ SO ₃	:	Sodium trifluorosulfonate / triflate

SEI	:	Solid electrode/electrolyte interface
SPEs	:	Solid Polymer Electrolytes
THF	:	Tetrahydrofuran
TGA	:	Thermogravimetric Analysis
TiO ₂	:	Titanium dioxide
VTF	:	Vogel-Tamman-Fulcher
λ	:	Wavelength
XRD	:	X-ray Diffraction
ZnSO ₄	:	Zinc sulfate

University of Malaya

CHAPTER 1: INTRODUCTION

1.1 Background of the Present Work

In this research work, poly (vinylidene fluoride-co-hexafluoropropylene) (PVdF-HFP) based gel polymer electrolyte films were prepared and studied. Lithium triflate (LiCF_3SO_3) and sodium triflate (NaCF_3SO_3) salts serve as dopants and ethylene carbonate (EC) and propylene carbonate (PC) have been used as plasticizing agents.

(PVdF-HFP) was used as a host polymer and provides a medium for the ions conduction. PVdF-HFP is a copolymer with formula $-(\text{C}_2\text{H}_2\text{F}_2)_m-(\text{C}_3\text{F}_6)_n-$. Figure 1 shows the molecular structure of PVdF-HFP. Every polymer has functional group that can chemically react or bond with the salt. The functional group of the PVdF-HFP copolymer is fluorinated groups, $-(\text{C}-\text{F})-$. The fluorine atom from this group is expected to coordinate bond with the lithium and sodium ions from the doping salts.

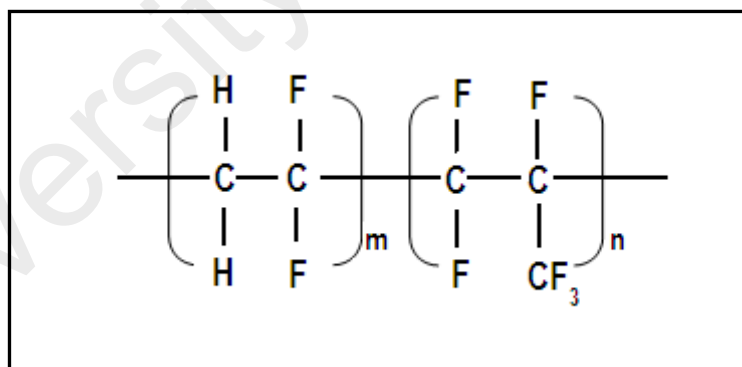


Figure 1.1: Molecular structure of PVdF-HFP

In this work, the effect of adding two triflate based salts with different cations i.e lithium and sodium on the properties of PVdF-HFP polymer electrolytes was investigated. Although most of the interest in polymer electrolytes studies is focused on lithium ion-conducting systems, the sodium ion-conducting systems have also been the

subject of much attention for many researchers. One of the earliest studies of polymer electrolytes containing sodium triflate was reported by Schantz (Schantz, Sandahl, Börjesson, Torell, & Stevens, 1988), where sodium triflate salt has been dissolved in polyether.

The chemical structures of lithium triflate and sodium triflate are shown in Figure 2(a) and 2(b), respectively. Lithium and sodium have similar chemical properties because they are in the same group in the periodic table. However, sodium is more reactive than lithium. This is because the outermost shell electron in sodium is much further than the one in lithium. The attraction between the electron and the sodium nucleus would be weaker and sodium readily and easily loses its electron to the surrounding and becomes a positive ion. This is one of the most important criteria of inorganic salts. The same properties are expected in the triflate salt and sodium is expected to dissociate easily from the triflate anion. Triflate anion is larger than other anions such as tetrafluoroborate (BF_4^-) and perchlorate (ClO_4^-). The lattice energy of the salt with larger anion is lower and it is expected to promote greater dissociation of the salt, thereby providing higher conductivity of ions. In the present study, the anion of both salts is the same i.e. triflate. Therefore, the effects of different cations on the conductivity, morphological, structural and thermal properties of PVdF-HFP – based gel polymer electrolytes system can be investigated. The highest conducting sample from Li-system and Na-system will be used as electrolyte in rechargeable batteries.

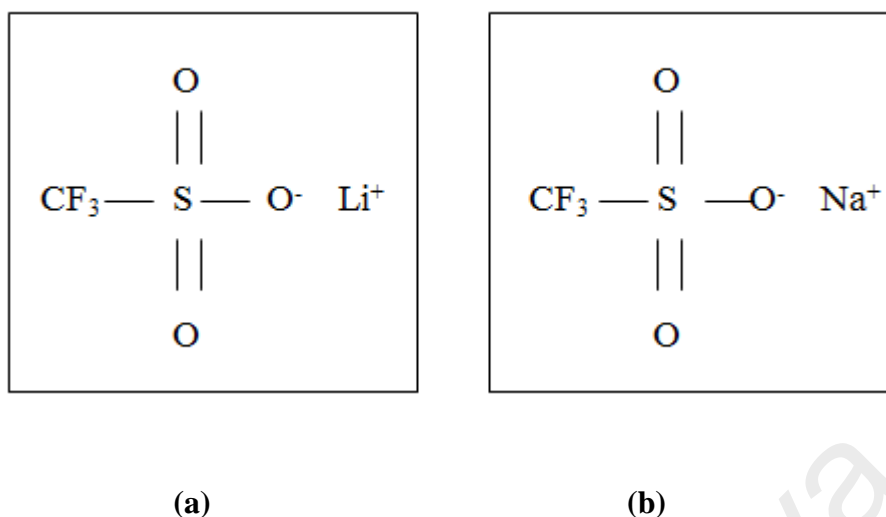


Figure 1.2: The chemical structure of (a) lithium triflate and (b) sodium triflate

1.2 Objectives of the Present Work

The objectives of this study are:

- 1) To prepare and characterize two systems of gel polymer electrolyte (GPE) films based on PVdF-HFP as a polymer host i.e. PVdF-HFP/EC/PC/ LiCF₃SO₃ and PVdF-HFP/EC/PC/ NaCF₃SO₃;
- 2) To investigate the effect of different salts (i.e Li CF₃SO₃ and NaCF₃SO₃) contents on their electrical , structural, thermal and electrochemical properties;
- 3) To determine the performance of electrochemical cells using the gel polymer electrolyte film that exhibited the highest conductivity as an electrolyte from both systems.

1.3 Organization of the Thesis

This thesis has been discussed in nine chapters. The first chapter provides the background and objectives of the study.

Chapter two is a brief idea of battery system and overview of polymer electrolytes including the conceptual, theoretical and materials aspects of the polymer electrolytes. This chapter also summarized an overview of the past works done on polymer electrolytes. It also present some discuss about ion conduction mechanism in gel polymer electrolytes system.

Chapter three outlines the experiments carried out to prepare the samples and the techniques used to characterize the GPE samples. The flow charts of sample preparation are provided to have a better understanding. The characterizations of the samples are done by using various techniques include impedance spectroscopy, transference number, Fourier Transform Infrared (FTIR), X-Ray Diffraction (XRD), RAMAN spectroscopy, Field Emission Scanning Electron Microscopy (FESEM), Thermogravimetric analysis (TGA) , Differential Scanning Calorimetry (DSC), Linear Sweep Voltammetry (LSV) and Cyclic Voltammetry (CV).

Chapter four to chapter eight present the analysis and discussion of the results from all experiments. The results of electrical conductivity studies of the PVdF-HFP-based polymer electrolytes films at various temperatures using impedance spectroscopy and the effect of different sizes of cations (Li^+ and Na^+) in enhancing the electrical conductivity of PVdF-HFP film will be presented in chapter four. This chapter also presents the result from transference number measurements. The results of thermal studies using DSC and TGA will be discussed in chapter five. Chapter six gives detail studies on the structural and morphological studies carried out using FTIR, Raman,

XRD and FESEM. The relationship between molecular structure and electrical performance are also described in this chapter. Chapter seven presents the electrochemical studies performed using LSV and CV. The results of battery performance have been discussed in chapter eight. Finally, chapter nine concludes the thesis with some suggestions for further work.

University of Malaya

CHAPTER 2: LITERATURE REVIEW

2.1 Electrolytes and Batteries

Electrolytes are solutions that containing free ions that make the solutions electrically conductive, which electricity is passed and causes ion to move towards cathode and anode respectively thus conducting current. Therefore, the solution of electrolytes is always required in batteries, even in dry cell.

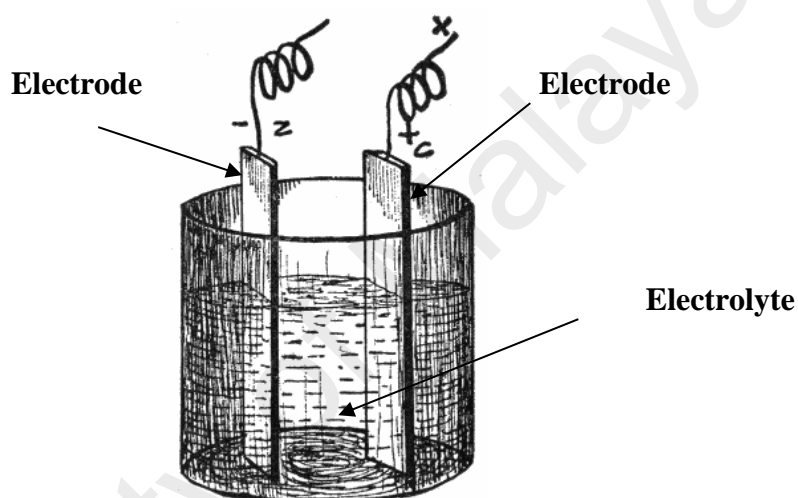


Figure 2.1: Basic structure of primary battery

(“Battery_diagram,” 2013)

Batteries are devices that transform chemical energy stored in a material into electricity. The simplest battery consists of two electrodes. It is very simple and convenient way to make the electricity portable. Figure 2.1 shows the conventional battery with three basic components i.e the anode, cathode and electrolyte solution. Inside the battery, the chemical reaction produces electrons. Batteries use this chemical reaction to do work on charge and produce a voltage between their output terminals. The basic element is called an electrochemical cell and makes use of an oxidation/reduction reaction. In order to understand how the battery works in general

the standard zinc-copper battery can be used. The schematic for zinc-copper battery is shown in Figure 2.2.

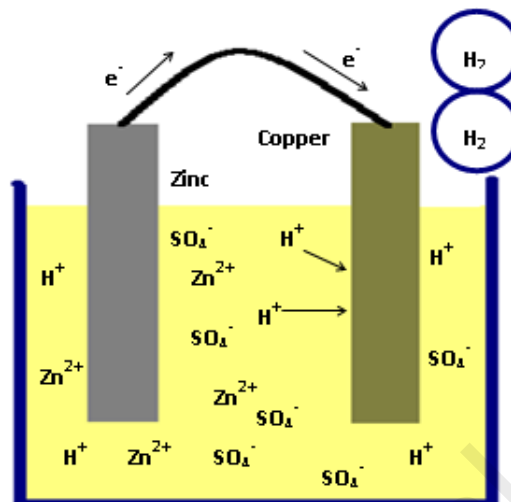


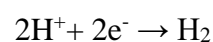
Figure 2.2: Schematic representation of the working mechanism of a zinc-copper battery

The working mechanisms of this battery system are as follow:

- The acid molecules break up into three ions: two H^+ ions and one SO_4^- ion.
- The zinc atoms on the surface of the zinc rod lose two electrons ($2e^-$) to become Zn^{2+} ions. This reaction is called oxidation



- The Zn^{2+} ions combine with the SO_4^- ion to create $ZnSO_4$, which dissolves in the acid.
- The electrons flow through the wire and combine with hydrogen on the copper rod, so hydrogen gas begins bubbling off the copper rod. This reaction is called reduction



There are two types of batteries i.e. primary (disposable) and secondary (rechargeable), both of which convert chemical energy to electrical energy. Primary batteries can only be used once because they use up their chemicals in an irreversible reaction. Secondary battery is a system that is capable of repeated use. It can be recharged because the chemical reactions they use are reversible; they are recharged by running a charging current through the battery, but in the opposite direction of the discharge current. The chemical reactions that occur in secondary batteries are reversible because the components that react are not completely used up. Rechargeable batteries need an external electrical source to recharge them after they have expended their energy, which reverses the chemical reactions that occur during discharge/use.

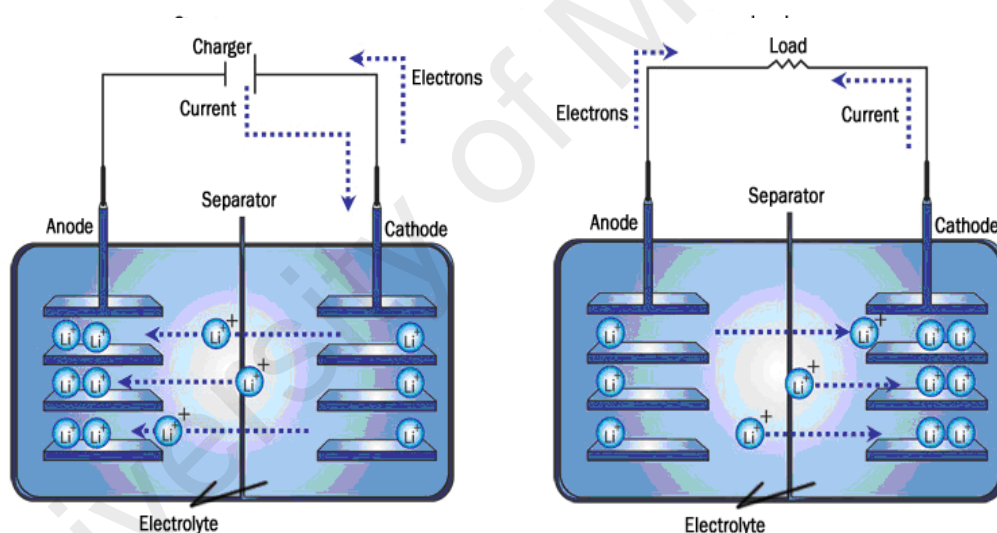


Figure 2.3: Schematic of charge and discharge process for secondary battery

(“Charge/discharge_process,” 2013)

Figure 2.3 shows the schematic of charge and discharge process for rechargeable battery. During the charge reaction, lithium ions in the positive electrode are ionized and moves to the negative electrode through the electrolyte. During the discharge, the

lithium ions return to the positive electrode, reverting to its original phase. This simple migration of lithium ions gives the battery a long shelf life and a long cycle life.

To date there are a few batteries in the market that use a variety of chemicals to power their reaction such as

- 1) **Zinc-carbon battery:** Also known as a standard carbon battery, zinc-carbon chemistry is used in all inexpensive AA, C and D dry-cell batteries. The electrodes are zinc and carbon, with an acidic paste between them that serves as the electrolyte.
- 2) **Alkaline battery:** Used in common Duracell and Energizer batteries, the electrodes are zinc and manganese-oxide, with an alkaline electrolyte.
- 3) **Lithium photo battery:** Lithium, lithium-iodide and lead-iodide are used in cameras because of their ability to supply power surges.
- 4) **Lead-acid battery:** Used in automobiles, the electrodes are made of lead and lead-oxide with a strong acidic electrolyte (rechargeable).
- 5) **Nickel-cadmium battery:** The electrodes are nickel-hydroxide and cadmium, with potassium hydroxide as the electrolyte (rechargeable).
- 6) **Nickel-metal hydride battery:** This battery is rapidly replacing nickel-cadmium because it does not suffer from the memory effect that nickel-cadmiums do (rechargeable).
- 7) **Lithium-ion battery:** With a very good power-to-weight ratio, this is often found in high-end laptop computers and cell phones (rechargeable).
- 8) **Zinc-air battery:** This battery is lightweight and rechargeable.
- 9) **Zinc-mercury oxide battery:** This is often used in hearing-aids.
- 10) **Silver-zinc battery:** This is used in aeronautical applications because the power-to-weight ratio is good.

11) **Metal-chloride battery:** This is used in electric vehicles.

Some primary battery and secondary battery systems and their properties are listed in Table 2.1 and Table 2.2.

Table 2.1: Commercial primary battery systems

(Salkind, 1987)

Common Name	Cell Reaction	Nominal Voltage	Comments
Leclanche dry cell	$Zn + MnO_2 + 2 NH_4Cl = Zn(NH_3)_2Cl_2 + H_2 + Mn_2O_3$	1.5	Low cost, wide range of sizes
Zinc Chloride	$4Zn + 8MnO_2 + ZnCl_2 + 9H_2O = 8MnOOH + ZnCl_2 + 4ZnO + 5H_2O$	1.5	Intermediate cost and performance
Alkaline-Manganese	$2Zn + 3MnO_2 = 2ZnO + Mn_3O_4$	1.5	Sets standard for cylindrical cells
Silver-Zinc	$Zn + Ag_2O = 2Ag + ZnO$	1.6	Higher voltage than Zn/HgO or Zn/Air
Mercury-Zinc	$Zn + HgO = Hg + ZnO$	1.35	Sets standard for button cells
Air-depolarized	$2Zn + O_2 (Air) = 2ZnO$	1.4	Twice capacity of mercury, limited active stand
Li/CuO	$2Li + CuO = Li_2O + Cu$	1.5	Potential replacement for Leclanche and Zinc Chloride
Li/FeS	$2Li + FeS = Li_2S + Fe$	1.6	Replacement for Zn/HgO and Zn/Ag ₂ O No mercury
Li/SO ₂	$2Li + 2SO_2 = Li_2S_2O_4$	2.8	Military battery Low temperature Excellent storage
Li/SOCl ₂	$4Li + 2SOCl_2 = 4LiCl + S + SO_2$	3.6	High voltage High energy density

Li/CF _x	$x\text{Li} + \text{CF}_x = x\text{LiF} + \text{C}$	2.7	High voltage Long shelf life Wide operating temperature
Li/MnO ₂	$\text{Li} + \text{MnO}_2 = \text{LiMnO}_2$	2.8	High voltage Long shelf life Wide operating temperature
Li/I ₂	$2\text{Li} + \text{I}_2 = 2\text{LiI}$	2.8	Heart pacemaker

Table 2.2: Commercial secondary battery systems
(Salkind & Falk, 1969)

Common Name	Cell Reaction	Nominal Voltage	Comments
Lead acid	$\text{Pb} + \text{PbO}_2 + 2 \text{H}_2\text{SO}_4 = 2\text{PbSO}_4 + 2\text{H}_2\text{O}$	2.10	Lowest cost Largest sales Available sealed
Nickel-Cadmium	$2\text{NiOOH} + \text{Cd} + 2\text{H}_2\text{O} = 2\text{Ni(OH)}_2 + \text{Cd(OH)}_2$	1.3	High rate Available sealed
Nickel-Iron	$2\text{NiOOH} + \text{Fe} + 2\text{H}_2\text{O} = 2\text{Ni(OH)}_2 + \text{Fe(OH)}_2$	1.37	Limited production Long cycle life Old technology
Nickel-Hydrogen	$\text{H}_2 + 2\text{NiOOH} = 2\text{Ni(OH)}_2$	1.35	Special space battery Long cycle life High self-discharge
Silver-Zinc	$\text{Zn} + \text{AgO} + \text{H}_2\text{O} = \text{Zn(OH)}_2 + \text{Ag}_2\text{O}$	1.86	Two step discharge Limited cycle life High energy density
Lithium-MoS ₂	$\text{Li} + \text{MoS}_2 = \text{LiMoS}_2$	2.3	Developed, commercialized and withdrawn

2.1.1 Development of Lithium Ion Rechargeable Battery

Technologies of lithium ion rechargeable batteries (LIB) were pioneered by Sony Corporation. Since the introduction of LIB on the market first in the world in June 1991 (Nagaura & Tozawa, 1990) the LIB has been employed in most of today's high-performance portable electronic devices as diverse as cellular phones, video cameras, notebook computers, portable minidisk players and others. The cells used layered oxide chemistry, specifically lithium cobalt oxide. Although lower in energy density, lithium ion batteries are inherently safer than lithium-metal cells. There are several important differences between Lithium batteries and Lithium-ion batteries. Lithium batteries are not rechargeable but Li-ion batteries are rechargeable. From chemical standpoint lithium batteries use lithium in its pure metallic form while Li-ion batteries use lithium compounds that are much more stable than the elemental lithium used in lithium batteries. Figures 2.4 shows the examples of commercial primary lithium-battery and lithium-ion rechargeable batteries.



(a)



(b)

Figure 2.4: Examples of commercial (a) primary lithium-battery and (b) lithium-ion rechargeable batteries

In many battery systems, the lithium ion secondary batteries have following advantages compared to other batteries system:

- 1) High energy density: generally 110-120 Wh/kg, three of four times of nickel-cadmium batteries
- 2) High working voltage: average 3.6 V, to be equal to three nickel-cadmium or nickel-metal hydride batteries in series connection
- 3) High rate of discharging and charging ability
- 4) Long life and no environmental pollution: no poisonous materials such as Cd, Pb and Hg

Besides the wide use for portable devices such as cell phones, digital cameras, laptops, etc., lithium-ion batteries also used as power sources for implantable medical devices, professional power tools, robots, Light Electric Vehicles, UPS systems, various military applications, and they can substitute conventional nickel systems in order to minimize the mass and volume of the power subsystems in aerospace applications. Moreover, for thermodynamic and kinetic reasons, lithium-ion battery is a promising candidate for automotive applications that require battery technologies with improved energy and power density as well as an extended cycle life.

Despite its overall advantages, lithium-ion technology also has some drawbacks. It is fragile and should have a protection circuit to maintain safe operation. They require protection from being over charged and discharged too far, so that they need to have the current maintained within safe limits. A major disadvantage of the lithium ion battery is their cost because it is more expensive than similar capacity NiMH or NiCd batteries. They are much more complex to manufacture in order to protect the battery from damage due to overcharging or undercharging. In fact, the batteries need the most expensive materials such as specialized carbon for the anode, electrolyte solvents, electrolyte salts, cathode materials and separator. Liquid electrolyte for lithium-ion cells

also requires highly purified electrolyte solvents. Figure 2.5 shows the internal structure of lithium ion battery.

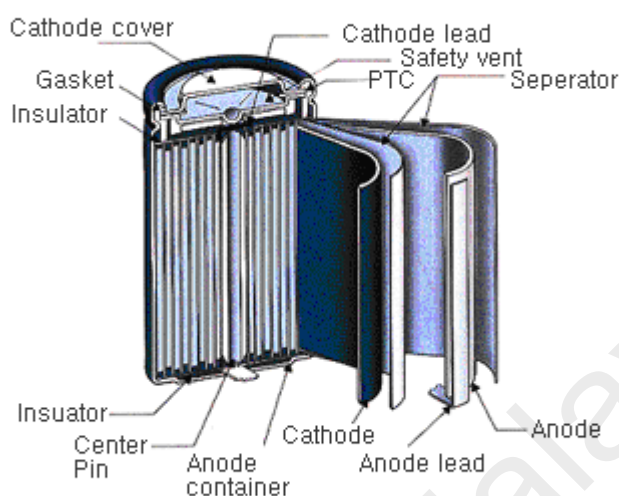


Figure 2.5: Structure of Li-ion battery

(Battery_structure, 2014)

2.1.2 Development of Sodium Ion Rechargeable Battery

Sodium-ion batteries have a potential to be a cheaper alternative for lithium-ion batteries. Although Li-ion batteries' high energy densities enable them to store a large amount of energy in a small space, the disadvantages of these batteries are their high cost and low stability. Sodium is similar to lithium in terms of its chemical properties, but approximately 1,000 times more abundant in the ground (26,000 ppm) and in the form of salt (NaCl) in normal seawater (15,000 ppm). This makes sodium-based batteries potentially more environmentally friendly and easier to recycle, as well as up to five times less expensive compared to lithium-based batteries.

In a new study, Young-Uk Park, et al. (Park et al., 2013), from Seoul National University and KAIST, Korea have designed a new cathode for sodium-ion batteries

that provides an energy density of 600 Wh kg^{-1} , which is the highest reported so far for sodium-ion batteries and even rivals the energy densities of some lithium-ion batteries. The new cathode material also has a greatly improved cycle life, bringing sodium-ion batteries a step closer to realization as part of a large-scale energy storage system. They reported that the material shows high cycling stability with 95% capacity retention for 100 cycles and 84% for 500 cycles, which the team attributes to the small volume change (2.9%) upon cycling - the smallest volume change among known Na intercalation cathodes.

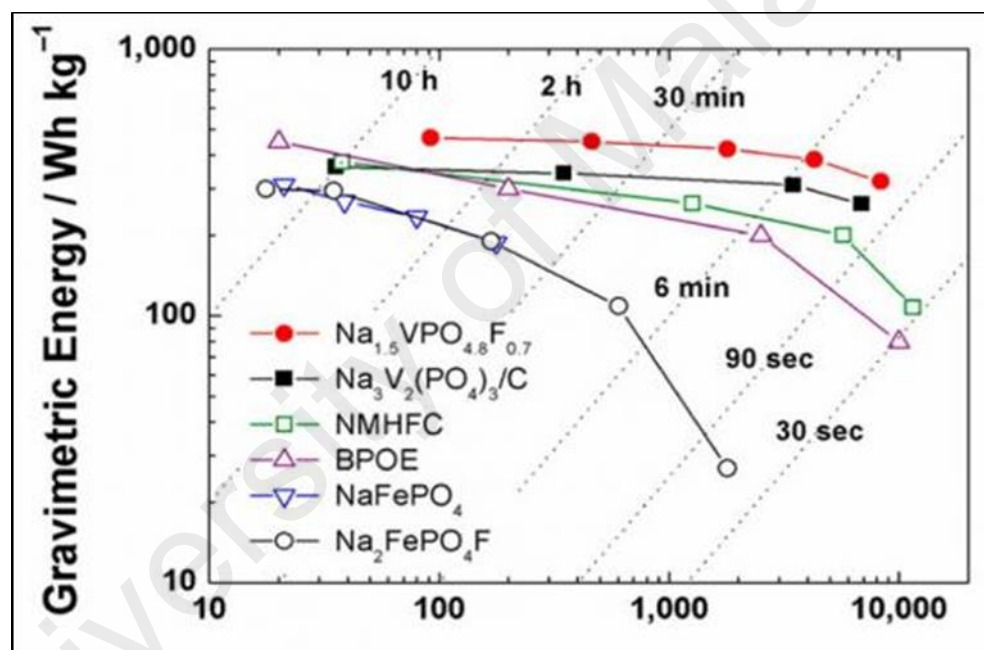


Figure 2.6: This Ragone plot for the new cathode material (red circles) and other cathode materials for Na-ion batteries show that the new cathode has the highest energy density for a wide range of charge and discharge rates

(Park et al., 2013).

2.2 Polymer Electrolytes in Lithium-Polymer Batteries

Lithium-polymer battery is a battery technology that similar to lithium-ion battery. It performs the same task with lithium-ion battery, but can be shaped in a small space. The

Li-polymer battery differentiates itself from other battery systems in the type of electrolyte used.

For the purpose of batteries or other reliable all-solid-state electrochemical device applications, the polymer electrolyte materials should inherently possess the following properties (Alamgir & Abraham, 1994; Gray, 1991; Song, Wang, & Wan, 1999)

- **Ionic conductivity, $\sigma \geq 10^{-4} \text{ S cm}^{-1}$ at room temperature:** This enables us to achieve a performance level close to that of the liquid electrolyte-based devices.
- **Ionic transference number $t_{ion} \sim 1$:** This is not only absolutely desirable but the polymer electrolyte should preferably be a single-ion (namely, cation) conducting system. For battery applications, the polymer electrolyte should perfectly act as an ion conducting medium and as an electronic separator. However, the majority of the polymer electrolytes reported so far, although exhibiting negligible electronic conduction, show the cationic transference number ~ 0.5 . This is indicative of the fact that at the maximum only half of the potential transporting ions move in the polymer electrolytes (Bruce, Hardgrave, & Vincent, 1992; Doyle & Newman, 1995; Evans, Vincent, & Bruce, 1987). Obviously, the larger the cationic transference number (close to unity), the smaller would be the concentration polarization effect in the electrolytes during charge–discharge steps, and hence, the higher would be the power density achievable in the battery (Song et al., 1999).
- **High chemical, thermal and electrochemical stabilities:** The solid-state electrochemical devices are fabricated by sandwiching the polymer electrolyte membranes between appropriate cathode and anode materials. In order to avoid undesired chemical reactions proceeding at the

electrode/electrolyte interfaces, the polymer electrolytes should possess a high chemical stability. Furthermore, to have a wider temperature range during battery operations, polymer electrolytes should be thermally stable. They should also have a good electrochemical stability domain extending from 0 V to as high as 4–5V.

- **High mechanical strength:** The polymer electrolytes should be mechanically stable, so that the scaling up and large-scale manufacturing of the devices could be realized
- **Compatibility with the electrode materials:** Finally, the polymer electrolytes should be compatible with the variety of electrode materials. Hence, adequate and possibly non-toxic anode/cathode materials should be identified. Presently, major effort has been diverted to explore such active electrode materials which would improve the performance level of the electrochemical devices.

Electrolytes that containing polymer as a material host has been widely studied during the last 20 years. The electrolytes that are well known as polymer electrolyte was proposed by Wright and Fenton in 1973 (Fenton, Parker, & Wright, 1973) but their technological significances are fulfilled and appreciated by Armand and his group few years later (Armand, Chabagno, Duclot, 1979). In the polymer electrolytes, ions can move with the segmental motion of the polymer chain as shown in Figure 2.7. In other words, the polymer acts as medium for ion motions in the electrolytes.

Generally, polymer electrolytes so-called ion conducting polymer consists of inorganic salts (ion contributor) dissolved in a polymer host. A polymer must be able to solvate salt; through interaction between the cations of the salt and the lone pair

electrons provided by the polymer. The conceptual structure of lithium polymer battery is shown in Figure 2.8.

There are several general properties to be considered in order to perform successfully as an electrolyte in the batteries.

- i. Polymer that forms salt complexes should have polar group (Lewis bases) on the polymer chain, to solvate the salt effectively
- ii. The salts with low lattice energy are most likely to form polymer-salt complexes. These salts usually contain univalent alkali ions with larger anions (e.g. CF_3SO_3^- , ClO_4^- , HPO_4^- , etc.)
- iii. Polymers with low cohesive energy density and high flexibility (as indicated by low glass transition temperature) have the greatest tendency to interact with salts.
- iv. The plasticizer should have low viscosity, high dielectric constant, low melting point and high boiling point: help to increase the amorphous nature by reducing the polymer crystallinity, dissociate ion-pairs into free cations and anions thereby leading to an overall enhancement in conductivity.
- v. The polymer electrolyte system should have an amorphous characteristic: ionic conductivity in polymer electrolytes is associated with the amorphous phase

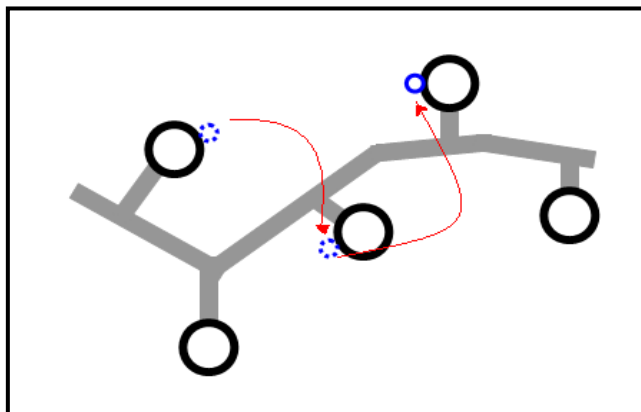


Figure 2.7: Ions move in polymer chain

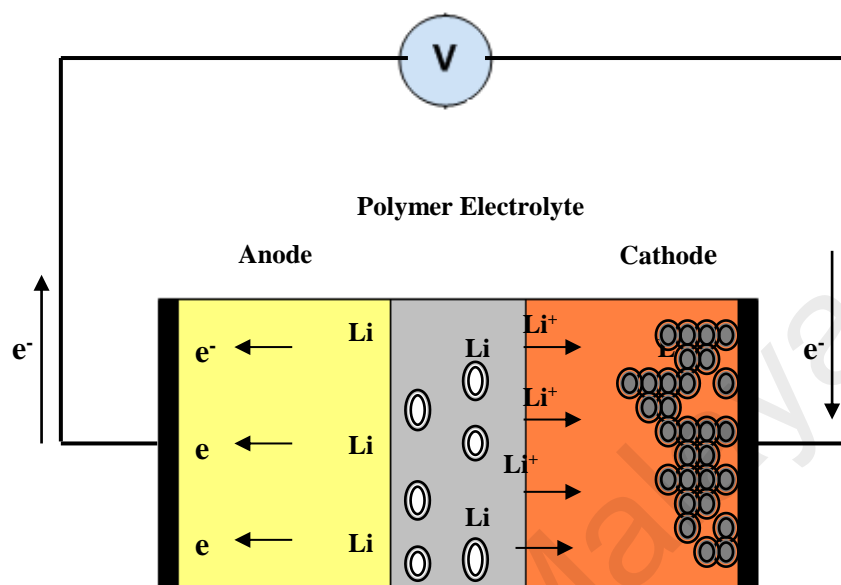


Figure 2.8: Conceptual structure of lithium polymer battery

2.2.1 Development of Polymer Electrolytes

There are many types of polymer electrolytes such as (i) dry solid polymer electrolytes (SPEs) (ii) liquid polymer electrolytes and (iii) gel polymer electrolytes. Among the polymer electrolytes studies, gel polymer electrolytes (GPE) are found to be the best as compared to others, which have both solid and liquid like properties. It is hard to define gel because it is not solid state, also not liquid but it could be described as materials that can have properties ranging from soft and weak to hard and tough. Because of its unique character, it simultaneously has solid cohesion and liquids diffusivity properties.

The GPEs can be obtained by swelling the polymer in the solvents consisting of metal ions. Therefore, it can be thought as a liquid electrolyte entrapped in a polymer matrix. In addition, the GPEs can be made into a thin and flexible film. Since

it is flexible, it can be shaped and bent to fit the geometries of any devices. There are some advantages of GPE film;

- i. It possesses good mechanical strength as good as solid polymer electrolytes (SPEs) and good in degree of elasticity
- ii. It can give high ionic conductivity comparable to those of liquid electrolytes.
- iii. It can replace liquid electrolytes, as they are more stable in the term of chemical and electric stability
- iv. It is very helpful to prevent devices from drying out or leaking electrolyte

2.2.1.1 Polymer Matrix

In 1973, Wright and his group made polymer electrolytes that combine the lithium salt into polymer matrix based on poly (ethylene oxide) PEO (Fenton, Parker & Wright, 1973). Later, Armand and his co-workers (Armand, Chabagno & Duclot, 1979) explored the various device applications of these materials. The conductivity of the electrolytes is just 10^{-8} S cm^{-1} due to high crystallinity of the polymer matrix. Then it becomes an area of research interest around the world to find out a suitable polymer electrolyte for device applications.

Ionic conductivity is certainly the most important properties for polymer electrolytes. In order to improve the conductivity, many researchers therefore study many polymer matrixes that have different properties. The polymers that usually used in this research area are poly(acrylonitrile) (PAN), poly(methyl methacrylate) (PMMA), poly(vinyl chloride) (PVC), poly(propylene oxide) (PPO) and poly(vinylidene fluoride) (PVdF) researchers (Abraham, Jiang, & Carroll, 1997; Choe, Giaccari, Alamgir, & Abraham, 1995; Hong, Liqun, Xuejie, & Rongjian, 1992; Iijima, Y.; Tyoguchi, Y. & Eda, 1985;

Reich & Michaeli, 1975; Slane & Salomon, 1995; Tsuchida, Ohno, Tsunemi, & Kobayashi, 1983; Watanabe et al., 1984)

As a polymeric matrix of gel electrolytes, polymers should have several requirements such as:

- 1) good electrochemical stability toward oxidation and reduction at Li electrodes,
- 2) good compatibility with the electrolyte,
- 3) sufficient thermal stability
- 4) easy production at low cost
- 5) good mechanical strength of the final product

In the past three decades, PEO-based electrolytes were the major polymer host matrix used in batteries. PEO has a melting point of 65 °C, and is approximately 85% crystalline. Crystalline portion not only block ion paths but also reduce the system flexibility result in low conductivity ($<10^{-8}$ S cm⁻¹) and it is not satisfactory as a polymer solid electrolyte. PAN was also studied as polymer matrix in the electrolytes system since it has nitrogen atom on the backbone. This nitrogen atom is strong electron donor like ether oxygen in PEO and has low cohesive energy. PAN based electrolytes has been studied by many researchers (Abraham & Alamgir, 1990; Huang, Frech, Johansson, & Lindgren, 1995; Reich & Michaeli, 1975; Watanabe et al., 1984) . They reported that PAN systems have shown higher conductivity ($>10^{-3}$ S cm⁻¹) than PEO. In fact, the electrolytes have good dimensional stability and electrochemical stability window exceeding 4.5V (Abraham & Alamgir, 1990; Watanabe et al., 1984). However, PAN did not attain a stable interface with lithium metal. Previous reports clearly demonstrated that the interfacial resistance of PAN based electrolytes with lithium cathode is increases with time (Hong et al., 1992; Slane & Salomon, 1995). The poor

interfacial stability affects the cyclability of the rechargeable lithium battery thus, puts restriction on the application of PAN based polymer electrolytes to the lithium polymer batteries.

The possibility of using PMMA as polymer host has been explored by Iijima and his group (Iijima, Tyoguchi & Eda, 1985). The ionic conductivity of PMMA remains very close to that of liquid electrolyte but the mechanical stability is relatively poor. Studies have also been made on PVC-based electrolytes (Abraham & Alamgir, 1990; Mary Sureshini, Nishimoto, & Watanabe, 1996). Recently, Stephan et al. have attempted to enhance the mechanical strength of PMMA electrolytes by blending them with PVC. A PMMA/PVC blend electrolyte with ratio of 7:3 with 70% plasticizer content was found to be optimal in mechanical strength and conductivity points of view (Stephan et. al, 1999, Stephan et. al, 2000).

PVdF as a host has attracting much attention of many researchers due to its promising properties. It is semicrystalline polymer with high thermal stability and the electrolytes have high anodic stability due to strong electron withdrawing functional group. It is also has a high dielectric constant ($\epsilon_r = 8.4$) that assist in a greater ionization of lithium salts (Abraham et al., 1995). Many efforts have been done on the PVdF based electrolytes and the conductivity obtained is about $10^{-3} \text{ S cm}^{-1}$. However, by using the copolymer i.e PVdF-HFP could give better result on the conductivity. The HFP units have been introduced to the PVdF in order to keep the good solvating properties of the polymer and lower its high crystallinity. The high crystallinity phase is unsuitable for ionic conduction. By introducing the HFP unit will increase the amorphous phase therefore increase the ionic conductivity. Generally, the amorphous phase in the gel polymer electrolytes capable of trapping large amount of electrolytes while the

crystallinity phase acts as mechanical support so that, the free standing film can be obtained.

University of Malaya

2.2.1.2 Salts

The inorganic salt that most commonly studied in polymer electrolyte research such as lithium perchlorate (LiClO_4), lithium triflate (LiCF_3SO_3), lithium tetrafluoroborate (LiBF_4), lithium hexafluorophosphate (LiPF_6), copper (I) thiocyanate (CuCNS), and copper triflate (CuCF_3SO_3). The small ionic radius of lithium ion can provide high volumetric capacity. Thus, lithium ion conducting polymer electrolytes have been widely studied due to their potential use in rechargeable batteries.

The salt with large anion that has low lattice energy is the most suitable for polymer electrolytes system (Armand, 1994). The larger anion could promote the cation-anion dissociation and result more charge carriers for transportation. It is generally accepted that anions are mobile and in some systems net cation mobility is vanishingly small (disappear). Anions assist in cation transport by formation of ion pairs, triple ions and higher aggregates. With the assistance of polymeric chain segmental motion, the ionic cluster may itself move or it may act as transient center for the mobile species.

The lithium salts used for Li^+ conductive polymer electrolytes, such as lithium perchlorate (LiClO_4), lithium tetrafluoroborate (LiBF_4) and lithium triflate (LiCF_3SO_3) have larger anions and lower lattice energies to promote high conductivity, compared with halides such as lithium chloride (LiCl), lithium iodide (LiI) and lithium bromide (LiBr). Although most of the interest in polymer electrolytes focused on lithium ion-conducting polymer electrolytes, the sodium ion conducting analogs have also been the subject of much attention. One of the earliest studies on polymer electrolytes containing dissolved sodium triflate was reported by Schantz et.al (Schantz, Sandahl, Börjesson, Torell, Stevens, 1988). Some researchers have used triflate (CF_3SO_3) salt in conducting polymer electrolytes due to its large ionic radius compared to the complex anions ClO_4 and AsF_6 . The ionic size is also one of the factors in the increasing mobility of ions,

which the dipole interactions of the ions with polymer are weak. Hence, the conductivity of the polymer increased. Therefore, triflate salt can be a good candidate as a doping salt in the host polymer. The comparison study of lithium triflate and sodium triflate dissolved in poly(ethylenimine) and poly(ethylene oxide) was reported by many researchers i.e Rhodes et al., Sanders et al. and York et al. (Rhodes & Frech, 2000; Sanders, Snow, Frech, & Glatzhofer, 2003a; York, Frech, Snow, & Glatzhofer, 2001). Figure 2.9 shows the chemical structure of lithium triflate and sodium triflate salts.

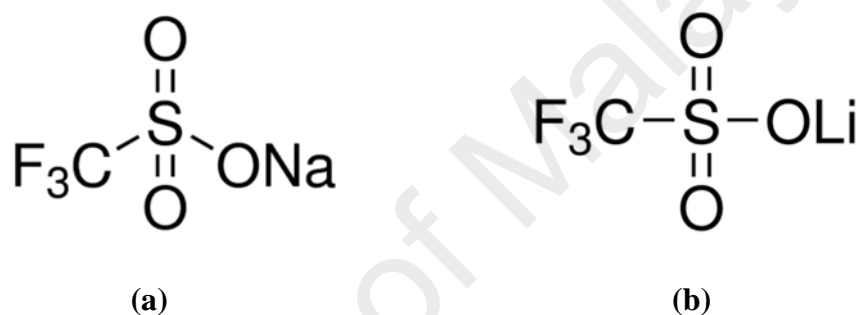


Figure 2.9: Chemical structure of (a) lithium triflate and (b) sodium triflate
(Lithium_trifluoromethanesulfonate, 2014, Sodium_trifluoromethanesulfonate, 2014)

2.2.1.3 Plasticizing Agent

Many efforts have been made to modify the structure of polymer electrolytes in order to improve their electrical, electrochemical and mechanical properties. These approaches include (a) synthesizing polymer (b) blending two polymers (c) adding plasticizers to polymer electrolytes and (d) adding inert fillers to make composite polymer electrolytes (Rajendran, Babu, & Sivakumar, 2008) . The most popular method is adding low-volatility liquids with high dielectric constants as plasticizer into the polymer electrolytes system (Abraham & Alamgir, 1990; Alamgir, Moulton, & Abraham, 1991). An organic solvent that used as plasticizing agent can be defined as a

chemical which reduces the stiffness of an amorphous polymer. The functions of the plasticizer are to decrease the glass transition temperature, dissolve the salt, make the polymer become amorphous and therefore allow the ions or ionic carriers to move freely hence raise the ionic conductivity of the electrolyte. Besides the plasticizing effect, the major function of the plasticizer is to associate with the ionic carriers and allow them to move faster.

The most common organic alkyl carbonate solvents are one or mixtures of the following: propylene carbonate (PC), ethylene carbonate (EC), diethyl carbonate (DEC), dimethyl carbonate (DMC), or ethyl methyl carbonate (EMC). The properties of some organic solvents commonly used in rechargeable lithium batteries are summarized in Table 2.3. According to Li et al., a mixture of EC and PC could dissolve larger amount of lithium salt compared to other possible mixtures (Li & Balbuena, 1999). EC and PC are compatible with a wide range of polymers and salts and are commonly used in gel polymer electrolytes. They have higher dielectric constant compared to the other plasticizers that give them the ability to assist the dissolution and dissociation of salt; by improving the flexibility and segmental motion and solvate the cation that reduces ion-ion interactions (Akashi, Sekai, & Tanaka, 1998). The low viscosity of the plasticizers can increase the ionic mobility of the systems. Therefore, the combination of these two plasticizers help to prevent ion aggregation and increase the number of charge carriers thereby enhancing the electrical conductivity. The chemical structures of EC and PC are shown in Figure 2.10.

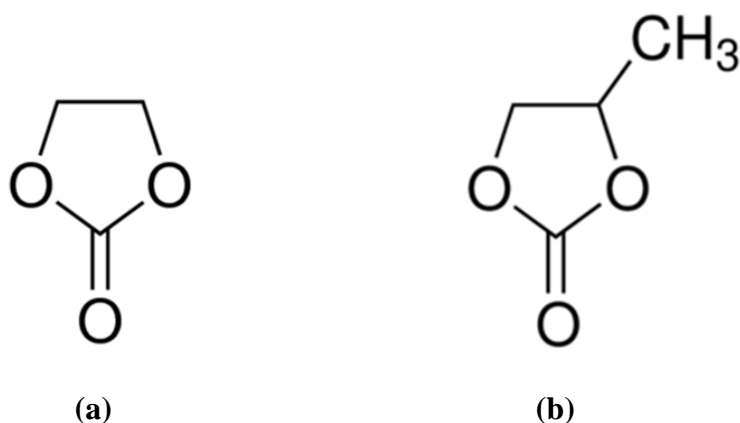


Figure 2.10: Chemical structure of (a) ethylene carbonate (EC) and (b) propylene carbonate (PC)

(Ethylene_carbonate, 2014, Propylene_carbonate, 2014)

The functions of the plasticizer in the polymer electrolyte are summarized as the following (Wang, Huang, Xue, Huang & Chen, 1999);

- i. Decreasing the glass transition temperature, T_g of the polymer and dissolving the crystallites of the polymer. This will lead to the increase of the mobility of the segmental chain of the polymer and help the transport of the charge carriers depending on the movement of the segmental chain
- ii. Interacting with the polymer molecules by way of dipolar interactions and therefore, increasing the polarities of the polymer and the plasticizer itself, which in turn, will help the dissociation of the salts in polymer electrolytes
- iii. Dissolving the salts so as to provide charge carriers for the polymer electrolytes
- iv. Destructing the coordination bond of cations with polymer and making more ions move into polymer electrolytes

Based on the above functions of the plasticizer in a polymer electrolyte, the requirement of plasticizer for polymer electrolyte are:

- 1) Compatible with the polymer and the electrodes
- 2) Thermodynamically stable
- 3) Low viscosity
- 4) High dielectric constant
- 5) Low melting point and high boiling point
- 6) Inexpensive and easily obtainable

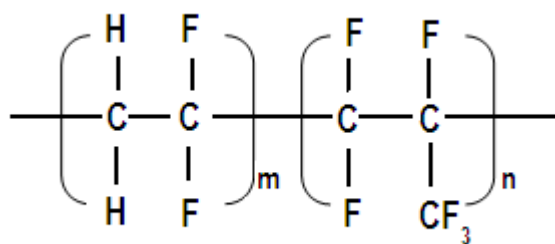
Table 2.3: Physical properties of some organic solvents
(Stephan, 2006)

Plasticizing Agent	Melting point (°C)	Boiling point (°C)	Density, g (cm ⁻³)	Dielectric constant, ϵ	Molecular weight	Solubility parameter, (J cm ⁻³) ^{1/2}
Dimethyl carbonate (DMC)	2.4	90	1.06	3.12	90.08	20.3
Diethyl carbonate (DEC)	-43.0	126	0.9752	2.82	118.13	18.0
γ -Butyrolactone (BTL)	-43.3	204	1.1284	39.0	86.09	25.8
Ethylene carbonate (EC)	36.4	248	1.3214	89.78	88.06	30.1
Propylene carbonate (PC)	-48.8	242	1.2047	66.14	102.09	27.2

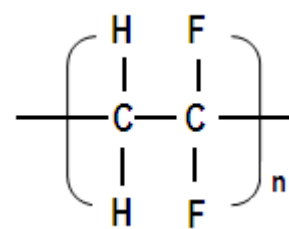
2.3 Development of PVdF-HFP-based polymer electrolytes

Poly (vinylidene fluoride-co-hexafluoropropylene) (PVdF-HFP) has been chosen as polymer host because of its various interesting properties like good film forming, high thermal and chemical stability. PVdF-HFP is copolymer where the PVdF copolymerized with HFP unit. Introduce the HFP unit to the PVdF backbone reduces the crystallinity of the neat PVdF making the flexibility of the copolymer greatly enhanced. The crystallinity (VdF) remaining in the system provide mechanical support for the formation of freestanding film while the amorphous (HFP) region capable of trapping large amount of electrolyte. Further, the polymer has high dielectric constant ($\epsilon = 8.4$), which helps for greater ionization of salt, and thus provide a high concentration of charge carriers. The strong electron-withdrawing functional group ($-\text{C}-\text{F}-$) in PVdF-HFP makes this polymer highly anodically stable (Song et al., 1999). Since copolymerization is one of the effective approaches to enhance the ionic conductivity, thus this copolymer can also improve the ionic conductivity of the electrolytes.

Because of the PVdF-HFP meets all the requirements to become a successful host in polymer electrolytes system, research works on this polymer have greatly increased in recent years. Saika and Kumar (D. Saikia & Kumar, 2005) did the comparison study between PVdF and PVdF-HFP based gel polymer electrolytes. They reported that the higher conductivity achieved for PVdF-HFP could be attributed to the higher amorphicity due to steric hindrance provided by CF_3 pendant group in HFP monomers that is randomly mixed with the VdF monomers in the polymer chain as shown in Figure 2.11.



Configuration of PVdF-HFP co-polymer



Configuration of PVdF polymer

Figure 2.11: Chemical structures of PVdF-HFP copolymer and PVdF homopolymer

Higher amorphicity provides more free volume for mobile Li⁺ ion resulting in higher conductivity. On the other hand, pure PVdF has higher degree of crystallinity because of single monomer throughout the polymer chain providing less free volume to the mobile Li⁺ ion, which results in lower conductivity. Stephan and his co-workers (Stephan, Kumar, Renganathan, & Kulandainathan, 2005) discussed the compatibility of PVdF-HFP gel polymer electrolytes with a combination of plasticizers EC and PC and three different lithium salts (LiCF₃SO₃, LiBF₄, LiClO₄). They found that the system consist of LiBF₄ salt exhibited maximum conductivity and was attributed to the low lattice energy of the salt. However, the films exhibited poor compatibility with lithium metal anode due to the formation of LiF in the layer.

For the plasticizing effects, most of the studies done on PVdF-HFP were used plasticizers to improve the ionic conductivity of polymer electrolyte. Saikia and Kumar (D. Saikia & Kumar, 2004a) was used the combination of EC and DEC to form gel polymer electrolytes consist of PVdF-HFP and PVdF separately. Takohiro et. al (Aoki, Ohta, & Fujinami, 2006) was used combination of EC and PC as plasticizing agent in the gel polymer electrolytes composed of PVdF-HFP and lithium tetrakis borate (LiTPSB). The result shows that the ionic conductivity of dry polymer electrolytes,

PVdF-HFP/ LiTPSB of $2 \times 10^{-8} \text{ S cm}^{-1}$ largely increase by addition of EC and PC to $2 \times 10^{-4} \text{ S cm}^{-1}$ due to increased flexibility of the ion conducting interfacial phase. Byoung-Koo and his group (Choi, Park, Joo & Gong, 2004) was studied the proton conducting gel polymer electrolytes consist of PVdF-HFP, H_3PO_4 and different organic solvents such as PC, EC, DMF and DMSO. The experimental data showed that the proton conductivity of PC and EC – based gel electrolytes is higher than DMF and DMSO-based gel electrolytes, possibly due to higher dielectric constant resulting in higher dissociation of H_3PO_4 therefore higher concentration of charge carriers.

Some researchers have discussed about blend PVdF-HFP with other polymer in order to enhance the conductivity of polymer electrolytes. Blending at least two polymers seems to be a good strategy to hold back the crystallinity and improve the conductivity which one of the polymers was applied to absorb the electrolyte's active species while the other one is tougher and inert, improving the mechanical property of polymer blend (Kim, Park, Rhee, 1996; Nicotera et al., 2006). Saikia and Kumar (Saikia & Kumar, 2005) studied the ionic transport in composite polymer electrolytes consist of PVdF-HFP and PMMA polymers, EC and PC as plasticizers, LiCF_3SO_3 as salt and fumed silica as filler. From the XRD analysis, they suggested that the blending method and the presence of filler, increase the conductivity of the film due to increase of amorphorcity, providing Li^+ more free volume and enhanced defect concentration along the polymer - SiO_2 . Aravindan et. al (Aravindan et. al, 2009) have prepared and characterized polymer electrolytes comprising the blending of PVdF-HFP and PEMA as host polymer, EC and DEC as plasticizing agent and incorporating NaCF_3SO_3 as the doping salt. They were added nanosized Sb_2O_3 as filler. The result also suggested that the high conductivity of the film studied could be attributed to the formation of amorphous domains/large free volume, which may be due to the strong interaction of filler particles with the polymer chains. The others works reported the blend polymer

electrolytes consisting PVdF-HFP are PVdF-HFP/PEMA (Sim, Majid, & Arof, 2012), PVdF-HFP/MG49 (Ataollahi et al., 2012), PVdF-HFP/PAN (Subramania, Sundaram, & Kumar, 2006), PVdF-HFP/PEG (Lee, Kim, & Bae, 2003), PVdF-HFP/PVAc (Choi, Lee, Park, & Ko, 2001), PVdF-HFP/PMMA (Lee & Park, 2001)

2.4 Ionic Mechanism in Conducting Polymer Electrolytes

Since electrolytes generally contain ion in solution, they are also known as ionic solution. A strong electrolyte is a good conductor because they consist of many ions in the solution. Conductivity in solutions is a measure of the ability of solution to conduct an electric current. The more ions there are in the solution, the higher its conductivity. Generally, ionic conductivity of electrolytes depends on the charge carrier concentration, n and carrier mobility, μ , as described by the relation

$$\sigma = \sum \mu_i n_i q_i \quad (2.1)$$

Where n , q and μ representing the charge carrier concentration, charge of mobile carrier and the mobility, respectively. Increases of conductivity value can be related to the increases of mobile charge (ion) which is contributed by salt concentration. The other aspect that govern the magnitude of conductivity of the polymer electrolytes are the degree of crystallinity and the nature of the salt and polymer. In polymer exist polar groups and it can be expected that polymers behave as solvents and dissolve salts to form stable ion-polymer complexes. According to the '*Breathing Polymeric Chain Model*' proposed by Chandra et. al (Chandra, Sekhon, & Arora, 2000), gel polymer electrolytes generally consist of free ions, ion aggregates and polymer chain dispersed in the gel matrix. The breathing of polymer by folding/unfolding of its chains result in

density/pressure fluctuation at the microscopic level that assist the motion of ions along with the dissociation of ion, aggregates which result in an increase of conductivity. The ion pairs that formed in the system are further solvated by polymer chains which result in a change of charge carrier concentration (η) and mobility (μ) (Sekhon, 2003). It is also generally accepted that anions are mobile and the anions assist in cation transport by formation of ion pairs, triple ions and higher aggregates. With the assistance of polymeric chain segmental motion, the ionic cluster may itself move or it may act as transient center for the mobile species. The scheme illustration of cation motion in polymer is shown in Figure 2.12.

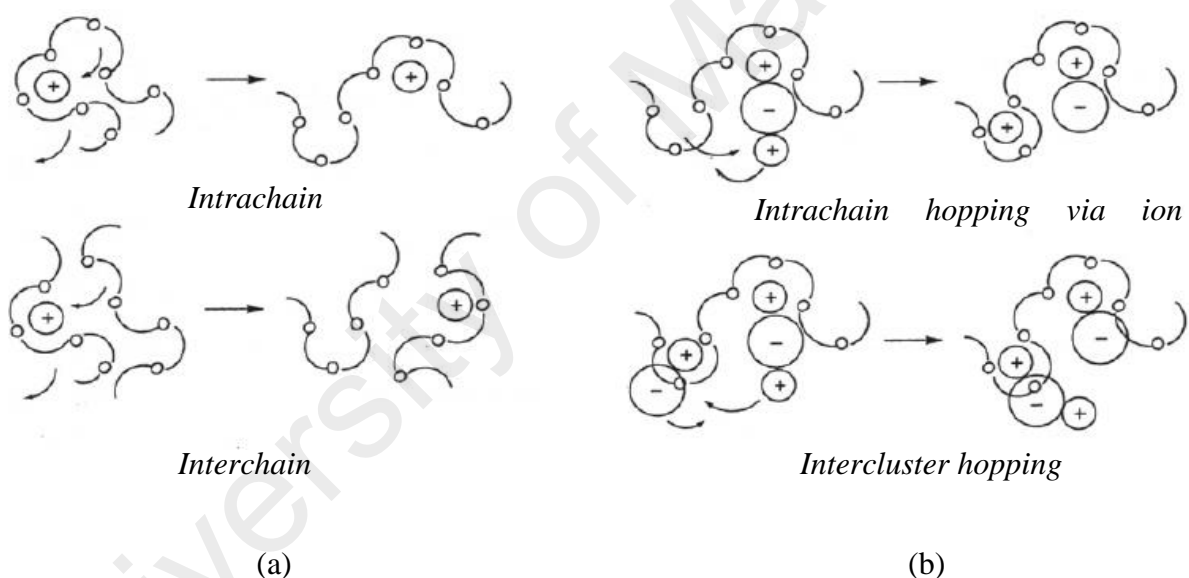


Figure 2.12: Representation of cation motion in polymer electrolyte (a) assisted by polymer chain motion only; (b) taking account of ionic cluster contributions

Generally, ionic conductivity of polymer electrolytes increases with temperature indicates it is thermally activated process. At higher temperatures, thermal movement of polymer chain segments and dissociation of salts would be improved, which increases ionic conductivity. Several theoretical models have been proposed to explain the ion

conduction process in polymer electrolytes and their conductivity variation as a function of temperature. The straight or curved lines observed when the conductivity is plotted in Arrhenius coordinates can be fit to the Arrhenius and Vogel-Tamman-Fulcher (VTF) forms. The linear variation of $\log \sigma$ versus $1000/T$ suggests an Arrhenius type thermally activated process which the conductivity can be expressed as:

$$\sigma = \sigma_0 \exp\left(\frac{-E_a}{kT}\right) \quad (2.2)$$

Where σ_0 is a pre-exponential factor, E_a is activation energy, k is Boltzmann constant and T is the absolute temperature in Kelvin. The E_a value can be evaluated from slope of the Arrhenius plot. The Arrhenius model is typical for conventional solid electrolytes as well as crystalline polymer electrolytes. The steady increase in conductivity with temperature reveals ionic transport via a simple ionic hopping mechanism decoupled from the polymer-chain breathing. Ion hopping mechanism happens between coordinating sites and local structural relaxations (Vieira, Avellaneda, & Pawlicka, 2007).

Another interesting feature of the conductivity plots is that they are gentle curves and not perfectly straight lines. So that, the temperature dependence on the ionic conductivity was not linear which is indicative of a conductivity mechanism involving ionic hopping motion coupled with the relaxation/breathing and/or segmental motion of polymeric chains. It also indicates that ion motion in polymer electrolytes was depended on the free volume and motion of the polymer chains in which the conduction occurs in amorphous region. The electrical conductivity temperature dependence for the ionic transport in the amorphous polymer electrolytes can be well described by the VTF equation:

$$\sigma = AT^{-1/2} \exp\left[-\frac{E_a}{k_b(T-T_0)}\right] \quad (2.3)$$

where A is the pre-exponential factor, k_b the Boltzmann constant, E_a is the apparent activation energy, which means the necessary energy required to move any chain segment for ion motion (Companik & Bidstrup, 1994), T_0 is normally called the equilibrium (ideal) glass-transition temperature corresponding to zero configuration, is related to the (kinetic) measured glass-transition temperature roughly by

$$T_0 \cong T_g - 50K \quad (2.4)$$

The kinetic glass-transition temperature, T_g can be observed as an endotherm in a thermal-analysis measurement. The simplest understanding of bent VTF conductivity behavior is that diffusion can occur only when the ion moves from one free volume space to another. In order to calculate the value of A and E_a , equation (2.3) can be rewritten as

$$\log_{10}(\sigma T^{1/2}) = \log_{10} A - 0.43 \frac{E_a}{k_b(T - T_0)} \quad (2.5)$$

The free volume model is the simplest way to understand the polymer segment mobility. It states that as temperature increases, the expansivity of the material produces local empty space, free volume, into which ionic carriers, solvated molecules or polymer segments themselves can move. The overall mobility of the material then is determined by the amount of volume present in the material. The free volume is calculated according to the simplest model, by the usual statistical argument of maximizing the number of ways in which the volume can be distributed (Cohen & Turnbull, 1959). One then obtains for the diffusivity D , the form

$$D = BRT \exp(-V^*/V_f) \quad (2.6)$$

which B and V^* are constant, R is the gas constant and V_f is the free volume. When the volume is expanded in terms of the volume at the glass transition temperature plus a linear term, the free volume theory yields the form (Cheradame, 1982; Killis, Lenest, Gandini, Cheradame, & Cohenaddad, 1984; Ratner, 1987)

$$D = D_o T \exp\left(\frac{-a}{T - (T_g - C_2')}\right) \quad (2.7)$$

where the constants a and C_2' are both inversely proportional to the free volume thermal expansion factor. Killis and co-workers (Killis, LeNest, Cheradame, & Gandini, 1982) shows that indeed there is a very close relationship between conductivity and polymer relaxation behavior.

The important concept for understanding of ionic motion in polymer is the issue of coupling between transport and relaxation: when the host polymer relaxes more rapidly, ionic conductivity increases. Angell (C. Angell, 1983, 1986) has generalized these concepts to differentiate two types of amorphous solid ion conducting polymers. He defines a decoupling ratio R as

$$R = \tau_s / \tau_\sigma \quad (2.8)$$

The dimensionless decoupling ratio R is the quotient of two different relaxation times: the structural relaxation time τ_s refers to viscosity or segmental relaxation, while the conductivity relaxation time τ_σ is inversely proportional to the conductivity. If R were close to unity, it would indicate that the ionic motion and the structural relaxation occur on the same time scale, thus suggesting that their rate determining steps are the same. Angell (Angell, 1986) has noted that for polymeric solid electrolytes $R \sim 10^{-3}$,

which implies (since it is substantially less than unity) strong residual ion-ion coupling, resulting in reduced conduction.

University of Malaya

CHAPTER 3: EXPERIMENTAL TECHNIQUES

3.1 Sample Preparation

3.1.1 Materials

Poly (vinylidene fluoride-co-hexafluoropropylene) (PVdF-HFP) with molecular weight of 450,000 g/mol, ethylene carbonate (EC), propylene carbonate (PC), lithium trifluoromethanesulfonate (LiCF_3SO_3) and sodium trifluoromethanesulfonate (NaCF_3SO_3) were supplied by Sigma Aldrich. The mixture of tetrahydrofuran (THF) and acetone from Sigma Aldrich was used as the solvent in casting gel polymer electrolyte films.

Table 3.1: Amounts of PVdF-HFP, plasticizers and salts in each group of gel polymer electrolytes system

Systems	PVdF-HFP (g)	EC (g)	PC (g)	LiCF_3SO_3	NaCF_3SO_3
Pure PVdF-HFP	2	-	-	-	-
PVdF-HFP + EC + PC	2	2	1	-	-
PVdF-HFP + EC + PC + LiCF_3SO_3	2	2	1	Varied from 5 to 30 wt.%	-
PVdF-HFP + EC + PC + NaCF_3SO_3	2	2	1	-	Varied from 5 to 30 wt.%

3.1.2 Preparation of Gel Polymer Electrolytes Systems

The fixed amount of PVdF-HFP was dissolved in a mixture of THF and acetone solvents and the mixture was stirred and heated until the solution turned into a clear and homogeneous. At the same time, the salt (LiCF_3SO_3 or NaCF_3SO_3) was dissolved in the mixture of EC and PC with the mass ratio of 2:1. The combination of EC and PC with ratio of 2:1 gives a prominently high conductivity which is $3.31 \times 10^{-8} \text{ S cm}^{-1}$ in the plasticized film without salt. The salt and plasticizing solvents then were stirred at room temperature for several hours. After complete dissolution, the salt solution was added to the polymer solution and the mixtures were continuously stirred for several hours. The gel polymer electrolyte films were prepared by varying the salt contents from 5 wt. % to 30 wt. %. When complete dissolution is achieved, the solution is then cast on to glass petri dishes and left to dry at room temperature. The solvent was allowed to evaporate slowly until the homogenous and mechanically stable gel films have formed. The films were then kept in the desiccators for further drying before the characterization to be carried out. Figure 3.1 shows the experimental flow chart in preparing the GPE films and the characterization techniques that used in analyzing the films.

3.2 Characterizations of Gel Polymer Electrolytes Films

1) Electrical Studies:

- i. Electrochemical Impedance: The impedance analysis was done in the frequency range of 50 Hz to 1 MHz to obtain conductivity value for all the GPE films at room temperature. The conductivity-temperature dependence studies were also performed on the films in temperature range of 303 – 373 K.
- ii. Transference number measurements: The D.C polarization method was used to measure the ionic transference number while the transference

number of cation was determined by the combination of A.C impedance and D.C polarization method.

2) Thermal Analysis:

- i. DSC analysis: The analysis was done to determine the value of glass transition temperature, T_g and other thermal properties in the GPE films.
- ii. TGA analysis: The measurement was performed in order to confirm the thermal stability of the GPE films.

3) Structural and Morphological Studies:

- i. FTIR & Raman spectroscopy studies: These studies were done in order to investigate the occurrence of complexation in the films.
- ii. XRD analysis: The analysis was used to identify the state of the GPE films i.e. either crystalline, semicrystalline or amorphous.
- iii. FESEM studies: The GPE films were analyzed using this technique in order to investigate the surface morphology of the films.

4) Electrochemical Studies

- i. CV analysis: The measurement was used to investigate the chemical reactivity (oxidation and reduction) of the GPE films. It can be used to determine whether the redox reactions are reversible or irreversible, and also to study the mechanism by which the reactions take place.
- ii. LSV analysis: The analysis was done in order to estimate electrochemical stability window or working voltage limit of the GPE films.

5) Cell fabrication: This is the final stage of the experimental procedure where the battery was assembled by sandwiching the GPE film between the respective electrodes in a sealed container and the charge/discharge cycling of the battery was studied.

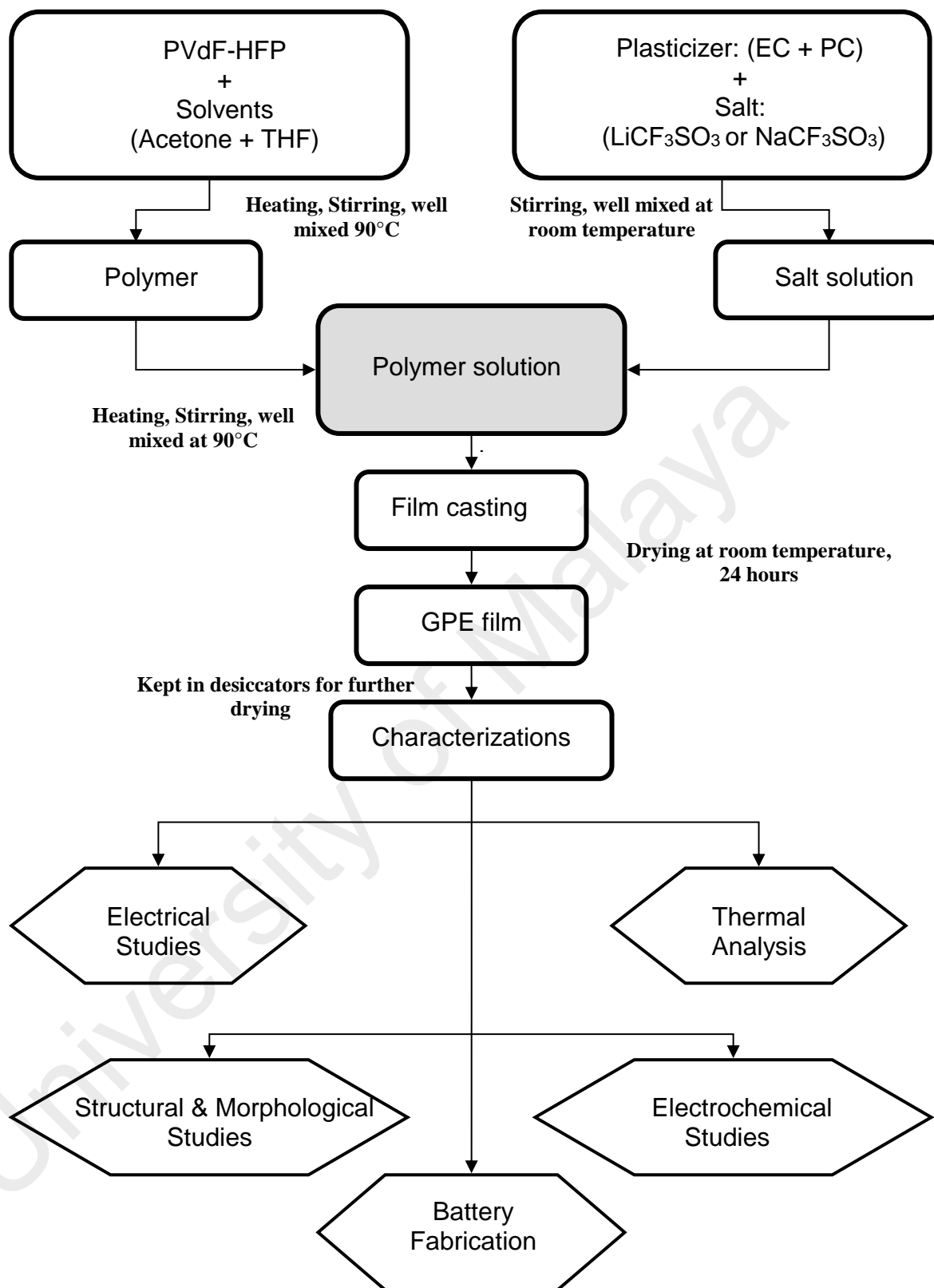


Figure 3.1: The experimental flow chart for the sample preparation method and characterization of the GPE films

3.3 Experimental Techniques

3.3.1 Electrochemical Impedance Spectroscopy (EIS)

Electrochemical Impedance Spectroscopy (EIS) method is a useful technique to characterize a physical process in terms of electrical measurements. The technique involves measurement and analysis of materials in which ionic conduction strongly predominates. Therefore, this technique is very valuable in the studies of rechargeable battery, fuel cells, corrosion.

Basically, in EIS studies the system response to the application of a periodic small amplitude A.C signal or voltage as a function of frequency. In D.C theory (a special case of A.C theory where the frequency equals 0 Hz) resistance is defined by Ohm's Law:

$$E = I R \quad (3.1)$$

Using this equation, a D.C potential (E) is supplied to a circuit, measure the resulting current, (I) and compute the resistance, R or we can determine any term of the equation if the other two are known. A resistor is the only element that impedes the flow of electrons in a D.C circuit. In A.C theory, where the frequency is non-zero, the analogous equation is:

$$E = I Z \quad (3.2)$$

As in equation (3.1), E and I are defined as potential and current, respectively. Z is defined as impedance, the A.C equivalent of resistance and the values are also measured in *ohms* (Ω). In the A.C circuit, there are other two elements that impede the flow of current i.e. capacitors and inductors. Therefore, the total impedance in the circuits is the combination of resistance, capacitance and inductances. The impedance can be

represented as complex quantity where a resistor only contributes to the real part of the impedance while the capacitance and inductance is the imaginary component. Both capacitors and inductors affect the magnitude and time-dependent characteristics /phase of an alternating current. A circuit is said to be largely capacitive when most of the opposition to current flow comes from its capacitive reactance and the current leads the applied voltage in phase angle. When most of the opposition to current flow comes from its inductive reactance, a circuit is said to be largely inductive and the current lags the applied voltage in phase angle. If the difference phase angle is closer to 90° , the circuit becomes more inductive (Advantages & Note, 2013).

Figure 3.2 shows a typical plot of a voltage sine wave (E) applied across a circuit and the resultant A.C current waveform (I). It can be seen that the two traces are different not only in amplitude, but are also shifted in time (difference phase between output and input signals). In the case of a purely resistive network, there will be changed in the amplitude but the two waveforms would not be shifted. They would be exactly in the same phase but different in amplitude.

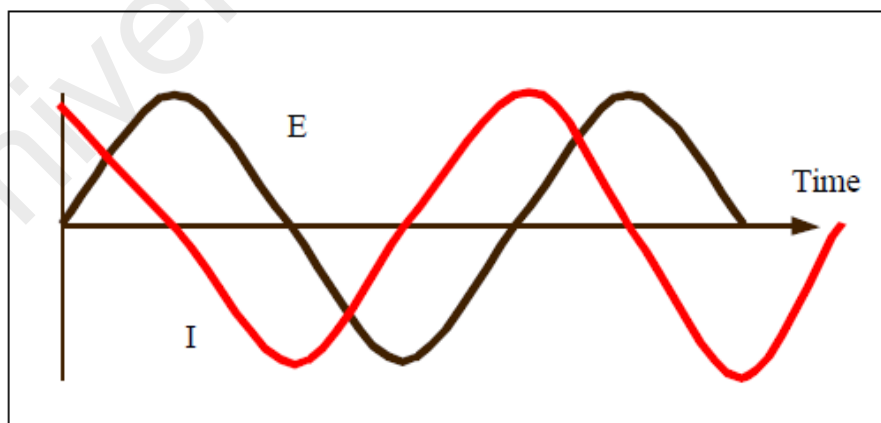


Figure 3.2: A.C. waveform for an applied potential and a resulting current.

The current sine wave can be described as;

$$I(t) = A\sin(\omega t + \theta) \quad (3.3)$$

Where;

$I(t)$ = instantaneous current

A = maximum amplitude

ω = frequency in radians per second = $2\pi f$ (here f = frequency in Hertz)

t = time

θ = phase shift in radians

The vector analysis is used to describe the A.C waveform in term of its amplitude and phase characteristic. Figure 3.3 and 3.4 show vector analyses for the resultant current waveform of Figure 3.2. Figure 3.3 shows the vector defined by phase angle (θ) and current magnitude ($|I|$) in term of x and y coordinates pair formed from the in-phase (x) and out-of-phase (y) components. The next approach is define the axes as real (I') and imaginary (I'') as shown in Figure 3.4.

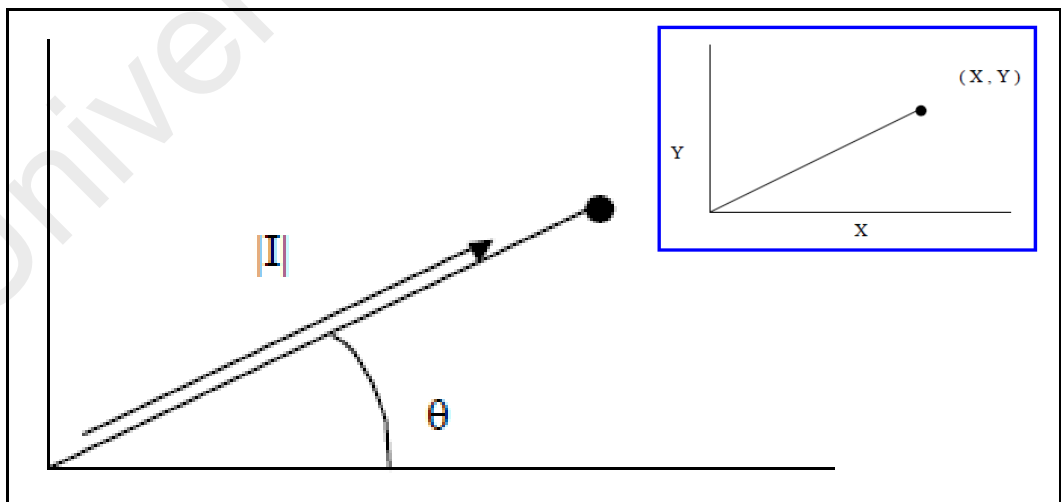


Figure 3.3: Vector in terms of Angle (θ) and Magnitude ($|I|$) Inset figure: Vector in terms of x and y coordinates

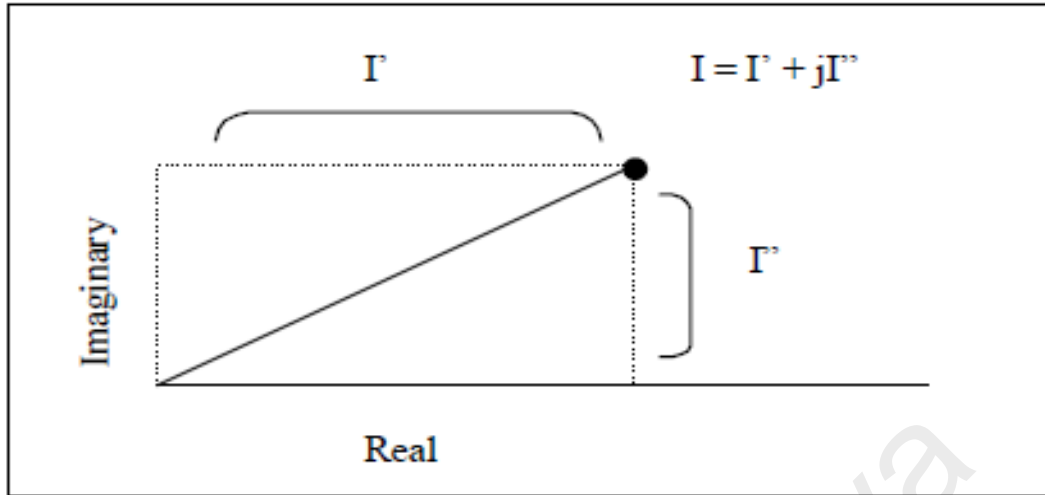


Figure 3.4: Vector in Terms of Real (I') and Imaginary (I'') coordinates

Using the complex number convention, an A.C current vector can be defined as the sum of its real and imaginary components:

$$I_T = I' + I'' j \quad (3.4)$$

where; $j = \sqrt{-1}$

Equation 3.2 can be used to calculate the impedance vector as the quotient of the voltage and current vectors:

$$Z_T = \frac{E' + E'' j}{I' + I'' j} \quad (3.5)$$

where the A.C voltage vector, E , can also be expressed as a complex number.

$$E_T = E' + E'' j \quad (3.6)$$

The resulting vector expression for the ac impedance,

$$Z_T = Z' + Z'' j \quad (3.7)$$

is defined in terms of the same coordinate axes as the current and voltage vectors.

The absolute magnitude of the impedance (that is, the length of the vector) can be expressed as

$$|Z| = \sqrt{Z'^2 + Z''^2} \quad (3.8)$$

and the phase angle can be defined by:

$$\tan \phi = \frac{Z''}{Z'} \quad (3.9)$$

In polar form, Z may be written as

$$Z(\omega) = |Z| \exp(j\omega) \quad (3.10)$$

where

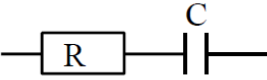

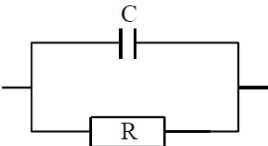
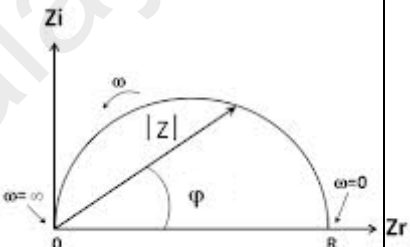
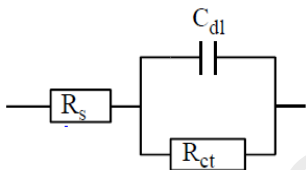
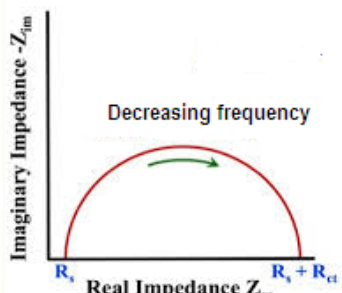
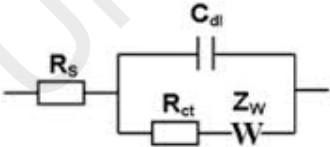
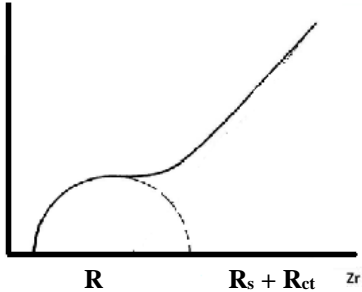
$$\exp(j\omega) = \cos(\phi) + j \sin(\phi) \quad (3.11)$$

The real and imaginary impedances are evaluated as a function of frequency. In general, the complex impedance may be written for any circuit by taking R for a resistance, $1/j\omega C$ for a capacitance and $j\omega L$ for an inductance. The data collected is analyzed in the form of impedance plots. Several examples of equivalent circuit and the impedance plot are shown Table 3.2. From the complex impedance plots bulk resistance of the sample is obtained. The room temperature ac conductivity of the sample (σ) can then be calculated using the equation:

$$\sigma = \frac{t}{R_b A} \quad (3.12)$$

where t is thickness of the film, A is the cross-sectional area and R_b is the bulk resistance.

Table 3.2: Example of equivalent circuits and the impedance plots in A.C impedance measurements.

Circuit element	Impedance equation	Impedance plot
	$Z(j\omega) = R - \frac{j}{\omega C}$	
	$Z(j\omega) = \frac{R}{1 + j\omega RC}$	
 <p data-bbox="316 1335 647 1424"> C_{dl} : Double layer capacitance R_{ct} : Charge-transfer resistance </p>	$Z(j\omega) = R_s - \frac{1}{1/R_{ct} + j\omega C_{dl}}$	
 <p data-bbox="344 1783 616 1816"> Z_w : Warburgh Impedance </p>	$\text{Re}(Z) = R_s + R_{ct} \left(1 + \frac{\lambda}{\sqrt{2\omega}} \right)$ $\text{Im}(Z) = \frac{R_{ct} \lambda}{\sqrt{2\omega}}$	

In this study, the electrical conductivity of gel polymer electrolytes was measured using a HIOKI 3532-50 LCR Hi Tester which is interfaced to a computer for data acquisition over the frequency range between 50 Hz and 1 MHz. Figure 3.5 shows the experimental setup for conductivity measurement. The film was placed between two stainless steel electrodes which acted as a blocking electrode for ions. The electrical conductivity is measured six times with different portions of the samples. The impedance measurements are also done to study the effect of temperature on the conductivity as discussed in Chapter 2. The conductivity-temperature dependence measurements are carried out to analyze the mechanism of ionic conduction in the GPE films. The conductivity - temperature studies are conducted in the temperature range between 303 K and 373 K.

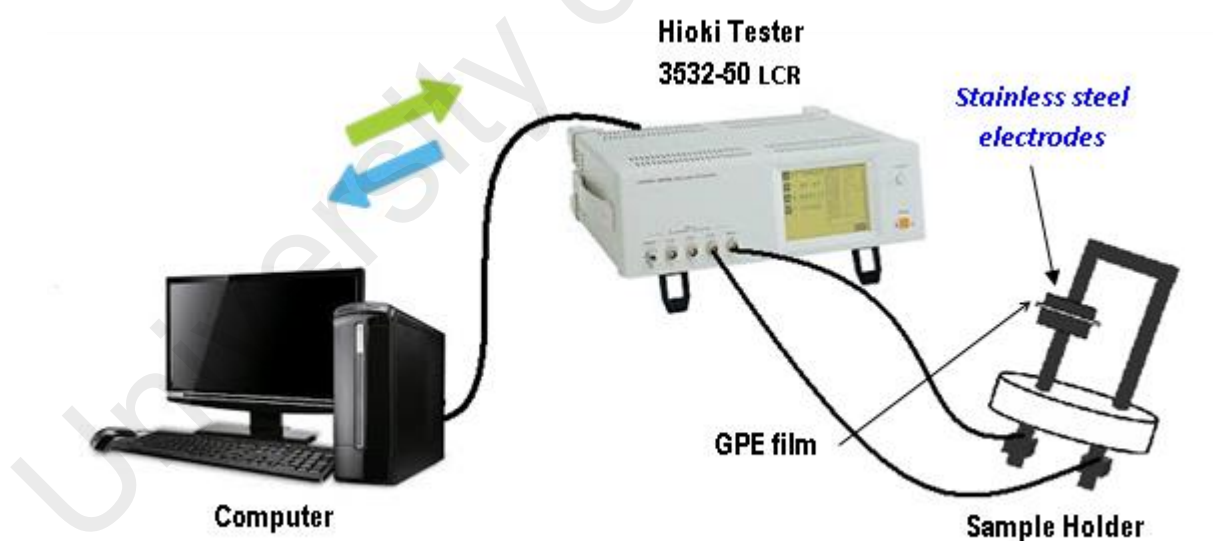


Figure 3.5: Experimental setup for conductivity measurement.

3.3.2 Transport number measurements

The transport number measurement was done to estimate the type of mobile ions that exist in the GPE films. The measurement can be used to determine what fraction of current is carried by which mobile species. In the polymer electrolytes the mobile species may refer to ionic (cation or anion) or free electron that will take part in the conduction process. The measurement can be carried out using DC polarization and combined AC impedance techniques as discussed below in brief.

DC polarization measurement to evaluate the ionic transport number (t_{ion})

The method also known as a Wagner's technique (Pandey, Agrawal, & Hashmi, 2009) is used to determine the ionic contribution to the total charge transport by measuring the residual electronic current passing through the gel polymer electrolytes. A fixed DC voltage is applied across the GPE film sandwiched between stainless steel blocking electrodes and the DC current passing through the sample is monitored as a function of time until the samples become fully polarized. Figure 3.6 shows the typical current versus time plot for DC polarization measurement. At the initial point of the plot, it can be seen that the peak current decrease rapidly with time. This is due to polarization of mobile ions at electrode/electrolyte interface. For pure ion conductor, the current decrease approaches zero while for the mixed ionic-electronic conductor, the current attains a residual constant value. The initial total current, (I_T) is the sum of ionic (I_i) and electronic currents (I_e);

$$I_T = I_i + I_e \quad (3.13)$$

The final current after polarization (constant residual current) is only due to electron conduction. From the plot of ‘current versus time’, the ionic transference number, t_i can be determined using the following equation;

$$t_i = \frac{I_i}{I_T} = \frac{I_T - I_e}{I_T} = 1 - \frac{I_e}{I_T} \quad (3.14)$$

In this work, the measurement was done using WONATECH system. A fixed voltage, 0.5 V is applied across the GPE film sandwiched between two stainless steel electrodes and the current is observed.

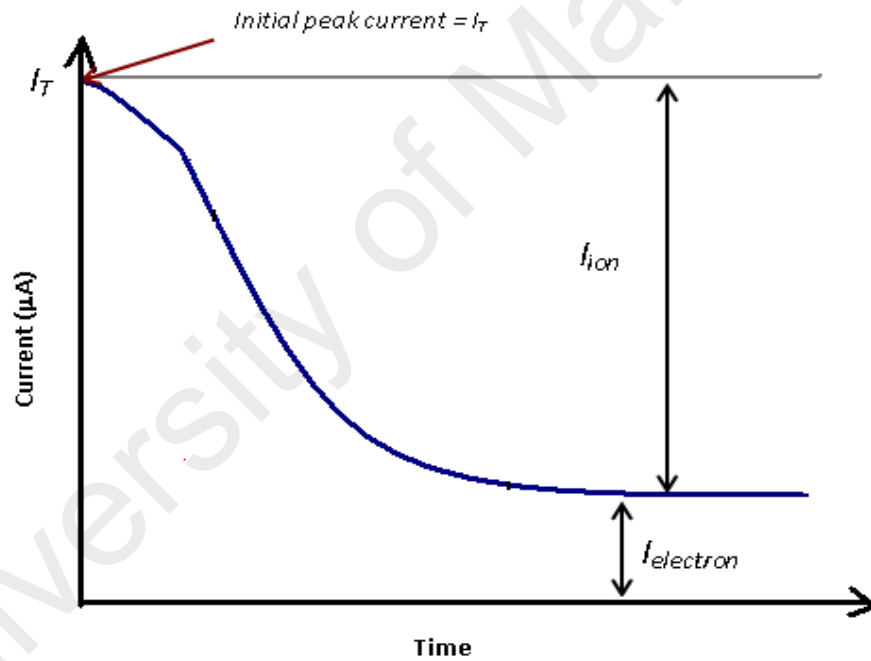


Figure 3.6: A typical current versus time plot for DC polarization measurement

Combined DC/AC method to evaluate the cationic transport number (t_+)

This measurement technique has been proposed by Evans and co-workers (Evans et al., 1987) to determine the cationic transference number, t^+ . In this work, A Hioki 3532 HIOKI 3532-50 LCR Hi Tester and Wonatech system were used to carry out the

experiments. The cation transference number was measured using Li |GPE| Li and Na |GPE| Na cell for lithium-based system and sodium-based system where the electrolyte sandwiched between two non-blocking metal electrodes. Firstly, the A.C impedance measurement was performed on the cell and the value of the resistance before the polarization, R_o is obtained from the complex impedance plot. Then the cell was polarized by applying a small DC voltage, ΔV across the cell and the current response is recorded with time, until a steady state value is observed. The value of initial, I_i and steady-state, I_s currents can be determined from the current versus time plot. Afterwards, the sample is immediately measured again using AC impedance to determine the value of resistance after polarization, R_s . The cationic transference number of the GPE samples was calculated from the following equation (Evans et al., 1987)

$$t_+ = \frac{I_s(\Delta V - I_o R_o)}{I_o(\Delta V - I_s R_s)} \quad (3.15)$$

where ΔV is the dc polarization voltage applied across the electrolyte film. Another equation that can be used to determine the cationic transference number is (Abraham et al., 1997):

$$t_+ = \frac{I_s R_f (\Delta V - I_o R_o)}{I_o R_o (\Delta V - I_s R_s)} \quad (3.16)$$

Where R_f represent final resistance of the electrolytes. This method will be used when the resistance before and after polarization is not the same.

3.3.3 Differential Scanning Calorimetry (DSC)

Differential Scanning Calorimetry (DSC) is a thermal analysis technique commonly used to determine glass transition temperature, T_g and melting temperature (crystalline point), T_m of polymeric materials. According to the classification, calorimetry is a technique for experimental quantification of heat that is either absorbed or released by a substance undergoing a physical or a chemical change. It can be used to measure the change in enthalpy associated with the process of a chemical reaction, such as heat of reaction (Δ_rH). Calorimetry can be conducted at either constant pressure or volume and allows one to monitor the change in temperature as a result of the chemical process being investigated.

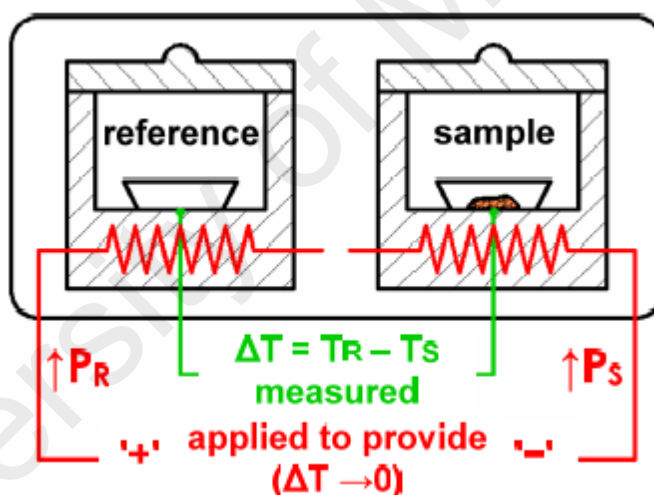


Figure 3.7: Schematic diagrams Differential Scanning Calorimeter
(Schematic_DSC, 2013)

The calorimeter consists of a sample holder and a reference holder as shown in Figure 3.7. The sample and reference sample are heated or cooled individually in a way that their temperatures are always equal. The differential heat flow between the sample and reference is continuously monitored. If a temperature difference is detected, then heat will be added to the cooler holder by supplying additional power to compensate for the difference. The difference between the power applied to the investigated specimen

and into the reference specimen is measured as a function of temperature and/or time.

Since the DSC is at constant pressure, heat flow is equivalent to enthalpy changes:

$$\left(\frac{\partial q}{\partial t}\right)_p = \frac{\partial H}{\partial t} \quad (3.17)$$

The heat flow difference between the sample and the reference is:

$$\Delta\left(\frac{\partial H}{\partial t}\right)_p = \left(\frac{\partial H}{\partial t}\right)_{sample} - \left(\frac{\partial H}{\partial t}\right)_{reference} \quad (3.18)$$

When $\Delta\delta H/\delta t$ is a negative value, the process is exothermic and releases heat; when $\Delta\delta H/\delta t$ is a positive value, the process is endothermic and requires heat input.

The output yielded by differential scanning calorimetry is called a differential thermogram, which plots the required heat flow against temperature. Data analysis is highly dependent on the assumption that both the reference and sample cells are constantly and accurately maintained at equal temperatures. The typical DSC thermograph is shown in Figure 3.8. The graph indicates the change in power (electrical heat) as the temperatures of the two cells are gradually increased. The area of the DSC thermogram (melting and crystallization peaks) can be used to estimate the enthalpy of transition, ΔH . A change in specific heat results in a small change in power, and can be either positive or negative depending on the particular process. The advent of an endothermic reaction will cause an increase in power as temperature increases, since additional heat is required to drive the reaction and still maintain the reference temperature. When an exothermic reaction occurs, the opposite effect is observed; power decreases because heat is released by the reaction and less power is required to maintain equivalent temperatures in the sample and reference holders.

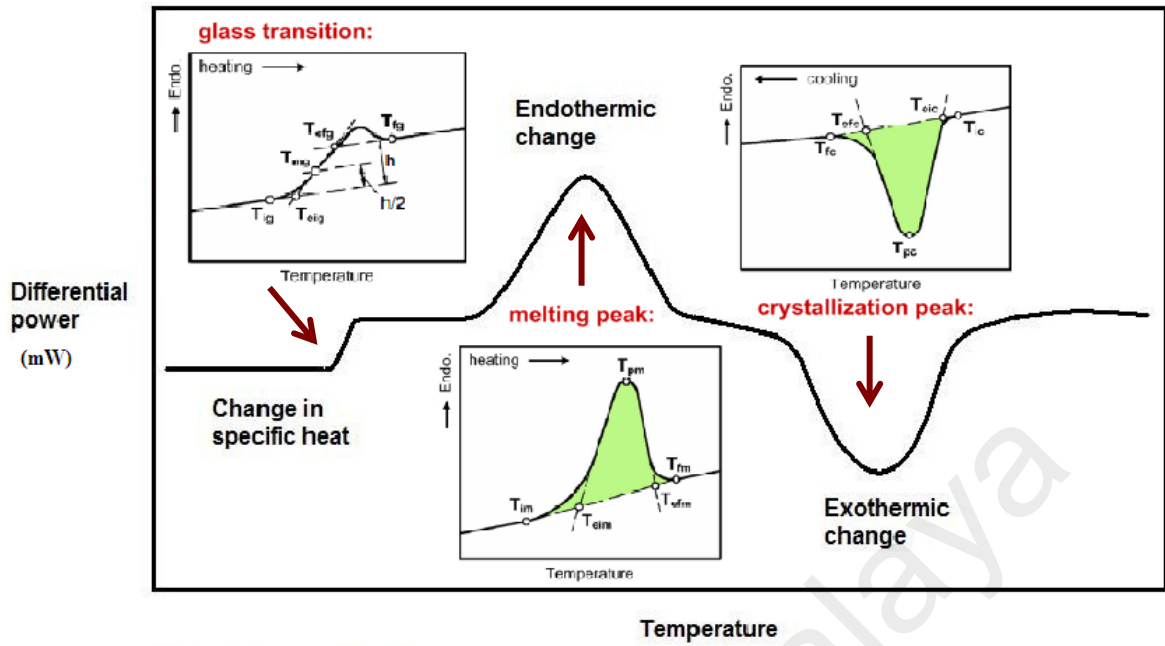


Figure 3.8: Typical DSC thermogram

In this work, DSC results of the GPE samples are obtained using Perkin Elmer DSC Instrument at Physics Department. The temperature range used is between $-50\text{ }^{\circ}\text{C}$ and $350\text{ }^{\circ}\text{C}$ with heating/cooling rate of $10\text{ }^{\circ}\text{C}/\text{min}$. The DSC plot was analyzed using TA Instrument Explorer software in order to find the glass transition temperature (T_g), melting point (T_m) and decomposition temperature (T_d) of the GPE films.

3.3.4 Thermogravimetry Analysis

Thermogravimetry analysis is the branch of thermal method based on the measurement of mass loss of material as a function of temperature or time when it is heated or cooled at a predetermined rate. It also provides information on the decomposition and thermal stability of the material at different temperatures and pressures of the environmental gases. It can analyze characterization of materials such

as polymers, to determine degradation temperatures, absorbed moisture content of materials, the level of inorganic and organic components in materials, decomposition points of explosives, and solvent residues.

The schematic principle of the TGA measurement is shown in Figure 3.9. The sample is heated under nitrogen or synthetic air with constant heat rate while the difference of the mass during this process is measured. A mass loss indicates that a degradation of the measured substance takes place. The reaction with oxygen from the synthetic air for example could lead to an increase of mass.

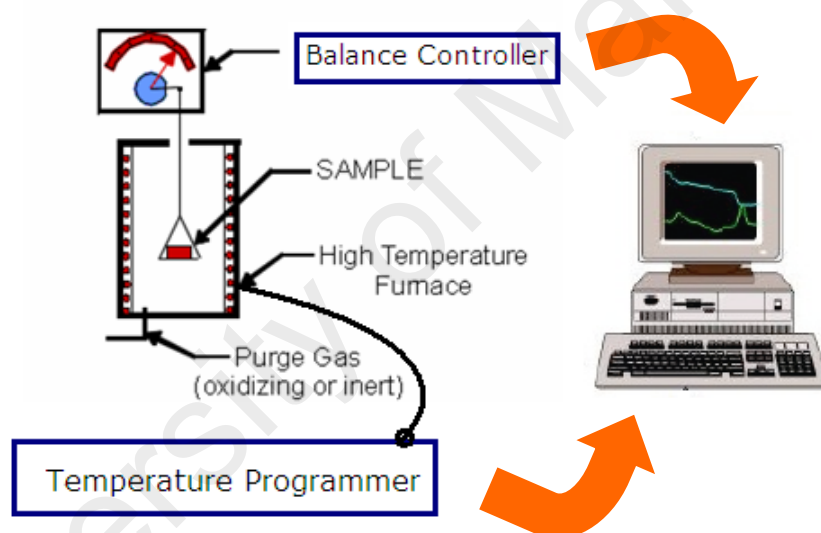


Figure 3.9: Schematic principle of TGA measurement

Mechanisms of Weight Change

At low temperatures, weight loss may originate from evaporation of residual moisture or solvent, but at higher temperatures weight loss can arise from a various processes including:

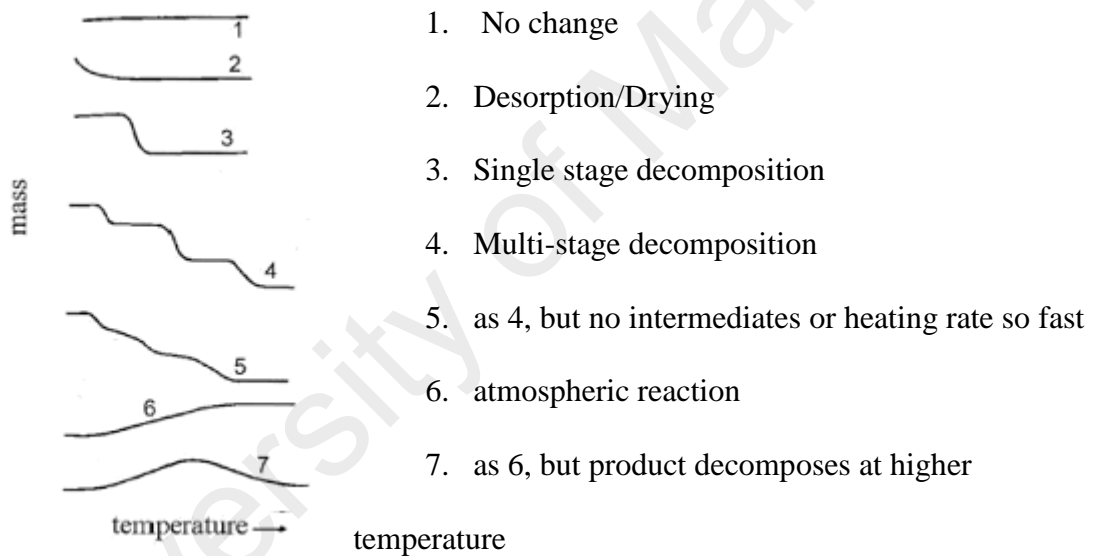
- 1) Decomposition: The breaking apart of chemical bonds
- 2) Evaporation: The loss of volatiles with elevated temperature

- 3) Reduction: Interaction of sample to a reducing atmosphere (hydrogen, ammonia, etc).
- 4) Desorption

Weight gain processes may also be observed and measured with TGA. For example:

- 1) Oxidation: Interaction of the sample with an oxidizing atmosphere
- 2) Absorption

Typical TGA curves



The results of a TGA measurement are usually displayed in a TGA curve. TGA curves are normally plotted with the mass change (Δm) expressed as a percentage on the vertical axis and temperature (T) or time (t) on the horizontal axis as shown in Figure 3.10.

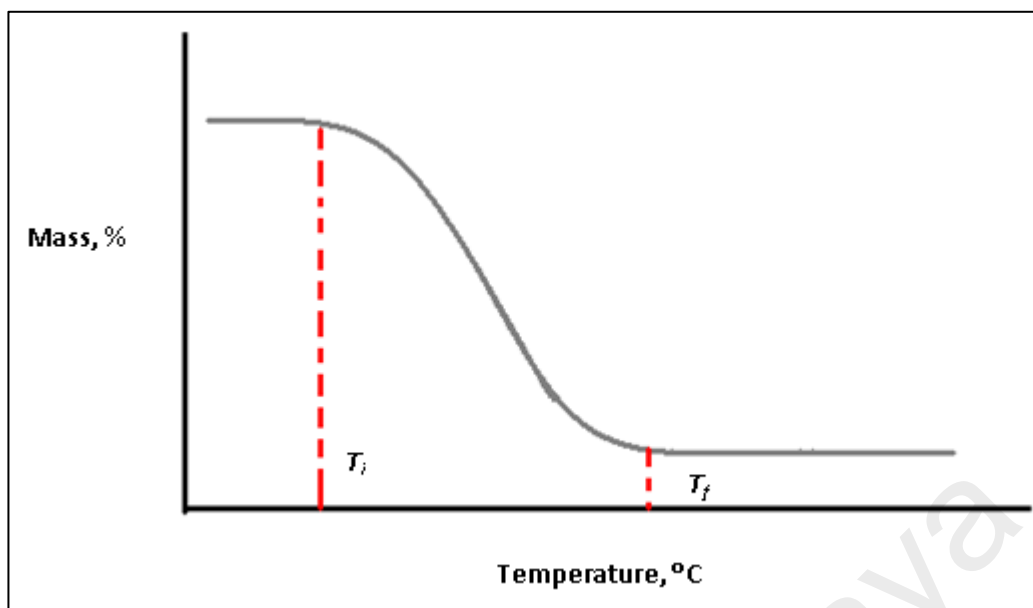


Figure 3.10: Typical TGA curve

The reaction is characterized by two temperatures, T_i and T_f , which are called the procedural decomposition temperature and the final temperature, respectively. T_i is defined as the lowest temperature at which the onset of a mass change can be detected by thermo balance operating under particular conditions and T_f as the final temperature at which the particular decomposition appear to be completed. We can also present derivative thermogravimetric (DTG) Curves in the thermogram to resolves changes more clearly. A DTG curve presents the rate of mass change ($\delta m/\delta t$) as a function of temperature, or time (t) against T on the (x axis) as shown in Figure 3.11 when substance is heated at uniform rate. In this figure, the derivative of the curve is shown by dotted lines.

In this work, TGA plots for all the GPE samples were obtained using Perkin Elmer Instrument. The experiment is conducted in temperature range from -90 to 350 °C with heating rate of 10 °C/min. The thermograms provide information such as the thermal

stability and percentage weight loss of the component(s) and the decomposition temperature of the polymer electrolyte films.

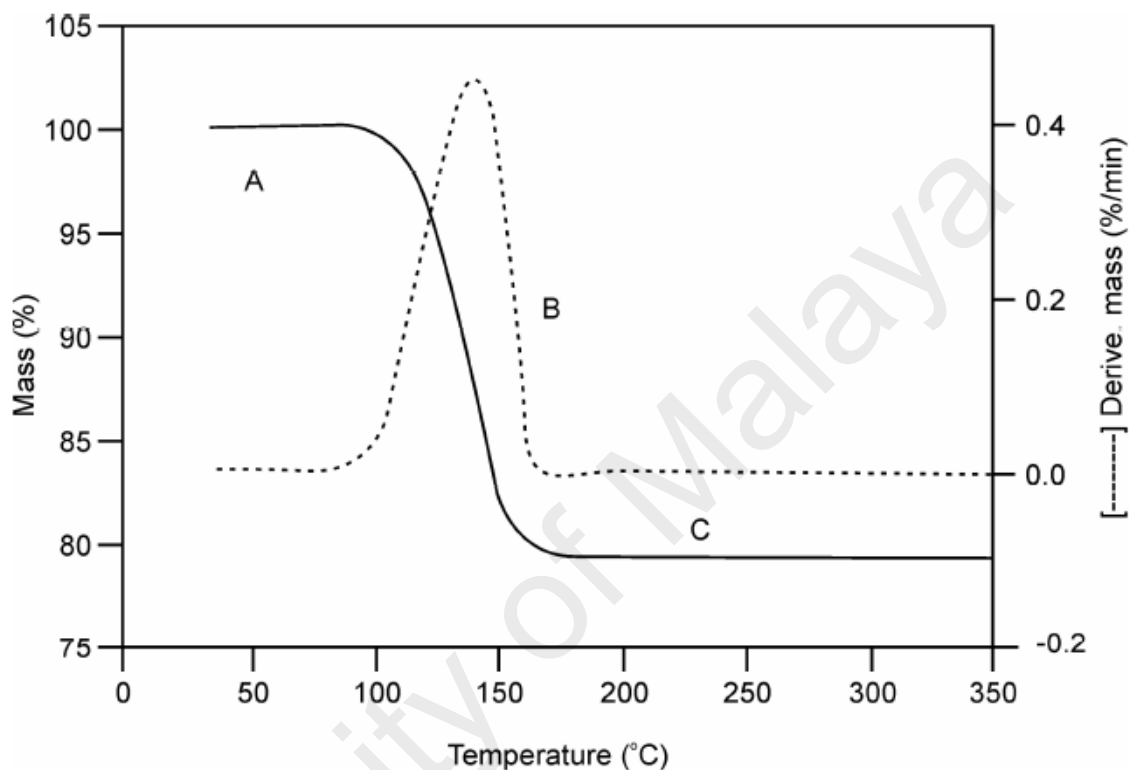


Figure 3.11: TGA -DTA Curve. Note the plateau of constant weight (region A), the mass loss portion (region B), and another plateau of constant mass (region C)

3.3.5 Fourier Transfer Infrared Spectroscopy (FTIR)

FTIR is a useful tool that is the most widely method used to obtain information about the chain structure, chemical composition and physical properties (i.e., chain orientation, crystallinity, and chain conformation or chain dynamics) of the polymer electrolytes sample.

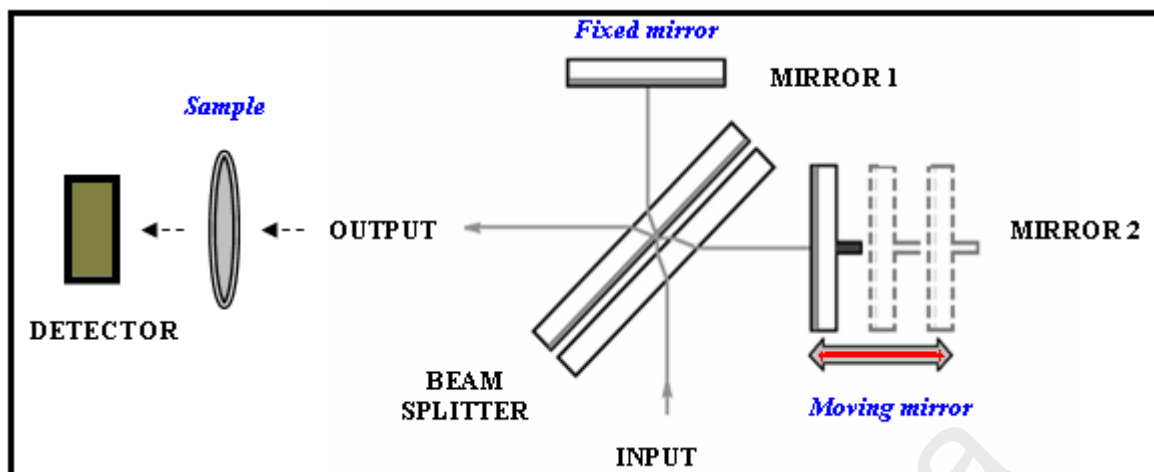


Figure 3.12: A Schematic of a generic Michelson interferometer

FTIR is based on the fundamental principles of molecular spectroscopy. It relies on the fact that the most molecules absorb light energy in the infrared region, known as their resonance frequencies. For example, the water molecule resonates around the 3450 wavenumber (given the symbol cm^{-1}), in the infrared region of the electromagnetic spectrum. Most of the commercially available FTIR spectrometers use the Michelson interferometer as shown in Figure 3.12. The basic Michelson Interferometer consists of:

- i. SOURCE: a broad-band light source which emits light covering the mid-IR range,
- ii. BEAM SPLITTER: a beam splitter made of KBr or CsI
- iii. MIRROR: Two front surface coated mirrors-one moving and one fixed
- iv. DETECTOR: The detectors used are specially designed to measure the special interferogram signal.

During the FTIR analysis, a small quantity of sample is introduced to the infrared cell, where it is subjected to an infrared light source, which is scanned from 4000 cm^{-1} to around 650 cm^{-1} . The sample is placed in the combined beam (just before the detector

in Figure 3.12). Radiation from the source strikes the beam splitter and separates into two beams. One beam is transmitted through the beam splitter to the fixed mirror and the second is reflected off the beam splitter to the moving mirror. The fixed and moving mirrors reflect the radiation back to the beam splitter. Again, half of this reflected radiation is transmitted and half is reflected at the beam splitter, resulting in one beam passing through the sample compartment and finally passes to the detector, and the second back to the source. The intensity of light transmitted through the sample is measured at each wavenumber allowing the amount of light absorbed by the sample to be determined as the difference between the intensity of light before and after the sample cell. This is known as the infrared spectrum or interferogram of the sample. Once interferogram is collected, it needs to be converted from intensity versus time spectrum into intensity versus frequency spectrum. The process of conversion is through mathematical function called a Fourier transform. The mathematical expression of Fourier transform can be expressed as

$$F(\omega) = \int_{-\infty}^{+\infty} f(x)e^{i\omega x} dx \quad (3.19)$$

And the reverse Fourier transform is

$$f(x) = \frac{1}{2\pi} \int_{-\infty}^{+\infty} f(\omega)e^{i\omega x} d\omega \quad (3.20)$$

where ω is angular frequency and x is the optical path difference between the beams travelling through the two arms of an interferometer. $F(\omega)$ is the spectrum and $f(x)$ is called the interferogram. It is clear that if the interferogram $f(x)$, is determined experimentally, the spectrum $F(\omega)$ can be obtained by using Fourier transform.

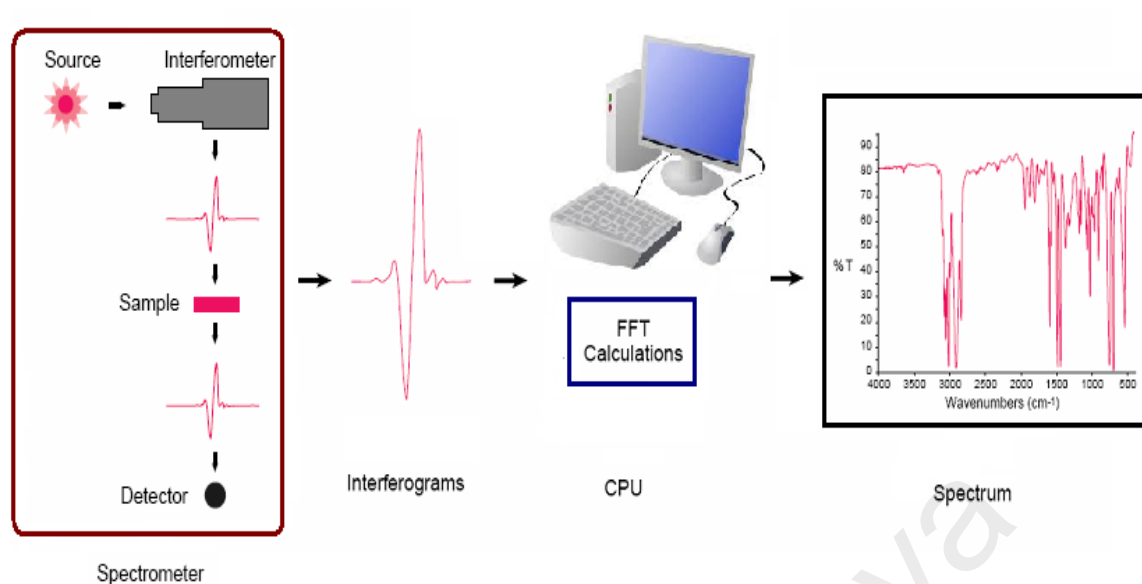


Figure 3.13: The sample analysis process
(Analysis_FTIR, 2013)

The IR region is commonly divided into three areas: near - IR ($400 - 10 \text{ cm}^{-1}$), mid - IR ($4000 - 400 \text{ cm}^{-1}$), and far - IR ($14000 - 4000 \text{ cm}^{-1}$). Infrared radiation is absorbed by organic molecules and converted into energy and cause groups of atoms to vibrate with respect to the bonds that connect them. When the radiant energy matches the energy of a specific molecular vibration, absorption occurs. A typical IR spectrum is shown in Figure 3.14. The wavenumber, plotted on the X-axis, is proportional to energy while the percent transmittance (%T) is plotted on the Y-axis. Absorption of radiant energy is therefore represented by a “trough” in the curve: zero transmittance corresponds to 100% absorption of light at that wavelength.

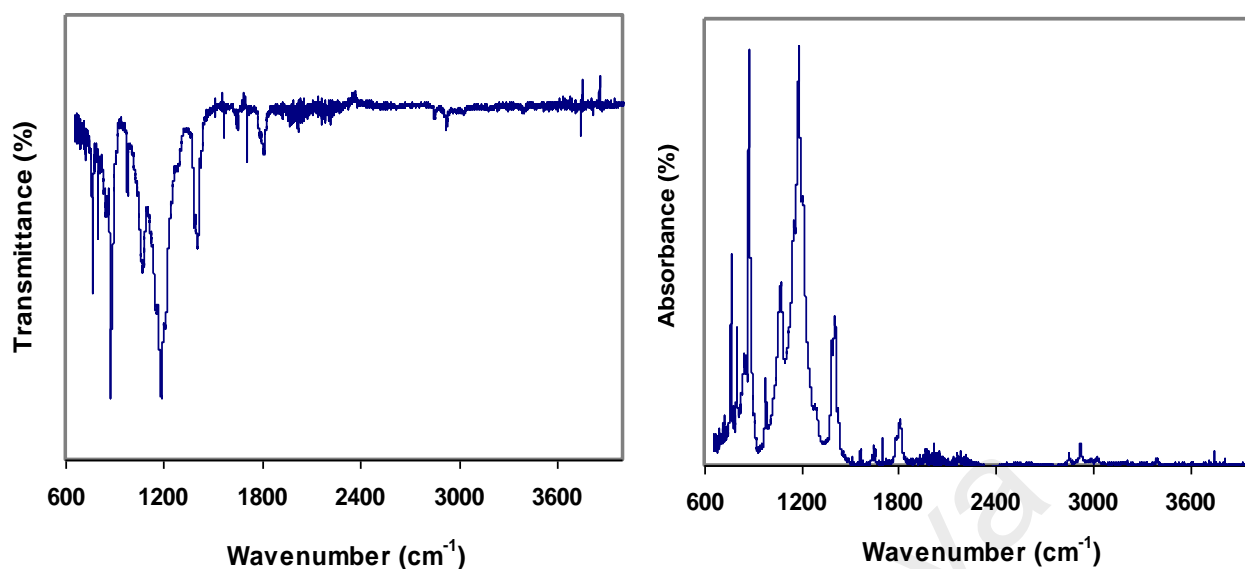


Figure 3.14: The IR spectrum of pure PVdF-HFP, plotted as transmission (left) and absorbance (right).

3.3.6 Raman Spectroscopy

Raman Spectroscopy is a method to measure modes of molecular motions, especially vibrations like the infrared spectroscopy. However, the physical technique of observing the vibration is different from the infrared spectroscopy. The infrared spectroscopy is based on absorption of photons while the Raman spectroscopy measures the light scattering, which studies the scattered photons. A few differences between the two spectroscopic methods are:

- 1) The most intense infrared bands are usually those arising from polar bonds such as O – H, N – H and C = O, while the most intense Raman bands are usually those arising from bonds having nearly symmetrical charge distribution such as C – C, C = C and S – S that are usually found in the substituent.

- 2) Thus, infrared spectroscopy is usually preferred for studying the substituent in polymer, while Raman spectroscopy is preferred for studying the conformation of a polymer.
- 3) Sample handling in Raman spectroscopy is much simpler than in infrared spectroscopy.

This technique based on light scattering of monochromatic light, usually from a laser source. Photons of the laser light are absorbed by the sample and then reemitted. Frequency of the reemitted photons is shifted up or down in comparison with original monochromatic frequency, which is called the Raman Effect. The fundamental equation is:

$$h\nu_0 + E_1 = h\nu_r + E_2 \quad (3.21)$$

Where;

h is the planck constant

ν_0 is the frequency of the incident light (photon)

ν_r is the frequency of the scattered light (photon)

E_1 and E_2 are the initial and the final energies of the molecule

The frequency shift $\nu_r - \nu_0 = \Delta \nu$ maybe either positive or negative in sign. Its magnitude is referred to as the Raman Frequency. The set of Raman frequencies of the scattering species constitutes its Raman Spectrum. The Raman frequency shift is expressed in term of wavenumbers instead of frequencies:

$$\nu = \nu_0 - \nu_r = \frac{E_2 - E_1}{hc} \quad (3.22)$$

where c is the velocity of light

Figure 3.15 shows the diagram for the most important processes involved in light scattering by molecules. Basically, there are two categories of light scattering:

- i. Elastic scattering where the scattered radiation is at the same frequency as the incident radiation, and
- ii. Inelastic scattering where the scattered radiation is at a different frequency.

Elastic scattering of molecules is called Rayleigh scattering. In Rayleigh scattering, the photon energy and molecular energy are both separately conserved. Rayleigh scattering has the highest probability of occurring and is the scattering that gives rise to the blue color of the sky. Raman scattering is inelastic: the total photon plus molecular energy is conserved but the vibrational energy changes and frequency shifts occur in the scattered radiation.

There are two types of Raman scattering phenomena which are distinguished by whether the frequency of incident light is shifted up or down. When the incident radiation is shifted to a lower frequency (lower energy), the scattered light is called Stokes scattering. In this type of scattering energy is transferred to the vibrational mode of the molecule which ends up in a higher vibrational energy state. Similarly, when the incident radiation is shifted to a higher frequency (higher energy), the scattered light is called anti-Stokes scattering. In this type of scattering energy is transferred from a vibrationally excited molecule, which ends up in a lower vibrational state after the scattering event.

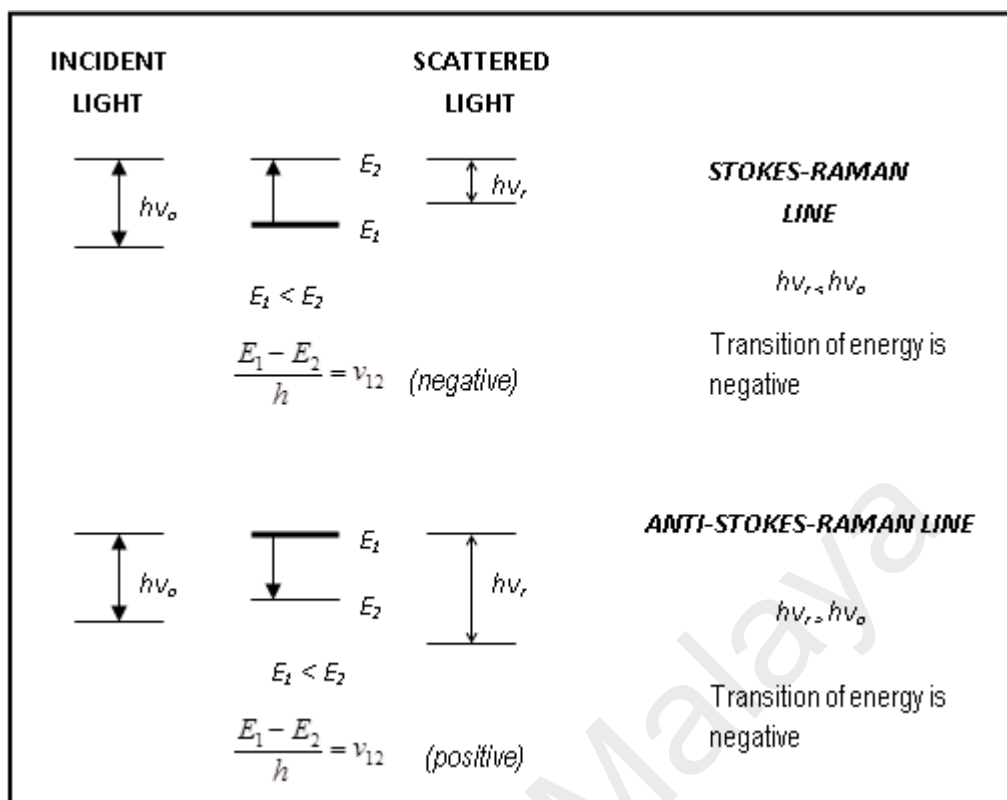


Figure 3.15: Diagram for the most important processes involved in light scattering by molecules

Figure 3.16 shows the typical Raman system. The system typically consists of four major components:

- i. Excitation source, usually a visible-light laser
- ii. Sample illumination system and light collection optics.
- iii. Wavelength selector (Filter or Spectrophotometer).
- iv. A signal processing system consisting of a detector and a data processing unit

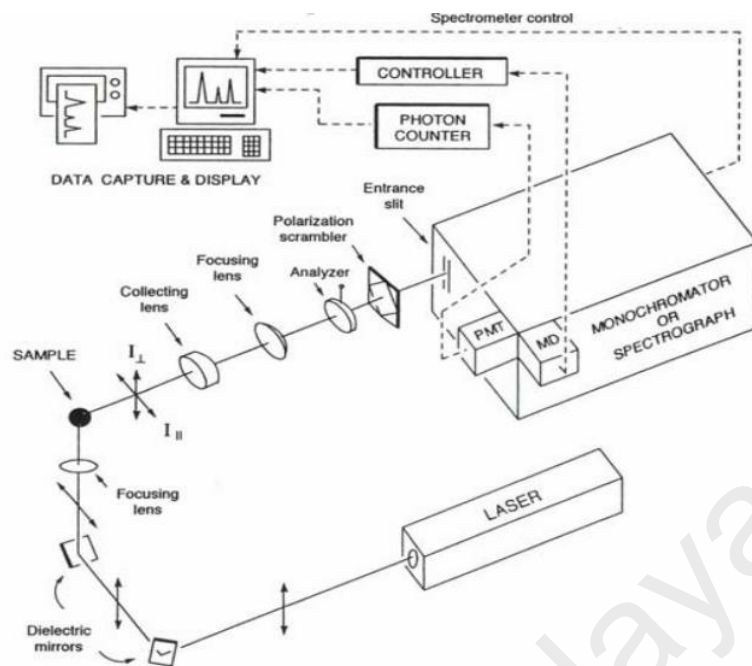


Figure 3.16: Schematic of typical Raman system

A sample is normally illuminated with a laser beam in the ultraviolet (UV), visible (Vis) or near infrared (NIR) range where photons of a single wavelength are focused onto the sample. The photons interact with the molecules excite the molecule from the ground state to a virtual energy state. The scattered light is collected with a lens and is sent through interference filter or spectrophotometer to obtain Raman spectrum of a sample. Figure 3.17 shows the typical Raman spectra.

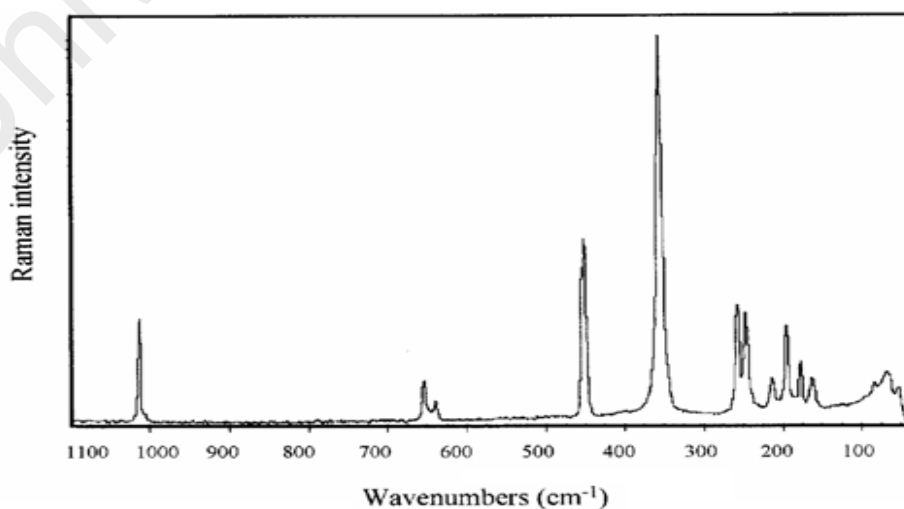


Figure 3.17: A typical Raman spectra

3.3.7 X-Ray Diffraction

X-ray diffraction is an analytical technique used to obtain the structural information of crystalline solids. The technique provides information include types and nature of crystalline phases present, structural make-up of phases, degree of crystallinity, amount of amorphous content, microstrain, size and orientation of crystallites.

A schematic of the x-ray diffractometer is shown in Figure 3.18. The main components are the x-ray source, a goniometer (or crystal orienter), a detection system, and a computer control system. The x-ray source is a high-vacuum tube, and the x-ray beam passes out of the tube through a thin window. A single crystal is generally mounted on the end of a glass fiber. This fiber is then attached to a metal pin which is secured to the goniometer head. The goniometer precisely orients the sample in the x-ray beam. As the x-rays pass through the crystal, the detector collects information to generate a diffraction pattern. Finally, the computer control system processes the information from the detector, and the structure of the crystal is solved.

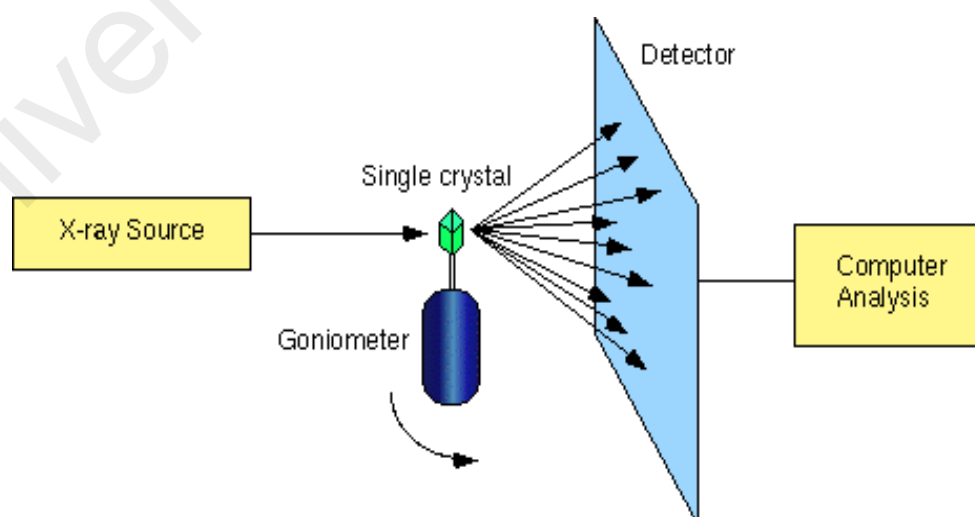


Figure 3.18: A schematic of an x-ray diffractometer
(Schematic_XRD, 2013)

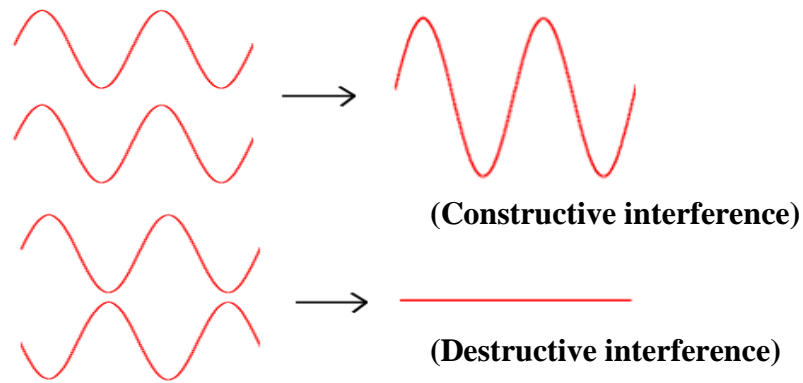


Figure 3.19: Constructive and destructive interferences

When X-rays are scattered from a crystalline solid they can constructively interfere, producing a diffracted beam. There are two types of interference depending on how the waves overlap one another. To understand how a diffraction pattern occurs, consider the diffraction patterns of two waves. Two waves of the same wavelength can come together either in phase or out of phase. If the two waves come together in phase, this means that the maxima and minima of both waves are at the same points. In other words, the hills and the valleys from both waves are lined up together. The waves reinforce or cause constructive interference, and the intensity of the resultant wave is increased. Conversely, two waves coming together out of phase have each minimum from one wave combining with a maximum of the other wave. The hills from the first wave line up with the valleys from the second wave while the valleys from the first wave line up with the hills from the second wave. This is called destructive interference and destroys the wave. Figure 3.19 shows constructive and destructive interferences.

In a crystal, x-rays are reflected from the different planes of atoms that are present. If two x-rays travel to two different planes, then one x-ray must travel further than the other. The x-rays may end up out of phase after they are reflected. Only at certain

angles of reflection do the two rays remain in phase. In the diffraction pattern, dark areas are caused by destructive interference while brighter areas are caused by constructive interference. The general relationship between the wavelength of the incident X-rays, angle of incidence and spacing between the crystal lattice planes of atoms is known as Bragg's Law, expressed as:

$$n\lambda = 2d \sin \theta \quad (3.18)$$

where n (an integer) is the "order" of reflection, λ is the wavelength of the incident X-rays, d is the spacing between the atomic planes (interplanar spacing of the crystal) and θ is the angle of diffraction. The concept used to derive Bragg's law is very similar to that used for Young's double slit experiment. The angle between the transmitted and diffracted beams will always be equal to 2θ . This angle can be obtained readily in experimental situations and the results of X-ray diffraction are therefore given in terms of 2θ .

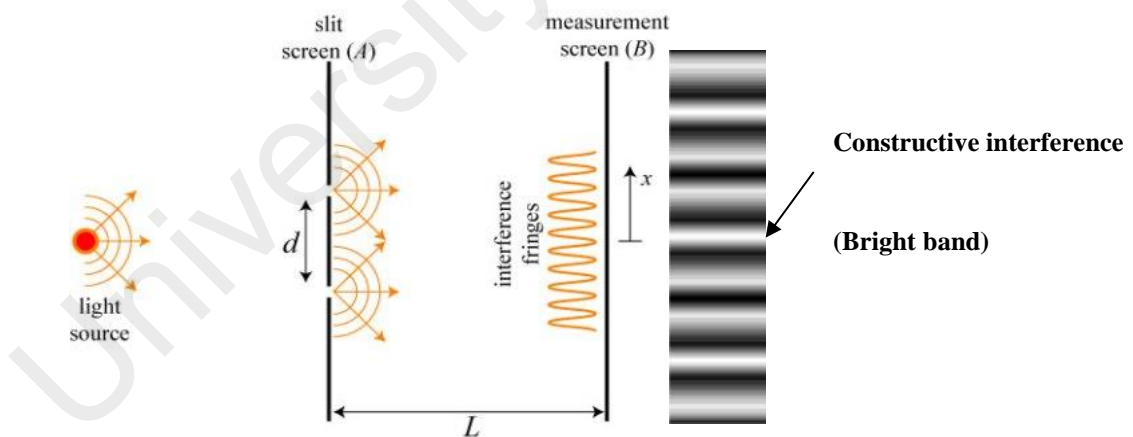


Figure 3.20: A simple schematic of the Young's double slit experiment
(Optics basics_ XRD, 2013)

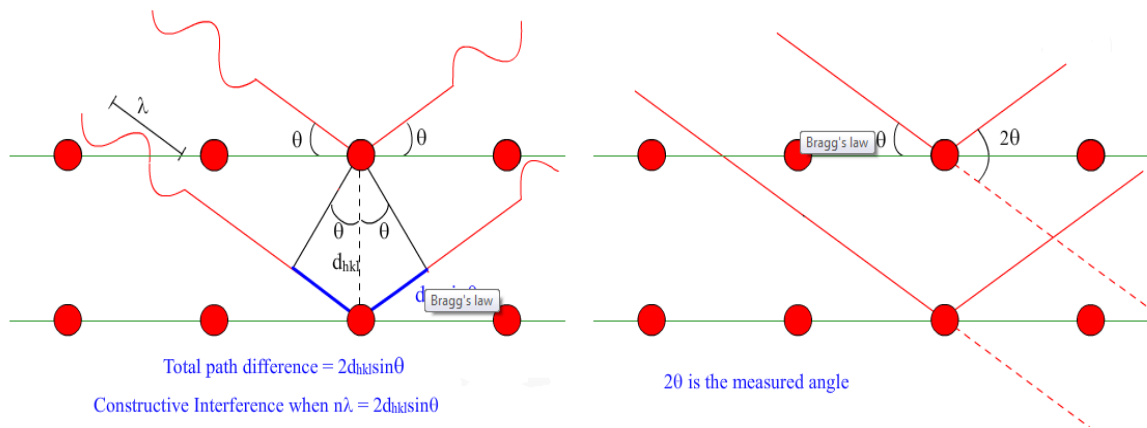


Figure 3.21: Bragg's Law reflection
 (Bragg's_Law, 2013)

In this work, the X'Pert PRO PANalytical diffractometer was used to investigate the nature of crystallinity and the amorphousness of the GPE films. The influence of the presence of solvent plasticizers and the amount of salt on the structural changes was observed.

3.3.8 Field Emission Scanning Electron Microscopy (FESEM)

FESEM is a technique that can be used by researchers in biology, chemistry and physics to observe small structure (as small as 1 nanometer) on the surface of cells and materials. It can be classified as a high vacuum instrument (less than 1×10^{-7} Pa in the gun zone). The vacuum allows electron movement along the column without scattering and helps prevent discharges inside the gun zone.

The main difference between FESEM and the conventional SEM is the emitter type. The conventional SEM generally used Thermionic Emitter as an electron gun. The emitter used electrical current to heat up the filament. The most common material used for filament is tungsten or lanthanum hexaboride (LaB_6). When the heat is enough to

overcome the work function of the filament material, the electrons can escape from the material itself. However, the thermionic source has disadvantages such as short lifetime, low brightness, and large energy spread. Beside that it is depend on high temperature to produce electron. Field Emission is good alternative of generating electrons that avoids these problems. A Field Emission Gun (FEG); also called a cold cathode field emitter, does not heat the filament. The emission is reached by placing the filament in a huge electrical potential gradient. The FEG is usually a wire of Tungsten (W) fashioned into a sharp point. The significance of the small tip radius (~ 100 nm) is that an electric field can be concentrated to an extreme level, becoming so big that the work function of the material is lowered and electrons can leave the cathode. FESEM uses Field Emission Gun producing a cleaner image, less electrostatic distortions and spatial resolution < 2 nm (that means 3 or 6 times better than SEM) (Principle_FESEM, 2013). However, field emitters must operate under ultrahigh vacuum (better than 10^{-9} Torr) to stabilize the electron emission and to prevent contamination.

Figure 3.22 shows the schematic diagram of FESEM microscope. FESEM works with electrons instead of light to form an image. These electrons are liberated by a field emission source and accelerated in a high electrical field gradient. The object is scanned by electrons according to a zig-zag pattern. Within the high vacuum column these so-called primary electrons are focussed and deflected by electronic lenses to produce a narrow scan beam that bombards the object. As a result secondary electrons are emitted from beam spot on the object. The angle and velocity of these secondary electrons relates to the surface structure of the object. A detector catches the secondary electrons and produces an electronic signal. This signal is amplified and transformed to a video scan-image that can be seen on a monitor or to a digital image that can be saved and processed further.

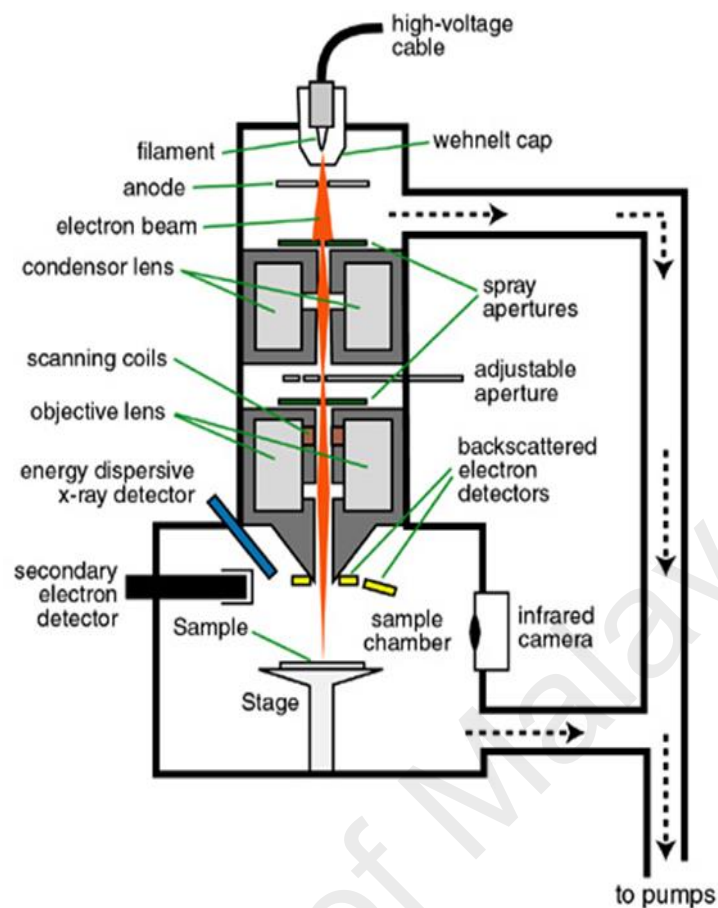


Figure 3.22: The schematic diagram of FESEM microscope
(Schematic_ FESEM, 2013)

The micrographs obtained from FESEM provide important information on the surface structure and morphology of almost of any samples. The nature and morphology of a polymer electrolyte film surface is one of important properties for the polymer electrolytes. In this work, FESEM micrographs of the samples are obtained using FESEM Quanta FEG 450 due to its variable vacuum strength which can retain the structure of the samples.

3.3.9 Linear Sweep Voltammetry

Linear Sweep Voltammetry (LSV) is the most basic potential sweep technique that commonly used by researchers today as it provides an efficient and straightforward assessment of the redox behavior of molecular systems. In other words, it can be used to analyze any chemical species that is electroactive, i.e. which can be made to oxidize or reduce.

In typical LSV method, a solution component is electrolyzed (oxidized or reduced) by placing the solution in contact with an electrode surface and then making that surface sufficiently positive or negative in voltage to force electron transfer. The experimental setup for this method uses combination of three electrode i.e reference electrode, working electrode (the electrode under study), and counter electrode and sometimes referred to as a three-electrode setup as illustrated in Figure 3.23. The current between working electrode and counter electrode is measured while the potential or voltage between reference electrode and working electrode is swept linearly in time. The potential of the electrode is the controlled parameter that causes the redox reaction. As the potential of the electrode becomes more positive, it becomes more strongly oxidizing. Conversely, if the potential of the electrode becomes more negative, it becomes more strongly reducing. The current measured is a measure of the electron flow i.e due to the electron transfer which takes place when oxidation and reduction occurs on the electrode surface. This type of current is known as a Faradaic current. In voltammetry, the Faradaic current is proportional to concentration.

In this research area, the LSV is widely used to evaluate the electrochemical stability of the electrolytes. The voltage is scanned with scan rate, v (V/s) for a given potential range of an electrolytes cell and presents result in the form of current-voltage plots as

shown in Figure 3.24. A sharp change is observed in the current when the electrolytes cell undergoes oxidation or reduction process within the measured voltage range. Therefore, we can predict and analyze the redox reaction by measuring the amount of current and voltage at this point. From the plot, it is observed that the current changes more significantly in the range of 4.6 – 5.2V and rapidly rises from 5.2V. This indicates that redox reaction occur at voltage higher than 4.6V and thus implies that the cell exhibit stable electrochemical characteristic up to 4.6V.

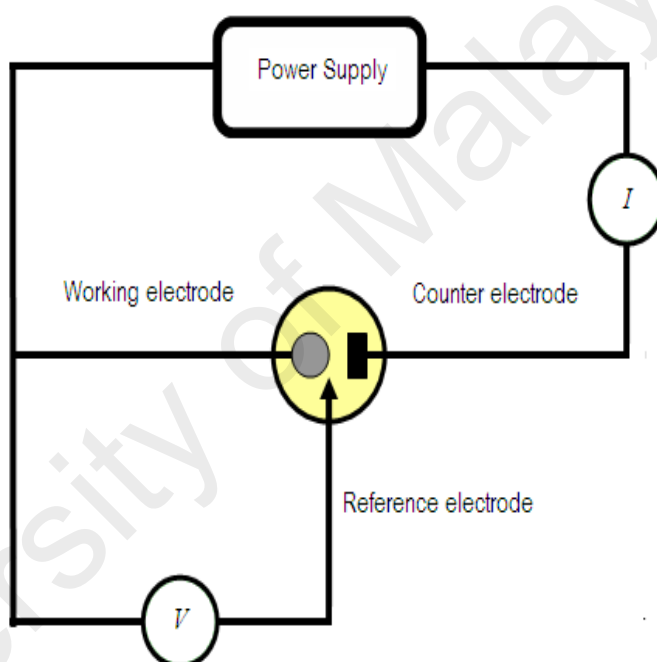


Figure 3.23: Schematic representation of the voltammetry experimental setup

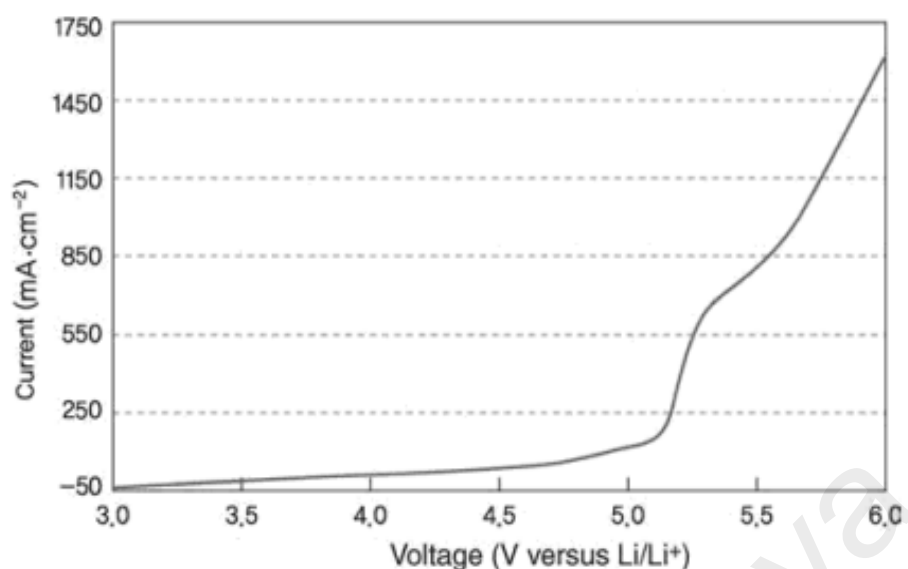


Figure 3.24: Current-Voltage profile of electrolytes cell under LSV
(Park, 2012)

In this work, linear sweep voltammetry was performed on stainless steel working electrode, with counter and reference electrode of lithium or sodium metal at scanning rate of 1.0 mV/s using WonATech system. The GPE film was cut into square shape with dimension of 2 cm by 2 cm. The technique was recorded on the SS|GPE|Li and SS|GPE|Na for lithium-based GPE film and sodium-based GPE film, respectively to determine the electrochemical stability window or working voltage limit of the gel polymer electrolytes.

3.3.10 Cyclic Voltammetry

Cyclic voltammetry (CV) is similar to linear sweep voltammetry where it is also observe changes in current by applying potential voltage under a constant scan rate. However, CV repeat the same experiment for each cycle which the potential scans run from the starting potential to the end potential, then reverse from the end potential back

to the starting potential. Figure 3.25 is a typical cyclic voltammogram that show the changes in current with varying applied potential. Many informations can be obtained from the cyclic voltammogram such as potential, reaction mechanism, quantity of electricity, reversibility and continuity (sustainability of reversible electrochemical reaction).

Cyclic voltammogram also provides several parameter which is the cathodic (E_{pc}) and anodic (E_{pa}) peak potentials, and also the cathodic (i_{pc}) and anodic (i_{pa}) peak currents, as shown in Figure 3.25. The values can be directly obtained from the program and the difference between potential peak of anodic and cathodic sweep, ΔE can be calculated. Theoretically, the potential difference of the redox peaks is 57 - 60 mV for reversible reaction. Larger differences or nonsymmetrical redox peaks indicating a nonreversible reaction.

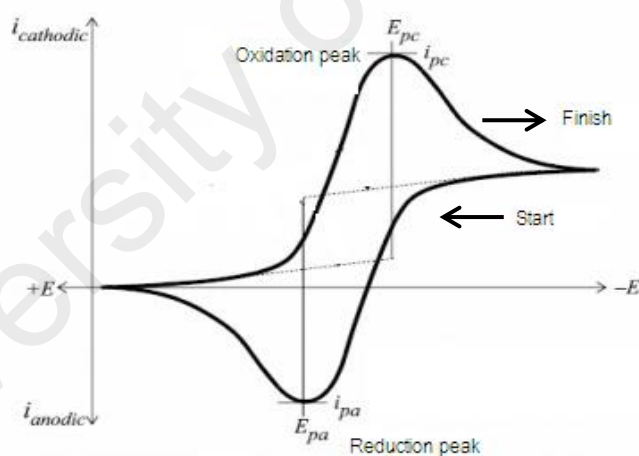


Figure 3.25: Current-voltage in cyclic voltammetry

In this work, cyclic voltammetry has been performed on symmetrical cells SS|GPE-Li|SS (Cell-I), SS|GPE-Na|SS (Cell-II), Li|GPE|Li (Cell-III) and Na|GPE|Na (Cell-IV) for the highest GPE film at room temperature from each system. The geometry of the

samples is similar to that used in LSV analysis. The studies have been carried out in order to confirm the conduction of Li^+ and Na^+ ions in the GPE film.

3.3.11 Battery Fabrication

The manufacturing of ion-polymer battery can be divided into the electrode process, assembly process and chemical process (inspections of charging-discharging).

Cathode and anode

For a cell to be characterized as a secondary battery, the electrode i.e. anode and cathode have to repeat charging and discharging via redox reaction process. For high energy density polymer ion battery, the positive electrode (cathode) is the metal oxide and the negative electrode (anode) is the active natural metals such as lithium, sodium, magnesium, zinc, calcium, etc. The anode materials should have a standard reduction potential similar to that of lithium/sodium so as to stabilize the released ions and provide a large electromotive force. There are various type of Lithium-ion cathode use in commercialized lithium secondary batteries such as Lithium Cobalt oxide (LiCoCO_2), Lithium Manganese Oxide (LiMn_2O_4), Lithium Iron Phosphate (LiFePO_4), Lithium Nickel Manganese Cobalt Oxide (LiNiMnCoO_2) and Lithium Nickel Cobalt Aluminum Oxide (LiNiCoAlO_2). Some widely used anode materials are $\text{Li}_3\text{-Co}_x\text{N}$ ($x = 0.2\text{-}0.6$), KC_8 , SnO_2 and Li_3Sb . The cathode and anode films are fabricated by spreading the materials on metal foils with the help of polymer binder solvents and supported by electron conducting materials such as carbon, acetylene black, etc.

The anode/cathode designations switch depending on whether the battery is charging or discharging. The electrode structure should be kept stable during the insertion and

extraction of ions within electrodes, while an electrolyte acts as an ion transfer medium. The electrolyte is ionically conductive, but electronically non-conductive. The ionically conductive electrolyte completes the electro-chemical circuit by carrying only ions between the active cathode and anode materials.

Generally, the electrolyte consists of an inorganic salt compound in an organic solvent, so that the electrochemical and thermal stability within the range of the working voltage can be maintained. In addition, separators made of polymers or ceramics have a high-temperature melt integrity, which prevents short circuits caused by electrical contact between the cathode and the anode.

In this work, metallic lithium/ sodium was used as an anode in assembly of polymer battery. The metals are readily available in market. However, the cathode was prepared in our laboratory by following these five steps: mixing, coating, drying and cutting. For the mixing process, the binder solution is produce by dissolving the polyvinylidene-flouride (PVdF) in NMP solvent. The lithium nickel cobalt oxide (LiNiCoO_2) and manganese oxide (MnO_2) were used as active material in lithium and sodium cathode, respectively. The super-P carbon was used as a conductive agent for both systems. The active materials and conductive agent using mixture of LiNiCoO_2 or MnO_2 (80%), super-P carbon (10%) and PVdF (10%) are mixed/dispersed in NMP solvent to produce homogeneous slurry. The slurry obtained was then coated onto Al foil under appropriate tension and dried at 80 °C (removing solvent in coated slurry) for a few hours. The coated foil then were cut into the appropriate size and dried in oven at 100 °C overnight.

Assembly process

The most electrochemically stable polymer electrolyte film which carries high conductivity at room temperature for each system was used as the electrolyte for the

lithium polymer cell fabrication. The cathode and anode obtained as described above. All battery components are dried thoroughly and the assembly process was done in the vacuum chamber. A gel polymer electrolyte film was assembled between the cathode and anode in a sealed container.

Charge/discharge cycling was carried out by using an electrochemical analyzer, WPG100e potentiostat/galvanostat system with a constant current of 1.0 mA for lithium and sodium cells. The cycle test of the lithium cell was performed from 1.5 to 4.0 V while the cycle test was performed from 1.5 to 3.0 V for the sodium cell.

University of Malaya

CHAPTER 4: ELECTRICAL STUDIES

4.1 Impedance Spectroscopy Analysis

The study of electrical conductivity of polymer electrolytes films is very important to investigate the ionic behavior and transport mechanisms of GPE films. Therefore, impedance spectroscopy analysis was performed on PVdF-HFP based gel electrolytes system to obtain the conductivity at room temperature. The impedance was measured from 50 Hz to 1 MHz. The films from the PVdF-HFP/EC/PC/LiCF₃SO₃ system and PVdF-HFP/EC/PC/NaCF₃SO₃ system with the highest room temperature conductivity were used to study the dependence of conductivity on temperature. The conductivity-temperature studies were carried out in the temperature range between 303K and 373K.

4.1.1 Room Temperature Impedance Spectroscopy Studies

4.1.1.1 Pure PVdF-HFP film and PVdF-HFP/EC/PC film

Figure 4.1 and 4.2 depict the Cole-Cole plots of pure PVdF-HFP film and PVdF-HFP/EC/PC film, respectively. The semicircle in the high frequency region represents the parallel combination of bulk resistance and bulk capacitance of the polymer electrolytes. From the figures, the value of bulk resistance, R_b can be obtained and the conductivity value of the films can be determined using equation (3.12). The conductivity at room temperature for pure PVdF-HFP film and PVdF-HFP/EC/PC film were calculated to be $1.86 \times 10^{-11} \Omega$ and $3.31 \times 10^{-8} \text{ S cm}^{-1}$, respectively. It was observed that the presence of solvent plasticizer EC and PC has drastically reduced the bulk resistance hence increased the conductivity values of the film. The increase in

conductivity value in this system implies that the plasticizer has dissolved the polymer and reduced the rigidity of polymer backbone. This will lead to the increase of the mobility of the segmental chain of the polymer. Since no ions have been introduced into this system, the conductivity is expected not to be high.

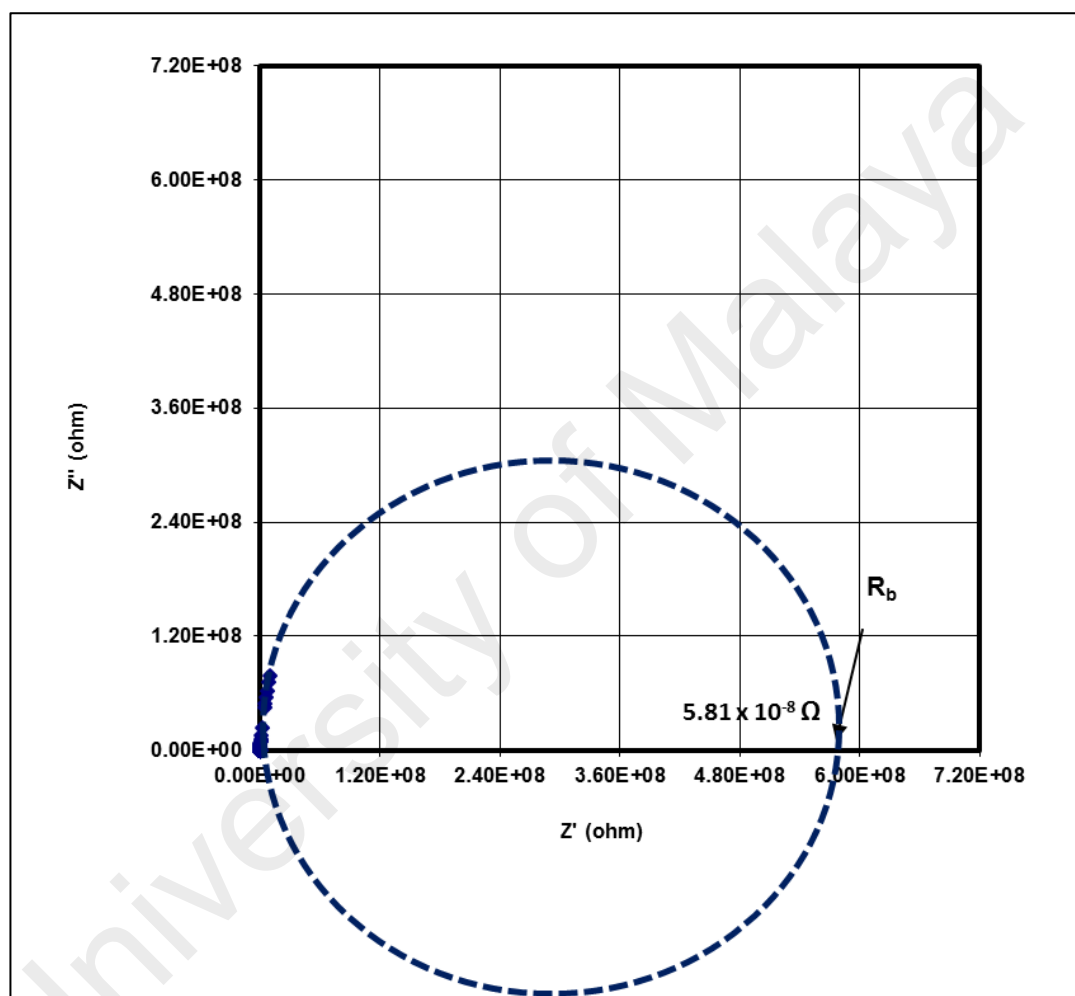


Figure 4.1: Cole-Cole plot for pure PVdF-HFP film

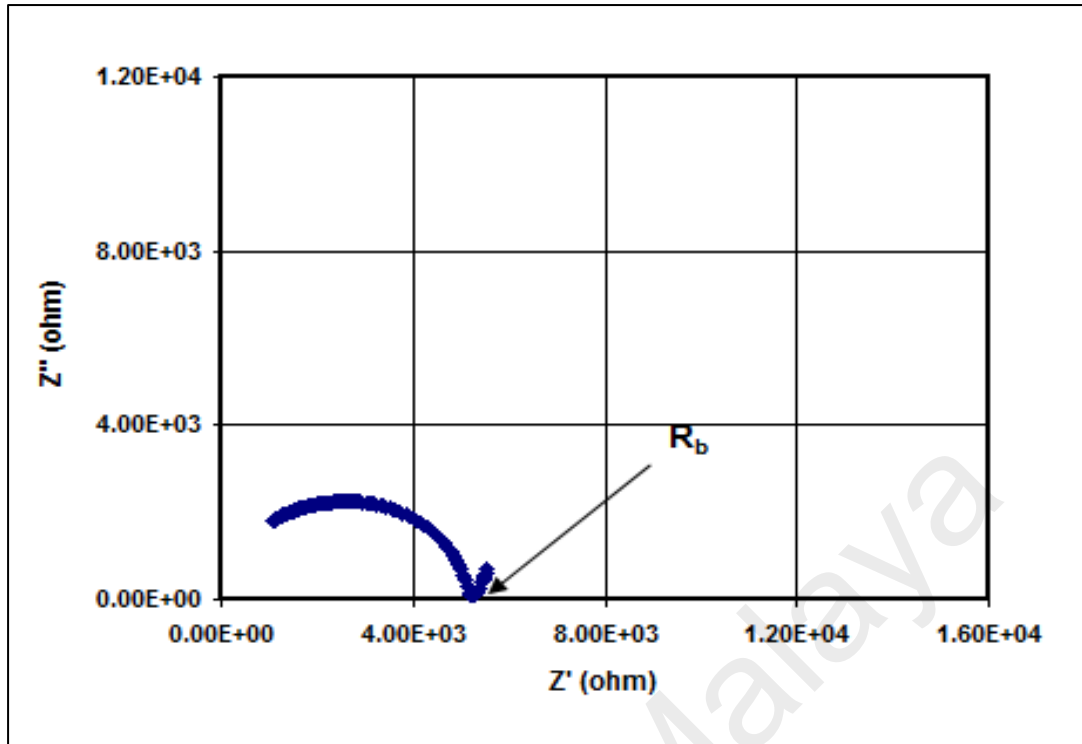


Figure 4.2: Cole-Cole plot for PVdF-HFP/EC/PC gel polymer electrolytes film

Figure 4.1 and 4.2 depict the Cole-Cole plots of pure PVdF-HFP film and PVdF-HFP/EC/PC film, respectively. The semi-circle in the high frequency region represents the parallel combination of bulk resistance and bulk capacitance of the polymer electrolytes. From the figures, the value of bulk resistance, R_b can be obtained and the conductivity value of the films can be determined using equation (3.12). The conductivity at room temperature for pure PVdF-HFP film and PVdF-HFP/EC/PC film are calculated to be 1.86×10^{-11} and $3.31 \times 10^{-8} \text{ S cm}^{-1}$, respectively. It was observed that the presence of solvent plasticizer EC and PC has drastically reduced the bulk resistance hence increased the conductivity values of the film. The increase in conductivity value in this system implies that the plasticizer has dissolved the polymer and reduced the rigidity of polymer backbone. This will lead to the increase of the

mobility of the segmental chain of the polymer. Since no ions have been introduced into this system, the conductivity is expected not to be high.

4.1.1.2 GPE system with LiCF_3SO_3 salt and NaCF_3SO_3 salt

Figure 4.3 shows the Cole-Cole plots of PVdF-HFP GPE films containing LiCF_3SO_3 salt with the composition from 5 wt.% to 30 wt.% of the salt. The disappearance of a depressed semicircle at high frequency for the films reveals the absence of capacitive nature of the samples. The bulk resistance, R_b values can be calculated from the intercept on the real impedance axis of the Cole-Cole plot. The values of bulk resistance, R_b and the conductivities at room temperature for all salt compositions in the PVdF-HFP/EC/PC/ LiCF_3SO_3 system are listed in Table 4.1.

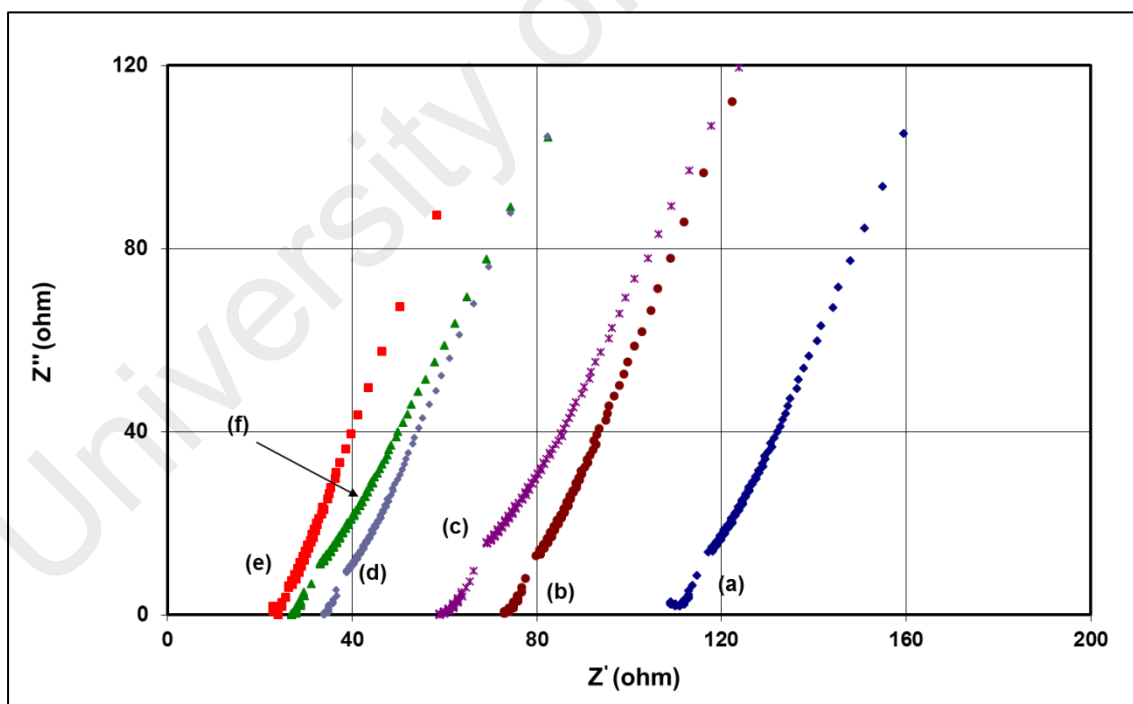


Figure 4.3: Cole-Cole plots for PVdF-HFP/EC/PC/ LiCF_3SO_3 gel polymer electrolytes film containing (a) 5 wt.% (b) 10 wt.% (c) 15 wt.% (d) 20 wt.% (e) 25 wt.% and (f) 30wt.% of LiCF_3SO_3 salt

Table 4.1: The compositions, the bulk resistance, R_b and the conductivity, σ of films in the PVdF-HFP/EC/PC/LiCF₃SO₃ system

LiCF ₃ SO ₃ content in GPE system (wt.%)	Average Bulk Resistance, R_b (Ω)	Average Conductivity, ($\sigma \pm \Delta \sigma$) (S/cm)
5	108.0	$(2.22 \pm 0.11) \times 10^{-4}$
10	61.0	$(5.40 \pm 0.34) \times 10^{-4}$
15	55.9	$(7.63 \pm 0.68) \times 10^{-4}$
20	32.1	$(1.02 \pm 0.07) \times 10^{-3}$
25	26.7	$(1.40 \pm 0.06) \times 10^{-3}$
30	32.7	$(1.13 \pm 0.08) \times 10^{-3}$

Figure 4.4 shows the variation of conductivity of the system containing different amounts of LiCF₃SO₃ in weight percentage. It can be observed that the conductivity increases as salt concentration increases, with a maximum value achieved at 25 wt.% of LiCF₃SO₃, and then decreased on further increase of the salt concentration (30 wt.%). The increase in conductivity is due to an increase in ionic mobility and free ion concentration (R. Kumar, Sharma, & Sekhon, 2005). Generally, ionic conductivity of electrolytes depends on the charge carrier concentration, n and charge carrier mobility, μ as described by relation $\sigma = nq\mu$, where q is the charge of a mobile carrier and the mobility, respectively. At low salt concentration, the LiCF₃SO₃ is highly dissociated. The number of mobile ions increases with increase in LiCF₃SO₃ concentration thus increasing the conductivity. The addition of plasticizing solvents such EC and PC also contributes to the conductivity enhancement by reducing the viscosity of the electrolytes and assist in the dissociation of the salt thereby increasing the number of free ions. The decrease in conductivity value at higher salt concentration of 30 wt.% may be due to increased formation of ion pairs and ion aggregates leading to the

creation of ion clusters which will decrease the number of free ions (Ramya, Selvasekarapandian, Savitha, Hirankumar, & Angelo, 2007). The presence of free ions, ion pairs and ion aggregates in the GPEs is further studied by FTIR spectroscopy and will be discussed in Chapter 6.

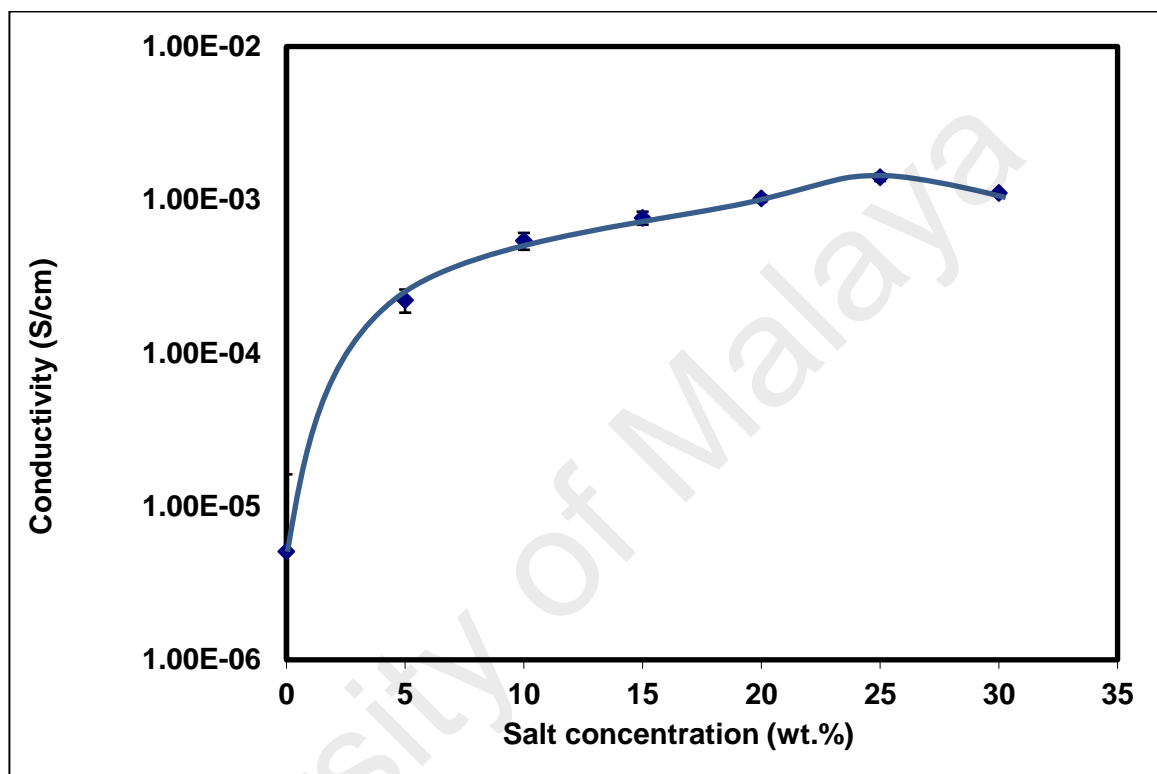


Figure 4.4: Variation of ionic conductivity with LiCF_3SO_3 salt in the GPE films

The Cole-Cole plots for the GPE films containing NaCF_3SO_3 salt are shown in Figure 4.5. Similar to Figure 4.3, the semicircle also completely disappear after the addition of the salt. This result suggests that, only the capacitive component of ion conducting polymer prevails (Selvasekarapandian, Hema, Kawamura, Kamishima, & Baskaran, 2010). It can be observed from the Table 4.2, the conductivity values continuously increase when more salt (up to 20 wt.%) has been added. The ionic conductivity as a function of salt concentration is shown in Figure 4.6. The same

behaviour as discussed in GPE-LiCF₃SO₃ system can be observed in this figure. The sharp increase in the conductivity value from 5 wt.% to 20 wt.% is due to the increase of charge carriers concentration and ionic mobility in this system. It can be observed from the figure that the conductivity increases with the increase of the amount of NaCF₃SO₃ up to 20 wt% and decrease with further addition of the salt. This is because when the salt content is increased, the number of free ions also increases, thus increases the diffusion of ions through their free volumes. Therefore, the conductivity increased. When more salt was added, the number of free ions also increases until it was saturated. These ions become closer to one another, decreasing the free volumes thus decreasing the conductivity. The maximum conductivity achieved for this system is $2.50 \times 10^{-3} \text{ S cm}^{-1}$ which is higher than the one in LiCF₃SO₃ system. This implies that the polymer and plasticizers, EC and PC have dissociated more NaCF₃SO₃ salt than LiCF₃SO₃ salt into ions. The small ionic radius and high electronegativity of lithium makes it the stronger Lewis acid than sodium. The stronger Lewis acidity of cation causes strong interaction, and co-intercalation tends to take place. At lower salt concentrations, the ions can move easily in the electrolytes due to the weaker bonding between Na⁺ ion with anion, Na⁺ ion with the polymer and the Na⁺ ion with solvent plasticizers. The presence of the plasticizers also help to destruct the coordination bond of Na⁺ with PVdF-HFP by providing free volumes and making more ions move in the polymer electrolytes, hence increase the conductivity. When more salt is added, the ion clusters are formed in the gel polymer electrolyte system. Even though the salt is dissolved by the polymer, this does not mean that cations and anions are well separated from each other. There is ample evidence that the ions interact with each other. These interactions lead to the formation of ion pairs and ion aggregates which can reduce the mobility of the charge carrier. In this case, EC and PC will play a vital role in dissociate the saturated amounts of salt in the GPE system to become free ions.

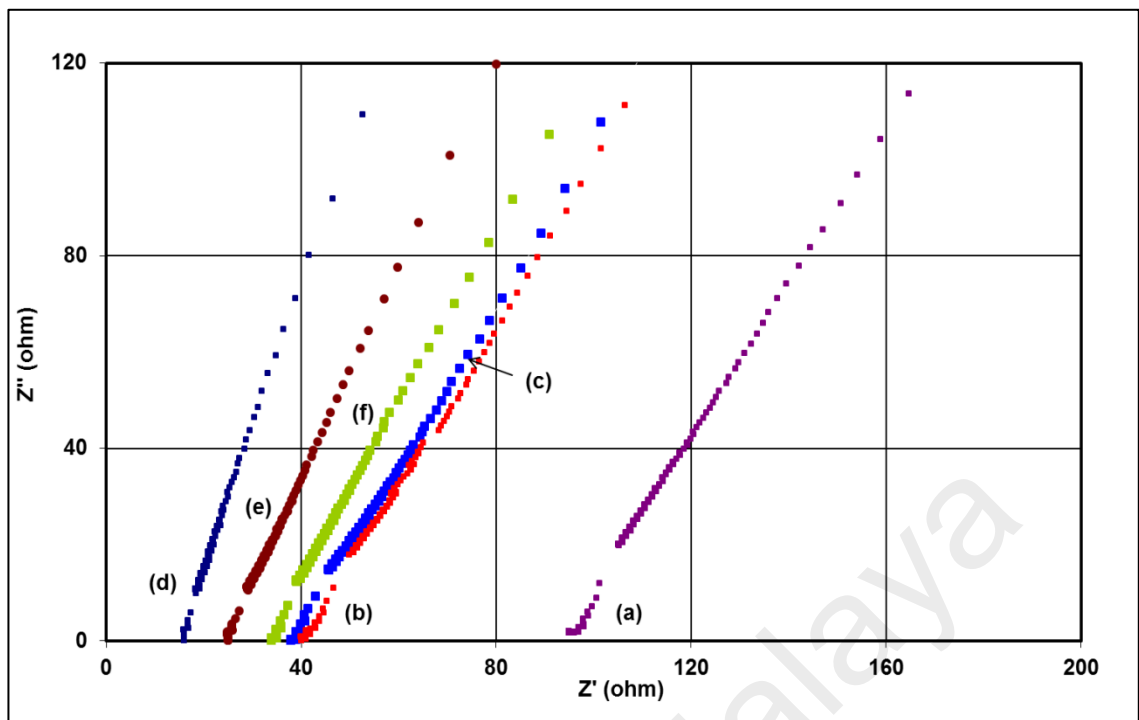


Figure 4.5: Cole-Cole plots for PVdF-HFP/EC/PC/NaCF₃SO₃ gel polymer electrolytes film containing (a) 5 wt.% (b) 10 wt.% (c) 15 wt.% (d) 20 wt.% (e) 25 wt.% and (f) 30wt.% of NaCF₃SO₃ salt.

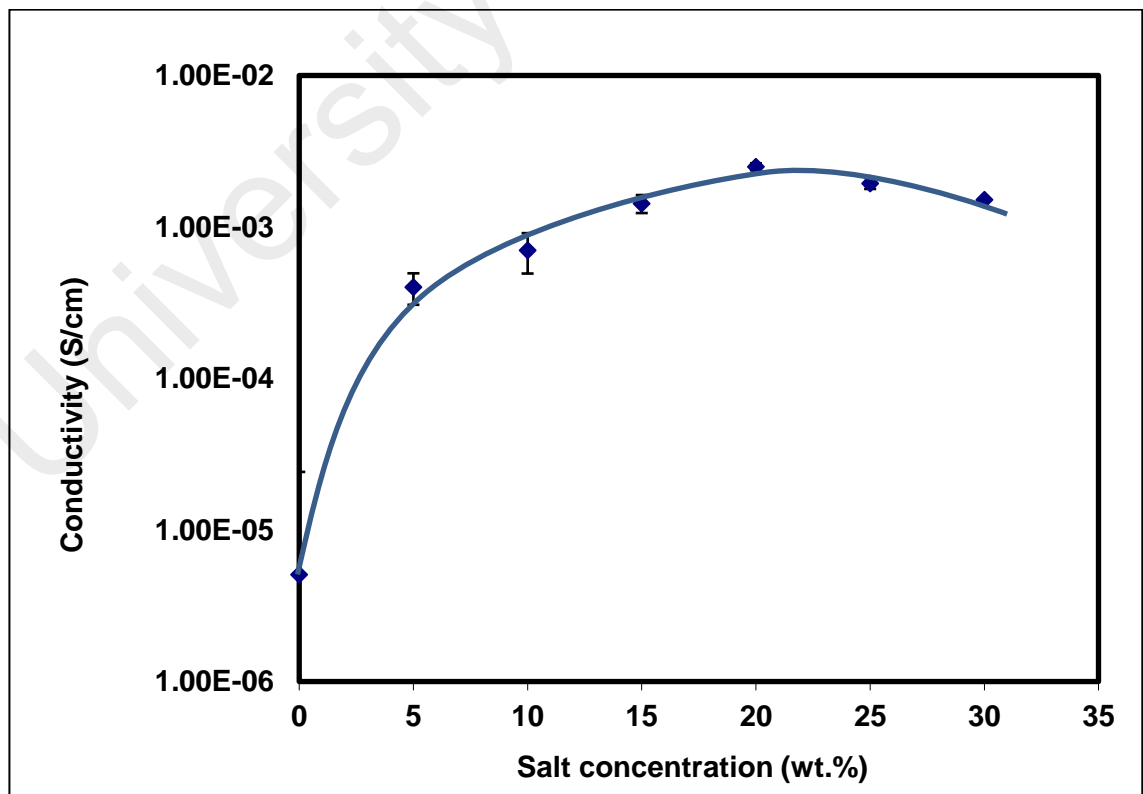


Figure 4.6: Variation of ionic conductivity with NaCF₃SO₃ salt in the GPE film.

Table 4.2: The compositions, the bulk resistance, R_b and the conductivity, σ of films in the PVdF-HFP/ EC/PC/NaCF₃SO₃ system

NaCF ₃ SO ₃ content in GPE system (wt.%)	Average Bulk Resistance, R_b (Ω)	Average Conductivity, ($\sigma \pm \Delta \sigma$) (S/cm)
5	91.6	$(4.01 \pm 0.19) \times 10^{-4}$
10	39.0	$(7.02 \pm 0.94) \times 10^{-4}$
15	32.0	$(1.43 \pm 0.21) \times 10^{-3}$
20	16.7	$(2.50 \pm 0.19) \times 10^{-3}$
25	23.7	$(1.95 \pm 0.13) \times 10^{-3}$
30	31.1	$(1.52 \pm 0.16) \times 10^{-3}$

4.1.2 Conductivity-Temperature Dependence Studies

The conductivity-temperature dependence has been studied to investigate the influence of temperature and salt concentrations on the ion transport mechanism of the GPE films. The study were done only for the samples containing 5 wt.%, 30 wt.% of salt and the highest conducting sample at room temperature from both systems. Figure 4.7 and 4.8 displays the variation in the conductivity-temperature dependence in the temperature range of 303 K to 373 K for GPE systems with LiCF₃SO₃ salt and NaCF₃SO₃ salt, respectively. In the temperature range of study, the conductivity is found to increase with temperature. The non-linear nature of the plots indicates that the ionic conduction in the gel polymer electrolytes dependent on the free volume and motion of the polymer chains in which the conduction occurs in amorphous region. This result can be described by the concept of free volume (Cohen & Turnbull, 1959; Grest & Cohen, 1980). As the temperature increases, the polymer expands to produce free volumes, which leads to enhance ionic mobility, whereby ions can move into the free

volume, causing the increase in conductivity. This will facilitate the movement of ions through the polymer matrix thereby increase the conductivity of the GPE films.

In order to give a better understanding into the ionic conduction mechanism of the GPE films, the conductivity-temperature data have been fitted to the Vogel-Tamman-Fulcher (VTF) equation as discussed in Chapter 2. From the VTF equation, it is clear that ionic conductivity could be improved by lowering the T_g . Generally, polymer complexes have a multiphase nature, consisting of salt-rich crystalline phase, pure polymer crystalline phase and amorphous phase with dissolved salt (Robitaille & Fauteux, 1986). In the crystalline phases, the polymer chains are rigid and thus the ion mobility is almost negligible and the overall conductivity is very low. At temperatures below the glass transition temperature, T_g , the diffusional motion of large chain segments is hindered by potential energy barrier. With increasing temperature the energy become great enough to overcome these barriers and segmental motion occur hence increase in the free volume of the system. Above the glass transition temperature, the thermodynamic theory of liquids may be used for the polymer where the amorphous region progressively increase, the polymer chain acquires faster internal modes in which bond rotations produce segmental modes which help the inter-chain and intra-chain ion movements (Reiter, Velická, & Míka, 2008). The increase in free volume due to increase of amorphous region would facilitate the motion of cationic charge carrier at temperature above T_g , thus increase the conductivity.

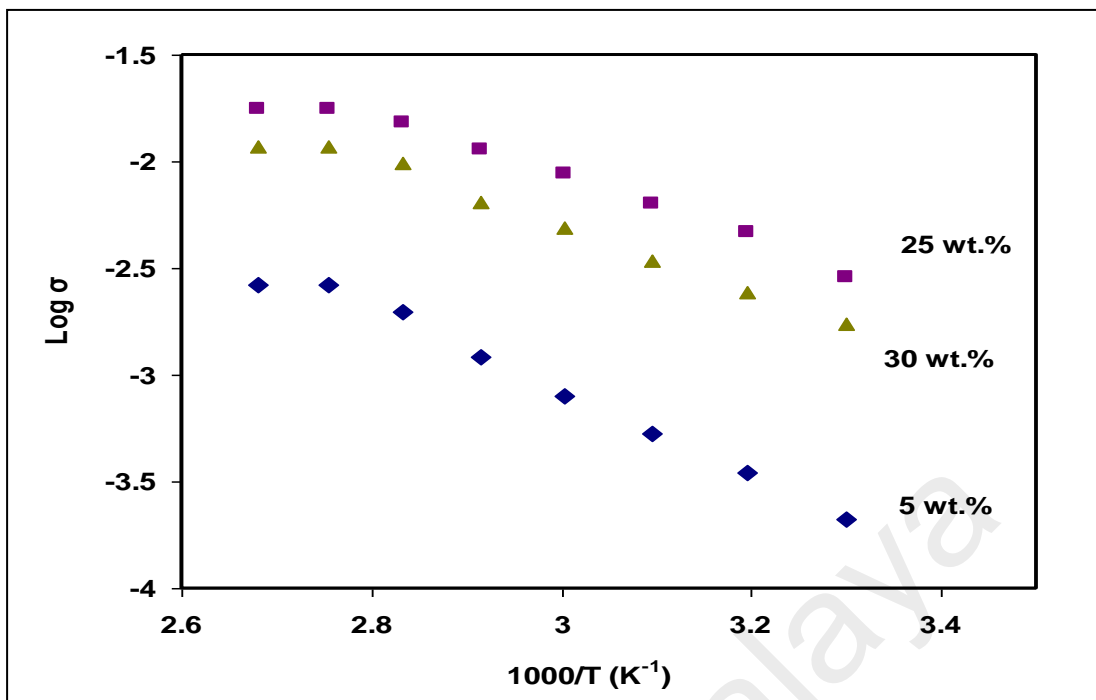


Figure 4.7: Log σ versus $1000/T$ plot for the GPE film containing (a) 5 wt.% (b) 25 wt.% and (c) 30 wt.% of LiCF_3SO_3 salt

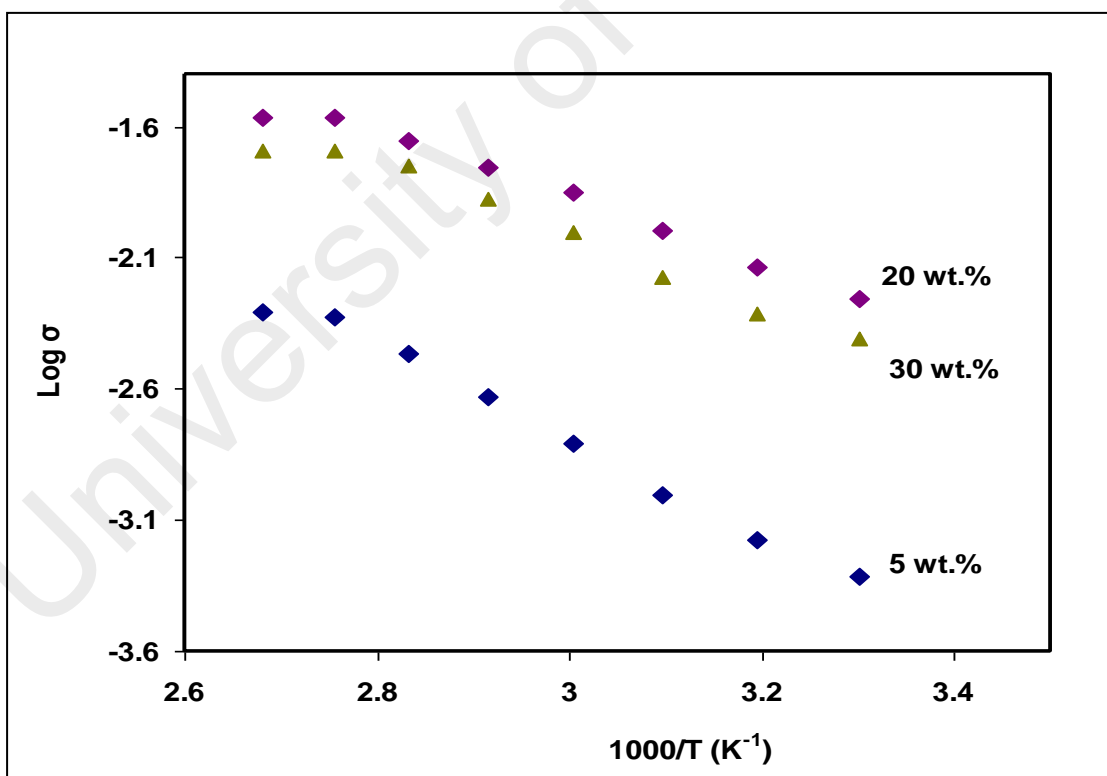


Figure 4.8: Log σ versus $1000/T$ plot for the GPE film containing (a) 5 wt.% (b) 20 wt.% and (c) 30 wt.% of NaCF_3SO_3 salt.

In the present study, the value of the glass transition temperature, T_g of the GPE films has been measured using Differential Scanning Calorimetry (DSC) which will be discussed in Chapter 5. The linear plots can be obtained by plotting the graph of $\log \sigma T^{1/2}$ versus $1000/(T-T_o)$ as shown in Figure 4.9 and 4.10 where $T_o = T_g - 50K$. The calculated values of parameter A and B (*pseudo-activation energy*) for each GPE film is summarized in Table 4.3. The conductivity result is in agreement with DSC result, where the sample with the lowest T_g value shows the highest conductivity. It can also be seen, the film containing 20 wt.% of NaCF_3SO_3 salt has the lowest pseudo activation energy and the highest ionic conductivity compared to the other GPE films. This result can be explained based on the Lewis acidity of the alkali ions (the Lewis acidity of Na^+ -ion is weaker than Li^+ -ion), i.e., the strength of the interaction of cations with the Lewis base of polymer electrolyte (Sagane, Abe, Iriyama, & Ogumi, 2005). The size of Na^+ is larger than Li^+ , thus the interaction between Na^+ and fluorine atom of PVdF-HFP chain is weaker than Li^+ . The electron donating functional group $\text{C} = \text{O}$ of EC and PC are also the possible site for the coordination with the cations. Due to the weak interaction, the de-bonding process between Na^+ ions and fluorine or oxygen atoms can easily take place, leading to an increase in the number of free ions. These free Na^+ ions then can move easily where ions can jump from one to another fluorine atom along the backbone of polymer hence increase the conductivity. This behaviour also can be understood on the basis that an increase of temperature increases the random thermal motion of Na^+ or Li^+ ions and reduces the correlations which arise from the Coulomb interaction between them.

Table 4.3: VTF parameters for the GPE films from LiCF₃SO₃ system and NaCF₃SO₃ system

Film PVdF-HFP/EC/PC + x	Pseudo-activation energy, B (eV)	T _g (°C)	T ₀ (K)	Number of charge carrier, A (S cm ⁻¹ K ^{1/2})
x = 5 wt. % LiCF ₃ SO ₃	0.102	-60	163	17.0
x = 25 wt. % Li CF ₃ SO ₃	0.080	-69	154	28.0
x = 30 wt. % Li CF ₃ SO ₃	0.083	-64	159	22.9
x = 5 wt. % Na CF ₃ SO ₃	0.097	-62	161	21.0
x = 20 wt. % Na CF ₃ SO ₃	0.076	-73	150	31.0
x = 30 wt. % Na CF ₃ SO ₃	0.079	-70	153	29.0

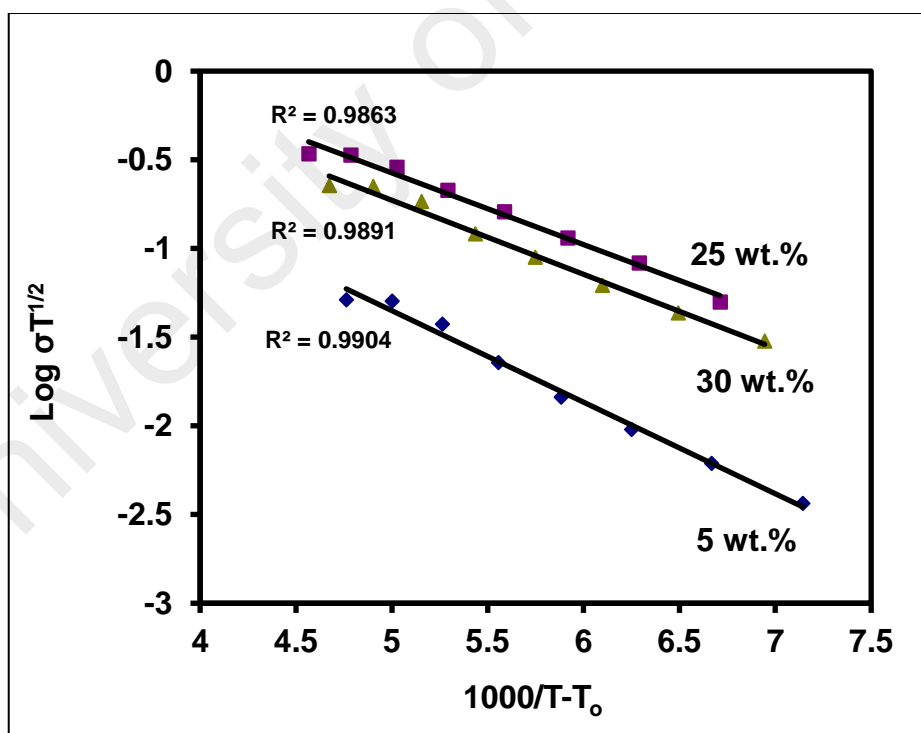


Figure 4.9: Log $\sigma T^{1/2}$ versus $1000/(T-T_0)$ plots for the GPE films containing (a) 5wt.% (b) 25 wt.% and (c) 30 wt.% of LiCF₃SO₃ salt

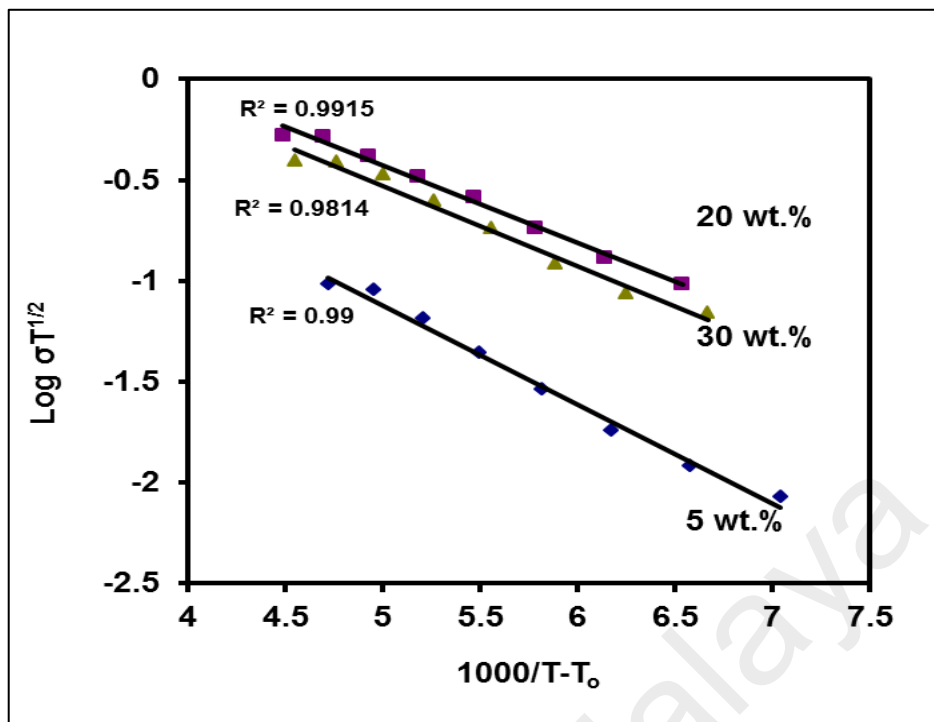


Figure 4.10: Log $\sigma T^{1/2}$ versus $1000/(T-T_0)$ plots for the GPE films containing (a) 5wt.% (b) 20 wt.% and (c) 30 wt.% of NaCF_3SO_3 salt

4.2 Transport Number Studies

4.1.2 Ionic Transport Measurement

In general the conductivity in a given electrolyte material is expressed by the transport number (t), which denotes the fraction of current carried by anions, cations or electrons in the material in terms of the total conductivity (σ_T). Therefore, the contributions of possible charge carriers into the charge transfer process are of practical importance as well (Lewandowski, Stepniak, & Grzybkowski, 2001). In this study, the transport number measurement was done by supplied D.C. electric potential of 0.5 V across the sample sandwiched between two blocking electrodes where the DC current was monitored as a function of time until it reached a constant value. The initial current

is the total current (i_t), due to the ions (i_{ion}) and electrons (i_{ele}). As the polarization builds up the i_{ion} is blocked and the final current is only the electronic current. After polarization of the SS | GPE | SS cell with the DC voltage, the current versus time plot has been drawn.

Figure 4.11 and 4.12 show the variation of normalized current with time for both PVdF-HFP/EC/PC/LiCF₃SO₃ and PVdF-HFP/EC/PC/NaCF₃SO₃ systems. The ionic transport number calculated using eq. (3.14) for both systems is tabulated in Table 4.4. From the table, the ionic transport number values are found to be in the range of 0.94 to 0.99 for all the compositions of GPE film. These results clearly suggest that the charge transport in these GPE systems is mainly due to ions and negligible contribution from electrons. It should be noted that increase in the conductivity value of the sample is due to the increase in the number of charge carriers as the highest conducting sample has the highest ionic transference number, $t_i = 0.99$. The high transference number may be associated with the effect of ion-ion and polymer-ion interactions on the microscopic parameter (Christie, Christie, & Vincent, 1999).

Table 4.4: Ionic transport number for the GPE film in PVdF-HFP/ EC/ PC/ LiCF₃SO₃ and PVdF-HFP/ EC/PC/NaCF₃SO₃ systems

Salt Content (wt.%)	Ionic Transport Number	
	PVdF-HFP + EC+ PC+ LiCF ₃ SO ₃	PVdF-HFP + EC+ PC+ NaCF ₃ SO ₃
5	0.942	0.964
20	-	0.994
25	0.989	-
30	0.983	0.989

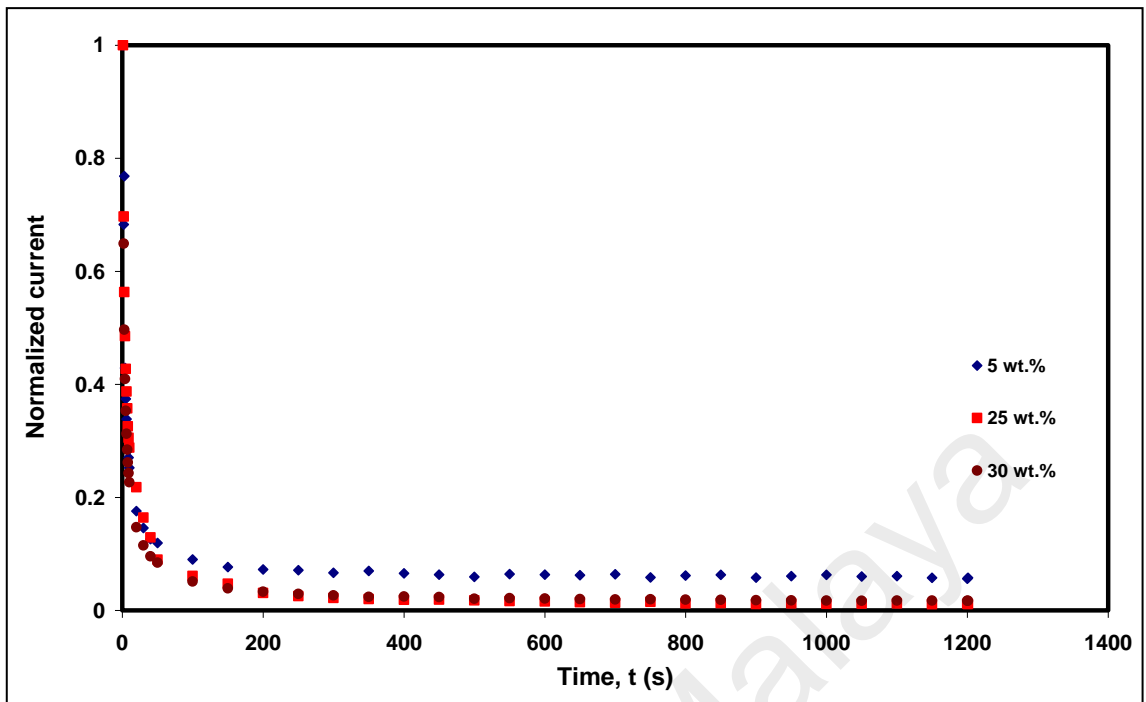


Figure 4.11: Normalized current versus time plots for films in PVdF-HFP/ EC/ PC/ LiCF₃SO₃ system

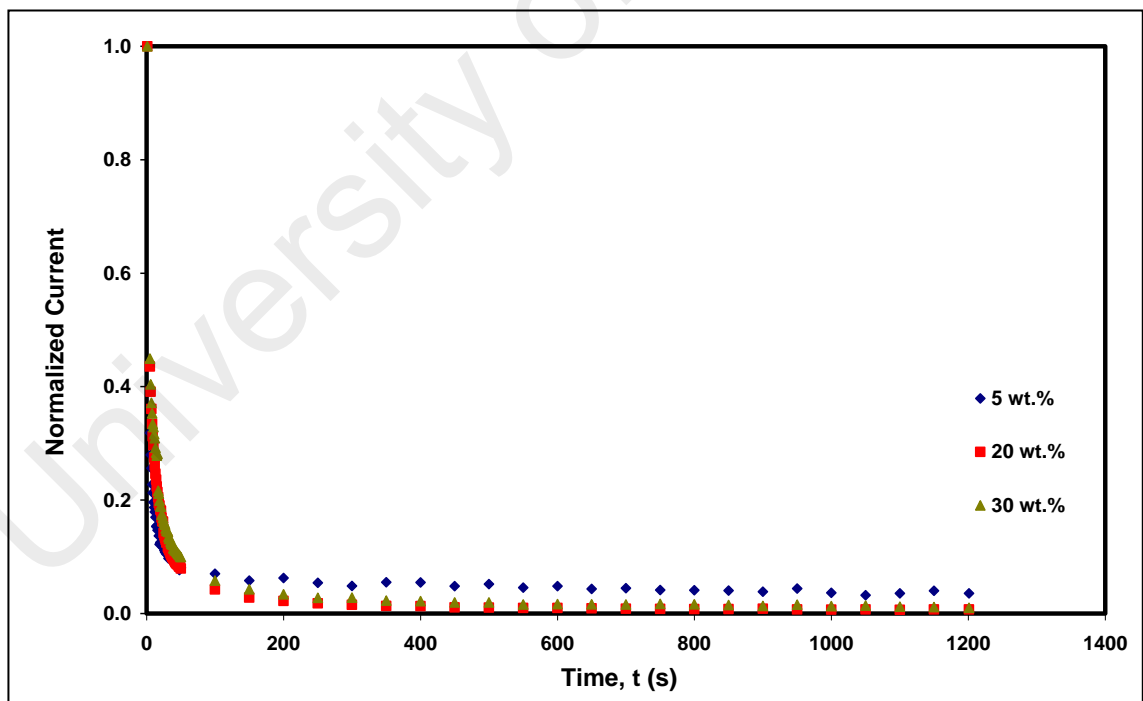


Figure 4.12: Normalized current versus time plots for films in PVdF-HFP/ EC/ PC/ NaCF₃SO₃ system

4.1.3 Cationic Transport Number Measurement, t_{Li^+} and t_{Na^+}

The cationic transport number measurement is an important study to evaluate the performance of the polymer electrolytes from their application point of view, particularly in rechargeable batteries. In this work, the combination of D.C. polarization and A.C. impedance technique were used to determine the cationic transport number of lithium t_{Li^+} and sodium t_{Na^+} ions in GPE films. The study was performed on the Li|GPE|Li and Na|GPE|Na cells containing 5 wt. %, 30 wt. % of salt and the highest conducting film from both systems where the electrolyte is sandwiched between two non-blocking metal electrodes. A constant potential of 0.5 V was applied to the cells and the current flowing through the cell was recorded as a function of the time as shown in Figure 4.3 and 4.14, respectively. The value of saturated current, I_s has been noted. As a part of the technique, the impedance plots of the above cells were recorded at room temperature prior to and after the polarization and the values of electrode-electrolyte contact resistances (R_b and R_i) were recorded.

Table 4.5: Transport number data and conductivity values for the GPE films in PVdF-HFP/EC/PC/LiCF₃SO₃ and PVdF-HFP/EC/PC/NaCF₃SO₃ systems

Sample GPE + x	Conductivity σ (S cm ⁻¹)	Transport Number	
		t_{ionic}	$t_{cationic}$
x = 5 wt.% LiCF ₃ SO ₃	2.22 x 10 ⁻⁴	0.942	0.41
x = 25 wt.% LiCF ₃ SO ₃	1.40 x 10 ⁻³	0.989	0.60
x = 30 wt.% LiCF ₃ SO ₃	1.13 x 10 ⁻³	0.983	0.51
x = 5 wt.% NaCF ₃ SO ₃	4.01 x 10 ⁻⁴	0.964	0.44
x = 20wt.% NaCF ₃ SO ₃	2.50 x 10 ⁻³	0.994	0.62
x = 30wt.% NaCF ₃ SO ₃	1.52 x 10 ⁻³	0.989	0.53

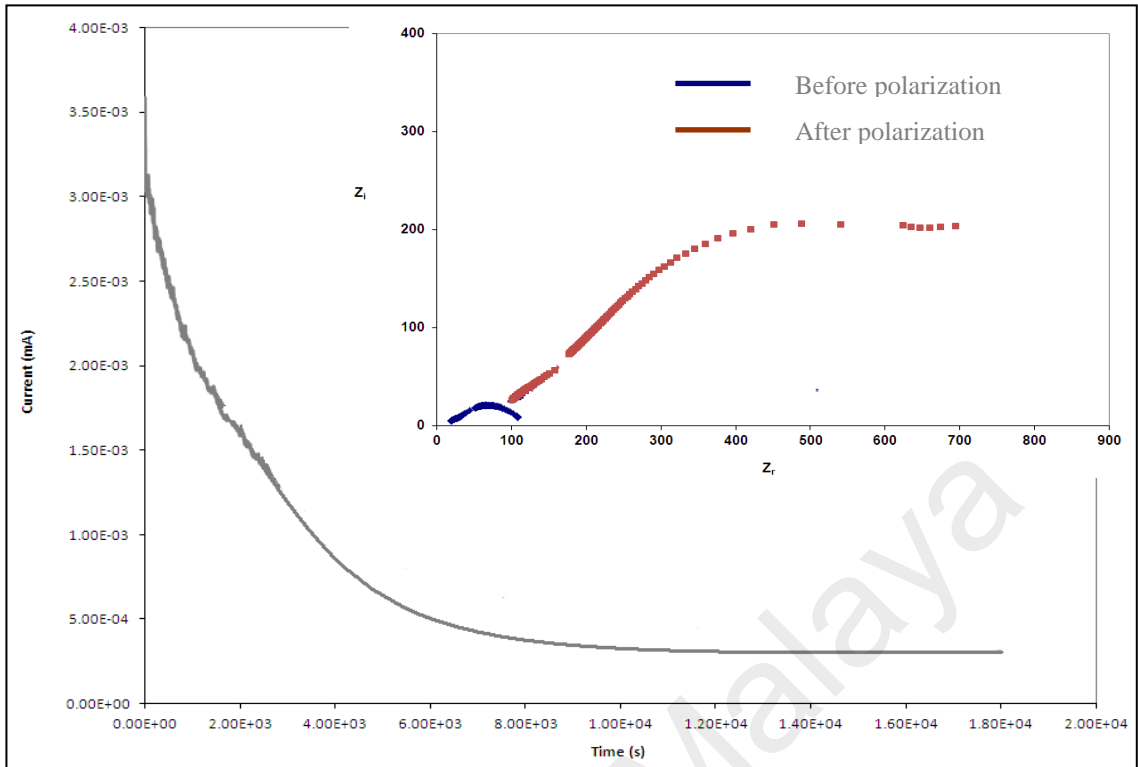


Figure 4.13: Normalized current versus time plot for PVdF-HFP/EC/PC + 25wt.% LiCF₃SO₃ film. Inset figure: Impedance plots of the cell before and after polarization

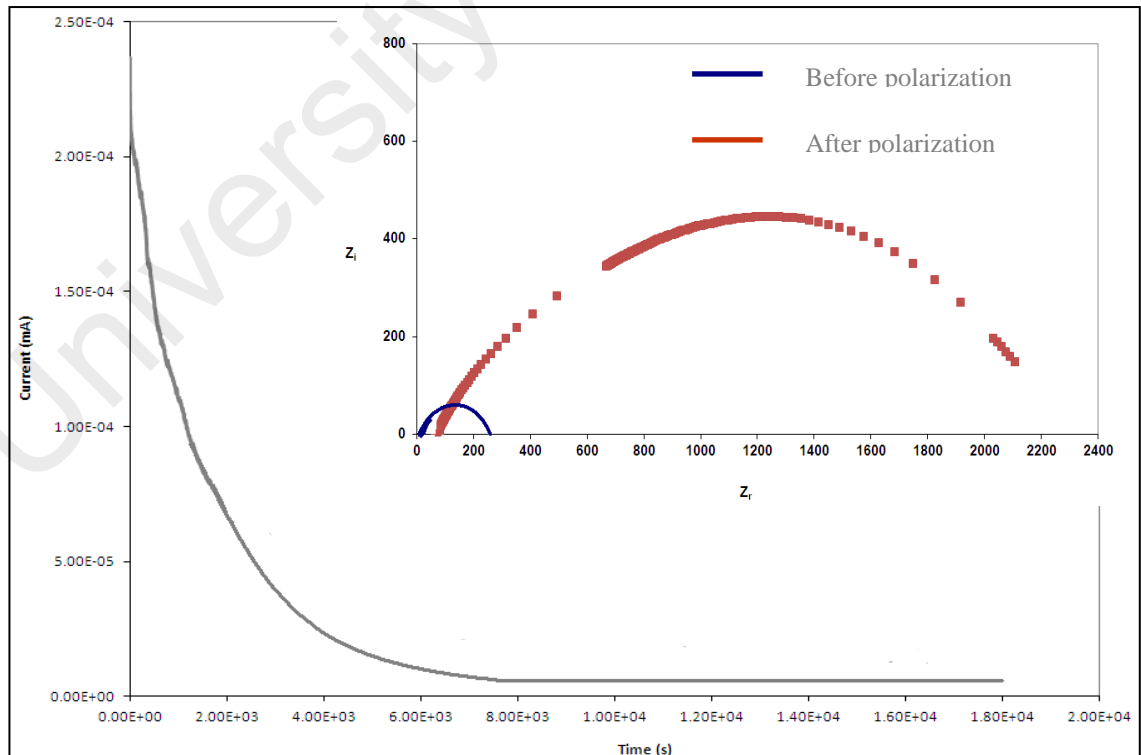


Figure 4.14: Normalized current versus time plot for PVdF-HFP/ EC/PC + 20 wt.% NaCF₃SO₃ film. Inset figure: Impedance plots of the cell before and after polarization.

Figure 4.13 and 4.14 show the normalized current versus time plots for films of PVdF-HFP/EC/PC + 25 wt.% LiCF₃SO₃ and PVdF-HFP/EC/PC + 20wt.% NaCF₃SO₃, respectively. The values of t_{Li^+} and t_{Na^+} for all the GPE film have been evaluated using equation (3.16). Table 4.5 lists the transference numbers calculated for all the GPE films. The t_+ for sample containing 25 wt.% LiCF₃SO₃ and 20 wt.% of NaCF₃SO₃ was calculated as 0.60 and 0.62, respectively. Therefore it is clear that a large proportion of current is carried by lithium and sodium ions in GPE-LiCF₃SO₃ system and GPE-NaCF₃SO₃ system, respectively. This also indicates the cationic species in the film relatively contributed more towards the overall conductivity which explains the high conductivity of these two GPE films. It is also suggested that the high value of the Li⁺ and Na⁺ transference number is attributed to the higher electrolytes retention capability of these gel polymer electrolytes due to its porous structure as shown in FESEM images which will be discussed in Chapter 6. There are large percentage of liquid electrolyte can be entrapped inside the pores and creates electrolytes channels within the polymer matrix which the cation can move faster and facilitates a higher transference number. The decrease in t_+ values at higher salt concentration (30 wt.% of salt) may be due to the ion pairs or multiplets/aggregates and hence the number of free ions for conduction are reduced.

CHAPTER 5: THERMAL ANALYSIS

Thermal analysis is a group of techniques in which the material properties (physical or chemical) of samples are monitored as a function of either temperature or time while the samples under investigation are subjected to a controlled temperature program. The temperature program may involve heating or cooling at a fixed rate, holding the temperature constant (isothermal), or any sequence of these. Differential Scanning Calorimeter has been performed in order to observe the change in transition temperature that is caused by the blending of polymer, salt and plasticizer. Thermogravimetric Analysis (TGA) is a mass depending technique and involves continuous monitoring of the weight of the sample as a function of temperature. TGA yields information regarding thermal stability, losses of residual volatiles and degradation of the material. DSC and TGA measurements were performed using Perkin Elmer instrument for selected samples with heating rate of 10°C/min. The DSC analyses were recorded in the temperature range of -90°C until 350°C. The DSC plot will be analyzed using TA Instrument Explorer software in order to find the glass transition temperature (T_g), melting point (T_m) and decomposition temperature (T_d) of the GPE films. TG experiment is conducted from room temperature to 600°C and the thermograms provide information such as the thermal stability and percentage weight loss of the component(s) and the decomposition temperature of the gel polymer electrolyte films.

5.1 Differential Scanning Calorimetry (DSC) Analysis

5.1.1 Pure PVdF-HFP

The DSC thermogram of a pure PVdF-HFP film is presented in Figure 5.1. The glass transition temperature, T_g of the film is observed at $-35\text{ }^\circ\text{C}$. Beyond T_g , a sharp endothermic peak is observed at around $144\text{ }^\circ\text{C}$ corresponds to the crystalline melting temperature (T_m) of pure PVdF-HFP. The figure also confirmed that the PVdF-HFP is a semi crystalline polymer which contained crystalline phase.

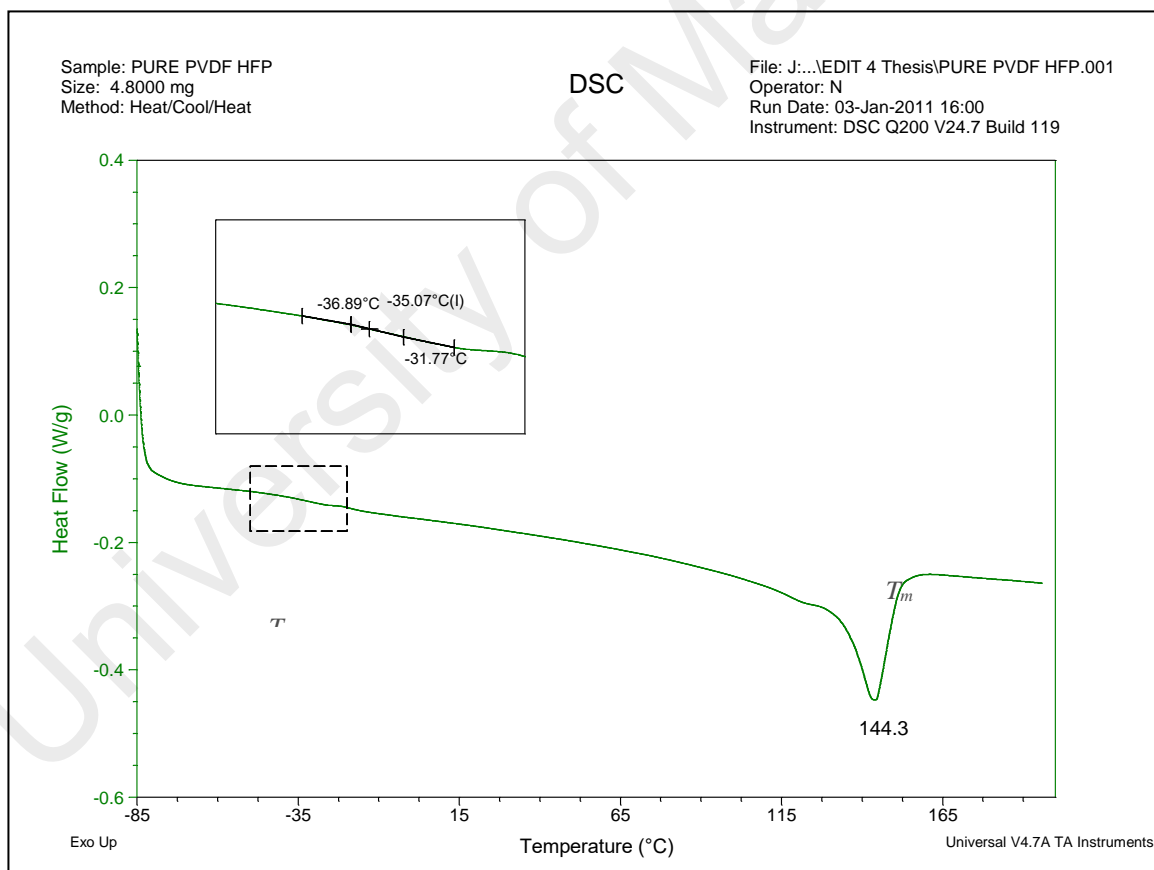


Figure 5.1: DSC thermogram of pure PVdF-HFP film.

5.1.2 PVdF-HFP/EC/PC

Figure 5.2 shows the DSC thermogram of PVdF-HFP/EC/PC film. It was observed that the T_g value of the film is decreased to -49.0°C . The decrease in T_g of pure PVdF-HFP when the plasticizers is added can be explained by morphological changes in PVdF-HFP system due to the plasticizing effect of the PVdF-HFP as observed in FESEM image, Figure 6.26 which will be discussed in Chapter 6. The presence of plasticizers in polymer increases the mobility of polymer segments which means that EC and PC help to soften the polymer backbone.

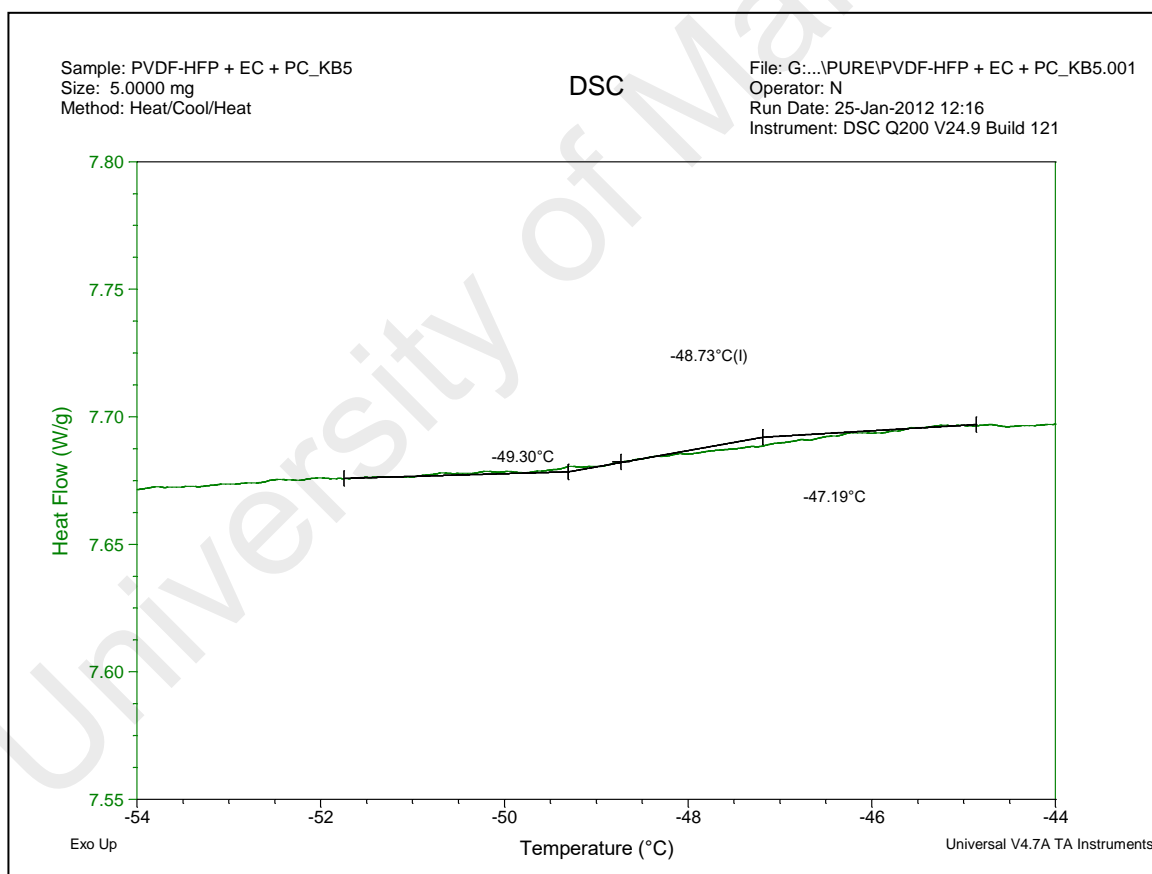


Figure 5.2: DSC thermogram of pure PVdF-HFP/EC/PC film.

5.1.3 PVdF-HFP/EC/PC/ LiCF₃SO₃ and PVdF-HFP/EC/PC/ NaCF₃SO₃ systems.

DSC thermograms of GPE film in the PVdF-HFP/EC/PC/ LiCF₃SO₃ and PVdF-HFP/EC/PC/ NaCF₃SO₃ systems have been depicted in Figure 5.3 to Figure 5.8, respectively. It can be seen that T_g of the GPE containing salt films has decreased compared to that of pure PVdF-HFP film. The change in T_g is due to the interaction of Li⁺ and Na⁺ cations with the fluorine atom in the PAN and also oxygen atom in plasticizers as discussed in FTIR analysis. The decrease of the T_g values is attributed to the increase of amorphous phase and the reduce in crystallinity of the film with the addition of LiCF₃SO₃ and NaCF₃SO₃ as confirmed by XRD patterns which will be discussed in next chapter. The decrease of T_g with increase in salt content is similar to that observed in the studies of an electrolyte based on the PVdF-HFP host matrix with the lithium salt (D Kumar, Suleman, & Hashmi, 2011; Ramesh & Lu, 2011b). In these cases, the presence of the salt may also contribute a plasticizing effect, lowering the T_g of the host polymer.

It also can be noted that the highest conducting films from both systems show the lowest T_g indicating that the conductivity is associated with the amorphous phase of the GPE films. As the ion transport mechanism in polymer electrolytes is dependant on the local motion of polymer segments, components which increase free volume may be expected to have a beneficial influence on conductivity. The result of the addition of LiCF₃SO₃ and NaCF₃SO₃ salts to the polymer electrolyte leads to conclude that in this system the salt exerts a plasticizing effect on the polymer structure. A further increase in salt content results in an increase in polymer rigidity caused by ionic crosslinking which impede segmental mobility and shift the T_g of the GPE to higher temperatures. The T_g and T_m values of the GPE samples studied are reported in Table 5.1.

Figure 5.9 illustrates the endothermic peak for GPE with LiCF_3SO_3 and NaCF_3SO_3 system respectively. It can be seen that the melting peak of crystalline phase of PVdF-HFP is broaden and shifted to lower temperature in the complexes. These indicate the crystalline phase of the GPE films are decrease with the presence of LiCF_3SO_3 and NaCF_3SO_3 salt. In other words, the films become more amorphous which makes the polymer electrolyte more flexible and facilitates segmental motion of the polymer thereby favouring an increased ionic conduction as well. Therefore, the DSC results have confirmed the results from the conductivity studies.

Table 5.1: Thermal and conductivity data for the GPE films.

Sample	Glass Transition Temperature T_g ($^{\circ}\text{C}$)	Melting Temperature T_m ($^{\circ}\text{C}$)	Conductivity r.t σ (S cm^{-1})
Pure PVdF-HFP	-35	144	1.86×10^{-11}
PVdF-HFP/EC/PC	-49	144	3.31×10^{-8}
GPE + 5 wt.% LiCF_3SO_3	-60	142	2.22×10^{-4}
GPE + 25 wt.% LiCF_3SO_3	-69	141	1.40×10^{-3}
GPE + 30 wt.% LiCF_3SO_3	-64	141	1.13×10^{-3}
GPE + 5 wt.% NaCF_3SO_3	-62	141	4.01×10^{-4}
GPE + 20 wt.% NaCF_3SO_3	-73	140	2.50×10^{-3}
GPE + 30 wt.% NaCF_3SO_3	-70	140	1.53×10^{-3}

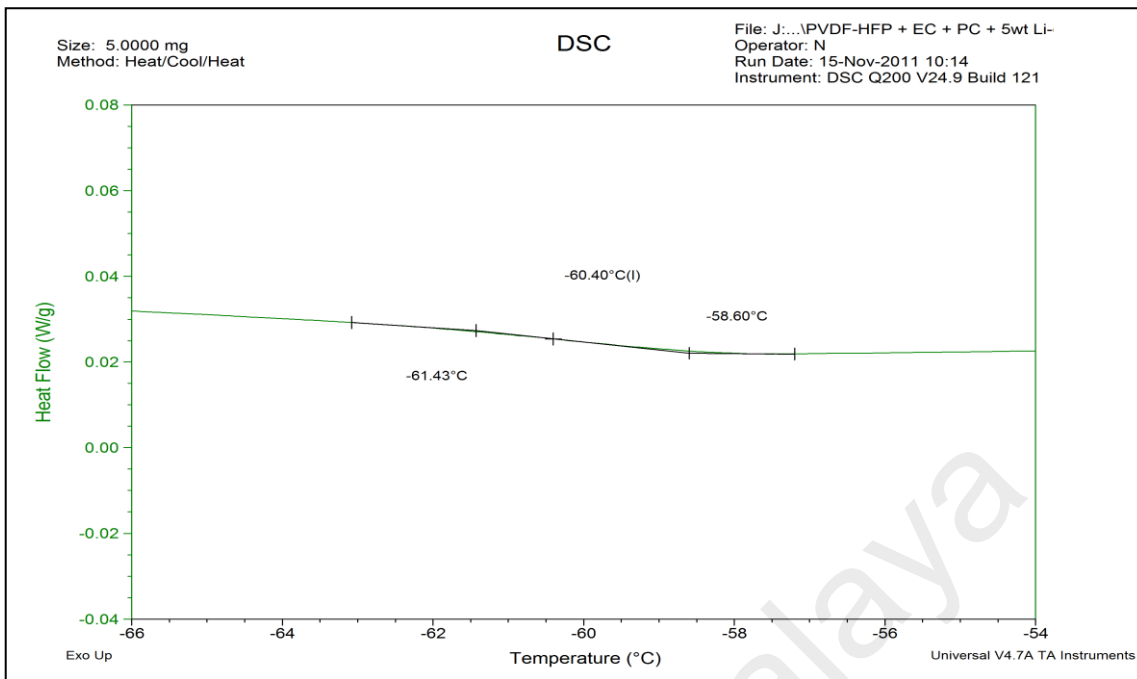


Figure 5.3: DSC thermogram of PVdF-HFP/EC/PC/5 wt.% LiCF₃SO₃ film

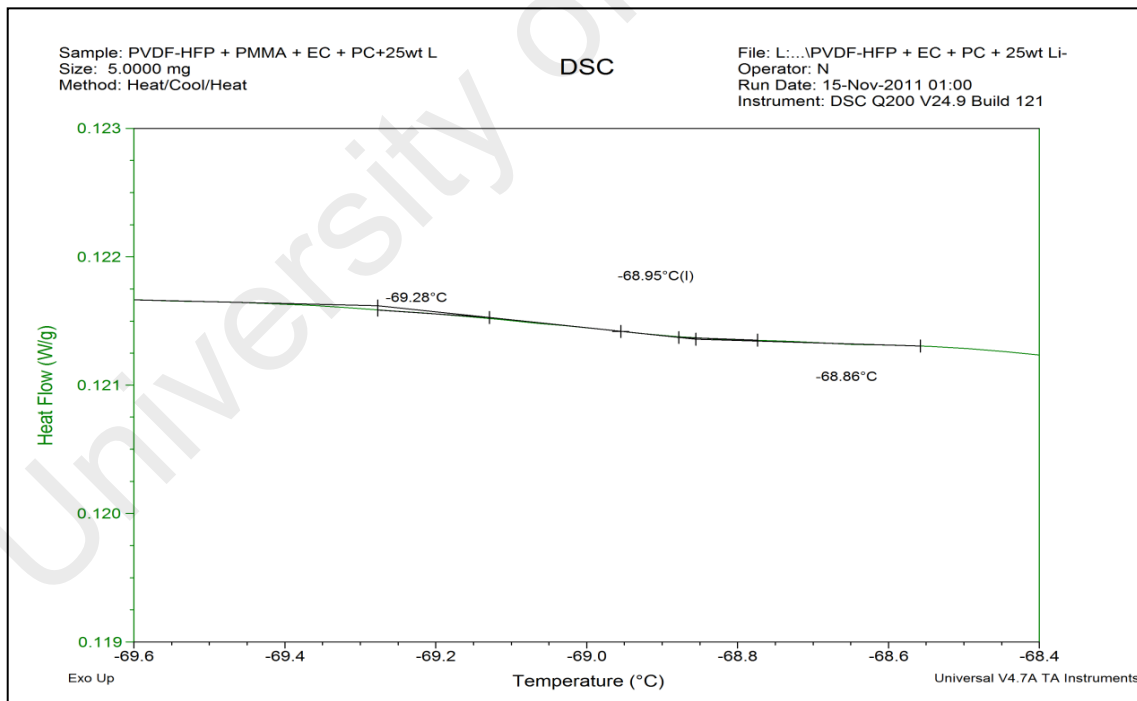


Figure 5.4: DSC thermogram of PVdF-HFP/EC/PC/25 wt.% LiCF₃SO₃

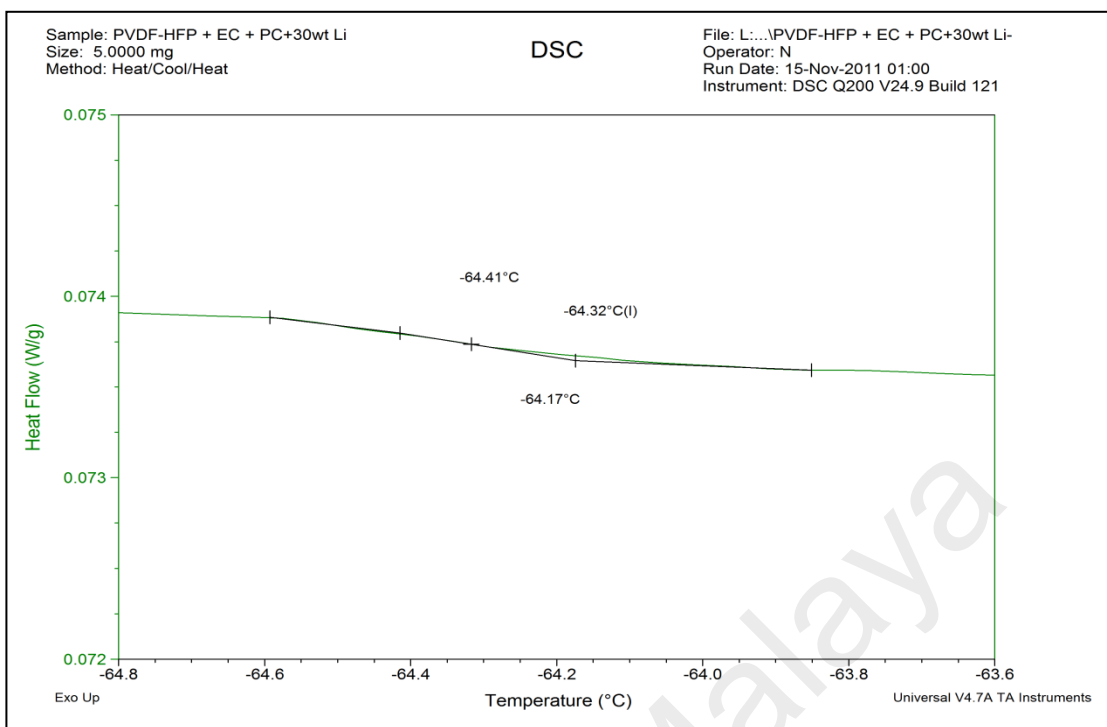


Figure 5.5: DSC thermogram of PVdF-HFP/EC/PC/ 30 wt.% LiCF₃SO₃

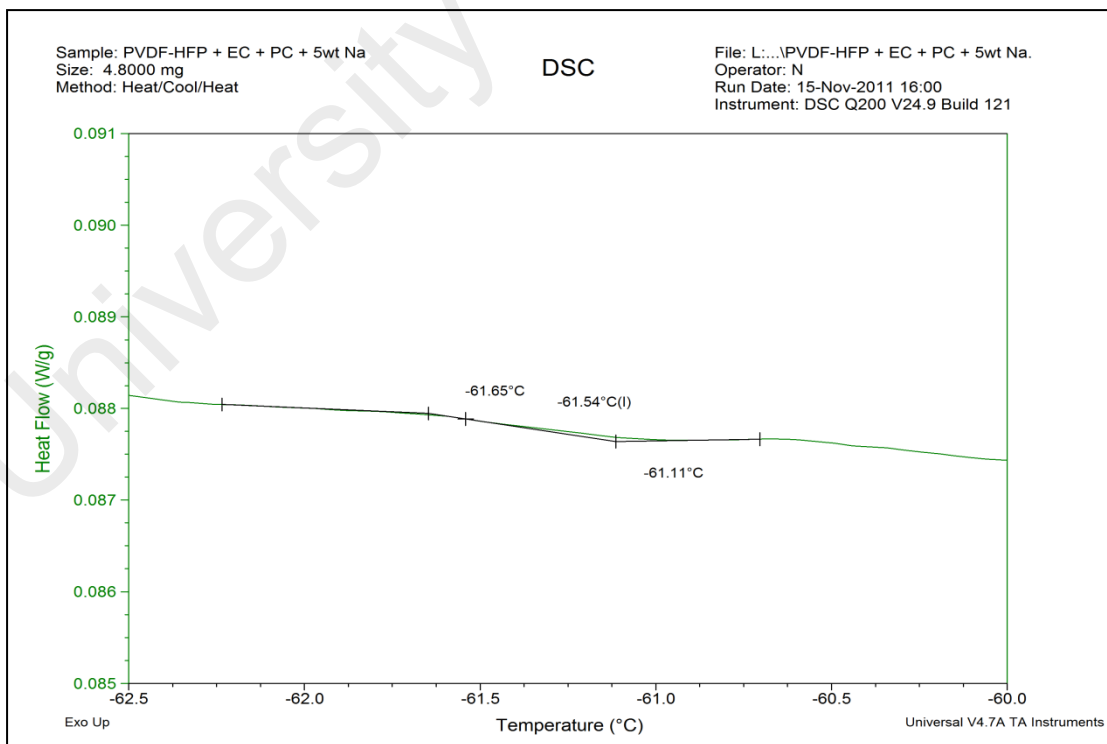


Figure 5.6: DSC thermogram of PVdF-HFP/ EC/ PC/5 wt.% NaCF₃SO₃

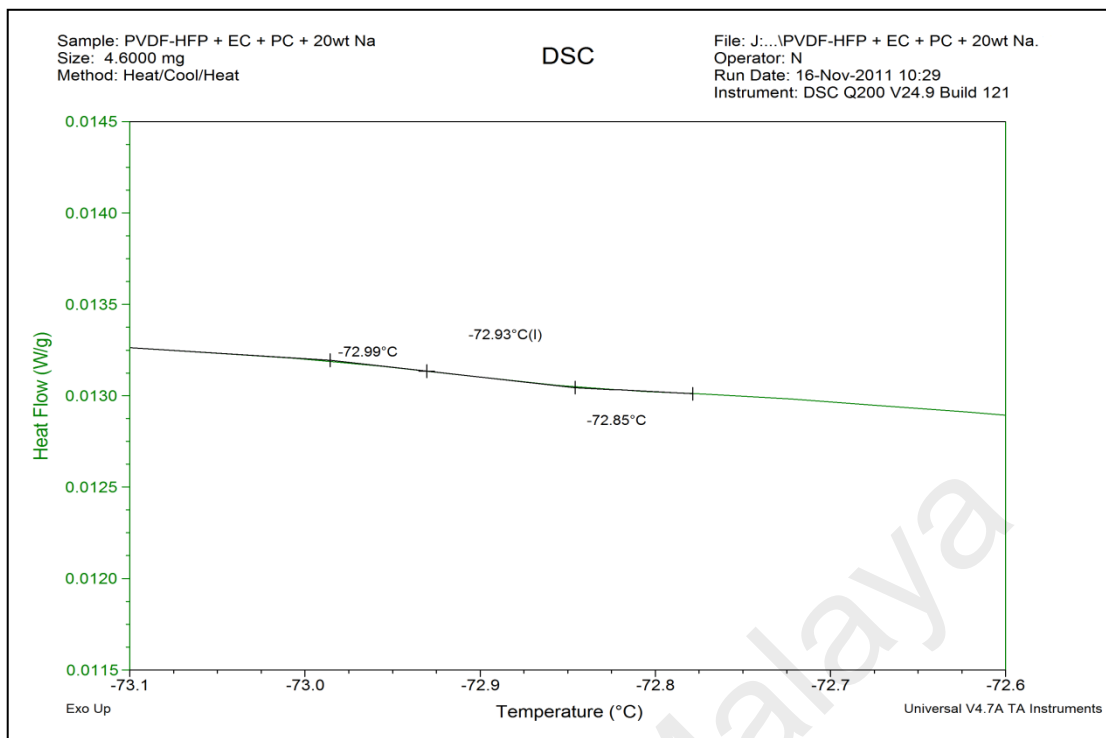


Figure 5.7: DSC thermogram of PVdF-HFP/EC/PC/20 wt.% NaCF₃SO₃

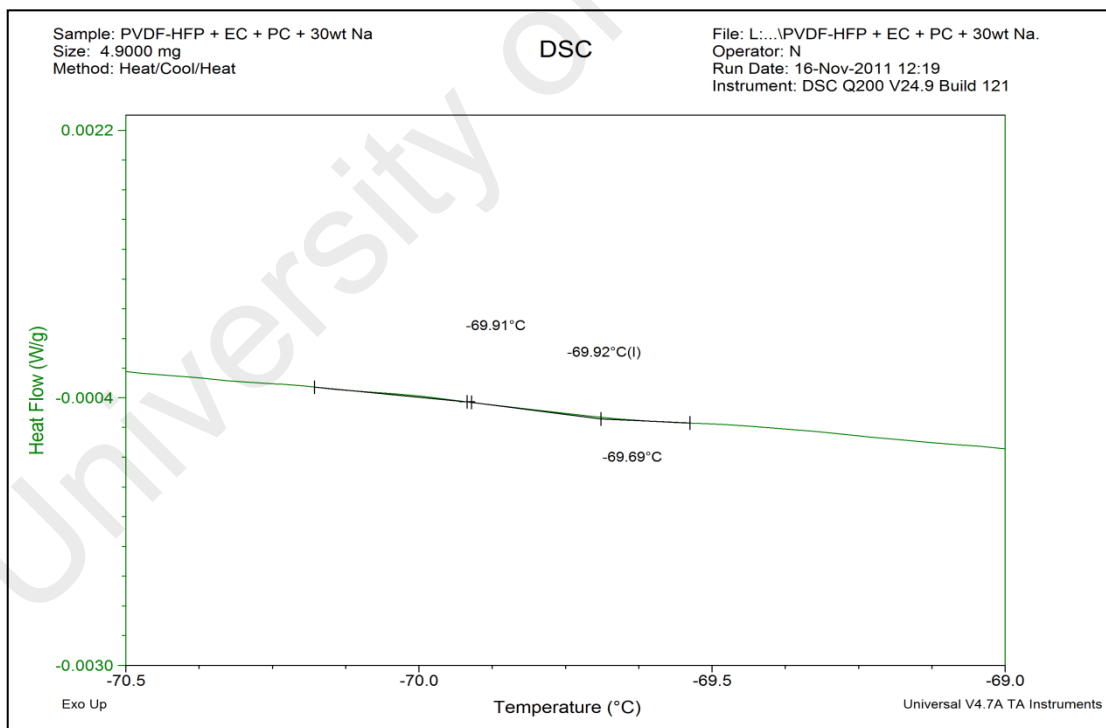


Figure 5.8: DSC thermogram of PVdF-HFP/ EC/ PC/ 30 wt.% NaCF₃SO₃

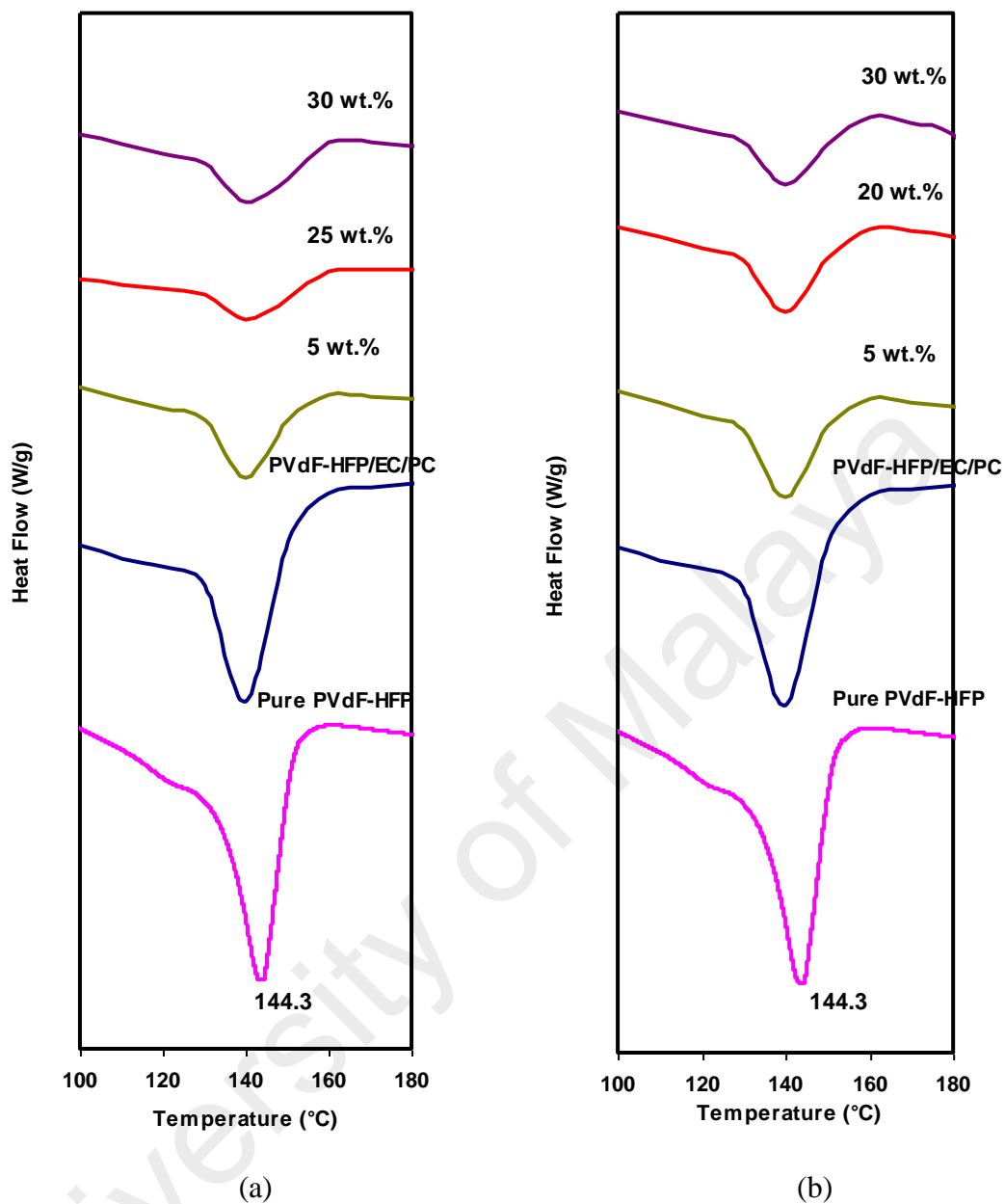


Figure 5.9: Melting temperature of (a) GPE + LiCF_3SO_3 system and (b) GPE + NaCF_3SO_3 system

5.2 Thermogravimetric Analysis (TGA)

5.2.1 Pure PVdF-HFP

Thermal analysis has been performed on the GPE films to determine the thermal stability of the films and to confirm that the solvent was completely removed from the preparation step. Figure 5.10 shows the TGA plots for pure PVdF-HFP. It is observed that pure PVdF-HFP film exhibit two-step decomposition pattern. First is the thermal transition of the film that occurs at 150 °C with a weight loss of about 5%. This indicates that the film is stable up to 150 °C, this is due to the melting of HFP unit in PVdF-HFP matrix (Nasef & Saidi, 2005). The second transition occurs at 461 °C with a major weight loss of about 72%. This result is predominantly caused by the heat decomposition of the polymer structure.

Sample: pure PVDF-HFP

File: G:...KB tgalpure PVDF-HFP.001.001

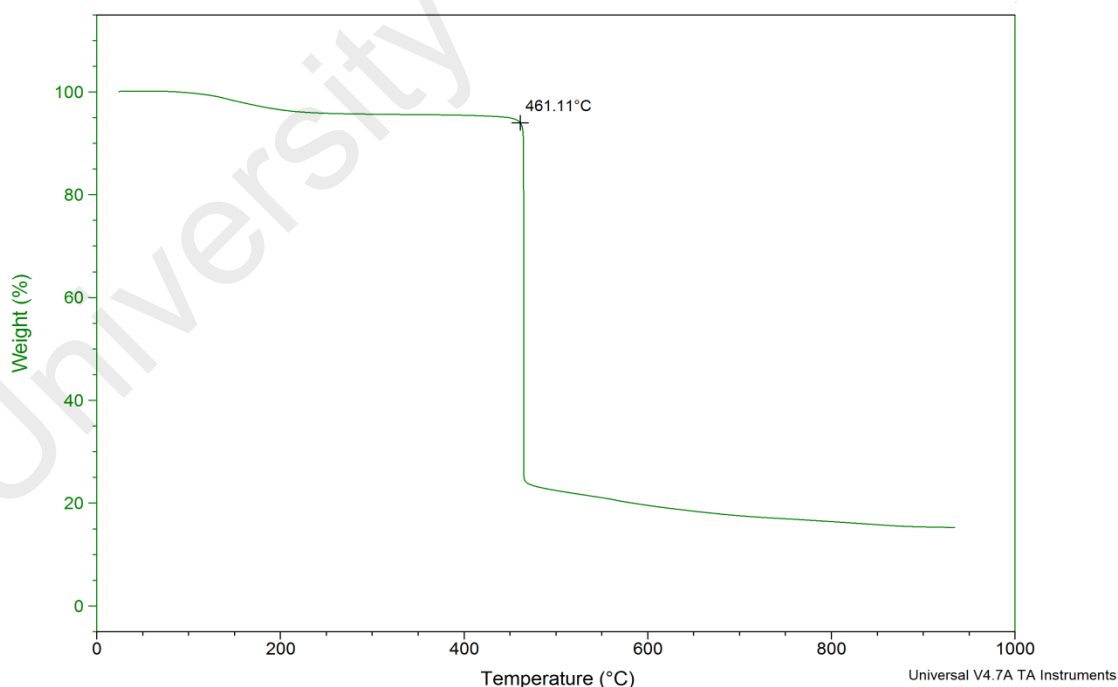


Figure 5.10: TGA thermograms of pure PVdF-HFP film.

5.2.2 PVdF-HFP/EC/PC

Figure 5.11 shows the TGA plots for the PVdF-HFP/EC/PC film. From the plot, the weight loss is observed in the initial stage at 122 °C corresponds to the evaporation of the PC and EC, which the loss of weight is about 31%. The initial decomposition of plasticized sample indicates that an addition of plasticizers decreases the thermal stability of the polymer system. The final step occurred at 438 °C is due to the degradation of the GPE film.

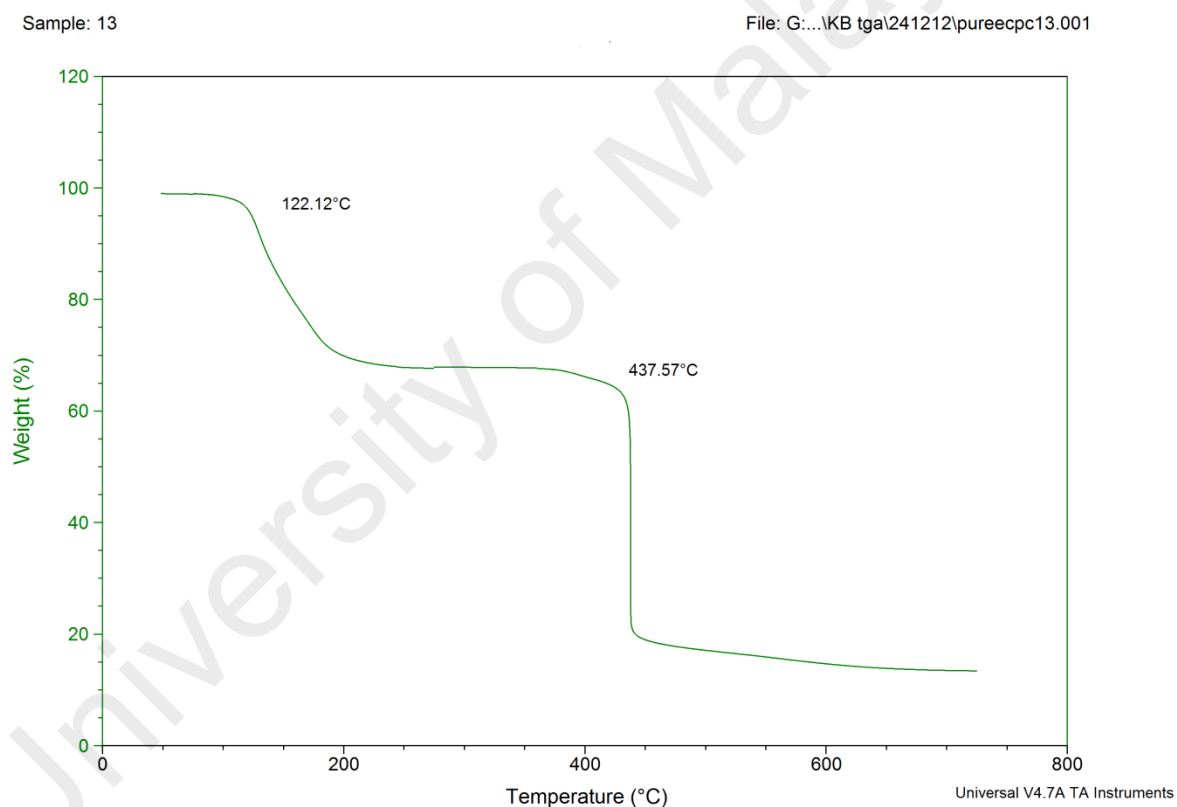


Figure 5.11: TGA thermograms of PVdF-HFP/EC/PC film.

5.2.3 PVdF-HFP/ EC/ PC/ LiCF₃SO₃ and PVdF-HFP/ EC/ PC/ NaCF₃SO₃ systems.

The TGA plots for the GPE films containing different compositions of LiCF₃SO₃ salt and NaCF₃SO₃ salt show the multi stage of weight loss as shown in Figure 5.12 and 5.13, respectively. The weight loss observed at the initial temperature below 100 °C is associated with the release of absorbed moisture. The weight loss between 150 and 200 °C is due to the melting of HFP component and the evaporation of EC and PC mixture. Further weight loss observed at higher temperatures between 370 and 450 °C indicates the decomposition of the polymer and their complexes.

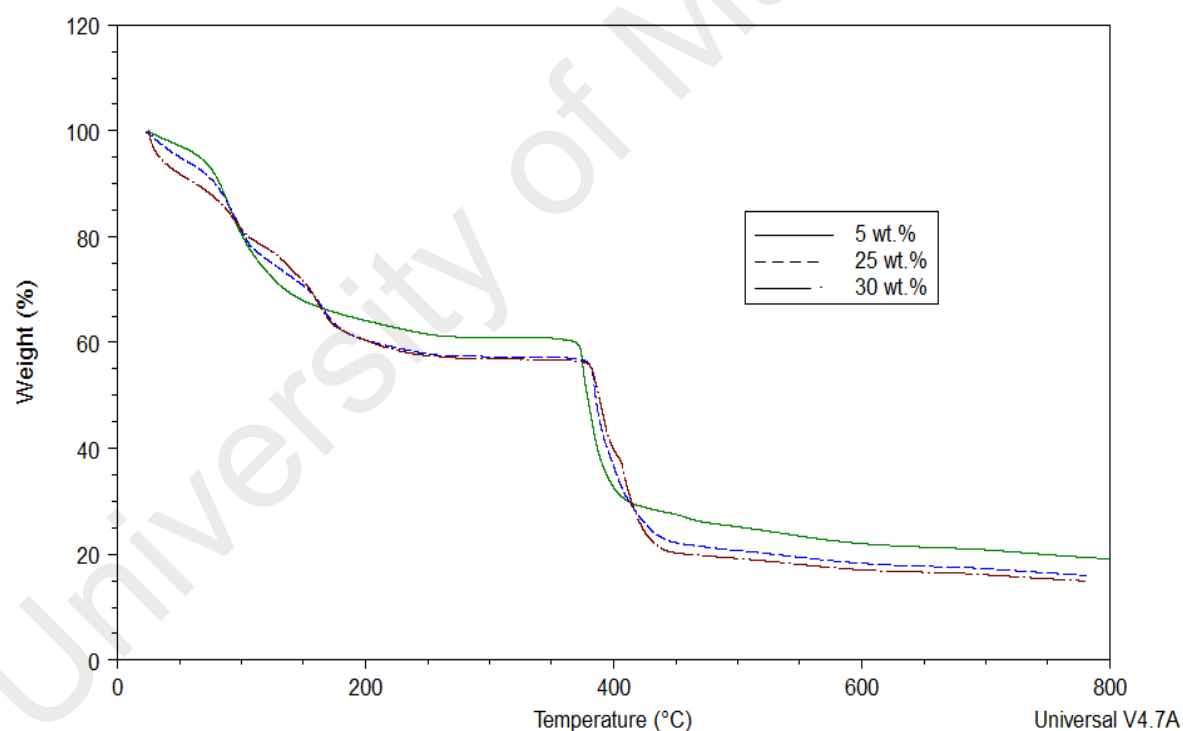


Figure 5.12: TGA plot for the films containing 5 wt.%, 25 wt.% and 30 wt.% of LiCF₃SO₃.

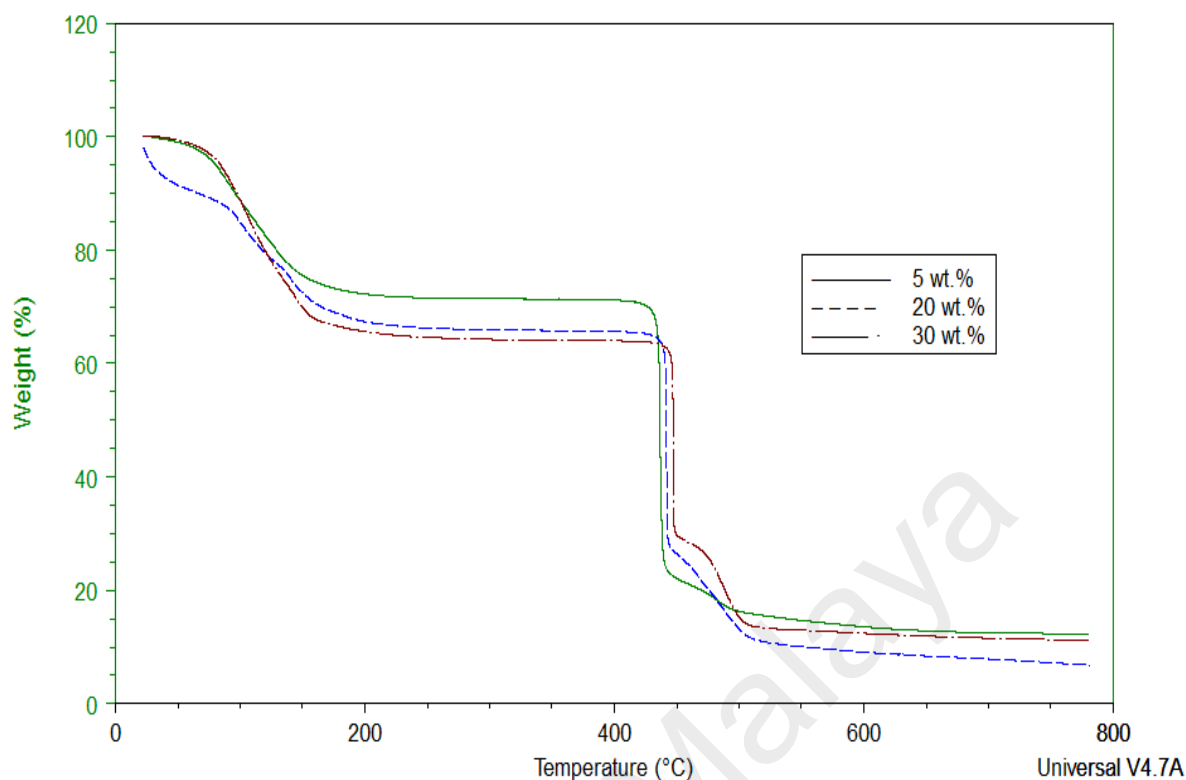


Figure 5.13: TGA plot for the films containing 5 wt.%, 20 wt.% and 30 wt.% of NaCF_3SO_3 .

The results of weight-loss ratios for all samples are summarized in Table 5.2. It can be seen that the first decomposition temperature increases when the salt was added to the PVdF-HFP/EC/PC film indicating that all GPE-salt complexes are thermally stable up to 128 °C. The weight loss percentages for all stages are observed to increase upon the addition of LiCF_3SO_3 salt. This is due to the presence of triflate anion group, which can be burnt off easily as carbon oxides, sulfur oxides and hydrogen fluoride as compared to the polymer host and lithium ions (Ramesh & Lu, 2011a). The weight loss of about 3% at temperature below 100 °C observed in TGA curve containing 20 wt.% NaCF_3SO_3 is due to the removal of moisture absorbed with sodium salt (Deepak Kumar & Hashmi, 2010). The result clearly shows that the highest conducting film from both systems (25 wt.% LiCF_3SO_3 and 20 wt.% NaCF_3SO_3) have a good thermal stability, whereas the 25 wt.% LiCF_3SO_3 shows the most thermally stable film up to ~ 179 °C,

which is higher than that of liquid electrolytes (80 °C) currently used in lithium ion batteries (Kuo, Chen, Wen, & Gopalan, 2002). Therefore, this type of GPE film with better thermal stability may enhance the performance and safety of the batteries. It is also observed that the amount of weight loss for the second region of decomposition decrease with increasing salt concentrations. This may be due to the higher amount of lithium salt and sodium salt that interacts with the polymer host, making the film more difficult to be decomposed (Ramesh & Lu, 2013).

Table 5.2: Decomposition temperatures and weight loss percentages of GPE films obtained from the TGA thermograms

GPE film	1 st decomposition T _{d1}	Weight lost at T _{d1} (%)	2 nd decomposition T _{d2}	Weight lost at T _{d2} (%)	Total weight loss (%) at 700 °C
Pure PVDF-HFP	155	5.2	461	72.0	84
PVDF-HFP/EC/PC	122	31.2	438	49.2	86
GPE +5 wt.% LiCF ₃ SO ₃	128	38.7	373	33.3	80.7
GPE +25 wt.% LiCF ₃ SO ₃	179	41.8	38.2	35.1	83.8
GPE +30 wt.% LiCF ₃ SO ₃	173	42.6	416	36.6	84.3
GPE +5 wt.% NaCF ₃ SO ₃	145	27.8	436	49.1	87.6
GPE +20 wt.% NaCF ₃ SO ₃	155	24.5	441	38.8	91.5
GPE +30 wt.% NaCF ₃ SO ₃	150	34.3	447	35.5	88.6

CHAPTER 6: STRUCTURAL AND MORPHOLOGICAL ANALYSIS

6.1 Fourier Transform Infrared Spectroscopy (FTIR) analysis

Infrared spectroscopy is a widely used technique for investigating chemical processes and structure. The Fourier Transform Infrared (FTIR) spectra were recorded in the range $4000\text{--}650\text{ cm}^{-1}$ with resolution of 1 cm^{-1} using Thermo Scientific Nicolet Smart ATR spectrophotometer to identify the complexation of the prepared GPE films. The purpose of this analysis is also to study the effect of adding plasticizers (EC and PC) and salts (LiCF_3SO_3 and NaCF_3SO_3) on pure PVdF-HFP film.

6.1.1 Pure PVdF-HFP

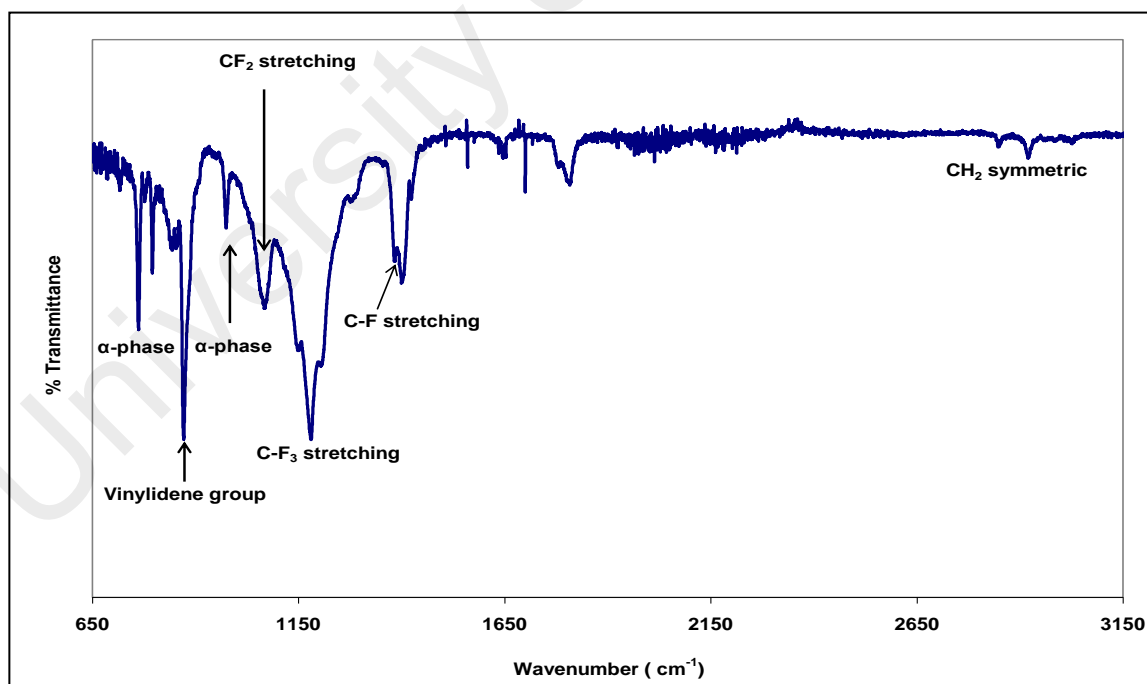


Figure 6.1: FTIR spectra of pure PVdF-HFP film in the region 650 cm^{-1} and 3150 cm^{-1}

Figure 6.1 shows the FTIR spectra of pure PVdF-HFP film in the wavenumber region from 650 to 3200 cm^{-1} . The vibrational bands in the pure PVdF-HFP spectra obtained from this work are consistent with that reported in literature review as listed in Table 6.1. Band at 763 cm^{-1} , and 976 cm^{-1} are assigned to α -phase of the semicrystalline PVdF-HFP. The band at 877 cm^{-1} is assigned to the amorphous phase of PVdF-HFP. The peaks at 1070 cm^{-1} , 1180 cm^{-1} and 1400 cm^{-1} are assigned to C – F₂ stretching, C – F₃ stretching and C – F stretching, respectively. Since the structure of PVdF-HFP involves a high density of CF groups, this vibrational bands is expected to be changed in the gel polymer electrolyte complexes (Saikia & Kumar, 2005).

Table 6.1: The vibrational modes and wavenumbers of pure PVdF-HFP

Wavenumber (cm^{-1})	Assignment of bands	Reference
1390,1410	C-F stretching	(Saikia & Kumar, 2005).
880	Vinylidene group/amorphous phase	(Saikia & Kumar, 2005), (Saikia & Kumar, 2004)
796, 848, 978, 1401	α -phase	(Saikia et al., 2011), (D Kumar et al., 2011)
1180	symmetrical stretching of –CF ₃	(Saikia, Han, & Chen-Yang, 2008), (Ramesh & Lu, 2011b)
1080	C-F ₂ stretching	(Saikia & Kumar, 2005), (Saikia & Kumar, 2004)
2971	CH ₂ symmetric	(Golcuk, Muftuoglu, Celik, & Bozkurt, 2013)

6.1.2 PVdF-HFP/EC/PC

Figure 6.2 shows the FTIR spectra of pure PC and pure EC film in the region between 650 cm^{-1} and 2250 cm^{-1} . In pure PC spectrum, the absorption peaks at 1179 cm^{-1} is due to C – O stretching and C – H wagging. As can be clearly seen from Figure 6.2 (a), the bands of ring stretching and ring breathing was observed as a sharp peak at 1047 cm^{-1} . The peak of C = O stretching band can be found at 1785 cm^{-1} . In pure EC spectrum, The peaks appeared at 717 cm^{-1} and 893 cm^{-1} are due to C = O bending and ring breathing, respectively. The skeletal stretching frequencies are found at 973 cm^{-1} , 1070 cm^{-1} and 1170 cm^{-1} . The group of frequencies at 1400 cm^{-1} and 1420 cm^{-1} are assigned to CH₂ wagging. The peak at 1470 cm^{-1} was assigned to CH₂ bending. Wang and co-workers reported that EC has a pair of intense doublets at 1770 cm^{-1} and 1798 cm^{-1} (Wang et al., 1996). These doublets are due to C = O stretching mode. In this work, the doublets are found at 1780 cm^{-1} and 1810 cm^{-1} . Table 6.2 lists the vibrational bands in pure PC and pure EC spectra obtained from this work and literature review.

Figure 6.3 shows the FTIR spectra of pure PVdF-HFP and PVdF-HFP/EC/PC film in the region between 650 cm^{-1} and 1650 cm^{-1} . The intensity of absorption peak observed at 873 cm^{-1} in pure PVdF-HFP spectrum is found to be decreased in plasticized films. The intensity of the peak of CF₂ stretching that found at 1080 cm^{-1} in pure PVdF-HFP is increased in the GPE films, which might be due to the addition of the plasticizing solvent, EC and PC. The changes in the position of vibrational modes indicate that the complexation between PVdF-HFP with EC and PC has occurred. The shifted peak from 1180 cm^{-1} in pure PVdF-HFP film to 1160 cm^{-1} in plasticized film can be suggested that the interaction has occurred between carbon atoms in the C – O group of PC and the fluorine atoms of C – F₃ group in PVdF-HFP.

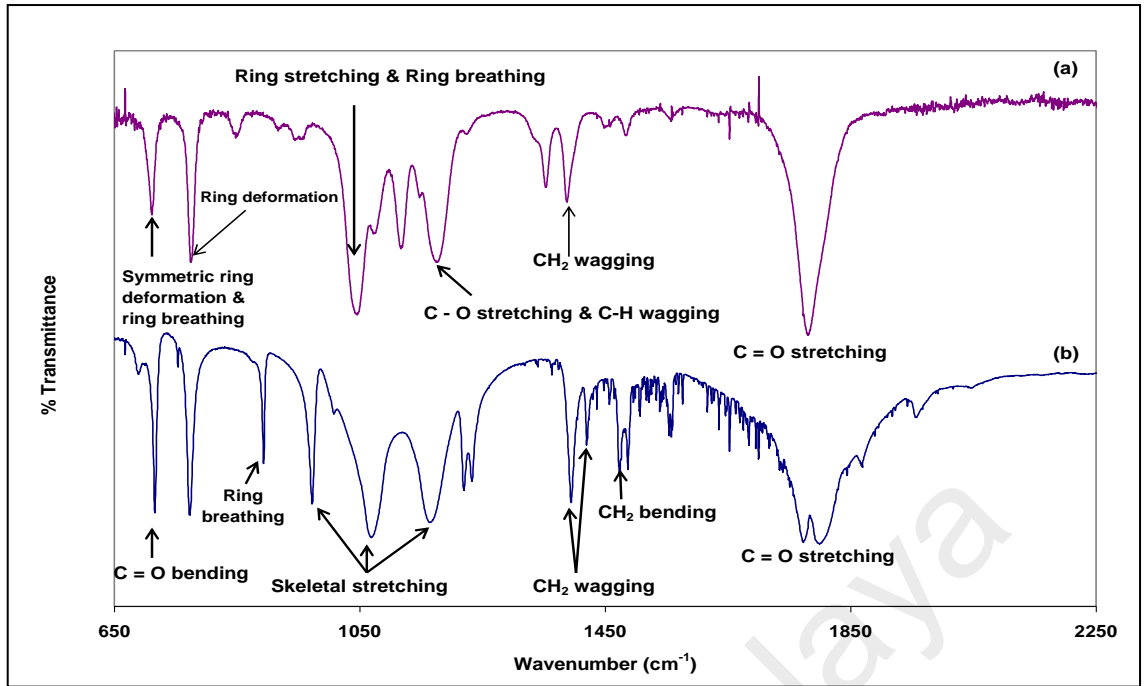


Figure 6.2: FTIR spectra of (a) pure PC and (b) pure EC in the range of 650 cm⁻¹ and 2250 cm⁻¹.

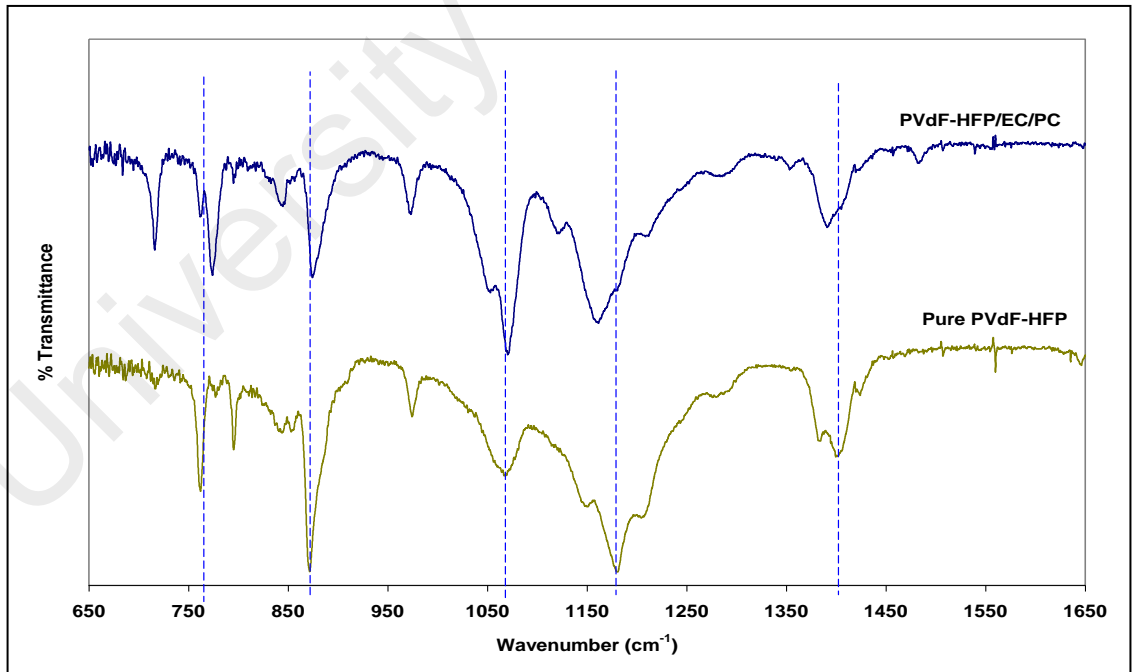


Figure 6.3: FTIR spectra of pure PVdF-HFP film and PVdF-HFP/EC/PC film.

Table 6.2: The vibrational modes and wavenumbers of pure EC and pure PC.

Assignment of bands	EC (wavenumber) (cm⁻¹)	PC (wavenumber) (cm⁻¹)	Reference	Wavenumbers obtained from the work (cm⁻¹)
C=O stretching	1810-1871, 1774 & 1803, 1773 & 1798, 1795	1789	(Deepa, Agnihotry, Gupta, & Chandra, 2004) (Huang et. al., 1996)	PC = 1785 EC = 1780 & 1810
Ring breathing	1067, 890	-	(Huang et. al., 1996)	893
Skeletal stretching	970,1076,1180	-	(Chintapalli & Frech, 1996)	973, 1070, 1170
CH ₂ wagging	1394, 1420	-	(Huang et. al., 1996)	1400, 1420
CH ₂ bending	1480	-	(Chintapalli & Frech, 1996)	1470
C=O bending	717	-	(Ramesh, Leen, Kumutha, & Arof, 2007)	717
Ring deformation	-	776	(Deepa et al., 2004)	776
Ring stretching + ring breathing	-	950,957	(Deepa et al., 2004)	1047
C-O stretching & C-H wagging	-	1179	(Deepa et al., 2004)	1178
Symmetric ring deformation + ringbreathing	-	712	(Deepa et al., 2004)	713

6.1.3 PVdF-HFP/EC/PC/ LiCF₃SO₃ and PVdF-HFP/EC/PC/ NaCF₃SO₃ systems

On addition of LiCF₃SO₃ and NaCF₃SO₃ salt into polymer electrolytes, the cation of the salt is expected to coordinate with lone pair of electrons present in fluorine atoms of host polymer, PVDF-HFP to form polymer-salt complexes. This interaction will influence the local structure of the polymer backbone and some modes of vibration will also be affected.

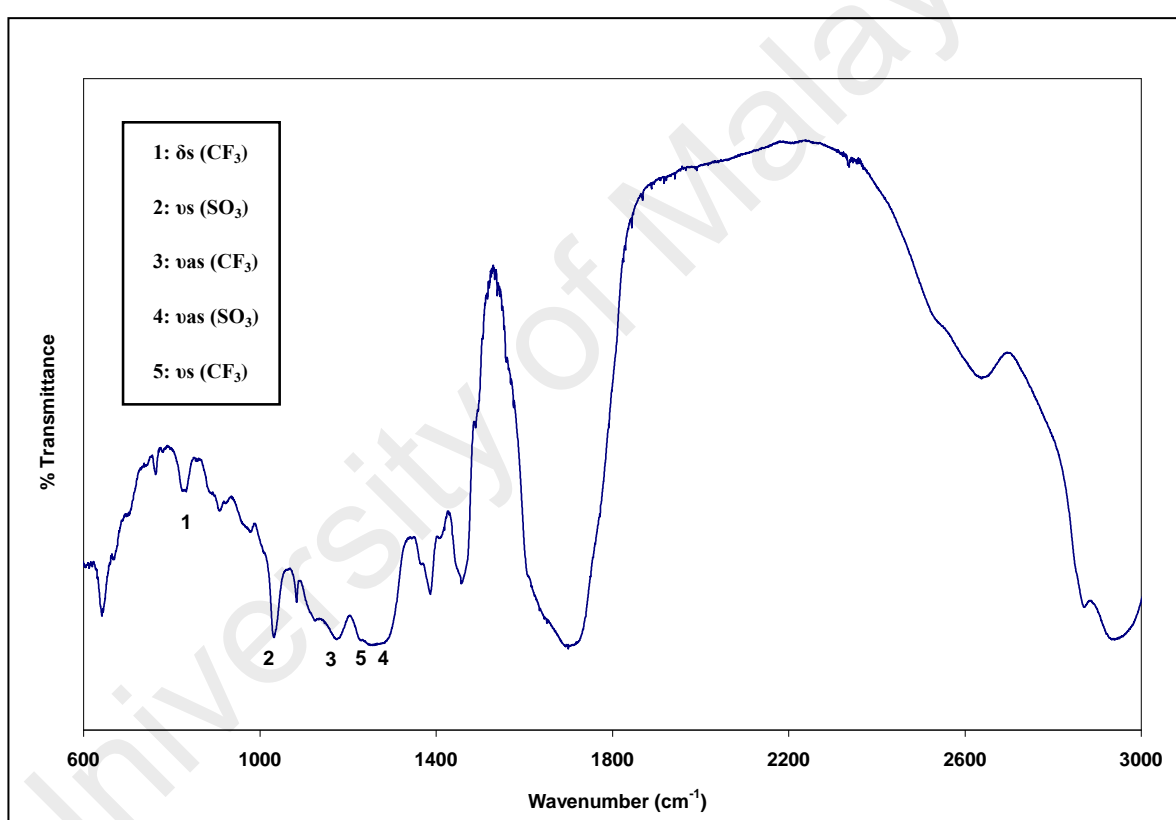


Figure 6.4: FTIR spectrum of LiCF₃SO₃ salt.

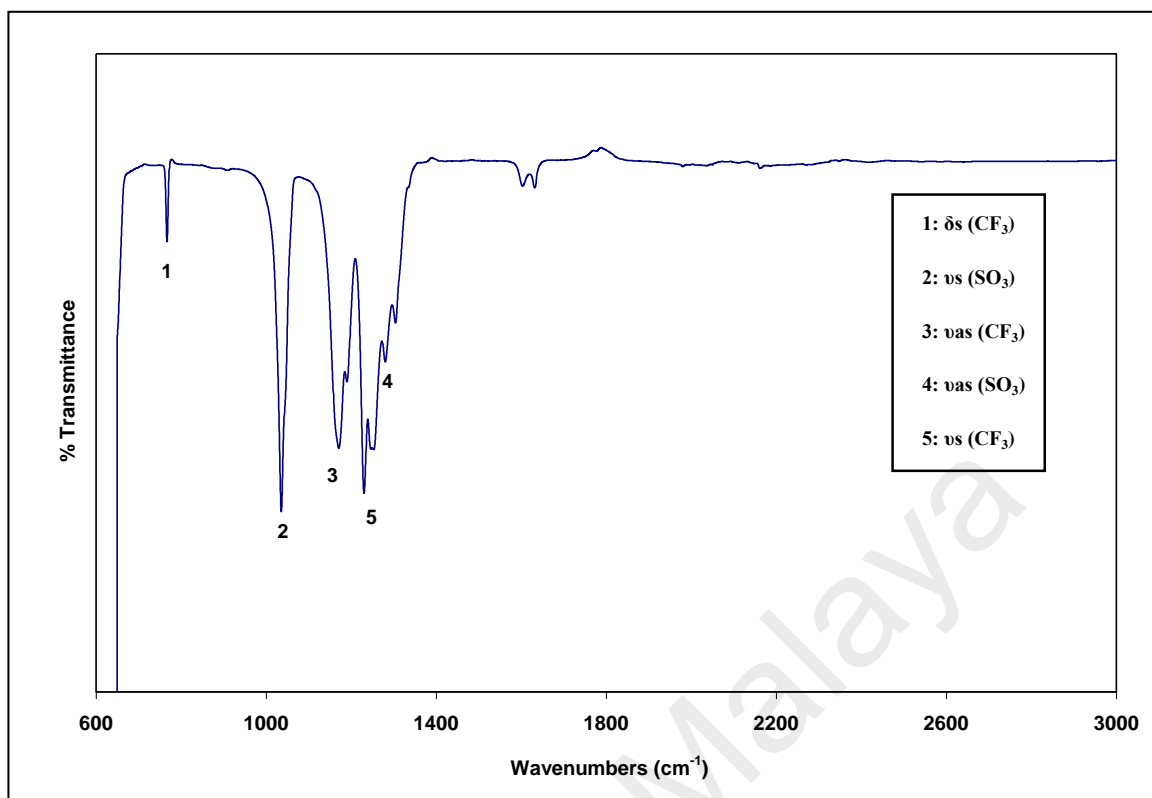


Figure 6.5: FTIR spectrum of NaCF_3SO_3 salt.

Figure 6.4 and 6.5 show the FTIR spectra for LiCF_3SO_3 and NaCF_3SO_3 salt in the region between 600cm^{-1} and 3000cm^{-1} . Since the anion of the salts is triflate [CF_3SO_3], they were expected to have a similar frequency bands as listed in Table 6.3 and Table 6.4. In spectroscopic studies of triflate containing polymer electrolytes, attention has been focused almost exclusively on the CF_3 symmetric deformation δ_s (CF_3) and SO_3 symmetric stretching ν_s (SO_3) modes. The δ_s (CF_3) have been well established to reflect the ionic association of the triflate anion at the SO_3 end through electronic distribution. The ν_s (SO_3) is particularly sensitive to ionic association since the oxygens of the triflate interact with the cations of the salt (Huang, Frech, & Wheeler, 1994).

Table 6.3: The vibrational modes and wavenumbers of LiCF₃SO₃ salt.

Vibrational modes	Wavenumbers (cm ⁻¹)	References	Wavenumbers obtained from the work (cm ⁻¹)
δ_s (CF ₃)	766,757	(Osman & Arof, 2003), (Sanders, Snow, Frech & Glatzhofer, 2003)	766
ν_s (SO ₃)	1033, 1043,1053,1062	(Wang et al., 1996)	1036
ν_{as} (CF ₃)	1182	(Angell, 1956)	1186
ν_{as} (SO ₃)	1272, 1257, 1302, 1260.	(Sanders, Snow, Frech & Glatzhofer, 2003)	1271
ν_s (CF ₃)	1230	(Angell, 1956)	1236

Table 6.4: The vibrational modes and wavenumbers of NaCF₃SO₃ salt.

Vibrational modes	Wavenumbers (cm ⁻¹)	References	Wavenumbers obtained from the work (cm ⁻¹)
δ_s (CF ₃)	766, 757	(Sanders, Snow, Frech & Glatzhofer, 2003)	769
ν_s (SO ₃)	1033, 1043,1053,1062	(Angell, 1956)	1037
ν_{as} (CF ₃)	1182, 1157	(Z. Wang et al., 1996), (Sanders, Snow, Frech & Glatzhofer, 2003)	1174
ν_{as} (SO ₃)	1272,1257, 1302,1271	(Sanders, Snow, Frech & Glatzhofer, 2003)	1282
ν_s (CF ₃)	1230	(Angell, 1956)	1232

Figure 6.6 and 6.7 show the FTIR spectra of pure PVdF-HFP film, PVdF-HFP/EC/PC film and gel polymer electrolyte films containing different concentrations

of LiCF_3SO_3 salt and NaCF_3SO_3 salt in the wavenumber region from 650 to 2600 cm^{-1} , respectively. The bands of SO_3 symmetric stretching [$\nu(\text{SO}_3)$] of pure LiCF_3SO_3 salt and NaCF_3SO_3 salt were observed at 1032 , 1042 and 1056 cm^{-1} as listed in Table 6.3 and 6.4 is due to free ions, ion pairs and ion aggregates, respectively. These bands were shifted to lower wavenumbers in the GPE films. The band due to in-plane deformation of CF_3 [$\delta(\text{CF}_3)$] of triflate salt was observed at 766 cm^{-1} . On addition of the salts into plasticized PVdF-HFP, several characteristics bands due to triflate anion were appeared in the FTIR spectra of GPE films. It is clearly observed that the characteristic bands of PVdF-HFP at 978 and 880 cm^{-1} which is assigned to α -phase and amorphous phase are broadened in the presence of EC, PC and triflate salt indicating that interaction occurred between polymer with EC, PC or salts. The intensity of the peak of CF_2 stretching that found at 1080 cm^{-1} in pure PVdF-HFP is increased in the GPE films for both systems, which might be due to the addition of the plasticizing solvent, EC and PC. It is also can be seen that the peak at 1180 cm^{-1} which is assigned to symmetrical stretching of $-\text{CF}_3$ of pure PVdF-HFP is shifted to 1170 cm^{-1} and become broadened with further addition of triflate salt. This suggested that the interaction has occurred between flourine atoms in PVdF-HFP and Li^+ or Na^+ in triflate salt. The $\text{C}=\text{O}$ stretching bands of EC and PC are found at 1780 cm^{-1} and 1810 cm^{-1} in pure EC and PC spectra become broadened with addition of salt in PVdF-HFP complexes. This indicates that the complexation has occurred due to the interaction through the Li^+ and Na^+ ions and the oxygen atoms of $\text{C}=\text{O}$ groups. These results also confirmed that the presence of plasticizing solvent will provide the pathway for ionic conduction in the GPE films.

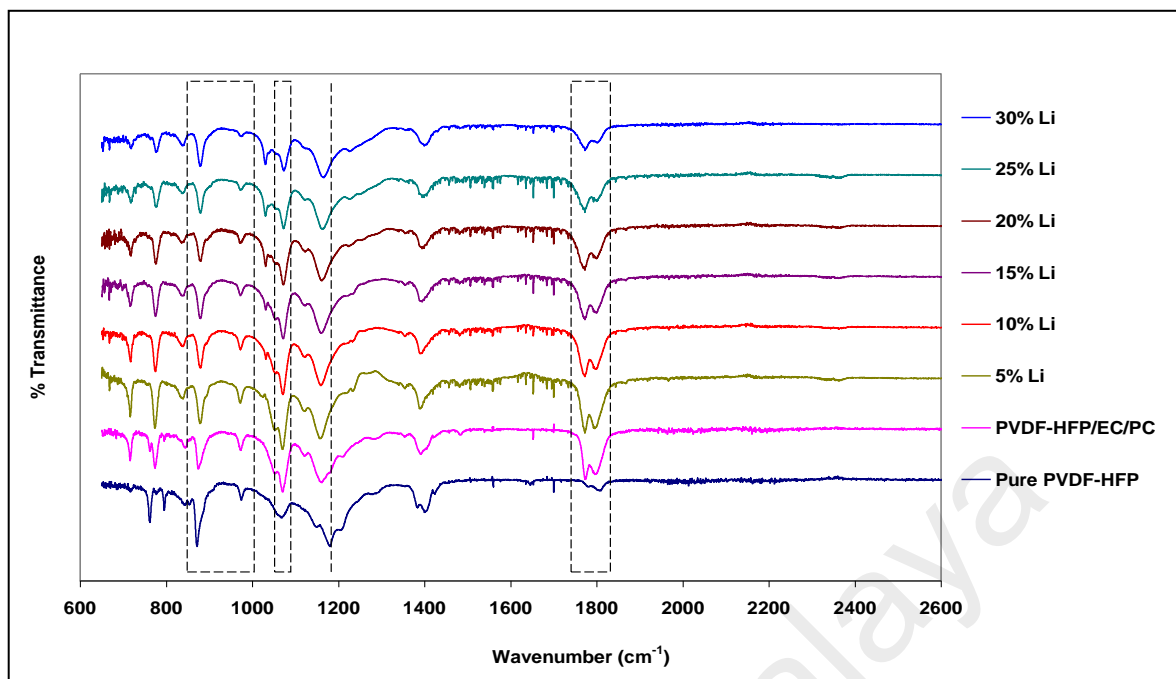


Figure 6.6: FTIR spectra of pure PVdF-HFP, PVdF-HFP/EC/PC and GPE films with different amount of LiCF₃SO₃ salt contents.

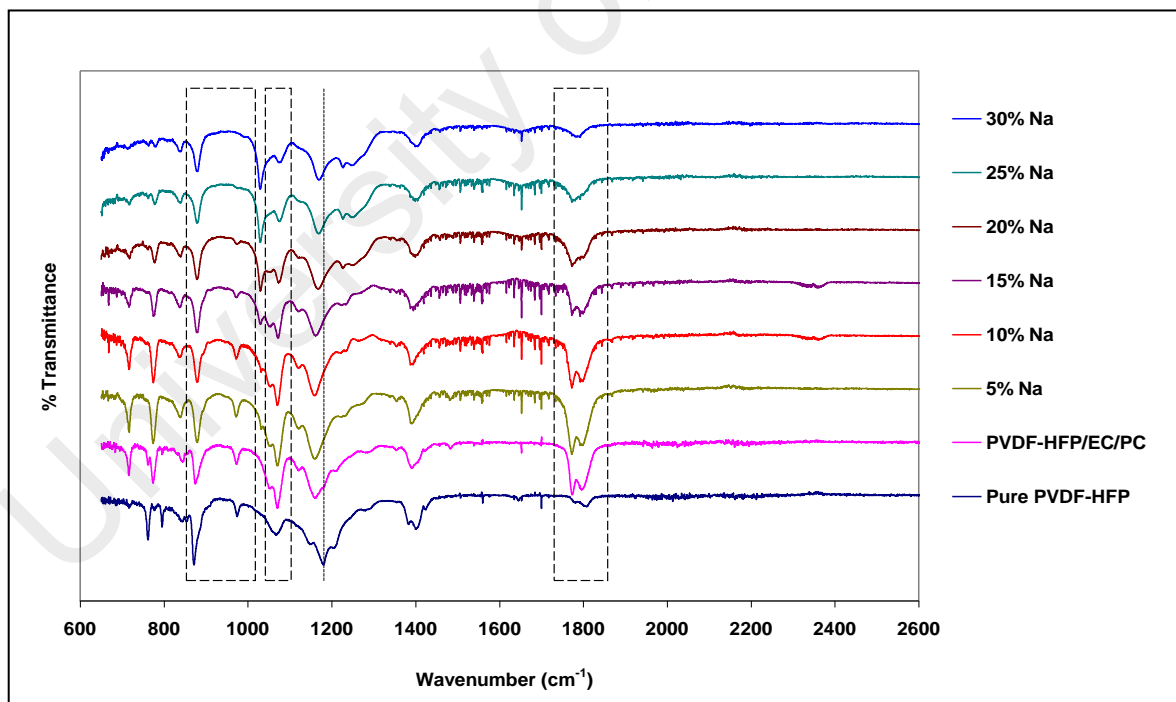


Figure 6.7: FTIR spectra of pure PVdF-HFP, PVdF-HFP/EC/PC and GPE films with different amount of NaCF₃SO₃ salt contents.

According to Jeong et. al (Jeong, Jo, & Jo, 2006), ion association of triflate anion occurs at the end of SO₃ thereby SO₃ symmetric stretching band [ν_s (SO₃)] is very sensitive to its coordination state of triflate anion. The band fitting of a Gaussian-Lorentzian peak in the region between 1000 and 1100 cm⁻¹ was applied in the FTIR spectra of GPE films in LiCF₃SO₃ system and NaCF₃SO₃ system as shown in Figure 6.8 and Figure 6.9. Band fitting of these regions has provided information pertaining to the free ions, ion pairs and ion aggregates of triflate anion and proved the occurring of ionic interaction in the GPE films. The bands assigned to free ions, ion pairs, ion aggregates and ring breathing of the plasticizing solvent are exhibited as region I, II, III and IV in Figure 6.8 and Figure 6.9. The amount of free ions, ion pairs, ion aggregates is represented by the area under the assigned bands. It can be observed from the figures that the amount of free ions (region I) increases while the amount of ion pairs (region II) and ion aggregates (region III) decreases with the addition of salt concentration of up to 25 wt.% and 20 wt. % of lithium and sodium salt, respectively. These results can be used to explain why the conductivity of PVdF-HFP GPE films exhibits a maximum at 25 wt.% of LiCF₃SO₃ and 20 wt.% of NaCF₃SO₃ for both system. High free ion concentration implies more ion dissociation over ion reassociation and vice versa (Kumar et al., 2005). At the highest concentration of triflate salt, the drop in conductivity is due to the large amount of ion pairs and ion aggregates and the small amount of free ions available. The mobility of ions is mostly influenced by the attractive coulombic forces that keep the ions into aggregates which causes the conductivity to decrease. The relationship between conductivity and ion states (free ions, ion pairs and ion aggregates) is shown in Figure 6.10, Figure 6.11 and 6.12, respectively.

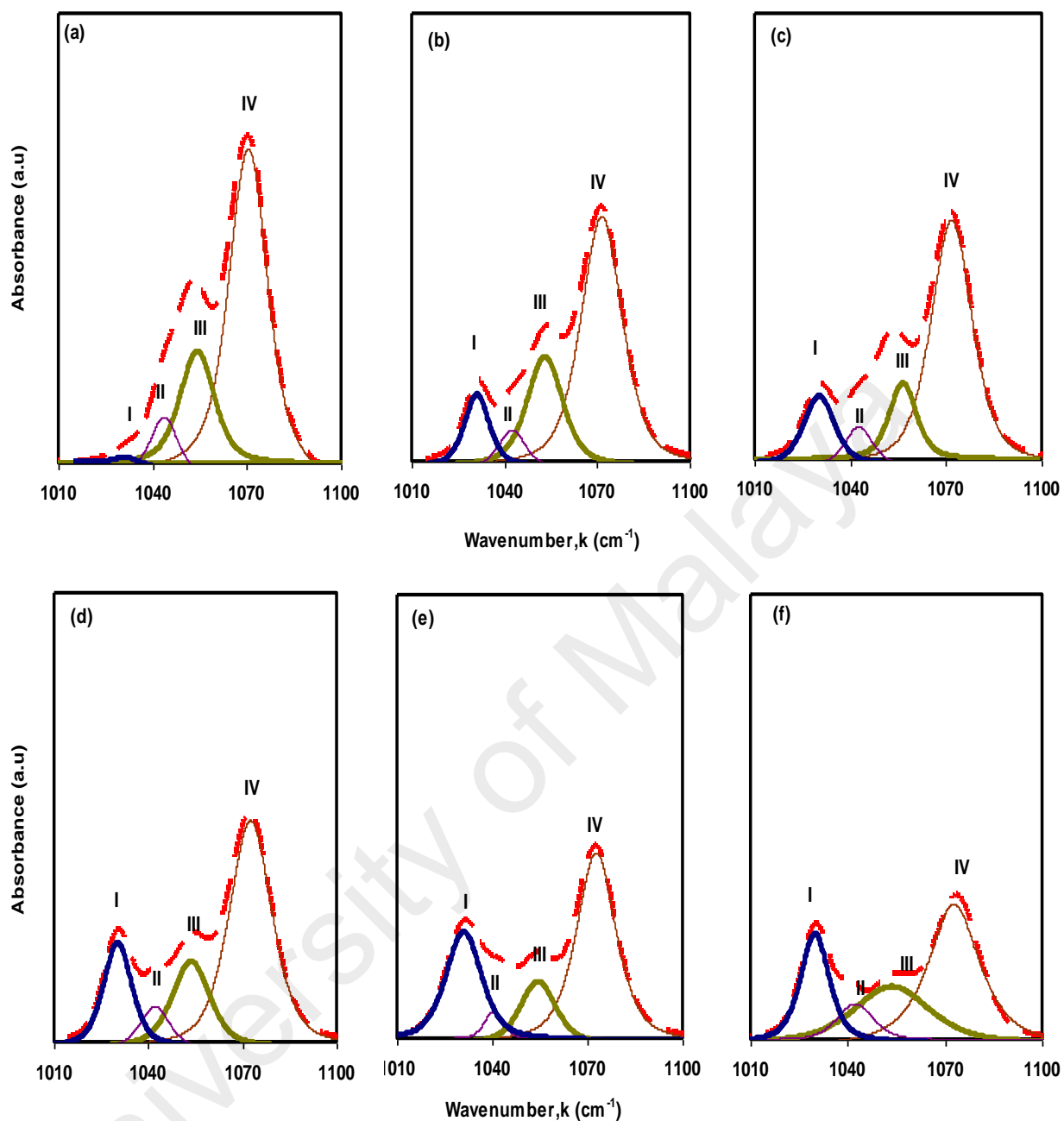


Figure 6.8: Deconvolution of FTIR spectra between 1000-1100 cm^{-1} for GPE films containing (a) 5 wt.% (b) 10 wt.% (c) 15 wt.% (d) 20 wt.% (e) 25 wt.% and (f) 30wt.% of LiCF_3SO_3 salt in the region (I) free triflate ions (II) ion pairs (III) ion aggregates (IV) ring breathing of the plasticizing solvent

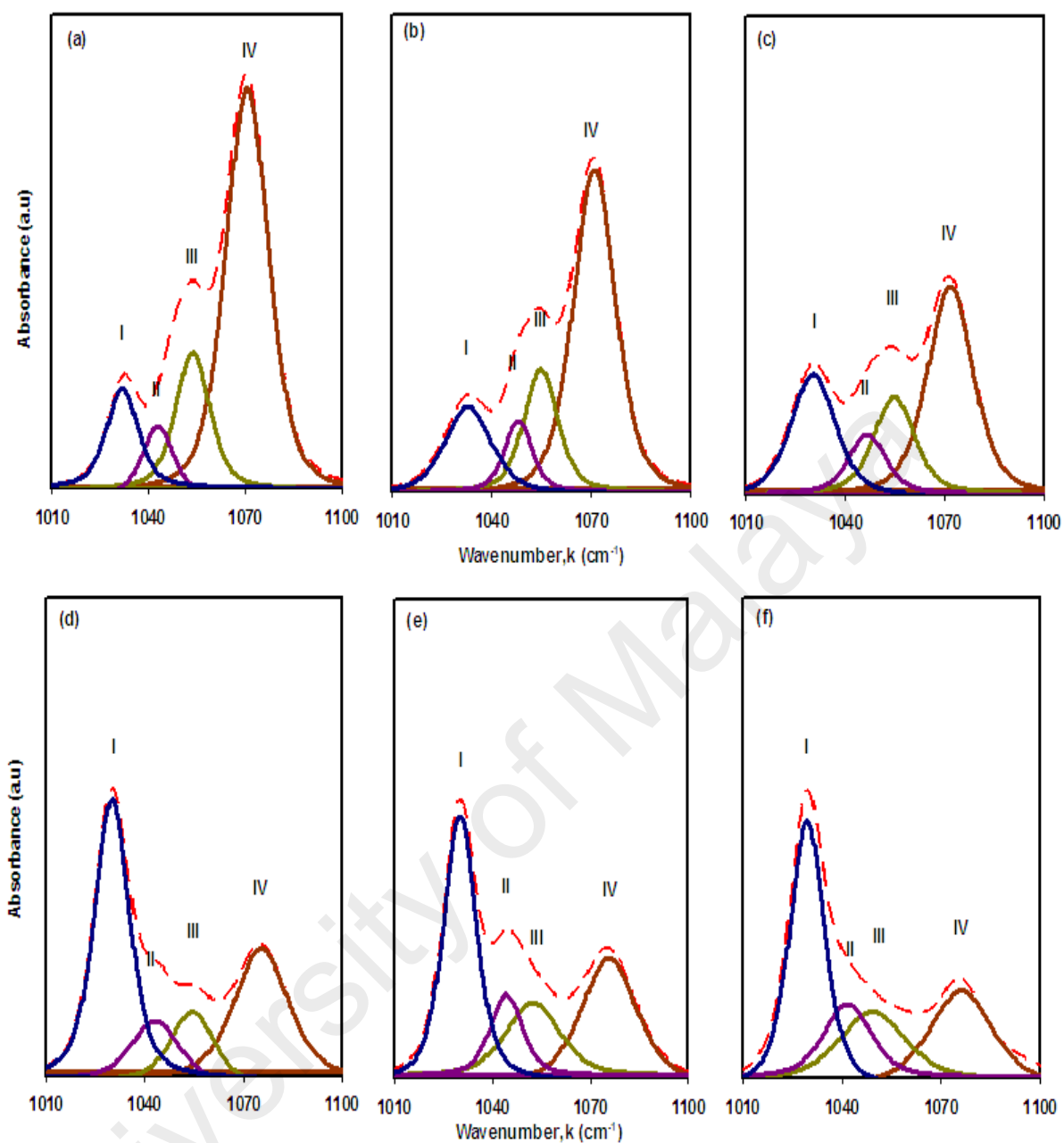


Figure 6.9: Deconvolution of FTIR spectra between 1000-1100 cm^{-1} for GPE films containing (a) 5 wt.% (b) 10 wt.% (c) 15 wt.% (d) 20 wt.% (e) 25 wt.% and (f) 30wt.% of NaCF_3SO_3 salt in the region (I) free triflate ions (II) ion pairs (III) ion aggregates (IV) ring breathing of the plasticizing solvent

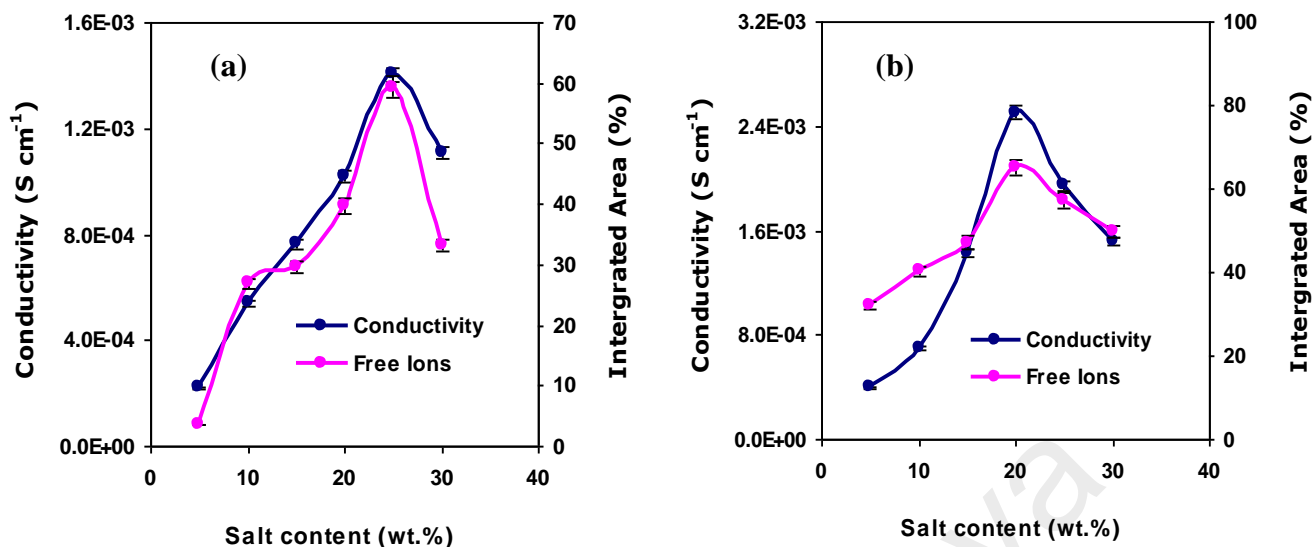


Figure 6.10: The plots of area under assigned decomposed of free ions band with conductivity versus the concentration of (a) LiCF₃SO₃ (b) NaCF₃SO₃ salt

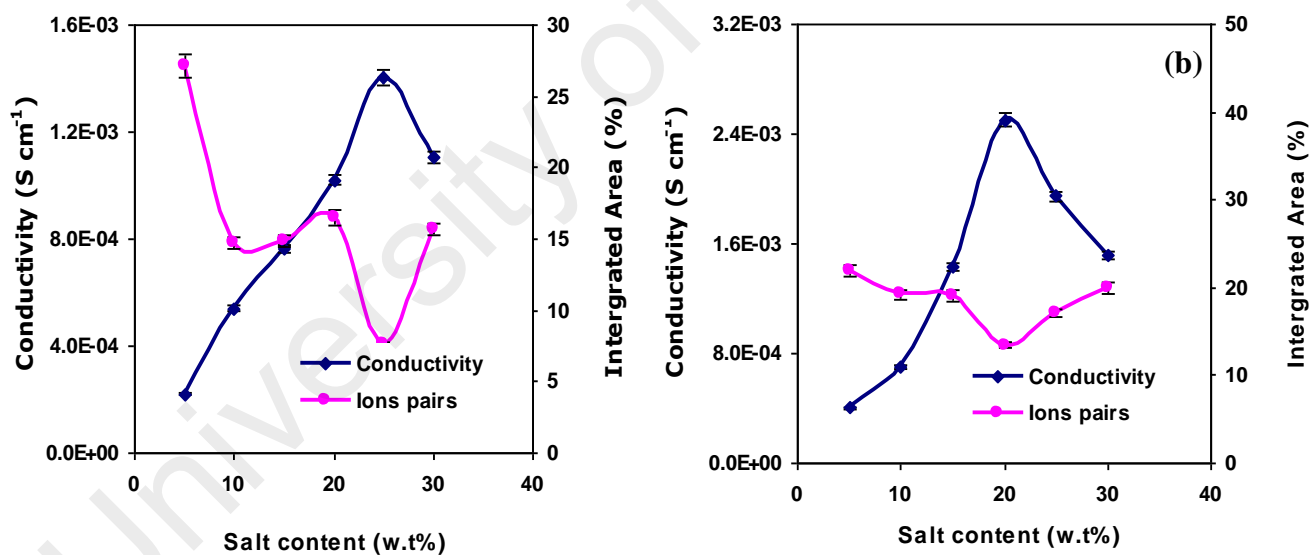


Figure 6.11: The plots of area under assigned decomposed of ion pair band with conductivity versus the concentration of (a) LiCF₃SO₃ (b) NaCF₃SO₃ salt

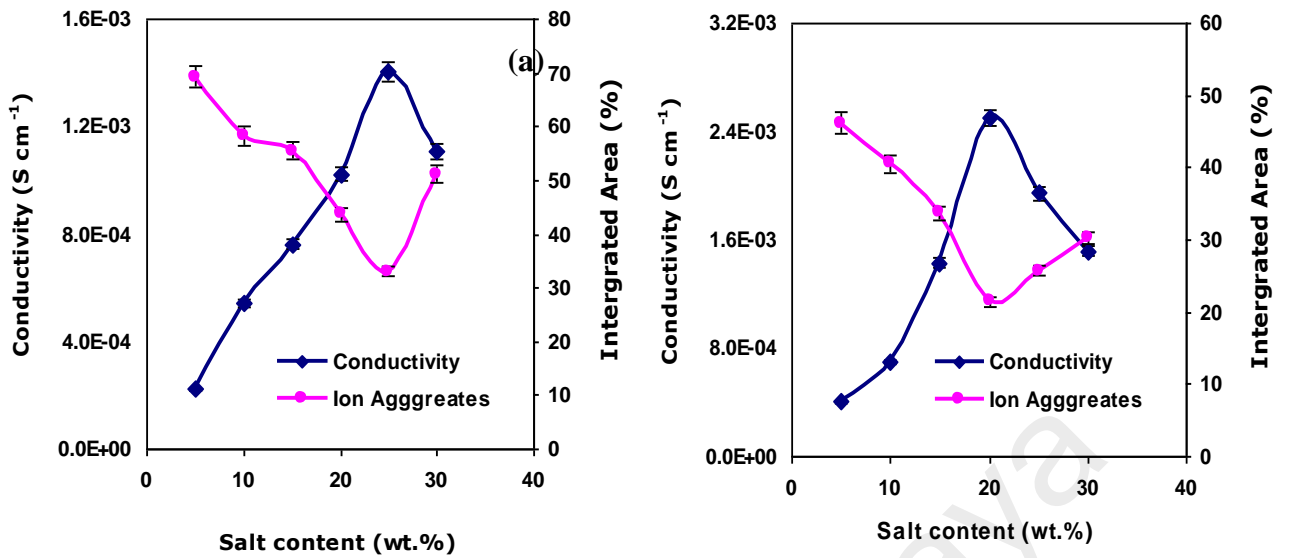


Figure 6.12: The plots of area under assigned decomposed of ion aggregate band with conductivity versus the concentration of (a) LiCF₃SO₃ (b) NaCF₃SO₃ salt

6.2 Raman Spectroscopy Analysis

Similar to FTIR spectroscopy, the Raman spectroscopy is one of the techniques that can be used to study the interaction between molecules in the GPE films. In FTIR, the infrared lights are absorbed in different amounts in a sample at distinct frequencies which correspond to the vibrational frequencies of the bonds in the sample. Contrary to FTIR, Raman is a light-scattering phenomenon which measures relative frequencies at which a sample scatters radiation, unlike FTIR spectroscopy which measures absolute frequencies at which a sample absorbs radiation. Whether Raman spectroscopy or FTIR spectroscopy, both methods have advantages and limitations, but when combined, these two methods become a powerful tool for performing materials characterization.

6.2.1 Pure PVdF-HFP and PVdF-HFP/EC/PC film

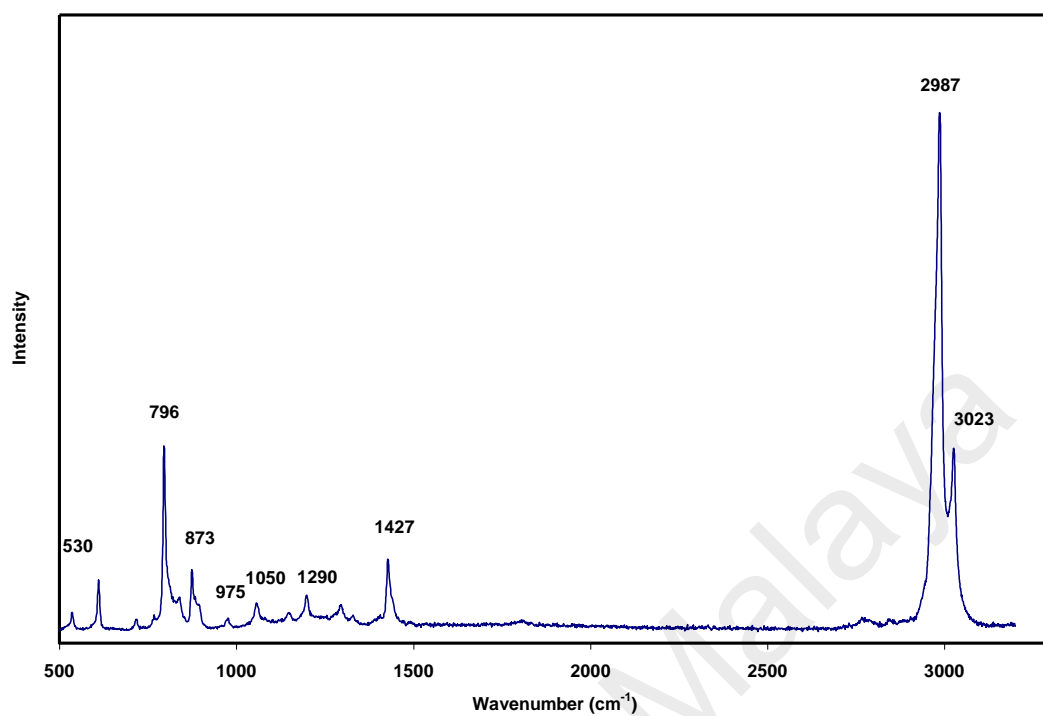


Figure 6.13: Raman Spectra of pure PVdF-HFP

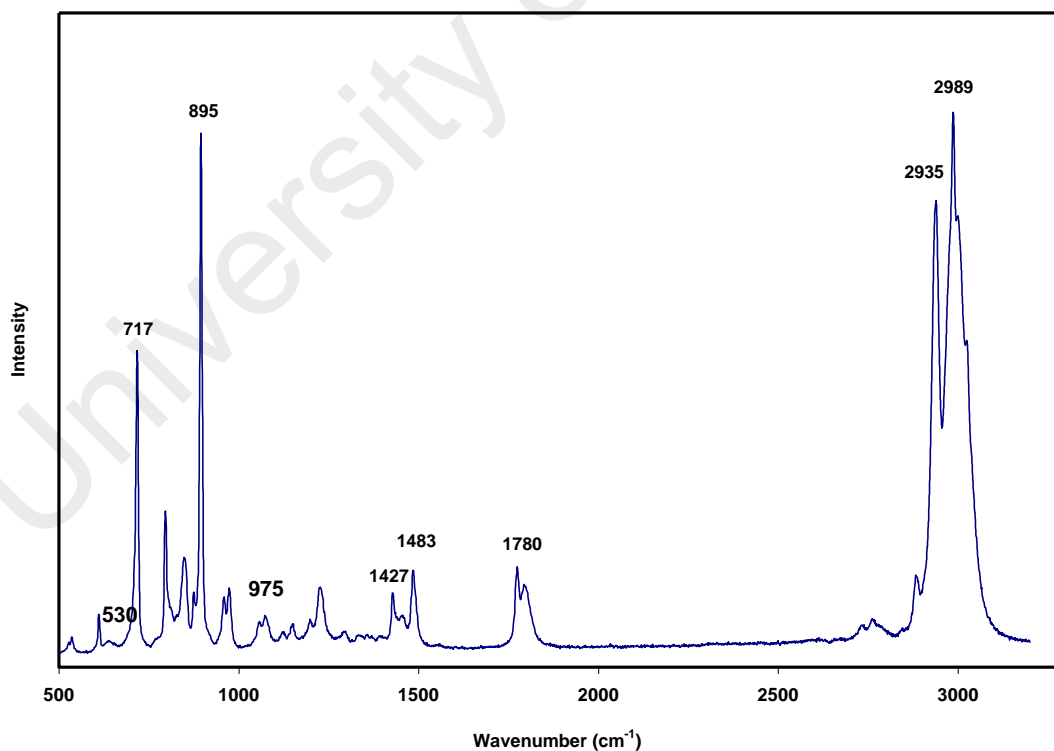


Figure 6.14: Raman spectra of PVdF-HFP/EC/PC film

Figure 6.13 and 6.14 presents raman spectra of pure PVdF-HFP and PVdF-HFP/EC/PC film, respectively. The raman spectra were obtained in the frequency range of 500 – 3200 cm^{-1} . The bands at 975, (1050 and 1290), and 1427 cm^{-1} are assigned to vinylidene, CF_3 group, $-\text{C}-\text{F}-$ and $-\text{CF}_2-$ stretching vibration and scissoring vibration of the vinyl group, respectively. The band at 873 cm^{-1} for the combination of C–C band and $\text{CCC}\delta$ skeletal bending of $\text{CF}-\text{CH}-\text{CF}$ is also be observed (Aravindan, Vickraman, Sivashanmugam, Thirunakaran, & Gopukumar, 2009). The peaks which appeared at 530 and 975 cm^{-1} are due to α phase of semi crystalline polymer PVdF-HFP. These peaks are observed to appear as a doublet in the PVdF-HFP/EC/PC complexes indicating the deformation of α -phase region which is due to the effect of solvent plasticizing on the crystalline structure of PVdF. The most intense peak at 796 cm^{-1} in pure PVDF-HFP spectrum is corresponding to the CH_2 rocking and the peak is becomes weak and completely absent in the PVdF-HFP/EC/PC complexes. It suggested that the interaction of the plasticizers with the polymer may reduce the intensity of the peak to form the amorphous phase in the GPE films. It also found that the band characteristic for plasticizer EC and PC, assigned to C=O bending and symmetric ring vibration appeared clearly at 717 and 895 cm^{-1} in the spectra.

6.2.2 PVdF-HFP/EC/PC/ LiCF_3SO_3 and PVdF-HFP/EC/PC/ NaCF_3SO_3 systems

Figure 6.15 and 6.16 displays Raman spectrum for the GPE system containing different amount of LiCF_3SO_3 and NaCF_3SO_3 content in the range of 600-1000 cm^{-1} , respectively. The CF_3 symmetric deformation δ (CF_3) band in CF_3SO_3^- for both system are found at 760 cm^{-1} which is close to the value observed in IR spectra i.e. 766 cm^{-1} . The band is shifted to 761 cm^{-1} at higher salt content. This indicates that there is possible interaction between the polymer with the Li and Na ions and also the

plasticizers with Li and Na ions in the GPE systems. The strong band at 795 cm^{-1} observed in pure PVdF-HFP spectra are found to be absent in the LiCF_3SO_3 and NaCF_3SO_3 GPE-complexes. It suggested that the interaction of the salt and plasticizers with the polymer may reduce the intensity of the peak to form the amorphous phase in the GPE films. It also found the intensity of the band at 717 and 895 cm^{-1} assigned to C=O bending and symmetric ring vibration plasticizers, EC and PC, is obviously lower in the GPE-complexes. Compared to pure PVdF-HFP film the reduction of the strong peaks in all GPE complexes indicated the interaction between plasticizers and other components of the films. In comparison, the band at 717 cm^{-1} is completely disappeared at higher NaCF_3SO_3 salt concentrations as shown in Figure 6.16. It indicates that there is stronger interaction between Na^+ ions and the oxygen atom in plasticizers than interaction of anions-cations of the salt. The SO_3 symmetric stretching $\nu_s(\text{SO}_3)$ band in CF_3SO_3^- for both systems is appeared at 1032 cm^{-1} as displayed in Figure 6.17 and 6.18, respectively. Similar to the $\delta(\text{CF}_3)$ band, the $\nu_s(\text{SO}_3)$ band also shifted to higher frequency i.e. 1033 cm^{-1} when more salt was added. It is clearly seen from the figures the $\delta(\text{CF}_3)$ band, the $\nu_s(\text{SO}_3)$ bands appeared as a strong band at highest salt composition i.e. 30 wt.% proving thereby that the increase of salt concentration leads to decrease of the amount of free anions and increase the number of ion pairs and aggregates. Therefore, this observation supports the conductivity studies where the conductivity tends to drop at higher salt concentrations after reaching the maximum value.

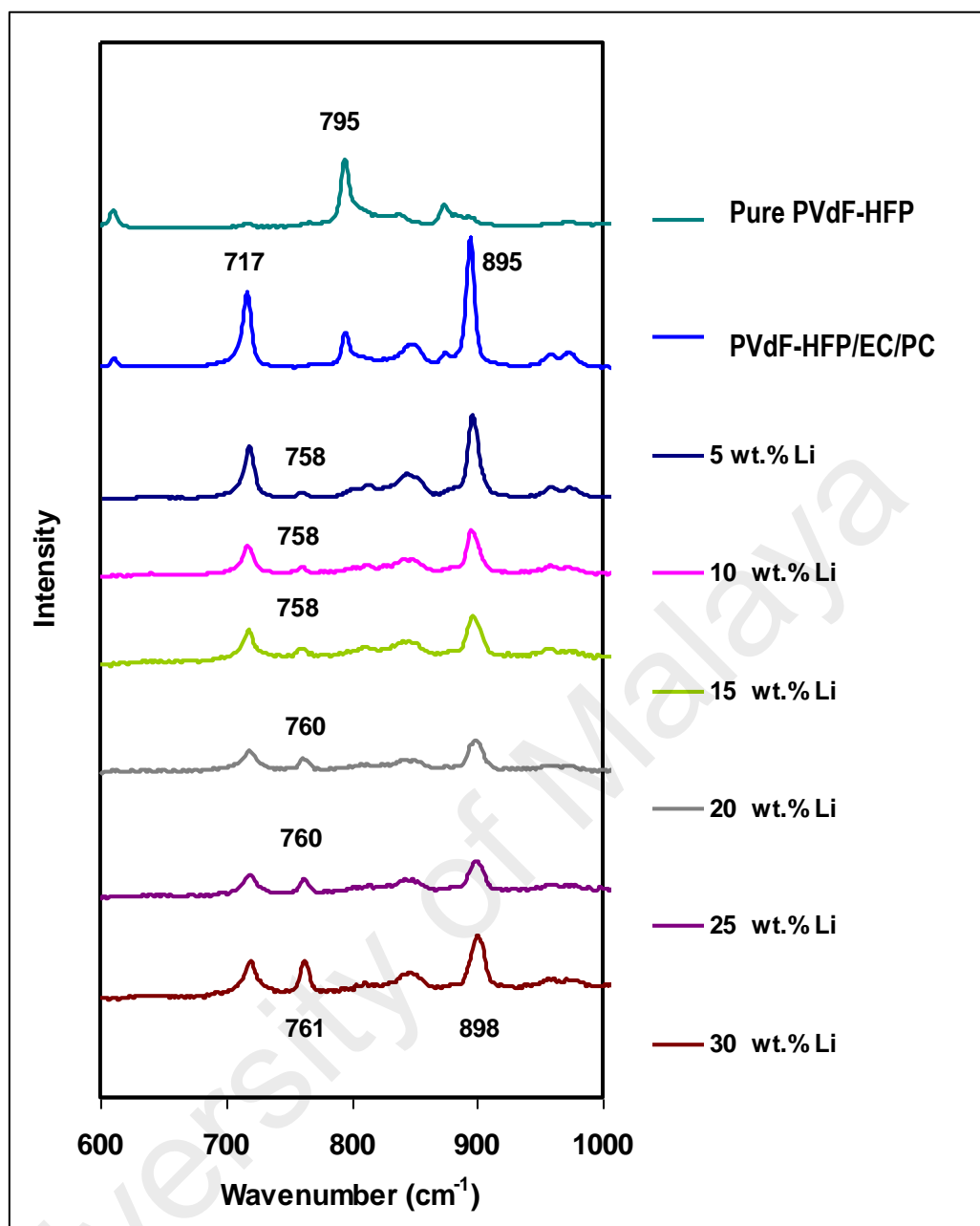


Figure 6.15: Raman spectrum of pure PVdF-HFP, PVdF-HFP/EC/PC and PVdF-HFP/EC/PC/LiCF₃SO₃ GPE with different salt compositions in the range of 600-1000 cm⁻¹

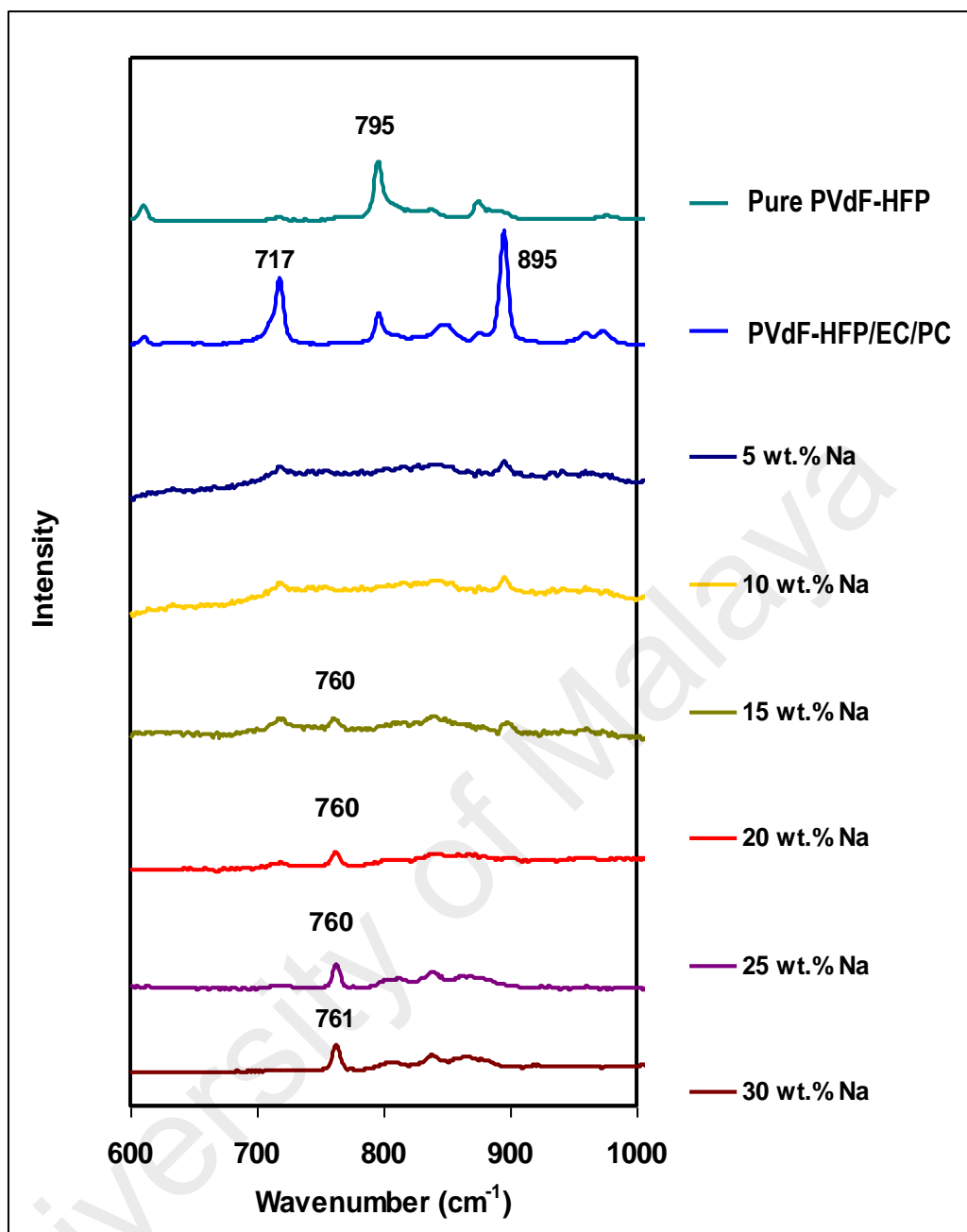


Figure 6.16: Raman spectrum of pure PVdF-HFP, PVdF-HFP/EC/PC and PVdF-HFP/EC/PC/NaCF₃SO₃ GPE with different salt compositions in the range of 600-1000 cm^{-1}

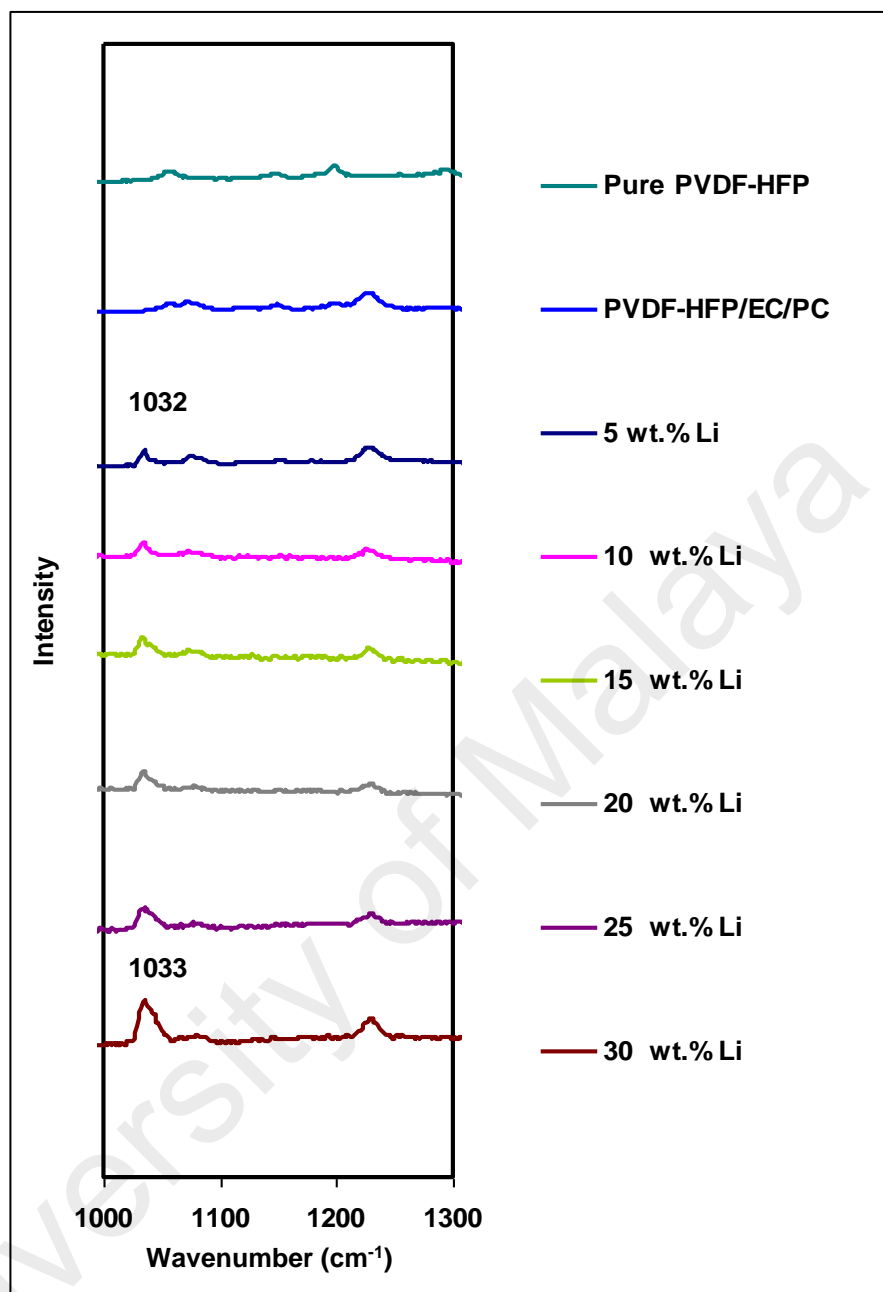


Figure 6.17: Raman spectrum of pure PVdF-HFP, PVdF-HFP/EC/PC and PVdF-HFP/EC/PC/LiCF₃SO₃ GPE with different salt compositions in the range of 1000 - 1300 cm⁻¹

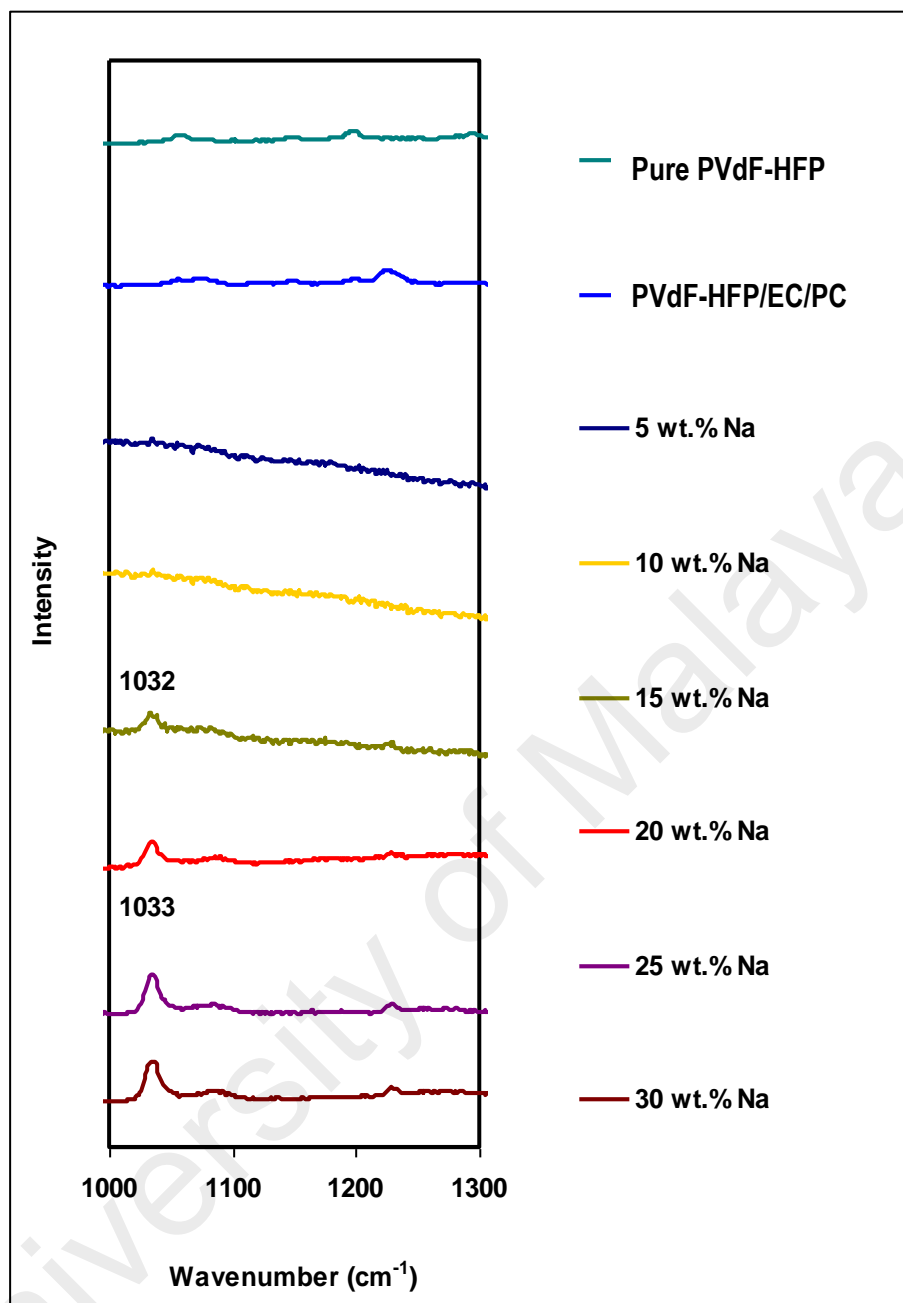


Figure 6.18: Raman spectrum of pure PVdF-HFP, PVDF-HFP/EC/PC and PVDFHFP/EC/PC/NaCF₃SO₃ GPE with different salt compositions in the range of 1000-1300 cm⁻¹

6.3 X-Ray Diffraction Analysis

The XRD is a very powerful determinative method that could be used to identify the structure of materials. In this work, the XRD was used to determine the structure of GPE system and the effect of salt and solvent plasticizers on the structure of host polymer, PVdF-HFP.

6.3.1 Pure PVdF-HFP and PVdF-HFP/EC/PC

Figure 6.19 shows the x-ray diffractogram of pure PVdF-HFP film. The XRD pattern of pure PVdF-HFP exhibit three peaks at $2\theta = 18.5^\circ$, 27.2° and 39.1° indicating semicrystalline nature of the polymer. These peak corresponding to crystalline phases of VdF α -phase crystals planes (Saikia & Kumar, 2004; Saikia, Han & Chen-Yang, 2008). The XRD pattern of PVdF-HFP/EC/PC film containing is shown in Figure 6.20. On addition of solvent plasticizers; EC and PC, the diffraction peaks of pure PVdF-HFP become broader and less intense. This can be attributed to the decrease in the degree of crystallinity or increase in amorphous phase of the polymer due to destruction of ordered arrangements of polymer chains and interaction of fluorine and oxygen atom of PVdF-HFP and plasticizers.

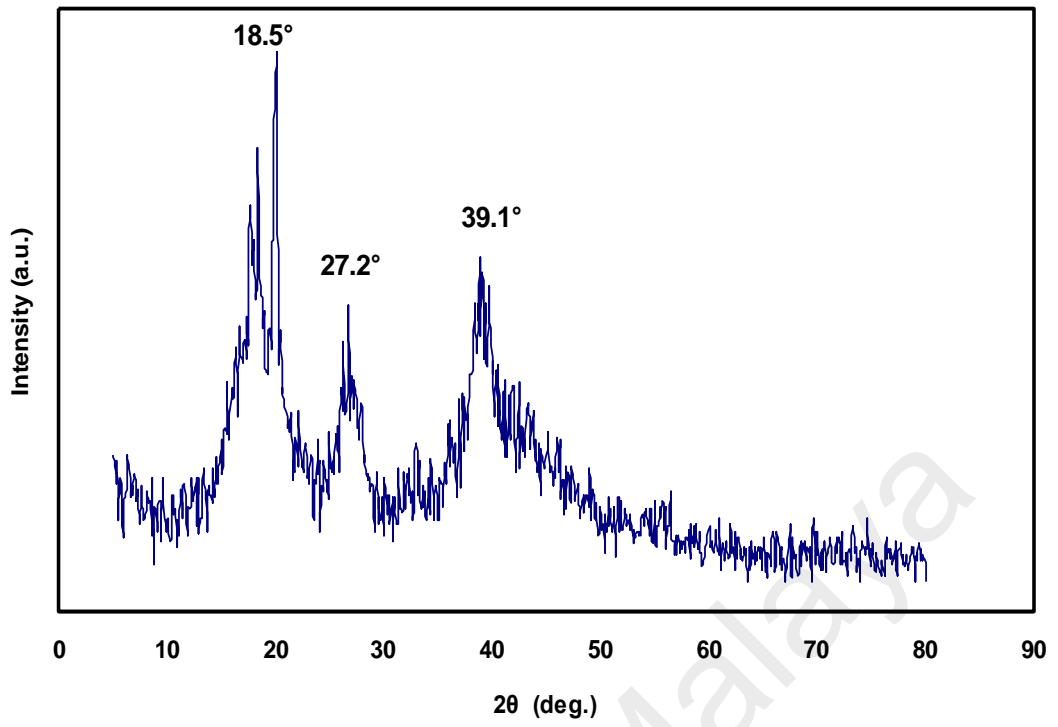


Figure 6.19: X-ray diffractogram of pure PVdF-HFP film

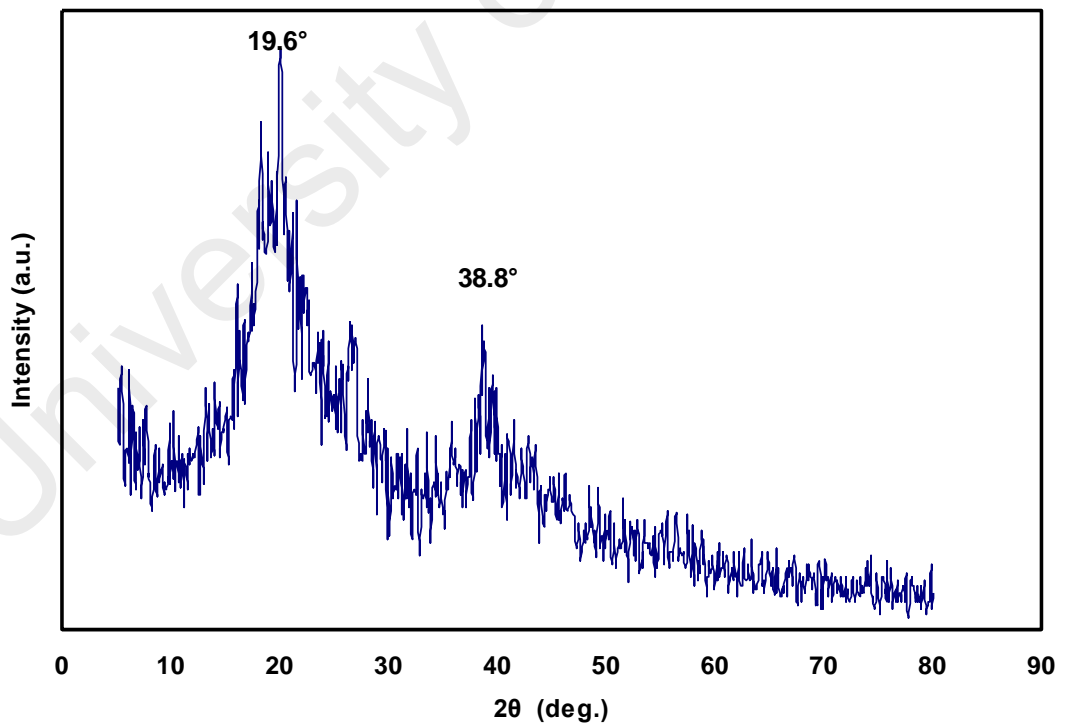


Figure 6.20: X-ray diffractogram of PVdF-HFP/EC/PC film

6.3.2 LiCF_3SO_3 and NaCF_3SO_3 Salts

The x-ray diffractogram of LiCF_3SO_3 salt and NaCF_3SO_3 salts are shown in Figure 6.21 and 6.22, respectively. The XRD pattern of LiCF_3SO_3 shows peaks at $2\theta = 16.7^\circ$, 19.8° , 20.3° , 22.5° , 24.6° , 25.5° , 33.0° , 33.6° and 41.7° . The strong peaks also can be found in NaCF_3SO_3 diffractogram which are observed at $2\theta = 23.7^\circ$, 32.9° , 34.8° , 42.7° , 48.7° , 53.5° and 56.20° . These reveal that both salts are crystalline in nature.

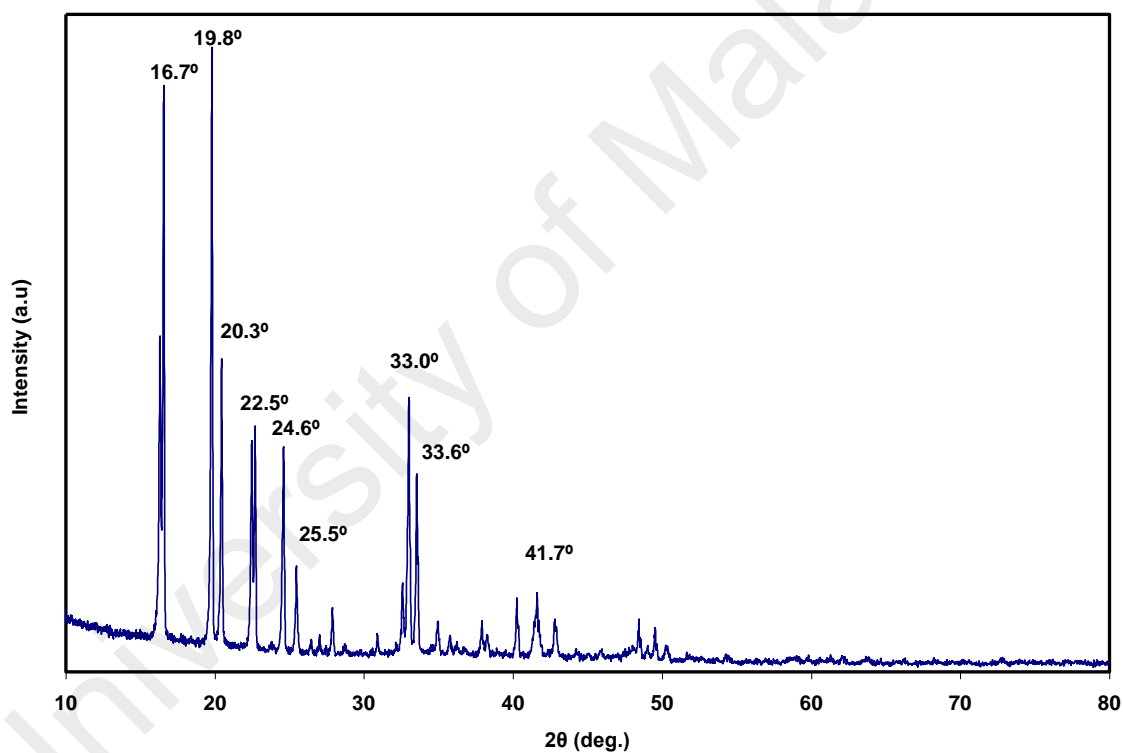


Figure 6.21: X-ray diffractogram of LiCF_3SO_3 salt.

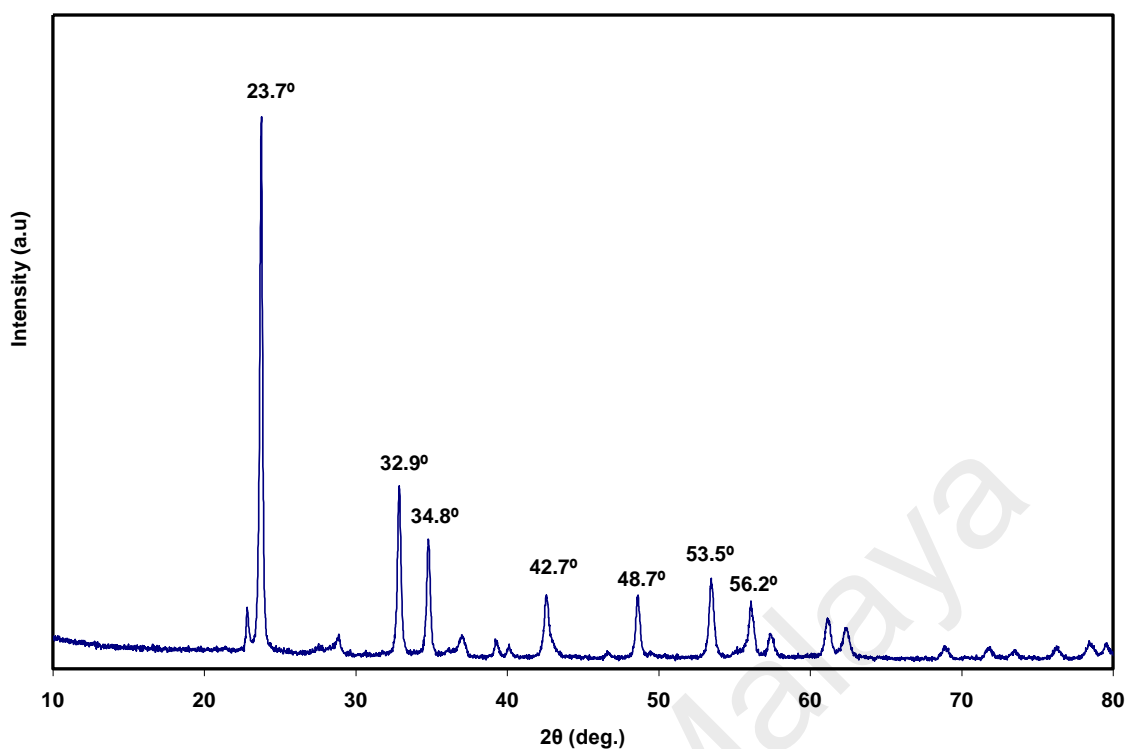


Figure 6.22: X-ray diffractogram of NaCF₃SO₃ salt.

6.3.3 PVdF-HFP/EC/PC/ LiCF₃SO₃ and PVdF-HFP/EC/PC/ NaCF₃SO₃ systems

Figure 6.23 shows the x-ray diffractogram of pure PVdF-HFP, PVdF-HFP/EC/PC and PVdF-HFP/EC/PC/LiCF₃SO₃ films containing different amounts of LiCF₃SO₃ salt. It can be observed that most of the peaks pertaining to pure LiCF₃SO₃ are absent in the polymer electrolyte films and indicates the complete dissolution of the salt in the polymer matrix PVdF-HFP and does not remain a separate phase. This observation is consistent with the FTIR results. The diffraction peak at 27.2° in pure PVdF completely disappeared in the GPE-complexes. On addition of the salt, the relative intensity of the characteristics peaks of PVdF-HFP/EC/PC at 38.8° is observed to decrease and become broaden indicates the reduction of crystalline phase in GPE-complexes. The film with 25 wt.% of LiCF₃SO₃ exhibit the most amorphous nature compared to the other films

thus leading to a highest conductivity in this system. This observation is in good agreement with the work done by Berthier and co-workers (Berthier et al., 1983). They reported that ionic conductivity in polymer electrolytes is associated with the amorphous phase of the studied samples. The x-ray diffractogram of pure PVdF-HFP, PVdF-HFP/EC/PC and PVdF-HFP/EC/PC/NaCF₃SO₃ films containing different amounts of NaCF₃SO₃ salt is shown in Figure 6.24. Similar to LiCF₃SO₃, all sharp crystalline peaks noticed NaCF₃SO₃ are absent in all GPE-complexes indicating the complexation has occurred between PVdF-HFP and NaCF₃SO₃ salt. The highest conductivity for this system is obtained from film containing 20wt.% of NaCF₃SO₃. It also can be observed that the XRD pattern of this film has the lowest intensity peak indicating the film is the most amorphous film. Therefore, the XRD analysis has confirmed that conductivity in the GPE films increases due to increase of amorphous phase in the films.

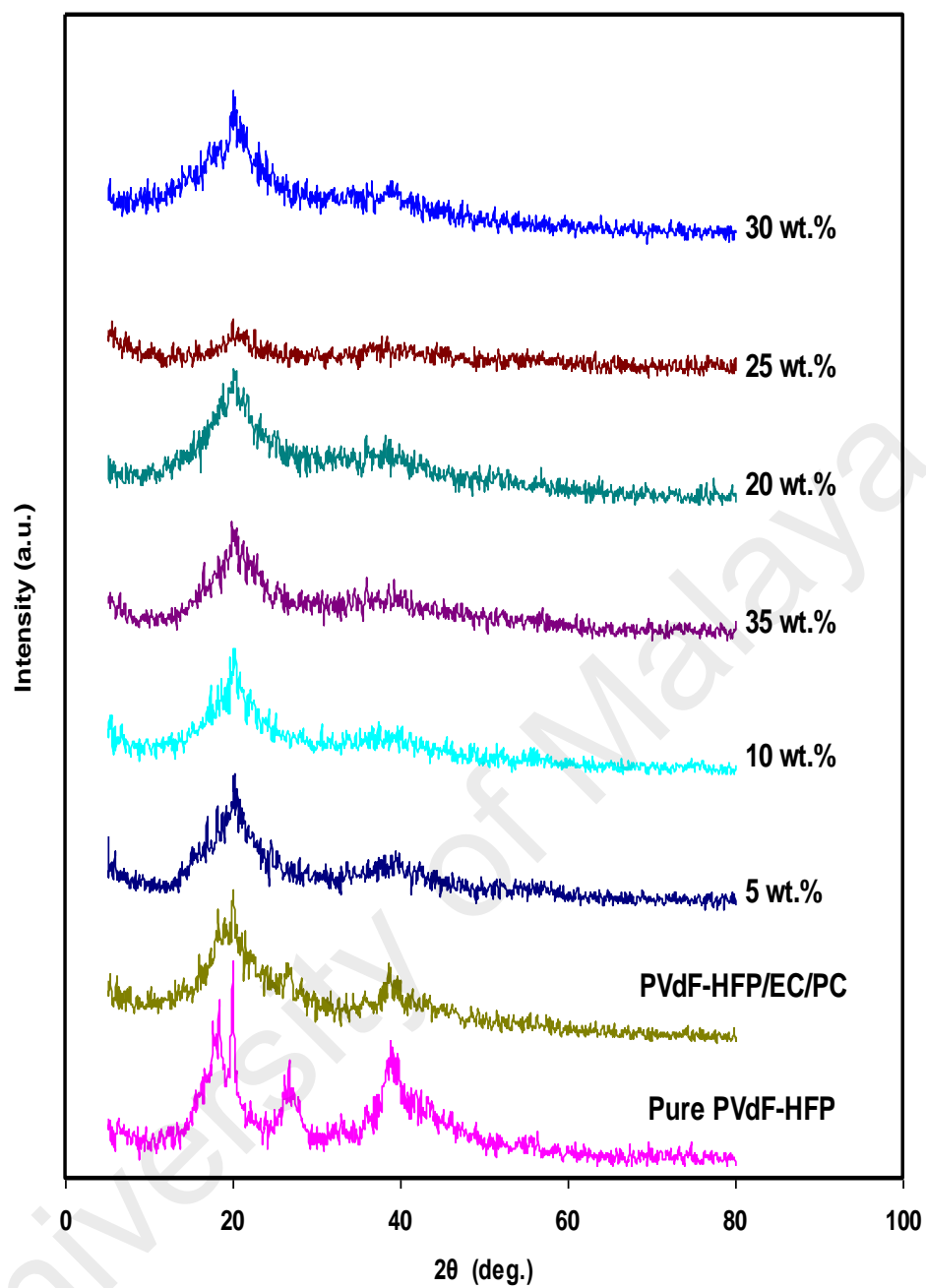


Figure 6.23: X-ray diffractogram of the GPE films in the PVdF-HFP/EC/PC/LiCF₃SO₃ system

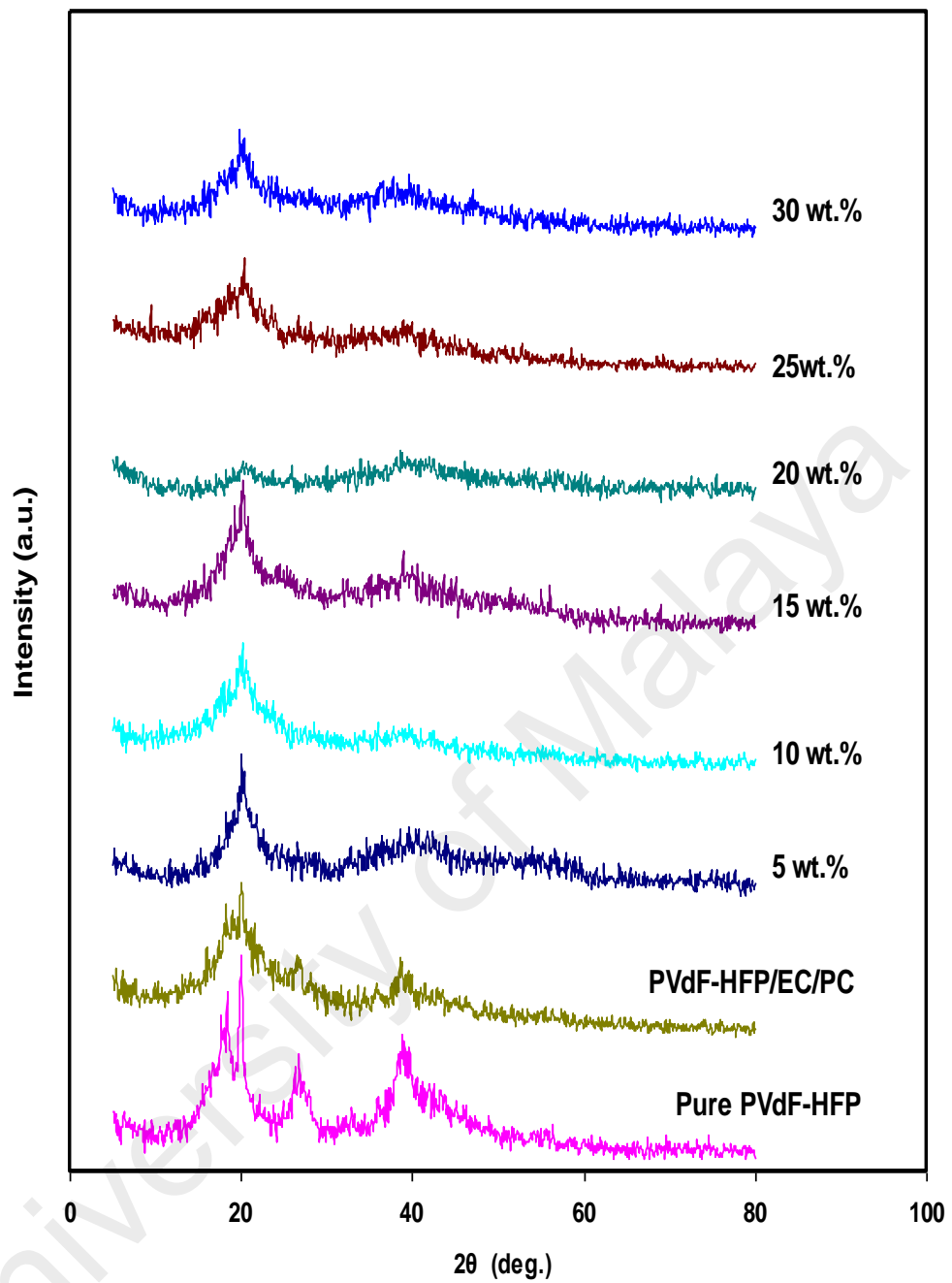


Figure 6.24: X-ray diffractogram of the GPE films in the PVdF-HFP/EC/PC/NaCF₃SO₃ system

6.4 Field Emission Scanning Electron Microscope Analysis

The FESEM was used to study the surface morphology features of the GPE films. Only three samples from each system were chosen for the study e.i. film with 5 wt. % of salt, film with highest conductivity and film with 30 wt. % of salt. This study was performed in order to examine the morphology changes on the surface of the polymer electrolytes with the addition of EC, PC, LiCF₃SO₃ and NaCF₃SO₃. All micrographs for the GPE films were obtained with the magnification of 3000 and 12000 X.

6.4.1 Pure PVdF-HFP and PVdF-HFP/EC/PC

Figure 6.25 shows the micrograph for pure PVdF-HFP film. A flaky surface structures separated by dark regions with unevenly sized pore was observed on the images of pure PVdF-HFP film indicating the semicrystalline nature that features both crystalline and amorphous regions. The pores are necessary for the transportation of the ions in the GPE films. The micrograph of PVdF-HFP/EC/PC film is shown in Figure 6.26. On addition of plasticizer, it is observed that there is a decrease in the spherulite and pores size. The crystalline texture that observed in pure film appeared to be decreased which results into the appearance of homogenous and smooth texture of the surface. These changes may be attributed to the effect of plasticization resulting in the reduction of crystallinity of host polymer and subsequent enhancement in the overall amorphous fraction in the film. It can therefore be inferred that the complexation between the polymer, PVdF-HFP and plasticizers has occurred. This result is consistent with the FTIR, Raman and XRD results that have been discussed in Section 6.1, 6.2 and 6.3, respectively.

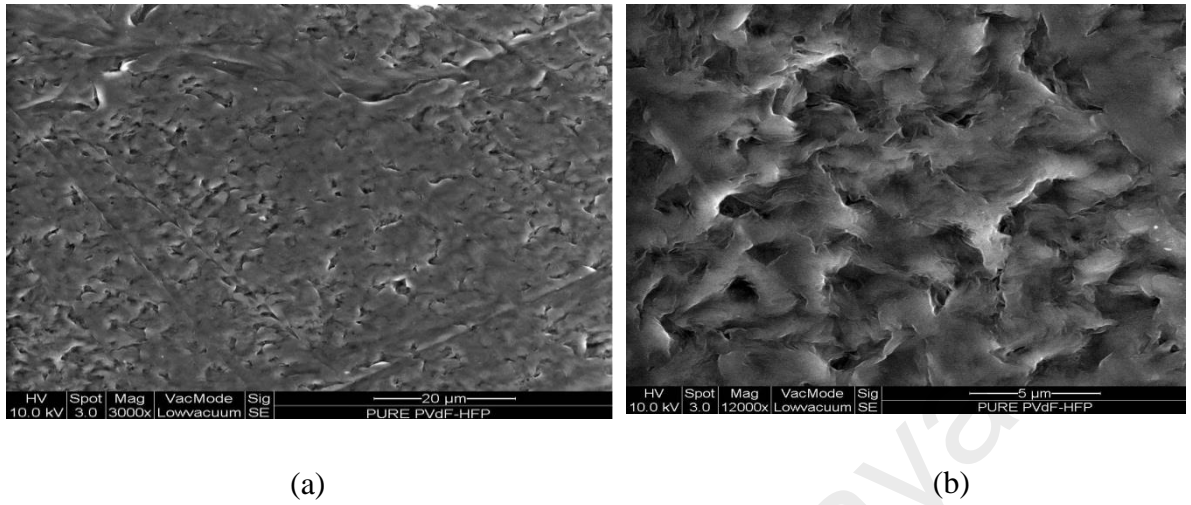


Figure 6.25: (a) Micrograph of pure PVdF-HFP film with the magnification factor of 3000X (b) Micrograph of pure PVdF-HFP film with the magnification factor of 12000X

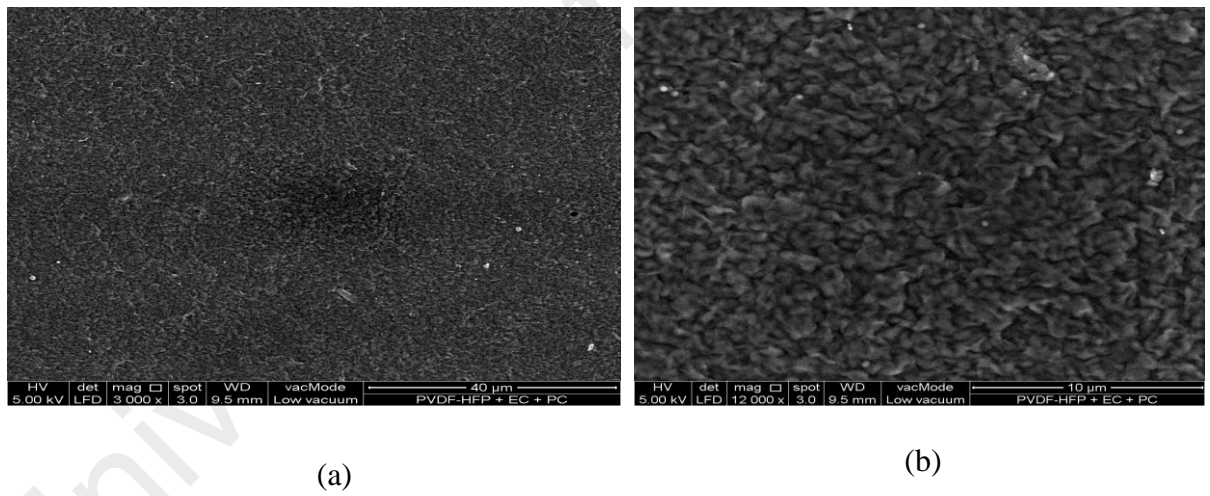


Figure 6.26: (a) Micrograph of PVdF-HFP/EC/PC film with the magnification factor of 3000X. (b) Micrograph of PVdF-HFP/EC/PC film with the magnification factor of 12000X

6.4.2 PVdF-HFP/EC/PC/LiCF₃SO₃

Figure 6.27 (a-c) shows the micrographs for PVdF-HFP containing 5 wt.%, 25 wt.% and 30 wt.% of LiCF₃SO₃, respectively. On the addition of salt, it is clearly observed the increase of pores size (dark region) with homogenous surface for all the GPE-complexes. It can be seen that the images in Figure 6.27 (a) and (c) is uniformly porous with small pores. The film with 30 wt.% of LiCF₃SO₃ salt shows a rougher surface than the 5 wt.% salt film. The pores are actually voids and present an obstruction to the movement of Li⁺ ions. This accounts for the poorer conductivities of these two GPE films compared to the film containing 25 wt.% salt. An interconnecting network of polymer structures seems to form in 25 wt.% LiCF₃SO₃ film, as shown in Figure 6.27 (b). These interconnecting structures may play a role in the increase of conductivity of this film because the network may present interconnecting pathways for Li⁺ ions to move through. These results revealed that the surface morphology of the GPE films is important and will affect the conductivity of the GPE films.

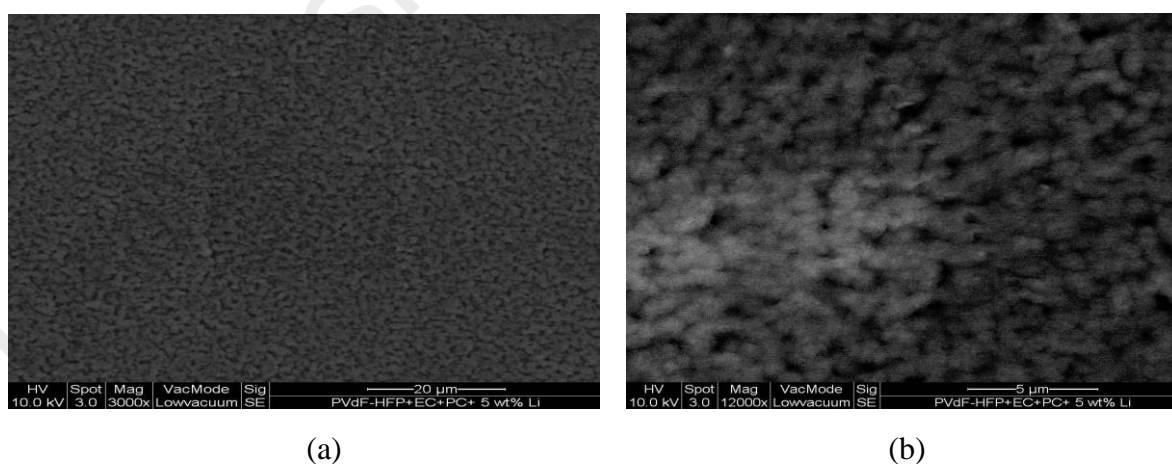
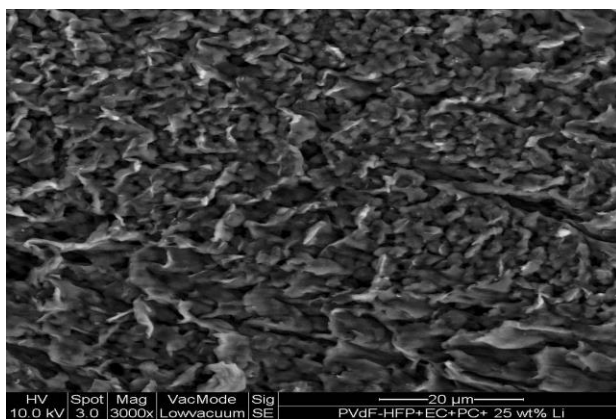
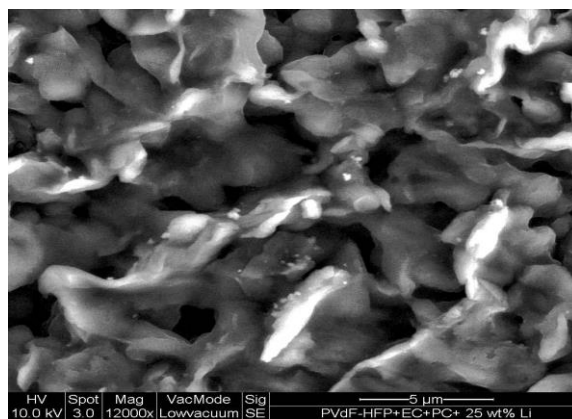


Figure 6.27: (a) Micrograph of PVdF-HFP/EC/PC/5wt.% of LiCF₃SO₃ film with the magnification factor of 3000X. (b) Micrograph of the film with the magnification factor of 12000X

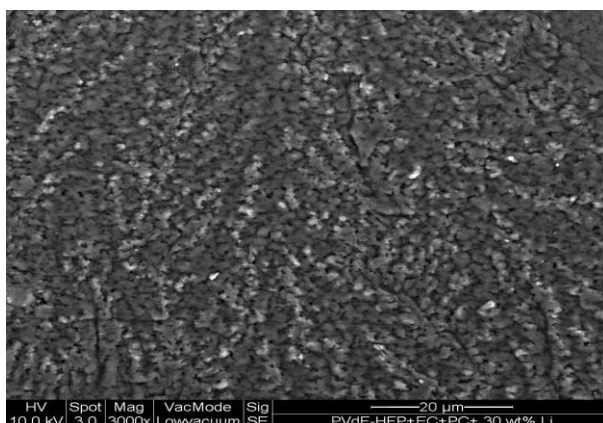


(a)

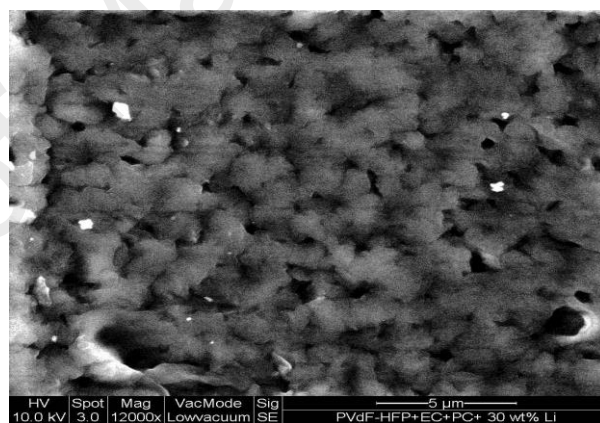


(b)

Figure 6.28: (a) Micrograph of PVdF-HFP/EC/PC/25wt.% of LiCF₃SO₃ film with the magnification factor of 3000X. (b) Micrograph of the film with the magnification factor of 12000X



(a)

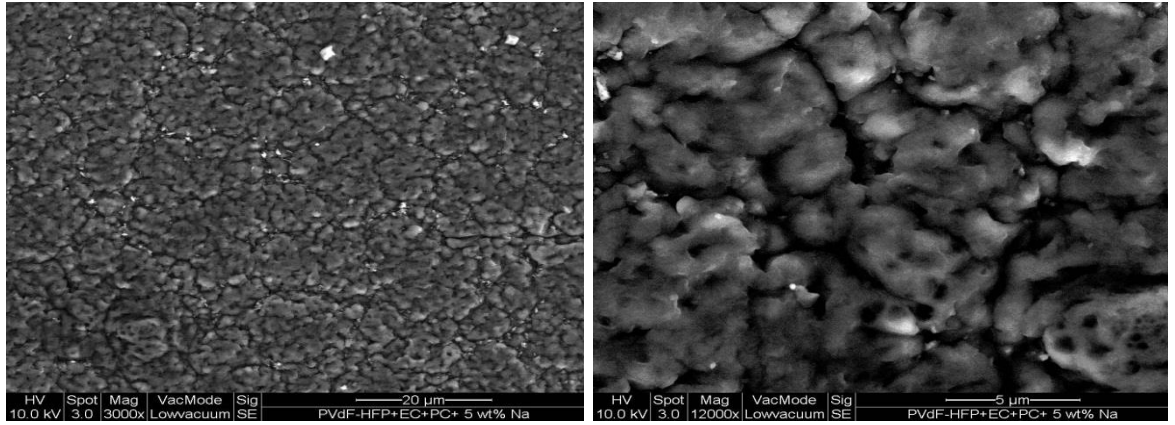


(b)

Figure 6.29: (a) Micrograph of PVdF-HFP/EC/PC/30wt.% of LiCF₃SO₃ film with the magnification factor of 3000X. (b) Micrograph of the film with the magnification factor of 12000X

6.4.3 PVdF-HFP/EC/PC/NaCF₃SO₃ System

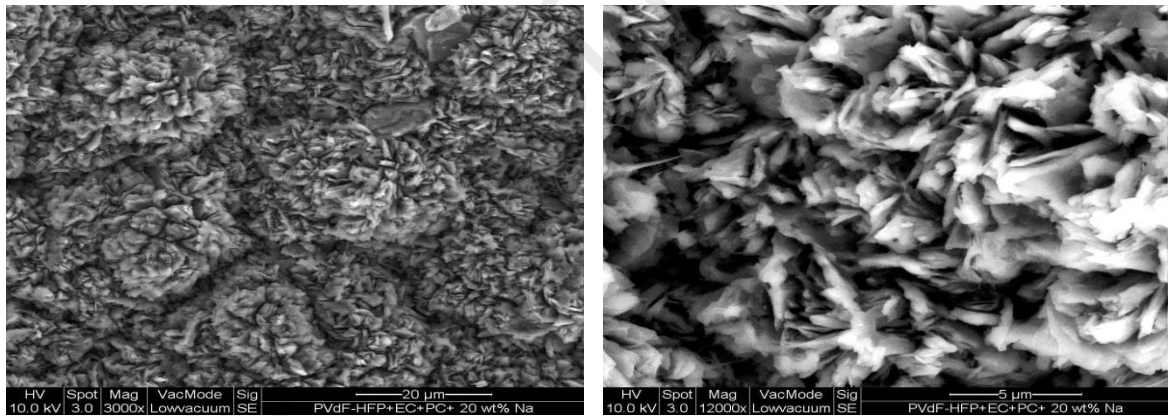
The FESEM micrographs for the PVdF-HFP/EC/PC/NaCF₃SO₃ films containing 5 wt.%, 20wt.% and 30 wt.% of NaCF₃SO₃ are presented in Figure 6.28 (a -c), respectively. Similar to LiCF₃SO₃ system, image at lower salt concentration i.e. 5 wt.% exhibit homogenous surface and uniform pores. When higher amounts of sodium salt are added to the films, i.e. 20 wt.% and 30 wt.% of NaCF₃SO₃, the surface morphology of the film change drastically. The films show flower-like aggregates with layered features. The surface morphology of highest conducting sample as shown in Figure 6.28 (b) experienced the greatest structural disorder suggested that on addition of plasticizers and salt into the polymer matrix has increased the total surface area for ion coordination. It also can be seen that the porosity in the GPE film containing 30 wt.% of NaCF₃SO₃ is slightly decreased therefore decrease the conductivity. Compared to the film with 25 wt.% of LiCF₃SO₃, the GPE film containing 20 wt.% NaCF₃SO₃ shows exhibit larger pore sizes and also large number of pores with overlapping layer aggregation. The pores are uniformly distributed on the surface which results in higher ionic conductivity. The difference in the pores size between both films could be due to the size of Na⁺ ion is bigger than Li⁺ ion. The overlapping layers shorten the pathway for the intra and inter-molecular coordination between ions and the polymer chains at the same time providing enough channels for the migration of ions, accounting for better ionic conductivity.



(a)

(b)

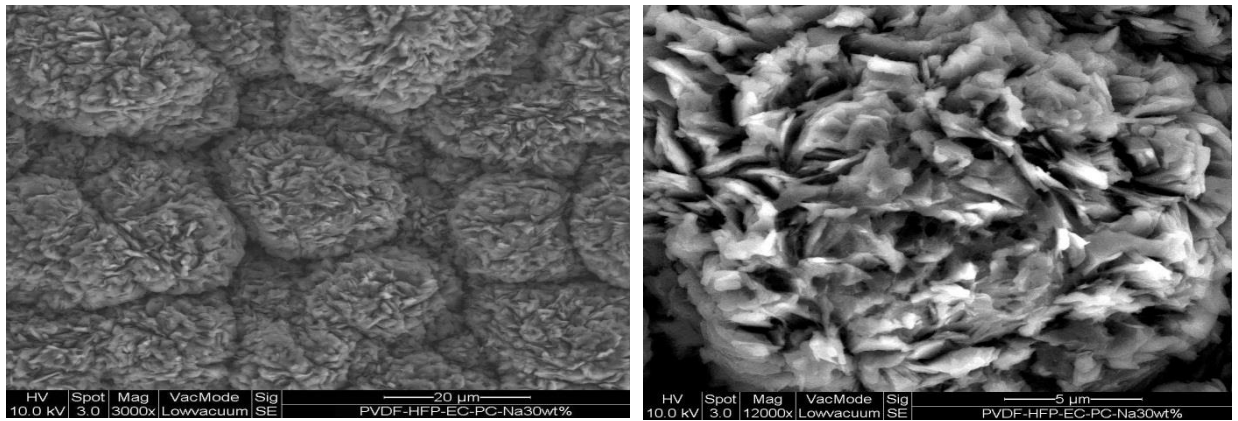
Figure 6.30: (a) Micrograph of PVdF-HFP/EC/PC/5 wt.% of NaCF_3SO_3 film with the magnification factor of 3000X. (b) Micrograph of the film with the magnification factor of 12000X



(a)

(b)

Figure 6.31: (a) Micrograph of PVdF-HFP/EC/PC/20 wt.% of NaCF_3SO_3 film with the magnification factor of 3000X. (b) Micrograph of the film with the magnification factor of 12000X



(a)

(b)

Figure 6.32: (a) Micrograph of PVdF-HFP/EC/PC/30 wt.% of NaCF₃SO₃ film with the magnification factor of 3000X. (b) Micrograph of the film with the magnification factor of 12000X

University of Malaya

CHAPTER 7: ELECTROCHEMICAL STUDIES

The electrochemical stability window i.e. working voltage range for the electrolytes is an important parameter to be evaluated from their application point of view as electrolytes in energy storage devices. In this work, the highest conducting film containing 25 wt.% of LiCF_3SO_3 and 20 wt.% of NaCF_3SO_3 salt was characterized through Linear Sweep Voltammetry (LSV) and Cyclic Voltammetry (CV) techniques by using WPG100e potentiostat/galvanostat system and the results obtained will be analyzed.

7.1 Linear Sweep Voltammetry

The LSV was performed on a SS | GPE | lithium and SS | GPE | sodium metal cells where stainless steel (SS) as working electrode, with counter and reference electrode of lithium/sodium metal. The voltage is swept from 0 V towards anodic (positive) values with a scan rate of 5 mV s^{-1} until a large current is obtained. As the potential is swept, a sudden rise of current is observed at certain potential, which is due to the electrolyte decomposition at the inert electrode interface. The resulting voltammogram of SS | GPE | Li-metal and SS | GPE | Na-metal cell are shown in Figure 7.1 and 7.2, respectively. The obtained current density at lower voltages is the combined results of the ionic conductivity of the polymer electrolyte and the interfacial resistance of lithium or sodium metal/polymer electrolyte. The onset of the current in the anodic high voltage range is assumed to result from a decomposition process associated with electrode (Slane & Salomon, 1995) and this onset voltage is taken as the upper limit of the electrolyte stability range. This voltage is generally located as the point of intersection of the extrapolated linear current in high voltage region with the voltage axis. The onset

voltages for anodic current for both cells are detected at around 3.2 V for lithium cell and 3.4 V for the sodium cell. This implies that 3.2 V and 3.4 V represents the electrochemical stability window or anodic stability of the GPE films which means that the films has good electrochemical stability ($>3.0\text{V}$) for use in lithium and sodium secondary cells.

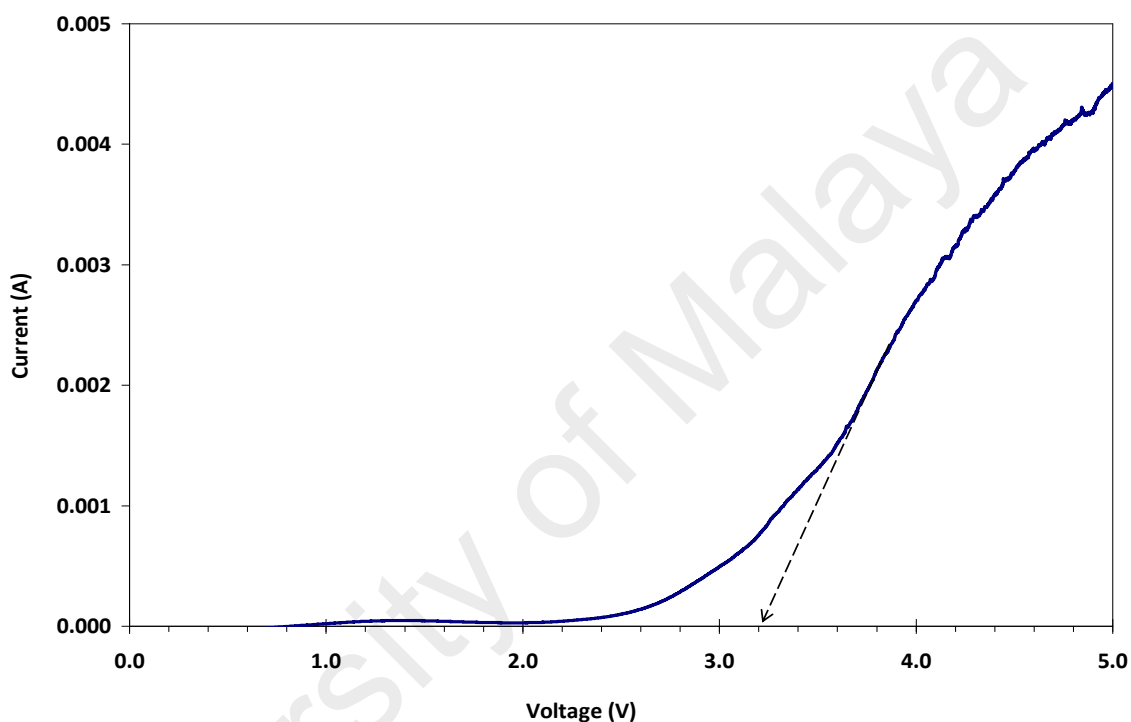


Figure 7.1: Linear sweep voltammogram of SS| GPE| Li cell for GPE containing 25 wt.% of LiCF_3SO_3 salt at scan rate of 5 mV s^{-1} .

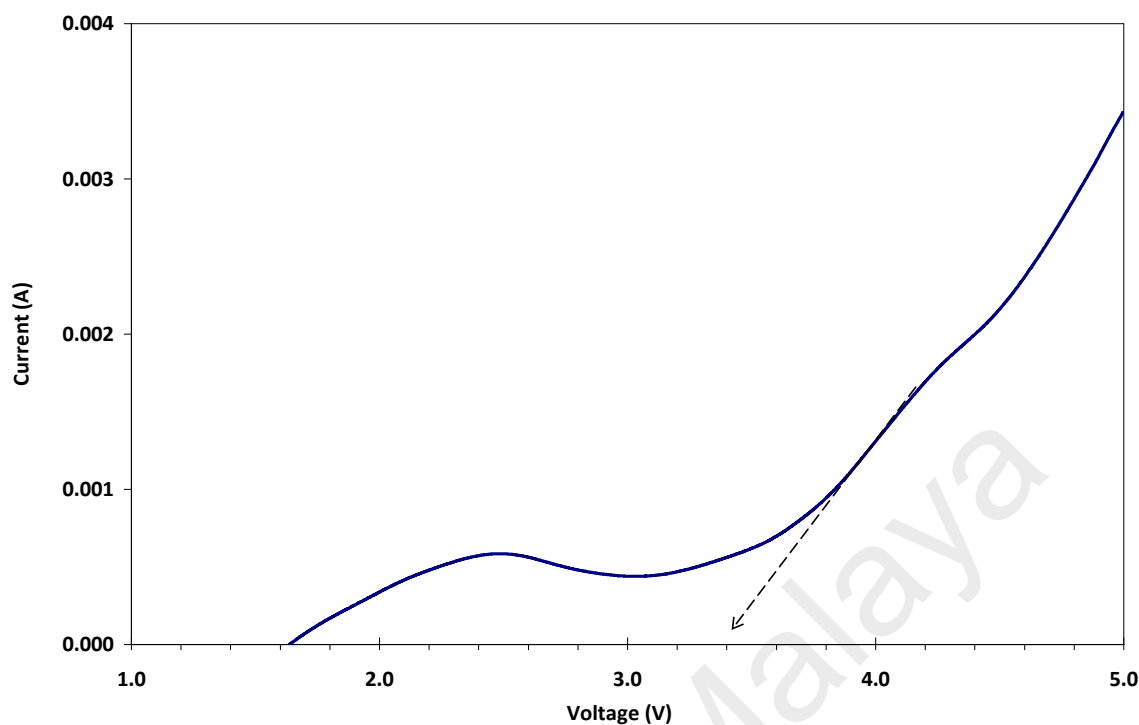


Figure 7.2: Linear sweep voltammogram of SS| GPE| Na cell for GPE containing 20 wt.% of NaCF₃SO₃ salt at scan rate of 5 mV s⁻¹

7.2 Cyclic Voltammetry

Cyclic voltammetry on the gel polymer electrolyte films were carried out in order to investigate the electrochemical behaviour at the interface between electrode and electrolyte. The electrolytes must be chemically stable to enable devices to attain extensive shelf lives in high voltage devices and they must be able to withstand the range of potential of the electrode couple. In the cyclic voltammetric analysis the sweep potential was firstly scanned in the positive direction and then the reversed direction. In the present work the comparative cyclic voltammetric studies have been performed on the symmetric cells of SS|GPE-Li|SS (Cell-I), SS|GPE-Na|SS (Cell-II), Li| GPE| Li (Cell-III) and Na| GPE| Na (Cell-IV) for the highest conducting film in PVdF-HFP/ EC/ PC/ LiCF₃SO₃ and PVdF-HFP/ EC/ PC/ NaCF₃SO₃ system at room temperature.

Figure 7.3 and 7.4 show the cyclic voltammograms for Cell-I and Cell-II where the GPE film was in contact with a stainless steel (SS) blocking electrode. The cyclic voltammetry (CV) of the cells were studied at 5 mVs^{-1} scan rate in the voltage range between -5.0 V and 5.0 V . As can be observed, there is only a very small current through the working electrode until the applied voltage reached a potential limit of the cells and the current related to GPE decomposition has increases on increase of the applied voltage above the potential limit. This could be due to non-interaction of the lithium and sodium ions in the gel polymer electrolyte with the SS electrodes.

Figure 7.5 and 7.6 show a cyclic sweeping between -5 and 5 V of Cell III and Cell IV, respectively. The figures present the CV curves for first, fifth, eighth and tenth cycle. It can be clearly observed from both figures that the peak current decrease during the initial cycle. It can be due to formation of passivation layer on electrode and stabilize afterwards. The presence of organic solvent in GPE system appears to influence the oxidation potential as reported by Kuo et al., 2002 (Kuo et al., 2002). The accumulation of free plasticizers aggregates at the interface facilitates ions migration and causes the anodic current to increase faster in the following sweeps than that in the first anodic sweep as shown in the figures. On cycling, there is no substantial change in the redox peak voltages and the overlapping of the subsequent sweeps indicates that the charge transfer reaction at the interface between the film and lithium/sodium metal is reversible and the gel polymer electrolyte is able to support fully reversible redox process. Therefore, it can be concluded that the film containing 25 wt.% of LiCF_3SO_3 and 20 wt.% of NaCF_3SO_3 GPE film have sufficient electrochemical stability and provide better cycle stability for the operation in the battery system.

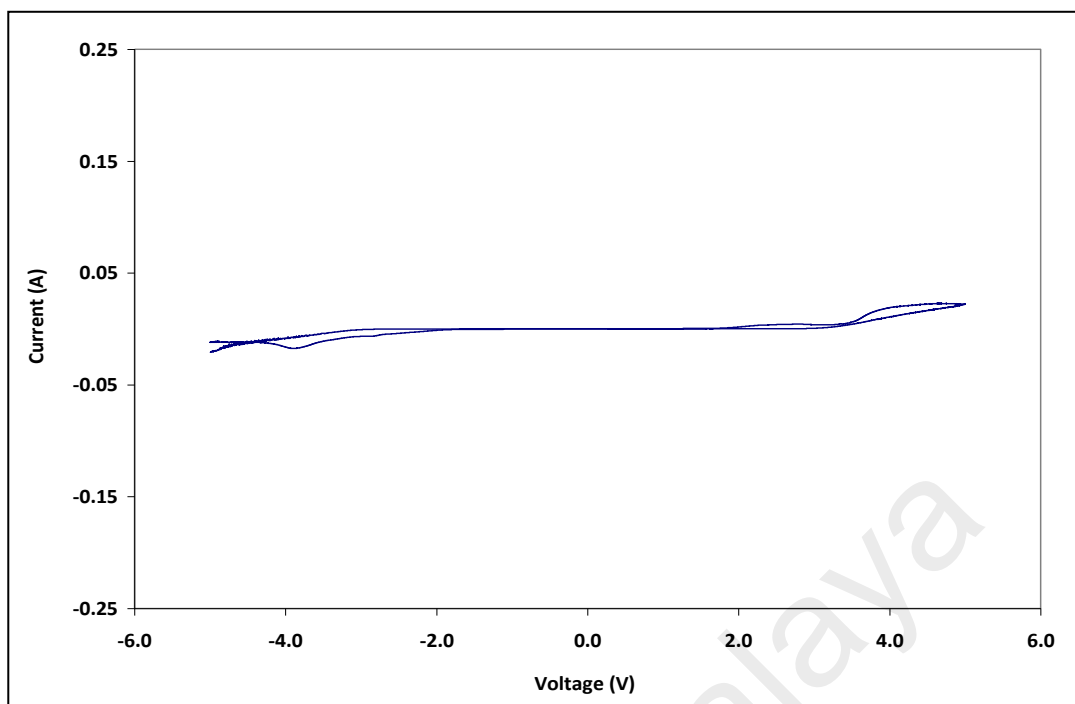


Figure 7.3: Cyclic voltammogram of cell-I: SS| GPE-Li| SS with 25 wt.% of LiCF_3SO_3 salt at scan rate of 5 mV s^{-1}

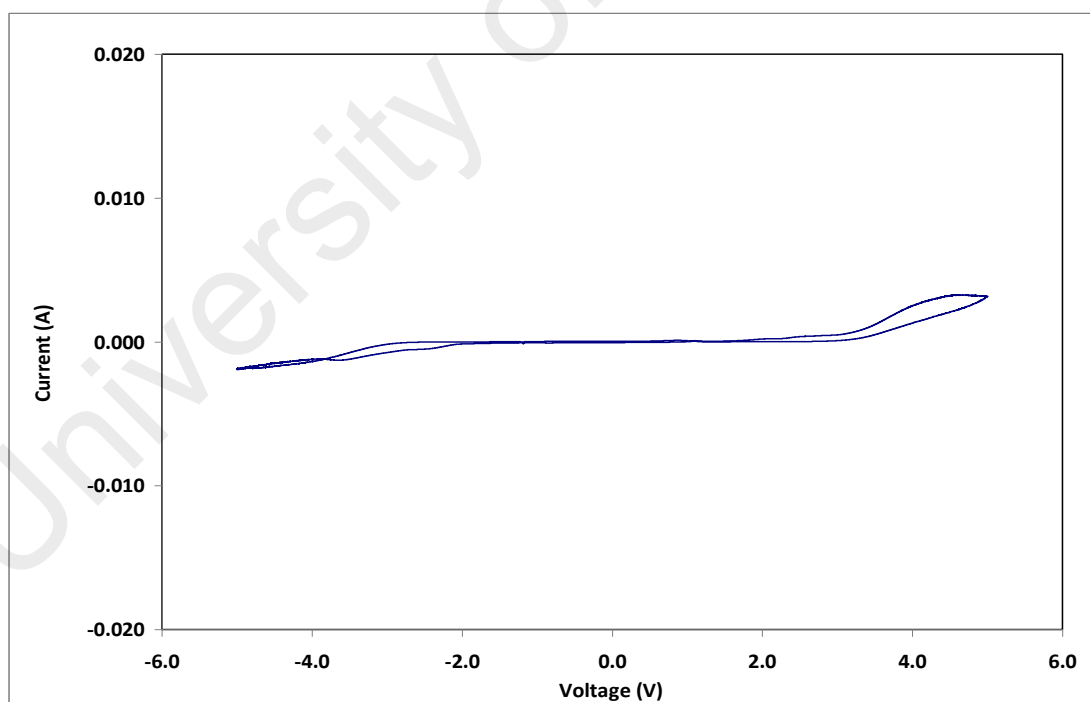


Figure 7.4: Cyclic voltammogram of cell-II: SS| GPE-Na| SS with 20 wt.% of NaCF_3SO_3 salt at scan rate of 5 mV s^{-1}

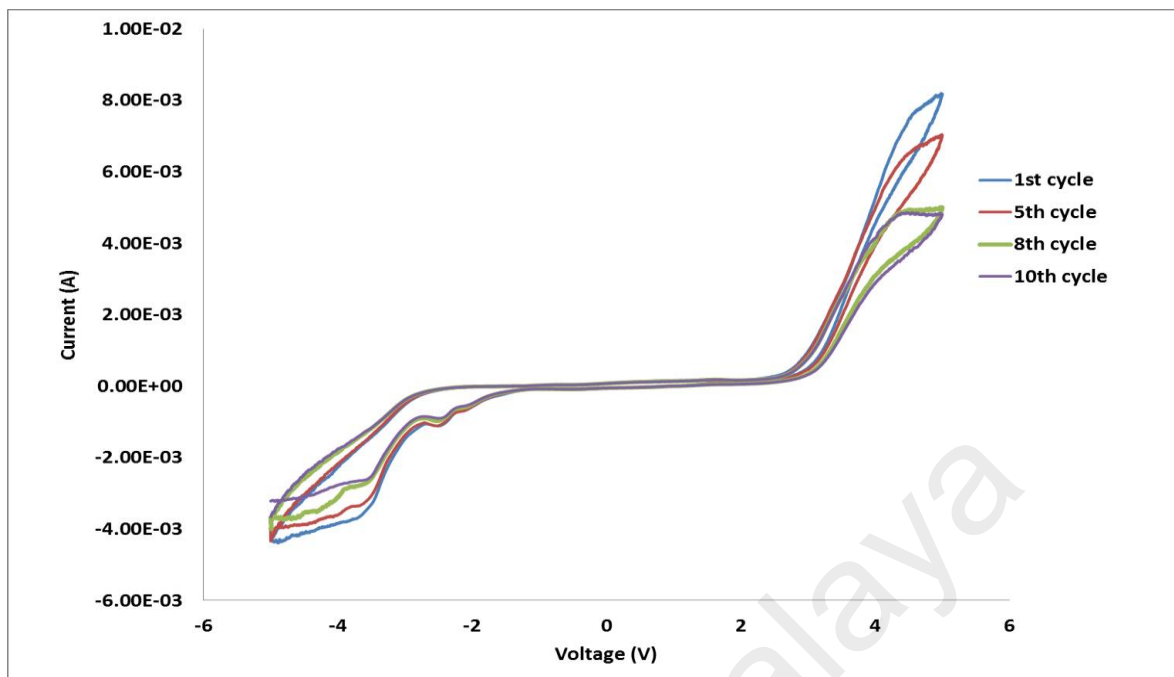


Figure 7.5: Cyclic voltammogram of cell-III: Li| GPE |Li with 25 wt.% of LiCF_3SO_3 salt at scan rate of 5 mVs^{-1}

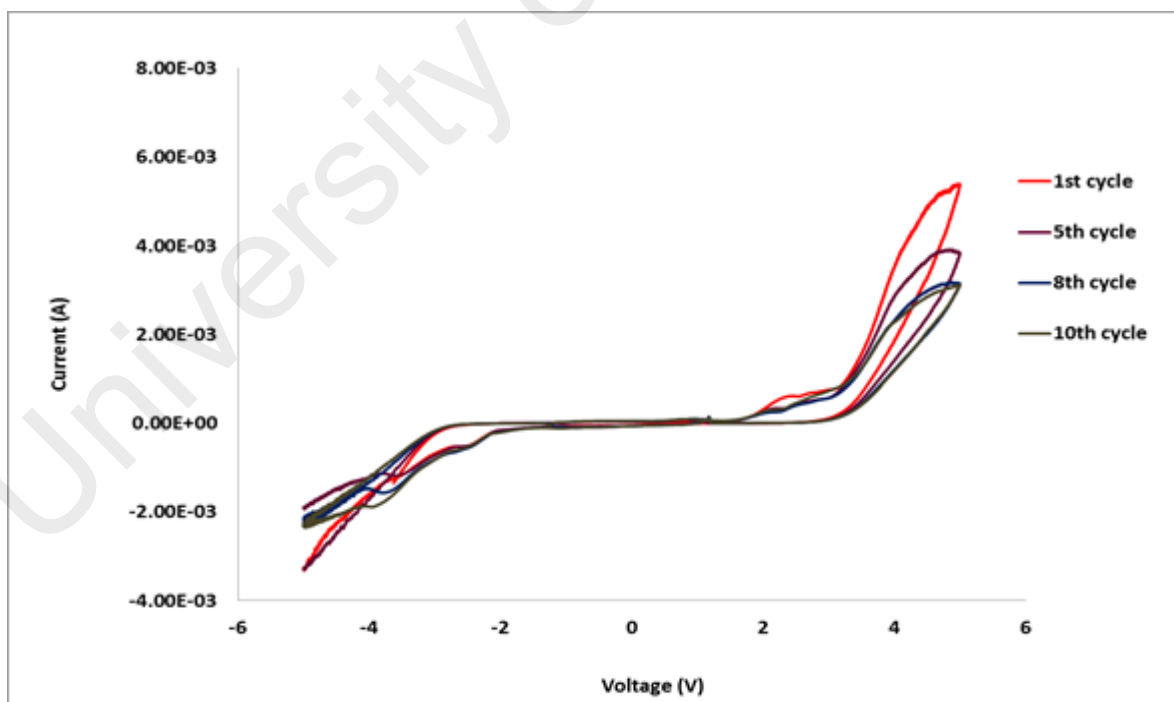


Figure 7.6: Cyclic voltammogram of cell-IV: Na| GPE |Na with 20 wt.% of NaCF_3SO_3 salt at scan rate of 5 mVs^{-1}

CHAPTER 8: CELL PERFORMANCES

8.1 Performances of Lithium Cell

In order to evaluate the electrochemical performance of lithium-ion polymer cells, the cells consisting of lithium nickel cobalt oxide (LiNiCoO_2) as a cathode, the PVdF-HFP-based gel polymer electrolyte containing 25 wt.% of LiCF_3SO_3 salt and lithium metal anode were prepared. In the present study LiNiCoO_2 was used because of its lower cost and higher capacity compared with LiCoO_2 (Ceder et al., 1998). LiCoO_2 and LiNiCoO_2 have a layered structure, where lithium and transition metal cations occupy alternate layers of octahedral sites in a distorted cubic close-packed oxygen-ion lattice. The layered metal oxide framework provides a two-dimensional interstitial space, which allows for easy removal of the lithium ions. Wang and Chen (Wang & Chen, 2014) have studied nanostructured LiNiCoO_2 and LiCoO_2 cathode material where the electrochemical results show the specific capacity achieved for LiNiCoO_2 and LiCoO_2 are 180 mAh/ g and 140 mAh/ g respectively. In this work, the lithium cell was assembled by sandwiching the GPE film between the respective electrodes in a sealed container.

As fabricated, the cell with the optimized gel polymer electrolytes exhibited an open circuit voltage (OCV) of 3.53 V. The cell was charged to 4.0 V with current of 1.0 mA, followed by discharging at 1.0 mA to 1.5 V and the charge-discharge process was repeated up to 10 cycles at room temperature. Figure 8.1 shows the voltage profile of the LiNiCoO_2 | GPE | Li cell with discharge capacity for ten cycles. The highest capacity of 164 mAh/ g achieved at the first cycle. Lim and co-worker (Lim et al., 2012) were reported the cell studied based on PVdF-HFP gel polymer electrolytes using

LiFePO₄ cathode. The cell delivered initial discharge capacity of 156 mAh/ g, slightly lower than the value obtained in this research work. However, generally the fade in capacity mainly depends on the nature of cathode materials used. Figure 8.2 displays the discharge capacity versus number of cycle for LiNiCoO₂ | GPE | Li cell. It can be seen that the discharge capacities of the cell were gradually decrease with repetition of the cycle. The discharge capacity decreases to 118 mAhg⁻¹ after 5 cycles and to 79 mAhg⁻¹ after 10 cycles which show a capacity fading of 28% and 52%, respectively. The slight decrease in capacity might be due to physical changes in the interfacial properties between the positive electrode and the polymer gel electrolyte, which gradually increase the internal resistance of the cell during cycling. During discharging, the surface concentration drops faster than the bulk concentration as a implicating of the slow time constant for lithium ion transport. As discharge proceeds, the surface concentration ultimately decreases approach zero, which causes an abrupt drop in the cell voltage. The impact of concentration gradient is unavoidable with such low cationic transport number of the polymer electrolyte which accounts for the declined capacity.

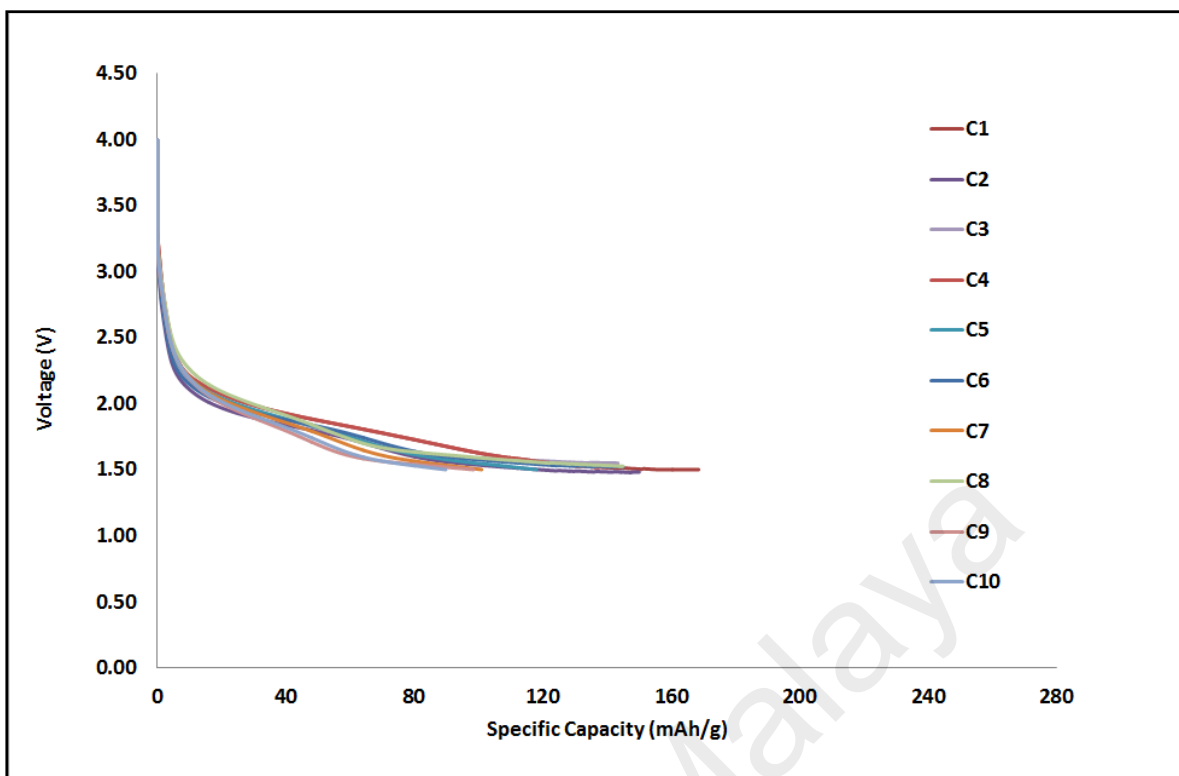


Figure 8.1: Variation of voltage of LiNiCoO₂ | GPE | Li cell during discharge with a current of 0.05 mA.

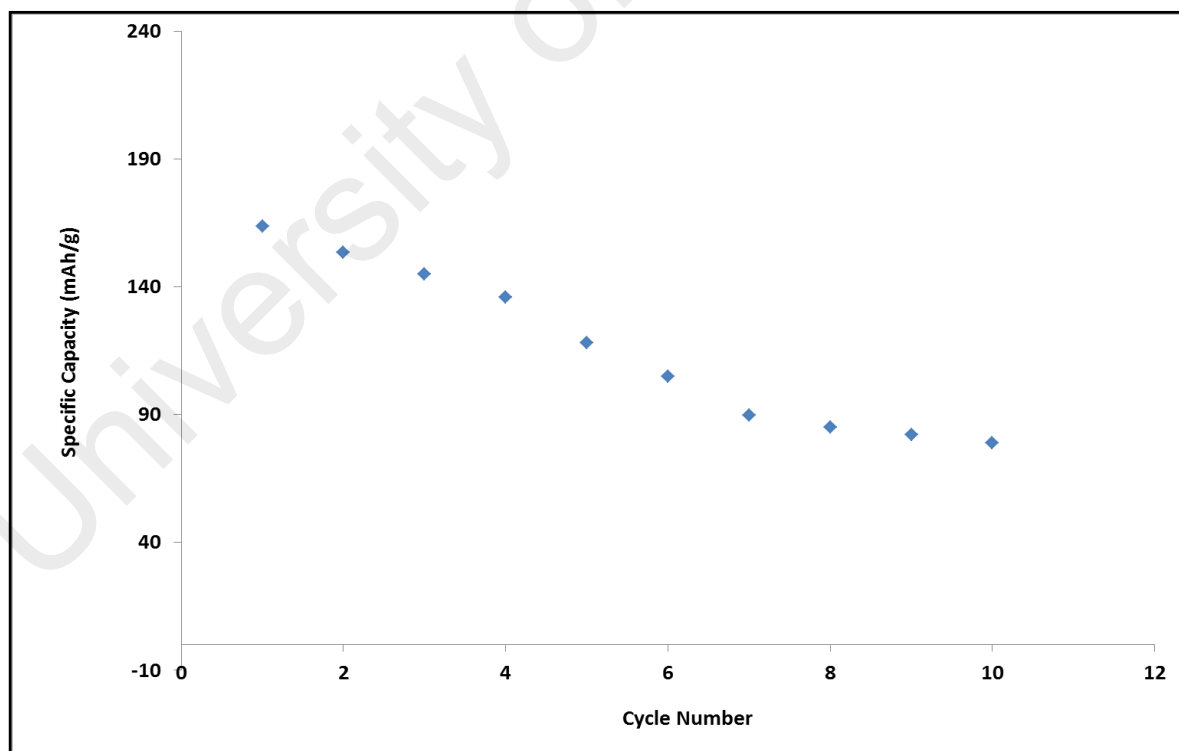


Figure 8.2: Discharge capacities of LiNiCoO₂ | GPE | Li cell as a function of cycle number.

8.2 Performances of Sodium Cell

In this research work, the sodium cell has been fabricated comprising a manganese oxide (MnO_2) as a cathode, sodium metal as an anode and optimized gel polymer electrolyte (GPE) film containing 20 wt.% of NaCF_3SO_3 salt. The open circuit voltage (OCV) of Na cell has been found to be ~ 2.5 V. The cell was charged to 3.0 V with current of 1.0 mA. The cell was then discharge to 1.5 V with the the current of 1.0 mA and the charge-discharge process was repeated up to 10 cycles. Figure 8.3 shows the voltage profile of the cell with discharge capacity for ten cycles. It is can be seen that the plot has a similar trend as observed in lithium cell, Figure 8.2 where the highest capacity is achieved at the first cycle with the value of 168 mAh/g. Figure 8.3 depicts the discharge capacities of MnO_2 | GPE | Na cell for ten cycles. It is also found that the charging and discharging processes were gradually decreased with the repetition of the cycle. Similar to lithium system, the discharge capacity of the sodium cell decrease to 66 mAhg^{-1} after cycle 5 cycles and 50 mAhg^{-1} after 10 cycles which show a capacity fade of 61 % and 70 %, respectively. There could be many reasons for the capacity fading after the first cycle. In the cases of cell fabricated using metal oxides electrode and polymer electrolytes, it is believed that contact losses between oxides electrode and the electrolytes is the main cause for capacity fading during cycling (Kim, Lee, Kim, Park, & Seung, 2001; West, Zachau-Christiansen, & Jacobsen, 1983; Xia, Tatsumi, Fujieda, Prosini, & Sakai, 2000). The metal oxides particles such as manganese oxide and vanadium oxide change their volume during the course of intercalation of Na^+ into the oxide and elimination of the intercalated Na^+ . The changes of volume make the electrode-electrolyte contact poor, resulting in the capacity fading due to the increase in the cell resistance.

According to Hong et al., the larger size and different bonding characteristics of sodium ions influence the thermodynamic and/or kinetic properties of sodium-ion batteries, which leads to unexpected behavior in electrochemical performance and reaction mechanism, compared to lithium-ion batteries (Hong et al., 2013). As can be seen the capacity values at the first cycle achieved for sodium cell is slightly higher than value that obtained in lithium cell. However, there are several viewpoints when comparing these two types of cells. One of them is the fundamental properties of sodium that should be considered. Sodium and lithium have a similar tendency to lose electrons as measured by their electrochemical potential, which makes them good anode materials. However, sodium ions are nearly 25% larger than lithium ions. The larger size makes it more difficult to be inserted into the crystal structure of the electrodes, where the chemical reactions take place. As a result, the ions cannot move fast, thus make the charge/discharge process became slower than in lithium cell.

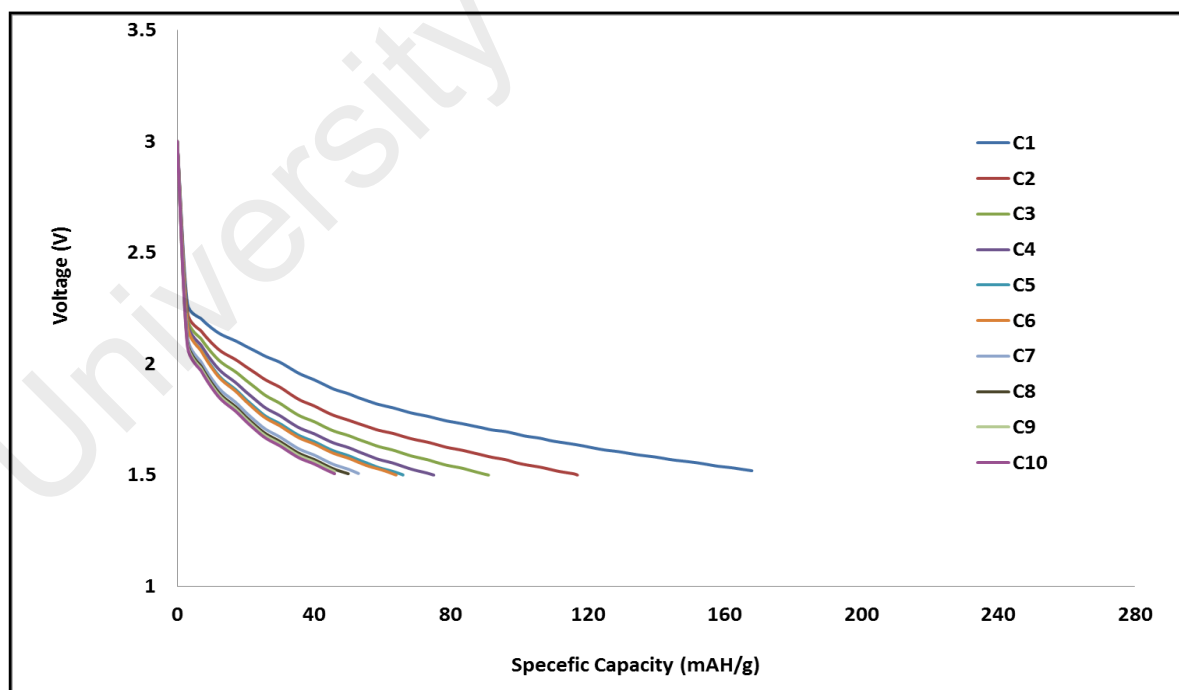


Figure 8.3: Variation of voltage of MnO₂ | GPE | Na cell during discharge with a current of 1.0 mA.

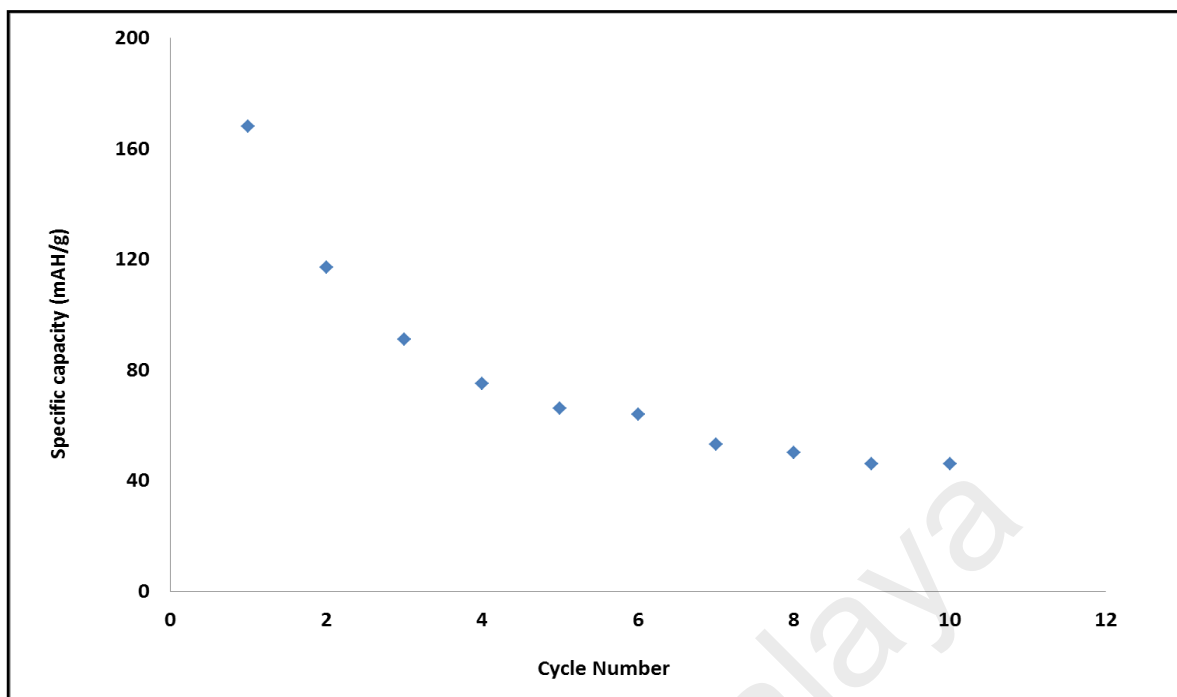


Figure 8.4: Discharge capacities of MnO₂ | GPE | Na cell as a function of cycle number.

University of Malaya

CHAPTER 9: DISCUSSION, CONCLUSION AND SUGGESTIONS FOR FURTHER WORK

The present work covers the work done on characterization of lithium and sodium ion conducting gel polymer electrolytes for their applications in solid state batteries. In this work, PVdF-HFP based gel polymer electrolytes containing lithium and sodium salts have been prepared with various compositions of salts using the solution casting technique. Several experimental methods have been done on these systems to study the effect of solvent plasticizers and salts on ionic conductivity, structural, morphology, thermal and electrochemical properties of the prepared samples.

The room temperature conductivity for pure PVdF- HFP film was achieved at $1.86 \times 10^{-11} \text{ S cm}^{-1}$. On addition of salts and plasticizer, the ionic conductivity of this film had increased. Table 9.1 summarizes the compositions of the films that achieved the highest conductivity for the three systems of gel polymer electrolytes.

Table 9.1: The compositions, and the conductivity, σ of films in the GPE films

System	Content			Conductivity (S cm^{-1})
	EC	PC	Salt	
PVdF-HFP/ EC/ PC	2g	1g	-	$(3.31 \pm 0.04) \times 10^{-8}$
PVdF-HFP/ EC/ PC + LiCF_3SO_3	2g	1g	25 wt. %	$(1.40 \pm 0.06) \times 10^{-3}$
PVdF-HFP/ EC/ PC + NaCF_3SO_3	2 g	1g	20 wt. %	$(2.50 \pm 0.19) \times 10^{-3}$

The conductivity variations at room temperature with LiCF_3SO_3 and NaCF_3SO_3 as depicted in Figure 4.4 and Figure 4.6 show similar trend where conductivity increase with salt content until the optimum salt concentration is reached. On addition of more

salt above the optimum concentration, the conductivity value drops. The optimizing salt concentration for both systems has increase the conductivity of PVdF-HFP/ EC/ PC film by five orders of magnitude. Charge carrier concentration and ionic mobility are two important factors which influence the conductivity of the polymer electrolyte. The conductivity generally depends on the concentration of salt and the degree of salt dissociation. Higher dissociation of salt resulting in higher number of mobile ions that is available for ion conduction. Therefore, the increase in conductivity is due to the increase of free mobile ions as more salt is dissolved into the solution. Conductivity continues to increase until the optimum salt concentration reached after which conductivity decreases. The additions of plasticizing solvent in the gel polymer electrolytes enhance the conductivity of polymer system. These plasticizers increase the amorphous content of the polymer matrix and tend to dissociate ion-pairs into free cations and anions thereby leading to an overall enhancement in conductivity. In the present work, the plasticizing solvents i.e EC and PC have played its role in softening the polymer backbone and accelerating the ion conductions which is responsible to the overall high conductivity.

The conductivity-temperature studies are carried out in temperature range of 303 K -373 K to understand the influence of temperature and salt concentrations on the ion transport mechanism of the GPE films. The temperature dependence of conductivity behavior obeys VTF pattern. The studies were done only for the samples containing 5 wt.%, 30 wt.% of salt and the highest conducting sample at room temperature from both systems. These studies indicate that the conductivity is increased when the temperature is increased. The increase in conductivity in temperature may be related to decrease in viscosity and hence increase the chain flexibility of the electrolytes which leads to an increase in mobility and dissociation rates of salt which result in an increase in conductivity. While non-linear nature of the VTF plots indicates that the ionic

conduction in the gel polymer electrolytes dependent on the free volume and motion of the polymer chains in which the conduction occurs in amorphous region.

The pseudo-activation energy, E_a , for the films was determined from the gradient of the VTF plots and the values were listed in Table 9.2. The activation energy can be defined as the energy required for ions to move. When the ion has acquired sufficient energy, it is able to break away from the donor site and continuously move to the next donor site. Therefore, it can be suggested that the value of E_a is the energy required to provide a conductive condition for the migration of ions. It is known that ionic conductivity is proportional to the concentration of charge carriers and migration rate of charge carriers that is related to E_a . Therefore, from Table 9.2, it can be concluded that the conductivity behaviour of the PVdF-HFP based gel polymer electrolytes studied in this work not only depends on the charge carrier concentration but also the rate of migration of charge carries.

The film containing NaCF_3SO_3 salt has higher ionic conductivity and lower activation energy as compared to film containing LiCF_3SO_3 salt. This result can be explained based on the Lewis acidity of the alkali ions i.e., the strength of the interaction of cations with the nitrogen atoms of PVdF-HFP. The interaction between Li^+ ion and the nitrogen atom of PVdF-HFP is stronger than that of Na^+ ion. Thus, Li^+ ion transfer requires higher activation energy than Na^+ ion in polymer electrolytes. These results agreed well with the works reported by Sagane et al. and Abe et al. (Abe, Fukuda, Iriyama, & Ogumi, 2004; Sagane et al., 2005).

Table 9.2: VTF parameters for the GPE films from LiCF₃SO₃ system and NaCF₃SO₃ system

Film PVdF-HFP/EC/PC + x	Pseudo-activation energy, B (eV)	T _g (°C)	Number of charge carrier, A (S cm ⁻¹ K ^{1/2})
x = 5 wt. % LiCF ₃ SO ₃	0.102	-60	17.0
x = 25 wt. % Li CF ₃ SO ₃	0.080	-69	28.0
x = 30 wt. % Li CF ₃ SO ₃	0.083	-64	22.9
x = 5 wt. % Na CF ₃ SO ₃	0.102	-62	21.0
x = 20 wt. % Na CF ₃ SO ₃	0.080	-73	31.0
x = 30 wt. % Na CF ₃ SO ₃	0.083	-70	29.0

The ionic transport number (t_{ion}) for all the samples was directly determined using the DC polarization technique. The results confirmed that the total conductivity of the gel polymer electrolytes is predominantly due to ions. t_{ion} quantitatively gives the extent of ionic contribution to the total conductivity. In a pure ionic conductor, $t_{ion} = 1$, while it varies between 1 and 0 in the mixed (ionic + electronic) systems. The cationic transport number (t_+) is a key parameter to judge the performance of the electrolytes. The cationic transport number (t_+) was determined alternatively using combined DC polarization and AC impedance measurements and the results are listed in Table 9.3. It is clear that a large proportion of current is carried by lithium and sodium ions in GPE-LiCF₃SO₃ system and GPE-NaCF₃SO₃ system, respectively. The investigation also indicates the cationic species in the film relatively contributed more towards the overall conductivity which explains the high conductivity of these two GPE films.

Table 9.3: Ionic and cation transport number values for the GPE films in PVdF-HFP/ EC/PC/ LiCF₃SO₃ and PVdF-HFP/EC/PC/NaCF₃SO₃ systems

Sample GPE + x	Transport Number	
	t _{ionic}	t _{cationic}
x = 5 wt.% LiCF ₃ SO ₃	0.942	0.41
x = 25 wt.% LiCF ₃ SO ₃	0.989	0.60
x = 30 wt.% LiCF ₃ SO ₃	0.983	0.51
x = 5 wt.% NaCF ₃ SO ₃	0.964	0.44
x = 20wt.% NaCF ₃ SO ₃	0.994	0.62
x = 30wt.% NaCF ₃ SO ₃	0.989	0.53

DSC studies show that pure PVdF-HFP film has glass transition, T_g at $-35\text{ }^\circ\text{C}$ and upon the addition of plasticizers and salt, T_g values are decreases until a certain optimized concentration is achieved after which it increases again. This is corresponds with the room temperature conductivity value. It is also noticed that the highest conducting sample from each system shows the lowest T_g . Lower T_g usually leads to easier chain relaxation. An electrolyte with low T_g always implies fast ion conduction. The DSC thermographs also exhibit a decrease in T_m value due to the increases of salt concentration. The decrease in T_g and T_m values indicate a reduction in PVdF-HFP crystallinity which causes an increase in the amorphous phase. These observations suggest that the interaction between the polymer host backbone and salt affects the main chain dynamics of the polymer. The polymeric chain in the amorphous phase is more flexible, which results in the enhancement of segmental motion of the polymer, thus enhancing the conductivity. TGA analysis shows that the sample with higher salt concentration showed greater thermal stability. It also found that the highest conducting film from both systems have a good thermal stability, whereas the GPE film

containing 25 wt.% LiCF_3SO_3 shows the most thermally stable film up to $\sim 179^\circ\text{C}$, which is higher than that of liquid electrolytes (80°C) currently used in lithium ion batteries.

FTIR and RAMAN spectra studies have proved that the EC, PC, LiCF_3SO_3 salt and NaCF_3SO_3 salt have form complexes with the polymer host, PVdF-HFP. The complexation can be determined by the appearance of new peaks, the absence of peaks, the decrease or increase in intensity of the existing peaks in the FTIR spectra. The band fitting of the triflate anion absorbance region was done for both systems in order to study the ion dissociation of the salt. Band fitting of these regions has provided information pertaining to the free ions, ion pairs and ion aggregates of triflate anion and proved the occurring of ionic interaction in the GPE films. The XRD diffractograms that have been presented in Chapter 6 revealed that the film with the highest conductivity at room temperature is the amorphous film. Generally, the conductivity increases as the degree of crystallinity decreases with increase of the flexibility of the polymer backbone. The results from FESEM analysis are consistent with the FTIR, RAMAN and XRD studies. The micrographs show that the films with the highest conductivity at room temperature from each polymer electrolytes system have the amorphous phase. Therefore we can conclude that the presence of plasticizer in PVdF-HFP/salt system helps the formation of regular pores by destroys the crystallinity structure, hence absorbs more electrolytes solution to enhance the conductivity.

The GPE films for PVdF-HFP/EC/PC/ LiCF_3SO_3 and PVdF-HFP/EC/PC/ NaCF_3SO_3 systems are electrochemically stable up to 3.2 V and 3.4 V, respectively. This value of working voltage range appears to be high enough to be used as an electrolyte in lithium and sodium battery system. The cyclic voltammograms for both films exhibit good cycling performance and the cycling is reproducible up to 10 cycles. The LiNiCoO_2 |

GPE| Li and MnO₂| GPE| Na cells have been assembled and their performances have been evaluated as discussed in Chapter 8. Lithium cell show higher performance as well as higher voltage and but lower discharge capacity compared to the sodium cell. The specific capacities for both systems were found to decrease upon cycling. This is mainly due to the electrochemical irreversibility of lithium/sodium metal and the growth of the layer at the interface between electrode and the GPE film.

In addition to the studies carried out in the present work, there is a lot of scope for future work in the area of gel polymer electrolyte for electrochemical devices applications, particularly on development of rechargeable polymer-ion batteries. These are summarized as follows:

- i. There is a need to explore more Na⁺ ion conducting polymer/gel polymer electrolytes with other polymer hosts and salts. Sodium perchlorate (NaClO₄), sodium hexafluorophosphate (NaPF₆) and sodium tetrafluoroborate (NaBF₄) should be considered in an attempt to look for good sodium ion conducting polymer electrolytes.
- ii. Some other ionic liquids can be used as a solvent to form Li⁺ and Na⁺ ion conducting gel polymer electrolytes to obtain their better thermal and electrochemical stability.
- iii. The conductivity of the GPE films can be enhanced by blending the PVdF-HFP with other polymer such as PMMA and PEO. Blending polymer is a useful method to develop new materials with improved mechanical stability.
- iv. The different type of cathode materials such as V₂O₅ and MgNiO₂ can be used. Both of these materials are expected to give high discharge capacity with high stability of the battery.

REFERENCES

- Abe, T., Fukuda, H., Iriyama, Y., & Ogumi, Z. (2004). Solvated Li-Ion Transfer at Interface Between Graphite and Electrolyte. *Journal of The Electrochemical Society*, 151(8), A1120.
- Abraham, K. M., & Alamgir, M. (1990). Li⁺-Conductive Solid Polymer Electrolytes with Liquid-Like Conductivity. *J. Electrochem. Soc.*, 137(5), 1657.
- Abraham, K. M., Jiang, Z., & Carroll, B. (1997). Highly Conductive PEO-like Polymer Electrolytes. *Chemistry of Materials*, 9(3), 1978–1988.
- Advantages, T., & Note, A. T. (2013). Application Note AC-1 Subject: Basics of Electrochemical Impedance Spectroscopy Overview.
- Akashi, H., Sekai, K., & Tanaka, K. (1998). A novel fire-retardant polyacrylonitrile-based gel electrolyte for lithium batteries. *Electrochimica Acta*, 43(10-11), 1193–1197.
- Alamgir, M., & Abraham, K. M. (1994). *Lithium Batteries: New Materials, Developments and Perspectives*. (G. Pistoia, Ed.). Amsterdam: Elsevier.
- Alamgir, M., Moulton, R. D., & Abraham, K. M. (1991). *Primary and secondary lithium batteries*. (S. M. Abraham KM, Ed.). Pennington: Electrochem. Soc.
- Analysis_FTIR. (2013). Retrieved from Introduction to Fourier Infrared Spectroscopy, Thermo Nicolet (2001) from <http://www.thermonicolet.com>
- Angell, C. (1983). Fast ion motion in glassy and amorphous materials. *Solid State Ionics*, 9-10, 3–16.
- Angell, C. (1986). Recent developments in fast ion transport in glassy and amorphous materials. *Solid State Ionics*, 18-19, 72–88.
- Angell, C. L. (1956). The infra-red spectra and structure of ethylene carbonate. *Trans. Faraday Soc.*, 52(0), 1178–1183.
- Aoki, T., Ohta, T., & Fujinami, T. (2006). Lithium ion conductivity of gel polymer electrolytes containing insoluble lithium tetrakis(pentafluorobenzenethiolato) borate. *Journal of Power Sources*, 156(2), 589–593.
- Aravindan, V., Lakshmi, C., & Vickraman, P. (2009). Investigations on Na⁺ ion conducting polyvinylidene fluoride-co-hexafluoropropylene/poly ethylmethacrylate blend polymer electrolytes. *Current Applied Physics*, 9(5), 1106–1111.
- Aravindan, V., Vickraman, P., Sivashanmugam, a., Thirunakaran, R., & Gopukumar,

- S. (2009). LiFAP-based PVdF–HFP microporous membranes by phase-inversion technique with Li/LiFePO₄ cell. *Applied Physics A*, 97(4), 811–819.
- Armand, M. (1994). The history of polymer electrolytes. *Solid State Ionics*, 69(3-4), 309–319.
- Armand, M.B., Chabagno, J. M., Duclot, M. (1979). In Fast Ion Transport in Solids. In G. K. S. M. J. Duclot, P. Vashishta, N. Mundy (Ed.), (p. 131). New York.
- Battery_diagram. (2013). Retrieved from <http://www.gutenberg.org/files/38384/38384-h/images/fig40.png>
- Battery_structure. (2014). Retrieved from <http://www.tested.com/tech/1366-how-to-get-the-most-from-your-lithium-ion-batteries/>
- Berthier, C., Gorecki, W., Minier, M., Armand, M. B., Chabagno, J. M., & Rigaud, P. (1983). Microscopic investigation of ionic conductivity in alkali metal salts-poly(ethylene oxide) adducts. *Solid State Ionics*, 11(1), 91–95.
- Bragg's_Law. (2013). Retrieved from <http://www.doitpoms.ac.uk/tlplib/xray-diffraction/bragg.php>
- Bruce, P. G., Hardgrave, M. T., & Vincent, C. A. (1992). The determination of transference numbers in solid polymer electrolytes using the Hittorf method. *Solid State Ionics*, 53-56, 1087–1094.
- Ceder, G., Chiang, Y.-M., Sadoway, D. R., Aydinol, M. K., Jang, Y.-I., & Huang, B. (1998). Journal search results - Cite This For Me. *Nature*, 392(6677), 694–696.
- Chandra, S., Sekhon, S. S., & Arora, N. (2000). PMMA based protonic polymer gel electrolytes. *Ionics*, 6(1-2), 112–118.
- Charge/discharge_process. (2013). Retrieved from <http://www.howstuffwork.com>
- Cheradame, H. (1982). *IUPAC Macromolecules*. (H. Benoit & B. Rempp, Eds.). Pergamon Press, Oxford.
- Chintapalli, S., & Frech, R. (1996). Effect of plasticizers on high molecular weight PEO-LiCF₃SO₃ complexes. *Solid State Ionics*, 86-88, 341–346.
- Choe, H. S., Giaccari, J., Alamgir, M., & Abraham, K. M. (1995). Preparation and characterization of poly(vinyl sulfone)- and poly(vinylidene fluoride)-based electrolytes. *Electrochimica Acta*, 40(13-14), 2289–2293.
- Choi, B.-K., Park, S.-H., Joo, S.-W., & Gong, M.-S. (2004). Electrical and thermal properties of poly(vinylidene fluoride-hexafluoropropylene)-based proton

conducting gel-electrolytes. *Electrochimica Acta*, 50(2-3), 649–652.

Choi, N.-S., Lee, Y.-G., Park, J.-K., & Ko, J.-M. (2001). Preparation and electrochemical characteristics of plasticized polymer electrolytes based upon a P(VdF-co-HFP)/PVAc blend. *Electrochimica Acta*, 46(10-11), 1581–1586.

Christie, L., Christie, A. M., & Vincent, C. A. (1999). Measurement of the apparent lithium ion transference number and salt diffusion coefficient in solid polymer electrolytes. *Electrochimica Acta*, 44(17), 2909–2913.

Cohen, M. H., & Turnbull, D. (1959). Molecular Transport in Liquids and Glasses. *The Journal of Chemical Physics*, 31(5).

Companik, J. E., & Bidstrup, S. A. (1994). The viscosity and ion conductivity of polydimethylsiloxane systems: 1. Chain length and ion size effects. *Polymer*, 35(22), 4823–4833.

Deepa, M., Agnihotry, S. A., Gupta, D., & Chandra, R. (2004). Ion-pairing effects and ion-solvent-polymer interactions in $\text{LiN}(\text{CF}_3\text{SO}_2)_2/\text{PC}/\text{PMMA}$ electrolytes: a FTIR study. *Electrochimica Acta*, 49(3), 373–383.

Doyle, M., & Newman, J. (1995). Analysis of Transference Number Measurements Based on the Potentiostatic Polarization of Solid Polymer Electrolytes. *J. Electrochem. Soc.*, 142(10), 3465.

Ethylene_carbonate. (2014). Retrieved from <http://www.sigmaaldrich.com/catalog/product/aldrich/535559?lang=de®ion=DE>

Evans, J., Vincent, C. A., & Bruce, P. G. (1987). Electrochemical measurement of transference numbers in polymer electrolytes. *Polymer*, 28(13), 2324–2328.

Fenton, D. E., Parker, J. M., & Wright, P. V. (1973). Complexes of alkali metal ions with poly(ethylene oxide). *Polymer*, 14(11), 589.

Golcuk, S., Muftuoglu, A. E., Celik, S. U., & Bozkurt, A. (2013). Synthesis and characterization of polymer electrolyte membranes based on PVDF and styrene via photoinduced grafting. *J Polym Res*, 20(5).

Gray, F. M. (1991). *Polymer Electrolytes: Fundamentals and Technological Applications*. New York (VCH): John Wiley And Sons.

Grest, G. S., & Cohen, M. H. (1980). Liquid-glass transition: Dependence of the glass transition on heating and cooling rates. *Phys. Rev. B*, 21(9), 4113–4117.

- Hong, H., Liquan, C., Xuejie, H., & Rongjian, X. (1992). Studies on PAN-based lithium salt complex. *Electrochimica Acta*, 37(9), 1671–1673.
- Hong, S. Y., Kim, Y., Park, Y., Choi, A., Choi, N., & Lee, K. T. (2013). Charge Carriers in Rechargeable Batteries: Na Ions vs. Li Ions. Retrieved from <http://pubs.rsc.org/en/content/articlepdf/2013/ee/c3ee40811f>
- Huang, B., & Wang, Z.X., Li, G.B., Huang, H., Xue, R.J., Chen, L.Q. & Wang, F. S. (1996). Lithium ion conduction in polymer electrolytes based on PAN. *Solid State Ionics*, 85(1-4), 79–84.
- Huang, W., Frech, R., Johansson, P., & Lindgren, J. (1995). Cation-polymer interaction and ionic association in diglyme-LiCF₃SO₃ and diglyme-propylene carbonate-LiCF₃SO₃ complexes. *Electrochimica Acta*, 40(13-14), 2147–2151.
- Huang, W., Frech, R., & Wheeler, R. A. (1994). Molecular structures and normal vibrations of trifluoromethane sulfonate (CF₃SO₃⁻) and its lithium ion pairs and aggregates. *J. Phys. Chem.*, 98(1), 100–110.
- Iijima, Y.; Tyoguchi, Y. & Eda, N. (1985). No Title. *Denki Kagaku*, 53, 619.
- Jeong, S.-K., Jo, Y.-K., & Jo, N.-J. (2006). Decoupled ion conduction mechanism of poly(vinyl alcohol) based Mg-conducting solid polymer electrolyte. *Electrochimica Acta*, 52(4), 1549–1555.
- Killis, A., Lenest, J., Gandini, A., Cheradame, H., & Cohenaddad, J. (1984). Correlation among transport properties in ionically conducting cross-linked networks☆. *Solid State Ionics*, 14(3), 231–237.
- Killis, A., LeNest, J.-F., Cheradame, H., & Gandini, A. (1982). Ionic conductivity of polyether-polyurethane networks containing NaBPh₄: A free volume analysis. *Die Makromolekulare Chemie*, 183(11), 2835–2845.
- Kim, C. H., Lee, K. H., Kim, W. S., Park, J., & Seung, D. Y. (2001). Ion conductivities and interfacial characteristics of the plasticized polymer electrolytes based on poly(methyl methacrylate-co-Li maleate). *Journal of Power Sources*, 94, 163.
- Kim, D., Park, J. K., Rhee, H. W. (1996). Conductivity and thermal studies of solid polymer electrolytes prepared by blending poly(ethylene oxide), poly(oligo[oxyethylene]oxysebacoyl) and lithium perchlorate. *Solid State Ionics*, 83(1-2), 49–56.
- Kumar, D., & Hashmi, S. a. (2010). Ionic liquid based sodium ion conducting gel polymer electrolytes. *Solid State Ionics*, 181(8-10), 416–423.

- Kumar, D., Suleman, M., & Hashmi, S. (2011). Studies on poly(vinylidene fluoride-co-hexafluoropropylene) based gel electrolyte nanocomposite for sodium–sulfur batteries. *Solid State Ionics*, 202(1), 45–53.
- Kumar, R., Sharma, J. P., & Sekhon, S. S. (2005). FTIR study of ion dissociation in PMMA based gel electrolytes containing ammonium triflate: Role of dielectric constant of solvent. *European Polymer Journal*, 41(11), 2718–2725.
- Kuo, H.-H., Chen, W.-C., Wen, T.-C., & Gopalan, A. (2002). A novel composite gel polymer electrolyte for rechargeable lithium batteries. *Journal of Power Sources*, 110(1), 27–33.
- Lee, C., Kim, J.-H., & Bae, J.-Y. (2003). Polymer gel electrolytes prepared by thermal curing of poly(vinylidene fluoride)–hexafluoropropene/poly(ethylene glycol)/propylene carbonate/lithium perchlorate blends. *Polymer*, 44(23), 7143–7155.
- Lee, Y.-G., & Park, J.-K. (2001). Electrochemical characteristics of polymer electrolytes based on P(VdF-co-HFP)/PMMA ionomer blend for PLIB. *Journal of Power Sources*, 97-98, 616–620.
- Lewandowski, A., Stepniak, I., & Grzybkowski, W. (2001). Copper transport properties in polymer electrolytes based on poly(ethylene oxide) and poly(acrylonitrile). *Solid State Ionics*, 143(3-4), 425–432.
- Li, T., & Balbuena, P. B. (1999). Theoretical studies of lithium perchlorate in ethylene carbonate, propylene Carbonate, and {...}. *J. Electrochem. Soc.*, 146, 3613–3622.
- Lim, D.-H., Manuel, J., Ahn, J.-H., Kim, J.-K., Jacobsson, P., Matic, A., ... Kim, K.-W. (2012). Polymer electrolytes based on poly(vinylidene fluoride-co-hexafluoropropylene) nanofibrous membranes containing polymer plasticizers for lithium batteries. *Solid State Ionics*, 225, 631–635.
- Lithium_trifluoromethanesulfonate. (2014). Retrieved from <http://www.sigmaaldrich.com/catalog/product/aldrich/481548?lang=de®ion=DE>
- Manuel Stephan, a. (2006). Review on gel polymer electrolytes for lithium batteries. *European Polymer Journal*, 42(1), 21–42.
- Manuel Stephan, a., Gopu Kumar, S., Renganathan, N. G., & Anbu Kulandainathan, M. (2005). Characterization of poly(vinylidene fluoride–hexafluoropropylene) (PVdF–HFP) electrolytes complexed with different lithium salts. *European Polymer Journal*, 41(1), 15–21.

- Mary Sukeshini, A., Nishimoto, A., & Watanabe, M. (1996). Transport and electrochemical characterization of plasticized poly(vinyl chloride) solid electrolytes. *Solid State Ionics*, 86-88, 385–393.
- Nagaura, T. & Tozawa, K. (1990). Lithium ion rechargeable battery. *Prog. Batteries Solar Cells*, 9, 209–217.
- Nasef, M. M., & Saidi, H. (2005). No Title. *Materials Chemistry and Physics*, 25(In Press).
- Nicotera, I., Coppola, L., Oliviero, C., Castriota, M., & Cazzanelli, E. (2006). Investigation of ionic conduction and mechanical properties of PMMA–PVdF blend-based polymer electrolytes☆. *Solid State Ionics*, 177(5-6), 581–588.
- Optics basics_ XRD. (2013). Retrieved from <http://skullsinthestars.com/2009/03/28/optics-basics-youngs-double-slit-experiment>
- Osman, Z., & Arof, A. K. (2003). FTIR studies of chitosan acetate based polymer electrolytes. *Electrochimica Acta*, 48(8), 993–999.
- Pandey, G. P., Agrawal, R. C., & Hashmi, S. A. (2009). Magnesium ion-conducting gel polymer electrolytes dispersed with nanosized magnesium oxide. *Journal of Power Sources*, 190(2), 563–572.
- Park, J. (2012). Principles and Applications of Lithium Secondary Batteries.
- Park, Y., Seo, D., Kwon, H., Kim, B., Kim, J., Kim, H., ... Kang, K. (2013). A New High-Energy Cathode for a Na-Ion Battery with Ultrahigh Stability. *Journal of the American Chemical Society*.
- Principle_FESEM. (2013). Retrieved from http://areeweb.polito.it/ricerca/carbongroup/fac_fesem.html
- Propylene_carbonate. (2014). Retrieved from <http://www.sigmaaldrich.com/catalog/product/sial/310328?lang=de®ion=DE>
- Rajendran, S., Babu, R. shanker, & Sivakumar, P. (2008). *Investigations on PVC/PAN composite polymer electrolytes. Journal of Membrane Science* (Vol. 315).
- Ramesh, S., Leen, K. H., Kumutha, K., & Arof, A. K. (2007). FTIR studies of PVC/PMMA blend based polymer electrolytes. *Spectrochimica Acta Part A: Molecular and Biomolecular Spectroscopy*, 66(4-5), 1237–1242.
- Ramesh, S., & Lu, S.-C. (2011a). Atypical behaviors of BMIMTf ionic liquid present in ionic conductivity, SEM, and TG/DTG analyses of P(VdF-HFP)/LiTf-based solid

- polymer electrolyte system. *Journal of Materials Research*, 26(23), 2945–2951.
- Ramesh, S., & Lu, S.-C. (2011b). Effect of lithium salt concentration on crystallinity of poly(vinylidene fluoride-co-hexafluoropropylene)-based solid polymer electrolytes. *Journal of Molecular Structure*, 994(1-3), 403–409.
- Ramesh, S., & Lu, S.-C. (2013). A simple P(VdF-HFP)–LiTf system yielding highly ionic conducting and thermally stable solid polymer electrolytes. *Journal of Molecular Liquids*, 177, 73–77.
- Ramya, C. S., Selvasekarapandian, S., Savitha, T., Hirankumar, G., & Angelo, P. C. (2007). Vibrational and impedance spectroscopic study on PVP–NH₄SCN based polymer electrolytes. *Physica B: Condensed Matter*, 393(1-2), 11–17.
- Ratner, M. A. (1987). In *Polymer Electrolyte Reviews*. (J. R. MacCallum & C. A. Vincent, Eds.). London: Elsevier.
- Reich, S., & Michaeli, I. (1975). Electrical conductivity of small ions in polyacrylonitrile in the glass–transition region. *Journal of Polymer Science: Polymer Physics Edition*, 13(1), 9–18.
- Reiter, J., Velická, J., & Míka, M. (2008). Proton-conducting polymer electrolytes based on methacrylates. *Electrochimica Acta*, 53(26), 7769–7774.
- Rhodes, C. P., & Frech, R. (2000). A symmetry-based analysis of Raman and infrared spectra of the compounds (poly (ethylene oxide))₃ LiCF₃ SO₃ and (poly (ethylene oxide))₃ NaCF₃ SO₃, 137, 1131–1137.
- Sagane, F., Abe, T., Iriyama, Y., & Ogumi, Z. (2005). Li⁺ and Na⁺ transfer through interfaces between inorganic solid electrolytes and polymer or liquid electrolytes. *Journal of Power Sources*, 146(1-2), 749–752.
- Saikia, D., Han, C. C., & Chen-Yang, Y. W. (2008). Influence of polymer concentration and dyes on photovoltaic performance of dye-sensitized solar cell with P(VdF-HFP)-based gel polymer electrolyte. *Journal of Power Sources*, 185(1), 570–576.
- Saikia, D., & Kumar, a. (2004a). Ionic conduction in P(VDF-HFP)/PVDF–(PC + DEC)–LiClO₄ polymer gel electrolytes. *Electrochimica Acta*, 49(16), 2581–2589.
- Saikia, D., & Kumar, a. (2005). Ionic transport in P(VDF-HFP)–PMMA–LiCF₃SO₃–(PC+DEC)–SiO₂ composite gel polymer electrolyte. *European Polymer Journal*, 41(3), 563–568.
- Saikia, D., & Kumar, A. (2004b). Ionic conduction in P(VDF-HFP)/PVDF–(PC + DEC)–LiClO₄ polymer gel electrolytes. *Electrochimica Acta*, 49(16), 2581–2589.

- Saikia, D., Wu, H.-Y., Pan, Y.-C., Lin, C.-P., Huang, K.-P., Chen, K.-N., ... Kao, H.-M. (2011). Highly conductive and electrochemically stable plasticized blend polymer electrolytes based on PVdF-HFP and triblock copolymer PPG-PEG-PPG diamine for Li-ion batteries. *Journal of Power Sources*, 196(5), 2826–2834.
- Salkind, A. J. (1987). Proceeding of the Symposium in History of Battery Technology'. In A.J. Salkind (Ed.), . Pennington, New york.
- Salkind, A. J., & Falk, S. (1969). *Alkaline Storage Batteries*. (John Wiley, Ed.). New York.
- Sanders, R. A., Snow, A. G., Frech, R., & Glatzhofer, D. T. (2003a). A spectroscopic and conductivity comparison study of linear poly(N-methylethylenimine) with lithium triflate and sodium triflate. *Electrochimica Acta*, 48(14-16), 2247–2253.
- Sanders, R. A., Snow, A. G., Frech, R., & Glatzhofer, D. T. (2003b). A spectroscopic and conductivity comparison study of linear poly(N-methylethylenimine) with lithium triflate and sodium triflate. *Electrochimica Acta*, 48(14-16), 2247–2253.
- Schantz, S, Sandahl, J., Börjesson, L., Torell, L.M., Stevens, J. R. (1988). Ion pairing in polymer electrolytes; A comparative Raman study of NaCF₃SO₃ complexed in poly(propylene-glycol) and dissolved in acetonitrile. *Solid State Ionics*, 28-30, 1047–1053.
- Schematic_ FESEM. (2013). Retrieved from <http://www4.nau.edu/microanalysis/microprobe-sem/instrumentation.html>
- Schematic_DSC. (2013). Retrieved from http://www.fs.unilj.si/mma_bin.php?id=2010111100484104
- Schematic_XRD. (2013). Retrieved from Handout on X-Ray Diffraction generated for 626 instrumentations course, UW--Madison Chemistry Department, Spring, 1992, figure from the Web: <http://www.chem.wisc.edu/~newtrad/CurrRef/BDGTopic/BDGtext/BDGGraph.html>
- Sekhon, S. S. (2003). Conductivity behaviour of polymer gel electrolytes: Role of polymer. *Bulletin of Materials Science*, 26(3), 321–328.
- Selvasekarapandian, S., Hema, M., Kawamura, J., Kamishima, O., & Baskaran, R. (2010). Characterization of PVA–NH₄NO₃ Polymer Electrolyte and Its Application in Rechargeable Proton Battery. *Journal of the Physical Society of Japan*, 79(Suppl.A), 163–168.
- Sim, L. N., Majid, S. R., & Arof, a. K. (2012). FTIR studies of PEMA/PVdF-HFP blend polymer electrolyte system incorporated with LiCF₃SO₃ salt. *Vibrational*

Spectroscopy, 58, 57–66.

- Slane, S., & Salomon, M. (1995). Composite gel electrolyte for rechargeable lithium batteries. *Journal of Power Sources*, 55(1), 7–10.
- Sodium_trifluoromethanesulfonate. (2014). Retrieved from <http://www.sigmaaldrich.com/catalog/product/aldrich/367907?lang=de®ion=DE>
- Song, J. Y., Wang, Y. Y., & Wan, C. C. (1999). Review of gel-type polymer electrolytes for lithium-ion batteries. *Journal of Power Sources*, 77(2), 183–197.
- Subramania, a., Sundaram, N. T. K., & Kumar, G. V. (2006). Structural and electrochemical properties of micro-porous polymer blend electrolytes based on PVdF-co-HFP-PAN for Li-ion battery applications. *Journal of Power Sources*, 153(1), 177–182.
- Tsuchida, E., Ohno, H., Tsunemi, K., & Kobayashi, N. (1983). Lithium ionic conduction in poly (methacrylic acid)-poly (ethylene oxide) complex containing lithium perchlorate. *Solid State Ionics*, 11(3), 227–233.
- Vieira, D. F., Avellaneda, C. O., & Pawlicka, A. (2007). Conductivity study of a gelatin-based polymer electrolyte. *Electrochimica Acta*, 53(4), 1404–1408.
- Wang, C. M., & Chen, J. M. (2014). Nanotechnology Prospect for Rechargeable Li-ion Batteries. Retrieved from http://www.service.hkpc.org/hkiemat/previous/2008/mastec03_notes/CMWANG.PDF
- Wang, Z., Huang, B., Huang, H., Chen, L., Xue, R., & Wang, F. (1996). Infrared spectroscopic study of the interaction between lithium salt LiClO₄ and the plasticizer ethylene carbonate in the polyacrylonitrile-based electrolyte. *Solid State Ionics*, 85(1-4), 143–148.
- Wang, Z., Huang, B., Xue, R., Huang, X., Chen, L. (1999). Spectroscopic investigation of interactions among components and ion transport mechanism in polyacrylonitrile based electrolytes. *Solid State Ionics*, 121(1-4), 141–156.
- Watanabe, M., Rikukawa, M., Sanui, K., Ogata, N., Kato, H., Kobayashi, T., & Ohtaki, Z. (1984). Ionic conductivity of polymer complexes formed by poly(ethylene succinate) and lithium perchlorate. *Macromolecules*, 17(12), 2902–2908.
- West, K., Zachau-Christiansen, B., & Jacobsen, T. (1983). Electrochemical properties of non-stoichiometric V₆O₁₃. *Electrochimica Acta*, 28(12), 1829–1833.

Xia, Y. Y., Tatsumi, K., Fujieda, T., Prosini, P. P., & Sakai, T. (2000). Solid-state lithium-polymer batteries using lithiated MnO₂ cathodes. *Journal of Electrochemical Society*, 147, 2050.

York, S., Frech, R., Snow, A., & Glatzhofer, D. (2001). A comparative vibrational spectroscopic study of lithium triflate and sodium triflate in linear poly(ethylenimine). *Electrochimica Acta*, 46(10-11), 1533–1537.

University of Malaya

LIST OF PUBLICATIONS AND PAPERS PRESENTED

- [1] **K.B. M. Isa**, Z. Osman, A.K. Arof, L. Othman, N.H. Zainol, S.M. Samin, W.G. Chong, N. Kamarulzaman, "Lithium Ion Conduction And Ion-Polymer Interaction In PVdF-HFP Based Gel Polymer Electrolytes" *Solid State Ionics* 268 (2014) 288–293.
- [2] **K.B. Md. Isa**, L. Othman, N.H. Zainol, S.M. Samin, W.G. Chong, Z. Osman, A.K. Arof, "Studies on Sodium Ion Conducting Gel Polymer Electrolytes" *Key Engineering Materials* 594-595 (2013) 786–792.
- [3] Siti Mariam Samin, Mazwan Mansor, **Khairul Bahiyah Md Isa** and Zurina Osman, Comparison Studies of Blend and Unblend GPE Systems: Ionic Conductivity, Structural and Morphological Properties, *Advanced Materials Research*, 626(2013), 205-210.
- [4] N.H. Zainol, S.M. Samin, L. Othman, **K.B. M. Isa**, W.G. Chong, Z. Osman, "Magnesium Ion-Based Gel Polymer Electrolytes: Ionic Conduction and Infrared Spectroscopy Studies" *International Journal of Electrochemical Science* 8 (2013) 3602–3614.
- [5] Z. Osman, S.M. Samin, L. Othman, **K.B. Md Isa**, "Ionic Transport in PMMA-NaCF₃SO₃ Gel Polymer Electrolyte" *Advanced Materials Research* 545 (2012) 259–263.
- [6] W.G. Chong, Z. Osman, L. Othman, **K.B. Md. Isa**, "Ionic Conductivity and Dielectric Properties of Plasticized Polyacrylonitrile Based Solid Polymer Electrolyte Films" *Advanced Materials Research* 626 (2012) 211–214.
- [7] Z. Osman, **K.B. Md. Isa**, L. Othman, N. Kamarulzaman, K.B. Isa, L. Othman, N. Kamarulzaman, "Studies of Ionic Conductivity and Dielectric Behavior in Polyacrylonitrile Based Solid Polymer Electrolytes" *Defect and Diffusion Forum* 312-315 (2011) 116–121.